AFRL-PR-WP-TR-2002-2060

HIGH CYCLE FATIGUE (HCF) SCIENCE AND TECHNOLOGY PROGRAM

2001 Annual Report

Thomas M. Bartsch

Universal Technology Corporation
1270 North Fairfield Road
Dayton, OH 45432-2600

MAY 2002

FINAL REPORT FOR 01 JANUARY 2001 – 31 DECEMBER 2001

PROPULSION DIRECTORATE
AIR FORCE RESEARCH LABORATORY
AIR FORCE MATERIEL COMMAND
WRIGHT-PATTERSON AIR FORCE BASE, OH 45433-7251

NOTICE

USING GOVERNMENT DRAWINGS, SPECIFICATIONS, OR OTHER DATA INCLUDED IN THIS DOCUMENT FOR ANY PURPOSE OTHER THAN GOVERNMENT PROCUREMENT DOES NOT IN ANY WAY OBLIGATE THE US GOVERNMENT. THE FACT THAT THE GOVERNMENT FORMULATED OR SUPPLIED THE DRAWINGS, SPECIFICATIONS, OR OTHER DATA DOES NOT LICENSE THE HOLDER OR ANY OTHER PERSON OR CORPORATION; OR CONVEY ANY RIGHTS OR PERMISSION TO MANUFACTURE, USE, OR SELL ANY PATENTED INVENTION THAT MAY RELATE TO THEM.

THIS REPORT IS RELEASABLE TO THE NATIONAL TECHNICAL INFORMATION SERVICE (NTIS). AT NTIS, IT WILL BE AVAILABLE TO THE GENERAL PUBLIC, INCLUDING FOREIGN NATIONS.

THIS TECHNICAL REPORT HAS BEEN REVIEWED AND IS APPROVED FOR PUBLICATION.

Daniel E. Thomson, AFRL/PRTC

Theodore G. Fecke, AFRL/PRTC

WILLIAM E. KOOP, AFRL/PRT

Do not return copies of this report unless contractual obligations or notice on a specific document require its return.

REPORT DOCUMENTATION PAGE

Form Approved
OMB No. 0704-0188

1. REPORT DATE *(DD-MM-YY)*	2. REPORT TYPE	3. DATES COVERED *(From - To)*
May 2002	Final	01/01/2001 – 12/31/2001

4. TITLE AND SUBTITLE
HIGH CYCLE FATIGUE (HCF) SCIENCE AND TECHNOLOGY PROGRAM
2001 Annual Report

5a. CONTRACT NUMBER
F33615-98-C-2807

5b. GRANT NUMBER

5c. PROGRAM ELEMENT NUMBER
62203F

6. AUTHOR(S)
Thomas M. Bartsch

5d. PROJECT NUMBER
APPL

5e. TASK NUMBER
TO

5f. WORK UNIT NUMBER
04

7. PERFORMING ORGANIZATION NAME(S) AND ADDRESS(ES)

Universal Technology Corporation
1270 North Fairfield Road
Dayton, OH 45432-2600

8. PERFORMING ORGANIZATION REPORT NUMBER

9. SPONSORING/MONITORING AGENCY NAME(S) AND ADDRESS(ES)

Propulsion Directorate
Air Force Research Laboratory
Air Force Materiel Command
Wright-Patterson Air Force Base, OH 45433-7251

10. SPONSORING/MONITORING AGENCY ACRONYM(S)
AFRL/PRTC

11. SPONSORING/MONITORING AGENCY REPORT NUMBER(S)
AFRL-PR-WP-TR-2002-2060

12. DISTRIBUTION/AVAILABILITY STATEMENT
Approved for public release; distribution is unlimited.

13. SUPPLEMENTARY NOTES
Report contains color.

14. ABSTRACT

This fifth annual report of the National Turbine Engine High Cycle Fatigue (HCF) Program is a brief review of work completed, work in progress, and technical accomplishments. This program is a coordinated effort with participation by the Air Force, the Navy, and NASA. The technical efforts are organized under seven action teams—Materials Damage Tolerance Research, Forced Response Prediction, Component Analysis, Instrumentation, Passive Damping Technology, Component Surface Treatments, and Engine Demonstration—and two Programs—Test and Evaluation, and Transitions (ENSIP).

15. SUBJECT TERMS
high cycle fatigue, turbine engines, instrumentation, damping, forced response, test and evaluation, ENSIP, materials, surface treatments, laser shock peening, component analysis, damage tolerance

16. SECURITY CLASSIFICATION OF:			17. LIMITATION OF ABSTRACT:	18. NUMBER OF PAGES	19a. NAME OF RESPONSIBLE PERSON (Monitor)
a. REPORT	b. ABSTRACT	c. THIS PAGE			Daniel E. Thomson
Unclassified	Unclassified	Unclassified	SAR	236	19b. TELEPHONE NUMBER *(Include Area Code)* (937) 255-4826

HES&S 31-15093-1

Standard Form 298 (Rev. 8-98)
Prescribed by ANSI Std. Z39-18

Table of Contents

List of Figures

List of Tables

FOREWORD

This document, the fifth annual report of the National Turbine Engine High Cycle Fatigue (HCF) Science and Technology (S&T) Program, is a summary of the objectives, approaches, and technical progress of ongoing and planned future efforts.

High cycle fatigue (HCF) results from vibratory stress cycles induced by various aeromechanical sources. The frequencies can be thousands of cycles per second. HCF is a widespread phenomenon in aircraft gas turbine engines that historically has led to the premature failure of major engine components (fans, compressors, turbines) and in some instances has resulted in loss of the total engine and aircraft.

Between 1982 and 1996, high cycle fatigue accounted for 56% of Class A engine-related failures. HCF is a major factor negatively impacting safety, operability, and readiness, while at the same time increasing maintenance costs. In fiscal year 1994, HCF required an expenditure of 850,000 maintenance man-hours for risk management inspections. Estimates put the cost of high cycle fatigue at over $400 million per year.

The HCF S&T Program officially began in December 1994 with the specific purpose of helping to eliminate HCF as a major cause of aircraft turbine engine failures. Since its beginning the Program has been directed by an Air Force-led steering committee consisting of representatives from the Air Force, the Navy, the Army, and NASA along with an adjunct industry advisory panel, and an Executive Independent Review Team (EIRT). The Program's Technical Planning Team, S&T Action Teams, Test & Evaluation, and Transitions to the Engine Structural Integrity Program (ENSIP) support groups are all closely integrated and focused on highly effective development and transition of critical HCF turbine engine technology. In the fall of 2000, a parallel Steering Committee was established to oversee HCF-related data sharing and technology development efforts of mutual interests with the United Kingdom (UK). This action was taken after an extensive joint government review of both the US and UK HCF programs and an assessment of areas of potential technical collaboration and of issues critical to advanced turbine engine technology transition. The current Organizational Structure of the HCF Team is shown in Figure 0.1.

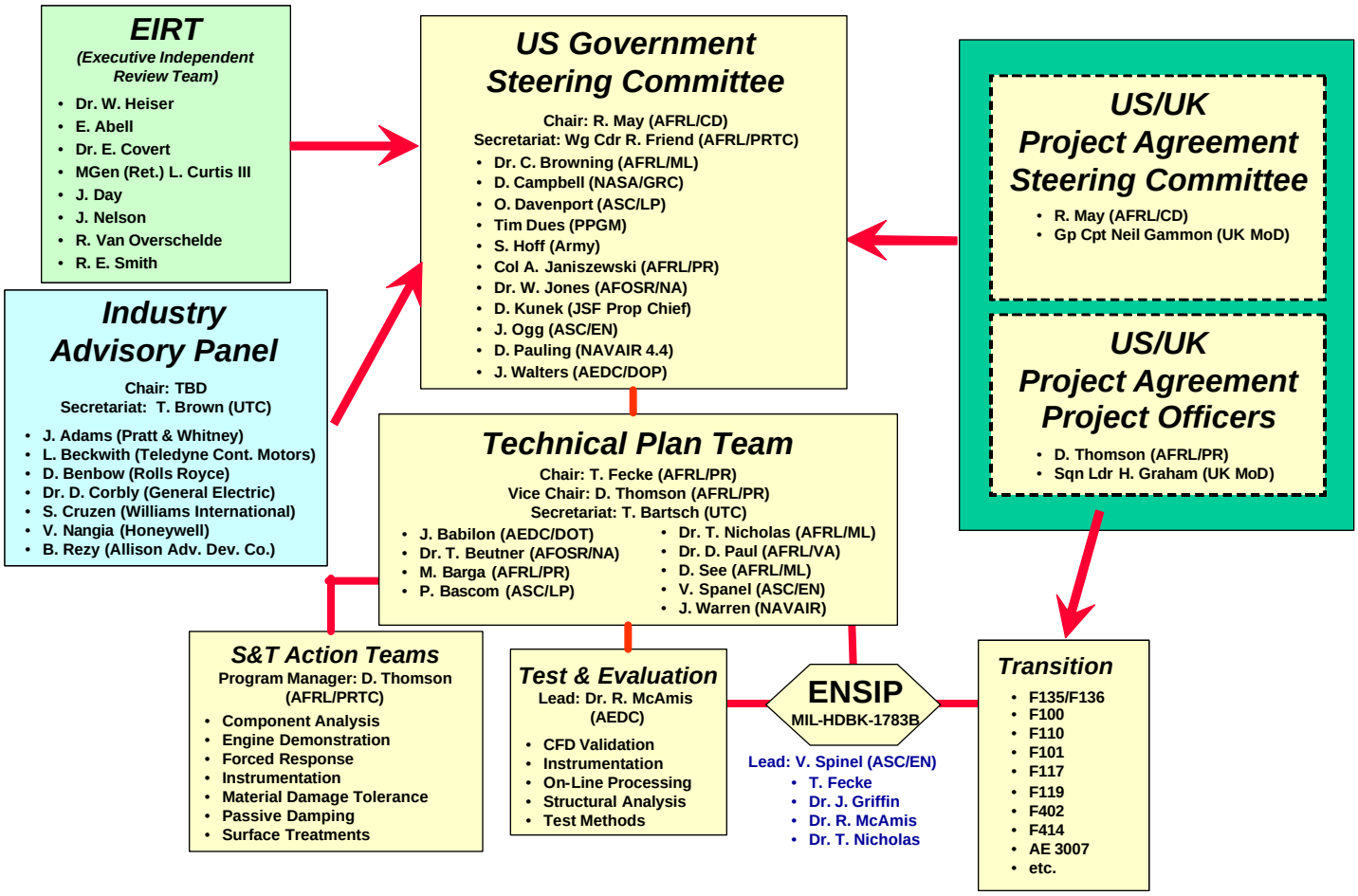

FIGURE 0.1 HCF Team Organizational Structure

Greatly improved safety and readiness and lower costs are all goals of the HCF Program. Specifically, the goals are as follows: to reduce HCF-related non-recoverable in-flight shutdowns by 50%; to virtually eliminate HCF related Class A mishaps; to virtually eliminate HCF-related precautionary stand-downs; and to reduce total engine maintenance costs by over 15 %.

The HCF S&T Program is also specifically directed at supporting the Integrated High Performance Turbine Engine Technology (IHPTET) Program and one of its goals: to reduce engine maintenance costs. This program will try to achieve that goal through technical action team efforts targeted at a 50% reduction of HCF-related maintenance costs. In addition, the program could contribute to a reduction in HCF-related "real" development costs of over 50%. When combined with the Test and Evaluation (T&E) program and future health monitoring approaches, the HCF S&T program should ensure the production of much more damage-tolerant high-performance engines.

The specific component objectives of the HCF S&T program are listed in Table 0.1 below:

TABLE 0.1 HCF S&T Program Objectives			
	Fans	**Compressors**	**Turbines**
Determine Alternating Stress Within…	20%	25%	25%
Damp Resonant Stress by…	60%	20%	25%
Reduce Uncertainty in Capability of Damaged Components by…	50%	50%	50%
Increase Leading Edge Defect Tolerance…	15x (5-75 mils)	n/a	n/a

The technical efforts are organized under seven action teams:

- Component Surface Treatments
- Materials Damage Tolerance Research
- Instrumentation
- Component Analysis
- Forced Response Prediction
- Passive Damping
- Engine Demonstration (added in 1999)

In addition to the HCF S&T Program, with its action teams, there is a Test and Evaluation Program (addressing test methods and facilities) and a Transition Program (addressing guidance documents) which support and are supported by all of the actions teams.

Action team technical and schedule research agendas, including highly focused exit criteria and program cost and funding baselines, are continually assessed and closely reviewed to ensure effective management discipline in this complex, high priority technology program.

Over the last several years, the technologies developed under the High Cycle Fatigue (HCF) Science and Technology (S&T) Program have helped solve several difficult field engine problems. As a result, there are now considerably fewer major HCF events. Excellent progress has been made in the HCF program. For the first time, it appears that this once arcane topic is being understood and managed to a point where significant cost reductions are being realized, positively impacting the operations, maintenance, and readiness of our combat forces. However, HCF is a very difficult technology challenge that has continued to involve multiple technology development and transition risks. During the fall of 1999, the HCF National Action Team completed a Project "Relook" study defining the efforts necessary to mitigate these critical risk issues—both current program "shortfalls" and "new requirements." Reprogramming plans were extensively reviewed and approved by both the HCF Industry Advisory Panel and a special committee. This reprogramming action extended the HCF program through 2006, with increased focus on advanced combat engine technology transition and greater attention to UAV/small engine issues. The current planning and programming efforts to increase UK participation and collaborative technology development should further enhance technology transition support to high priority collaborative propulsion development efforts.

Emphasis also continues to be placed on using the technology advancements developed in the HCF Technology Program to update the HCF-related portions of the Materials, Test, and Analysis sections of the Engine Structural Integrity Program (ENSIP) documentation.

In the future, the HCF S&T Program will continue as a very-high-priority national, and now international, effort. Meeting the total technology challenge could essentially eliminate engine HCF-related aircraft mishaps and greatly enhance overall aircraft system readiness.

Your comments regarding the work reported in this document are welcome, and may be directed to Mr. Daniel Thomson, the HCF Program Manager of the Air Force Research Laboratory Propulsion Directorate (AFRL/PRTC, Daniel.Thomson@wpafb.af.mil, 937-255-2611).

1.0 COMPONENT SURFACE TREATMENTS

BACKGROUND

The Component Surface Treatments Action Team (Surface Treatments AT) has the responsibility of fostering collaboration among individual HCF surface treatment efforts with the goal of increasing leading edge defect tolerance by 15x (5 mils to 75 mils). The Surface Treatments AT provides technical coordination and communication among active participants involved in Laser Shock Peening (LSP) and related technologies. Annual technical workshops have been organized and summaries of these workshops are disseminated to appropriate individuals and organizations. The Chair, Co-Chair, and selected Surface Treatments AT members meet as required (estimated quarterly) to review technical activities, develop specific goals for LSP programs, and coordinate with the Technical Plan Team (TPT) and Industry Advisory Panel (IAP). The Chairman (or Co-Chair) of the Surface Treatments AT keeps the TPT Secretary informed of AT activities on a frequent (at least monthly) basis. This AT includes members from government agencies, industry, and universities who are actively involved in surface treatment technologies applicable to engine HCF. The team is to be multidisciplinary with representatives from multiple organizations representing several component technologies as appropriate. The actual membership of the AT may change in time as individuals assume different roles in related projects.

ACTION TEAM CHAIRS

Chair
Mr. David W. See
U.S. Air Force
AFRL/MLMP, Bldg. 653
2977 P Street, Suite 6
Wright-Patterson AFB, OH 45433-7739
Phone: (937) 255-7279
Fax: (937) 656-4420

Co-Chair
Mr. Rollie Dutton
U.S. Air Force
AFRL/MLLM, Bldg. 655
2230 Tenth St., Suite 1
Wright-Patterson AFB, OH 45433
Phone: (937) 255-1305
Fax: (937) 255-3007

INTRODUCTION

The following pages summarize the schedules, backgrounds, and recent progress of the current and planned projects managed by this action team.

FIGURE 1.0 Component Surface Treatment Research Schedule

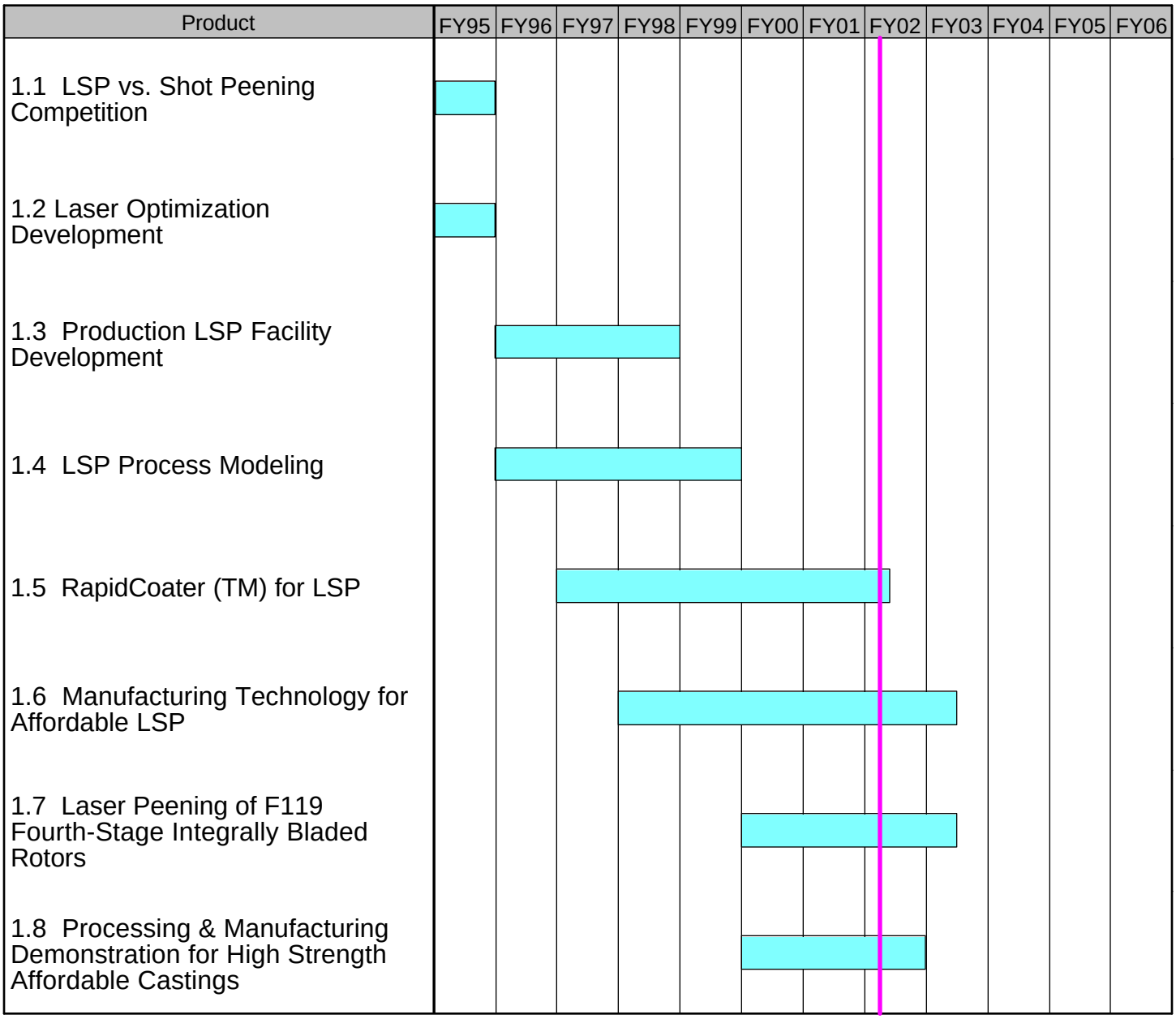

1.1 Laser Shock Peening (LSP) vs. Shot Peening Competition
FY 95

A comparative study between Laser Shock Peening (LSP) and the established surface treatment technology, shot peening, was conducted in 1995. This study evaluated the damage tolerance improvements produced by these processes, specifically rating their influence for enhancing the fatigue life of turbine engine fan blades damaged by foreign objects (FOD). The resulting data showed that *damaged* Laser Shock Peened F101 fan blades with a 250-mil notch actually demonstrated *greater* fatigue strength than the baseline *un*damaged untreated fan blades.

(Reference 2000 HCF Annual Report, Section 1.1 for more details.)

1.2 Laser Optimization Development
FY 95

(Reference 2000 HCF Annual Report, Section 1.2 for more details.)

1.3 Production LSP Facility Development
FY 96-98

The system, consisting of the laser, the facility, and the process, was successfully demonstrated in January 1998, and the laser is now available for use by the Air Force and industry.

(Reference 2000 HCF Annual Report, Section 1.3 for more details.)

1.4 LSP Process Modeling
FY 96-99

Background

The focus of this effort was to develop a predictive capability for the compressive residual stress distribution produced in a part or structure by laser peening. Using this capability tool will substantially shorten the development time and costs for applying laser peening to new applications and alloys.

In Phase I (FY 96-97) of this two-phase program, it was demonstrated that a residual stress profile could be modeled successfully for a single laser spot. The objectives of Phase II (FY 98-99) were (1) to develop models for predicting the in-material residual stress profiles produced by multiple-spot Laser Shock Peening, (2) to verify and validate the residual stress profiles by comparison to experimental measurements, and (3) to gather appropriate data for input to the models.

Final Results

A model for large-section thicknesses laser shock peened from one side was developed that showed good correlation with experimental residual stress profiles. The verification of the model was based on the comparison of residual stress measurements performed on LSP'd coupons with those predicted by the model. The residual stress profiles developed in a part were shown to be dependent on the laser peening intensity, the material, and the part geometry.

Thin and intermediate section thicknesses were also modeled with two-sided laser peening. This proved to be a much more difficult problem, and several constitutive equations for the material of interest were explored and tested with the models. Significant progress was made in defining the issues involved with modeling of residual stresses in thin sections. However, further work will be needed to reliably model the residual stresses produced by laser in thin sections.

Participating Organizations: LSP Technologies, Inc., Ohio State University, and University of Dayton Research Institute

Points of Contact:

Government
Mr. Joseph G. Burns
U.S. Air Force
AFRL/MLLM, Bldg. 655
2230 Tenth St., Suite 1
Wright-Patterson AFB, OH 45433-7817
Phone: (937) 255-1305
Fax: (937) 656-4420

Contractor
Dr. Allan H. Clauer
LSP Technologies, Inc.
6145 Scherers Place
Dublin, OH 43016-1272
Phone: (614) 718-3000 x12
Fax: (614) 718-3007

1.5 RapidCoater ä for LSP

FY 97-02

Introduction

One of the significant shortcomings of the current Laser Shock Peening process is slow processing, which is primarily due to the inability to apply and remove the opaque overlay (paint) rapidly. An opaque overlay is applied to the surface of a part for two reasons: to protect the surface of the part from the intense heat of the plasma and to provide a consistent processing medium for the laser beam. The application of these overlays is a time-consuming, labor-intensive process. Current practice requires the application and removal of the paint outside of the laser workstation. Under current practice, a part that requires multiple shots must be transported back and forth several times, from the laser workstation where it is peened, to a separate area where the overlay is removed and reapplied, then back to the laser workstation, and so on. Sections 1.5.1 and 1.5.2 below explain what is being done to solve this problem. Section 1.5.1 describes the development, selection, and demonstration of a prototype system to rapidly apply and remove the overlay system. Section 1.5.2 describes the development of a production system.

Another source of slow processing is due to the shape of the laser beam spot on the surface to be processed. The current laser beam shape is round, and as a result, overlapping of the laser beam spots, up to 30 percent, is required to provide 100 percent laser shock peen coverage. Decreasing the overlap

will increase the processing rates. Section 1.5.2 describes the development of laser beam optics to shape the round laser beam into a square laser beam.

The objective of this program was to develop and implement technologies that increase the rate of laser shock peening. The Points of Contact and Participating Organizations listed below apply to both of these efforts.

Participating Organizations: LSP Technologies, Inc.

Points of Contact:

Government
Mr. David W. See
U.S. Air Force
AFRL/MLMP, Bldg. 653
2977 P Street, Suite 6
Wright-Patterson AFB, OH 45433-7739
Phone: (937) 255-7279
Fax: (937) 656-4420

Contractor
Mr. David F. Lahrman
LSP Technologies, Inc.
6145 Scherers Place
Dublin, OH 43016-1284
Phone: (614) 718-3000 x44
Fax: (614) 718-3007

1.5.1 Rapid Overlay Concept Development

FY 97

Background and Final Results

The objective of this SBIR Phase I program was to identify and evaluate promising methods for applying and removing the opaque overlay rapidly during laser peening. Two coating application methods were investigated: (1) water-soluble paint applied with a spray gun; and (2) paint or ink application with an ink jet. The water-soluble paint/spray gun application method was selected as the most promising approach. The rapid overlay system concept was developed around this method. The rapid overlay demonstration test unit was assembled and tested to provide a working demonstration of the concept. The demonstration, which consisted of sequential application of the paint overlay, application of the overlay water film, firing the laser, and removal of the paint overlay in continuous, repetitive cycles, was successful. The successful demonstration system has been designated the RapidCoater™ System.

1.5.2 Development of a RapidCoater™ Manufacturing System

FY 98-01

Background

In Phase I of this program, it was demonstrated that it is possible to automate the application of the overlay while processing. The objectives of this Phase II program were to develop a rapid-overlay-application and removal system that can be integrated into a production laser peening system, develop a control system that will synchronize the coating process and interface it with the laser control system, and identify beam shaping optics to produce square laser beam spots. The production RapidCoater™

system accommodates a range of parts and operates reliably at the laser repetition frequency. This allows the RapidCoater™ system to be integrated into the production laser peening system.

An extension to this program was awarded that added two additional objectives. One of these objectives was to develop controls and monitors for the quality of the overlays being applied by the RapidCoater™ system to the surface of the part being processed. The other objective was to develop techniques to rapidly set-up and calibrate the laser beam monitors and the position of the laser beam on the part.

Recent Progress

In August 2000, the RapidCoater™ system was successfully demonstrated on a 1.5-inch by 0.75-inch patch on an F110 fan blade. A RapidCoater™ system with a dual-headed applicator, that applies paint to both sides of the fan blade, is shown in Figure 1.5.2.1, allowing both sides of the fan blade to be processed at the same time. The application of the opaque and transparent overlays, paint and water, respectively, was synchronized with the laser. The paint was applied first, followed by the overlay water, and sufficient time was allowed for the overlay water to establish a uniform thickness and pattern over the applied paint. After the laser pulse was delivered and the shock wave propagated through the material, the wash water on the RapidCoater™ system was activated to remove the paint and prepare the surface for the next laser pulse application. This demonstration was conducted with the F110-GE-100 fan blades at a processing rate of 0.25 Hz, because the Manufacturing Cell 2 laser system is currently capable of delivering one laser pulse every 4 seconds. However, without the Manufacturing Cell 2 laser, the RapidCoater™ system was demonstrated at a rate of 2 Hz while processing the same area on the F110 fan blade. In November 2001, several F110-GE-100 1st stage fan blades were LaserPeen™ processed for a component test. Some of these blades will be used in an engine test to be conducted in the first half of 2002.

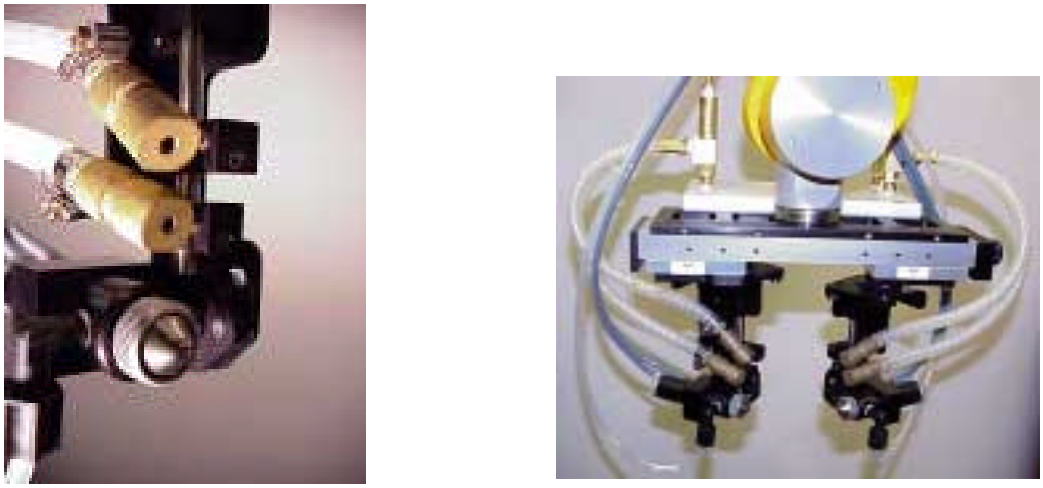

(a) (b)

FIGURE 1.5.2.1 A Single RapidCoater™ Head (a) for Single-Sided Processing and a Dual RapidCoater™ Head, and (b) for Processing a Thin Section, such as Compressor Blades

Laser peening rates are also a function of the laser beam spot shape. The current laser beam shape is round and as a result overlapping of the laser beam spots is required to provide 100 percent laser-shock-peen coverage. This overlap of the spots increases the processing time. However, if the spot

shape is square, the processing rates can be increased. Special optics were evaluated to produce square spots. A square beam was produced from a round beam as shown in Figure 1.5.2.2.

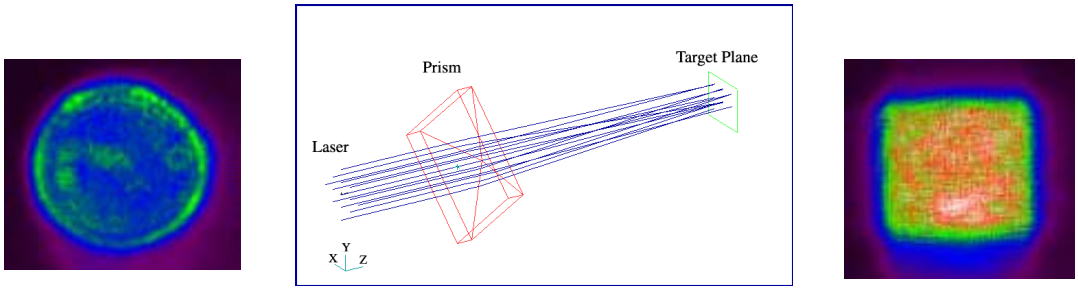

(a) (b) (c)

FIGURE 1.5.2.2 Spatial Profiles of the Laser Beam Showing the Transformation from a Round Spot (a) to a Square Spot (c) with the Use of Optics (b)

1.6 Manufacturing Technology for Affordable LSP

FY 98-03

Background

The overall focus of this project is to establish a commercial laser shock peening (LSP) processing capability and implement an affordable, production-capable LSP manufacturing cell for applications to gas turbine engine blades and other fatigue critical components.

The technical challenges associated with this program are all related to scaling the technology of the prototype production facility into a robust manufacturing facility. The program is focused on the development of advanced controls and monitors, semi-automated peening cells, a ruggedized laser system, and implementation of these subsystems into the LSP manufacturing cell. The project is divided into three phases.

Phase I: The purpose of Phase I was to mitigate the risks associated with the transition to manufacturing. This phase is divided into three areas:

1. Development and testing of new (or improved) controls and monitors, which will be used to increase the process reliability and reduce processing costs. The primary monitors (energy, temporal profile, and spatial profile) typically used for laser peening have been enhanced. "Secondary" laser monitors, process monitors, and quality control monitors have been demonstrated and will be down-selected for implementation into the new manufacturing cell.

2. Development of prototype small-parts and large-parts peening cells. This effort began in the final quarter of calendar year 1998 and was successfully completed in early 2000.

3. Initial commercialization planning and new application development.

This phase is completed.

Phase II: Phase II is the final design and build phase for the laser system and a small-parts peening cell. This phase is divided into two areas:

1. Design, fabrication, and integration of a manufacturing cell consisting of the laser system and a small-parts peening cell. This includes the down-selection and integration of the controls and monitors developed in Phase I.

2. Demonstration of the LSP manufacturing cell. The demonstration is currently scheduled for September 2002.

Phase III: Phase III is the commercial development phase. The objectives are to develop the new applications identified in Phase I and to demonstrate laser shock peening to the appropriate market sectors including the aerospace, medical, and automotive. This phase began in January 2000.

Recent Progress

Phase I. This phase of the program is essentially complete.

Phase II. The status of this phase of the program is as follows. The mechanical and electrical designs for the laser system have been completed. Assembly of the laser system is underway and nearing completion. Construction of the small parts and large parts laser peening cells is nearly completed as shown in Figure 1.6. An operational demonstration of a two-beam system is scheduled for September 2002.

Participating Organizations: LSP Technologies, Inc.

Points of Contact:

Government
Mr. David W. See
U.S. Air Force
AFRL/MLMP, Bldg. 653
2977 P Street, Suite 6
Wright-Patterson AFB, OH 45433-7739
Phone: (937) 255-7279
Fax: (937) 656-4420

Contractor
Dr. Jeff L. Dulaney
LSP Technologies, Inc.
6145 Scherers Place
Dublin, OH 43016-1284
Phone: (614) 718-3000 x11
Fax: (614) 718-3007

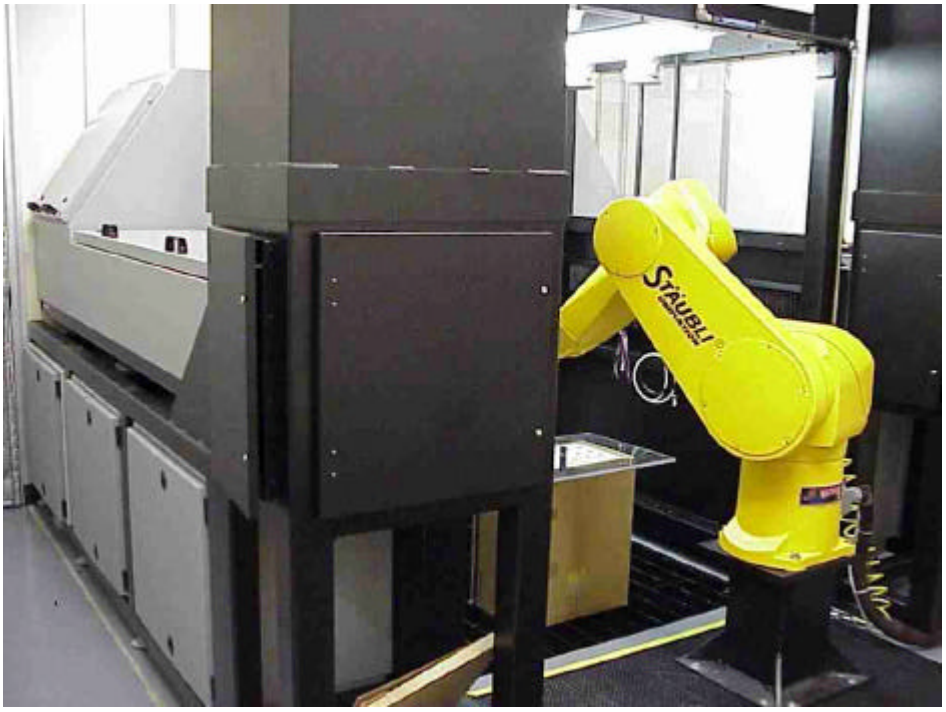

(a)

(b)

FIGURE 1.6 (a) The Small Parts Laser Peening Cell for Processing Parts such as Turbine Engine Airfoils, (b) The Large Parts Cell for Laser Peening Parts such as F119 IBRs.

1.7 Laser Peening of F119 Fourth-Stage Integrally Bladed Rotors

FY 00-03

Background

This program is in support of the F-22 System Program Office, which has an immediate need for additional fatigue resistance in the fourth-stage integrally bladed rotors (IBRs) on the F119 engine. There is a need to apply laser peening to the edges of the airfoils to meet the fatigue strength requirements for the IBRs. Laser peening is a repeatable manufacturing process that has wide application to many different types of gas turbine engine parts, but is currently being used in production only on individual blades. Laser peening produces deep compressive residual stresses in the surfaces of parts that improve fatigue life and resist crack propagation.

Air Force Manufacturing Technology Directorate is providing specific technology for insertion into the production manufacturing process for the fourth-stage F119 IBR, which includes an automated overlay applicator and robust controls and monitors for ensuring that the process remains within operating parameters.

There are two primary program goals:

1. Reduce the time to LaserPeen™ process a fourth-stage F119 IBR by a factor of 6 to 9 times.
2. Reduce the LaserPeen™ process cost for the fourth-stage F119 IBR by 50-75 percent.

The program is divided into four tasks:

Task 1: RapidCoater™ Overlay Applicator Design and Implementation
The current RapidCoater™ design used for individual blades will be modified to accommodate the specific geometry of the F119 fourth-stage IBR. The modified design shall be fabricated, tested, and optimized for the F119 fourth-stage IBR. Overlay coatings will be optimized to work with the RapidCoater™ for IBRs system.

Task 2: Production Hardening of the IBR Cell
The existing prototype large-parts peening cell will be modified to meet Pratt & Whitney's production requirements for the F119 fourth-stage IBR.

Task 3: Quality Control (QC) and Quality Assurance (QA) Controls and Monitors
QC and QA controls and monitors currently available in the small-parts peening cell will be integrated and adapted into the IBR peening cell. Additionally, an automated laser-beam-energy calibration system will be implemented into the IBR cell.

Task 4: Full Integration of the IBR Cell into the Manufacturing Cell
All aspects of integrating the IBR cell into the new manufacturing cell will be addressed in this task, including mechanical, electrical, computer, and optical interfaces.

Recent Progress

Several IBRs have been laser peened in the IBR cell and forwarded to Pratt & Whitney for evaluation and testing purposes (Fig. 1.7). Production laser peening of IBRs will begin in early 2002.

manipulate the RapidCoater™ head has been installed and is being integrated with other cell components. The IBR cell has been modified to improve robot-positioning capability. Additional cell improvements, and QA and QC monitors are being incorporated into the peening cell. The program is on schedule for a March 2003 completion.

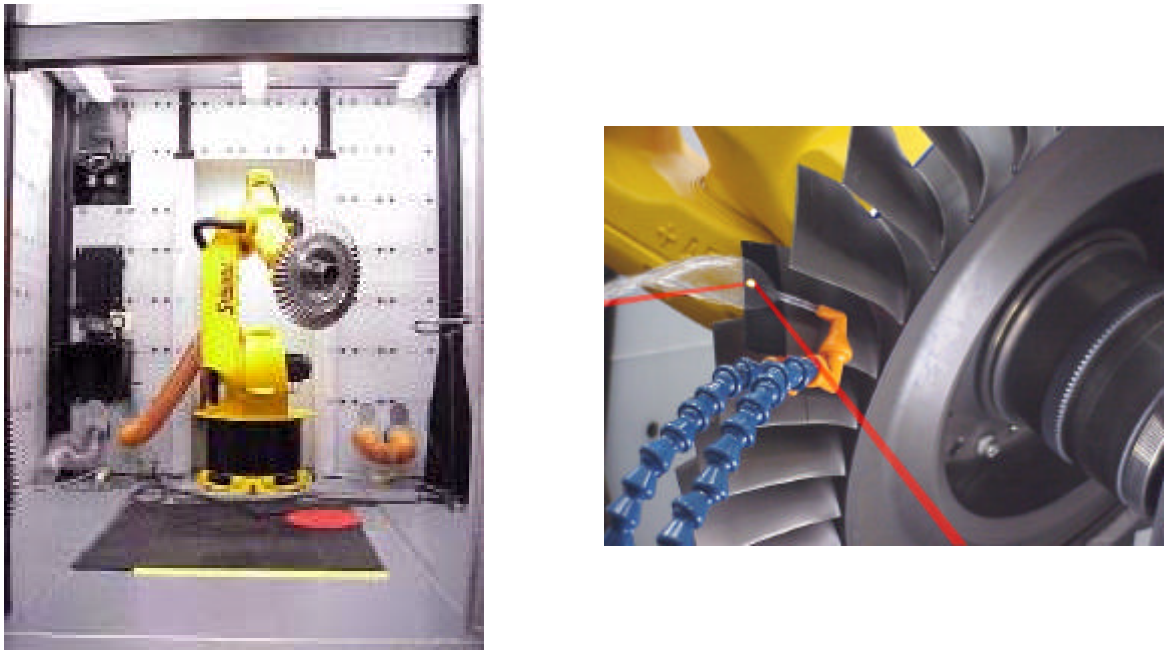

(a) (b)

FIGURE 1.7 (a) A 4th Stage IBR Positioned for Processing in the Large Parts Peening Cell, (b) A Close-up Schematic of Laser Peening of a 4th Stage IBR (Laser Beams Added for Visualization).

Participating Organizations: LSP Technologies, Inc.

Points of Contact:

Government
Mr. David W. See
U.S. Air Force
AFRL/MLMP, Bldg. 653
2977 P Street, Suite 6
Wright-Patterson AFB, OH 45433-7739
Phone: (937) 255-7279
Fax: (937) 656-4420

Contractor
Mr. Richard D. Tenaglia
LSP Technologies, Inc.
6145 Scherers Place
Dublin, OH 43016-1284
Phone: (614) 718-3000 x17
Fax: (614) 718-3007

1.8 Processing and Manufacturing Demonstration for High Strength Affordable Castings

FY 00-02

Background

Forged titanium blades for gas turbine engines are expensive and long-lead-time items. Recent advancements in vacuum die casting (VDC) have resulted in improvements to the quality of titanium alloy castings, and VDC is currently being considered as an alternative to precision forgings for producing static and rotating engine components. Although cast components are considerably less expensive than their forged counterparts, they must have equivalent fatigue life and resistance to foreign-object-damage-induced crack growth to be considered for engine applications.

Laser peening has been demonstrated to be an effective technique for increasing the fatigue life of engine components and increasing their resistance to crack growth after foreign object damage (FOD). Programs are in place to implement this technology on both forged blades and rotors. The purpose of this program is to investigate the feasibility of combining laser peening with VDC titanium alloy blades to produce more affordable turbine engine airfoils.

The tasks for this project included:

1. Assess the fatigue performance of cast titanium alloy blades that have been laser peened and compare to laser peened forged blades;

2. Determine the magnitude of the increased resistance to FOD in cast blades after laser peening;

3. Compare the resistance of compressive stresses produced by laser peening in cast and wrought alloys to thermal relaxation at elevated temperatures typical of engine operating temperatures;

4. Determine the comparative resistance to cyclical stress relaxation of cast titanium alloys processed by laser peening;

5. Estimate the potential cost benefits of using laser peened cast blades compared to unpeened and laser peened wrought blades.

Recent Progress

Thermal relaxation tests, cyclic stress relaxation tests, and component fatigue tests were completed. Preliminary results indicated the technical feasibility of producing laser peened vacuum die cast titanium alloy blades with equivalent fatigue life and FOD resistance compared with similarly peened forged (wrought) blades. However, some of the fatigue tests were inconclusive due to cracks not starting from the notches in the blades. Further testing should be performed to establish the equivalency of cast and wrought blades more definitively. Test samples and the fatigue test setup are shown in Figure 1.8.

Both cast and wrought Ti-6Al-2Sn-4Zr-2Mo samples were resistant to the thermal relaxation of compressive residual stresses at the temperatures investigated (400ºF and 900ºF). Cast and wrought Ti-6Al-2Sn-4Zr-2Mo and Ti-6Al-4V samples were also resistant to the relaxation of compressive residual stresses from laser peening under cyclic loading conditions. It was projected that laser peened

cast blades should cost 20-25% less than laser peened forged blades. The program is on schedule for a March 2002 completion.

(a)

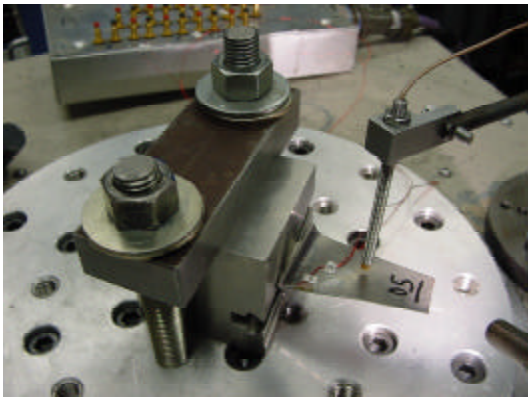

(b)

FIGURE 1.8 (a) Vacuum Die Cast Titanium Alloy Blades Prepared for Laser Peening, (b) Fatigue Testing of a Laser Peened Blade on an Electro-Dynamic Shaker Table.

Participating Organizations: Universal Technology Corporation, LSP Technologies, Inc., Pratt & Whitney, Howmet Research Corporation

Points of Contact:

Government
Mr. David W. See
U.S. Air Force
AFRL/MLMP, Bldg. 653
2977 P Street, Suite 6
Wright-Patterson AFB, OH 45433-7739
Phone: (937) 255-7279
Fax: (937) 656-4420

Contractor
Mr. Robert M. Neff
Universal Technology Corporation
1270 North Fairfield Road
Dayton, OH 45432-2600
Phone: (937) 426-8530
Fax: (937) 426-7753

1.9 Conclusions

The Component Surface Treatment Action Team has achieved the following:

1. Demonstrated that laser shock peening (LSP) of damaged turbine engine fan blades provides equal or better high cycle fatigue strength than undamaged, unpeened blades;

2. Completed testing that showed the ability of the laser peening process to stop both HCF crack initiation and crack propagation in turbine engine fan blades; and

3. Demonstrated a complete LSP system (laser, facility, and more affordable process) using equipment and facilities now available for government and industry use. Laser peening was successfully transitioned to the F101 and F110 engines. This has resulted in a 15x increase in

FOD tolerance for these engines, a major reduction in inspection man-hour costs, and increased flight safety.

Due to the excellent progress to date, engine contractors are now pursuing LSP approaches. Further cost reduction of the manufacturing facilities and processes for the LSP technique is now the major focus of this team. Engine manufacturers are currently pursuing LSP on fan and compressor integrally bladed rotors (IBRs).

The ultimate objective of the Component Surface Treatment Action Team and of all the efforts described in this section is to develop an affordable Laser Shock Peening system. The relationship of all these efforts is shown below in Figure 1.9.

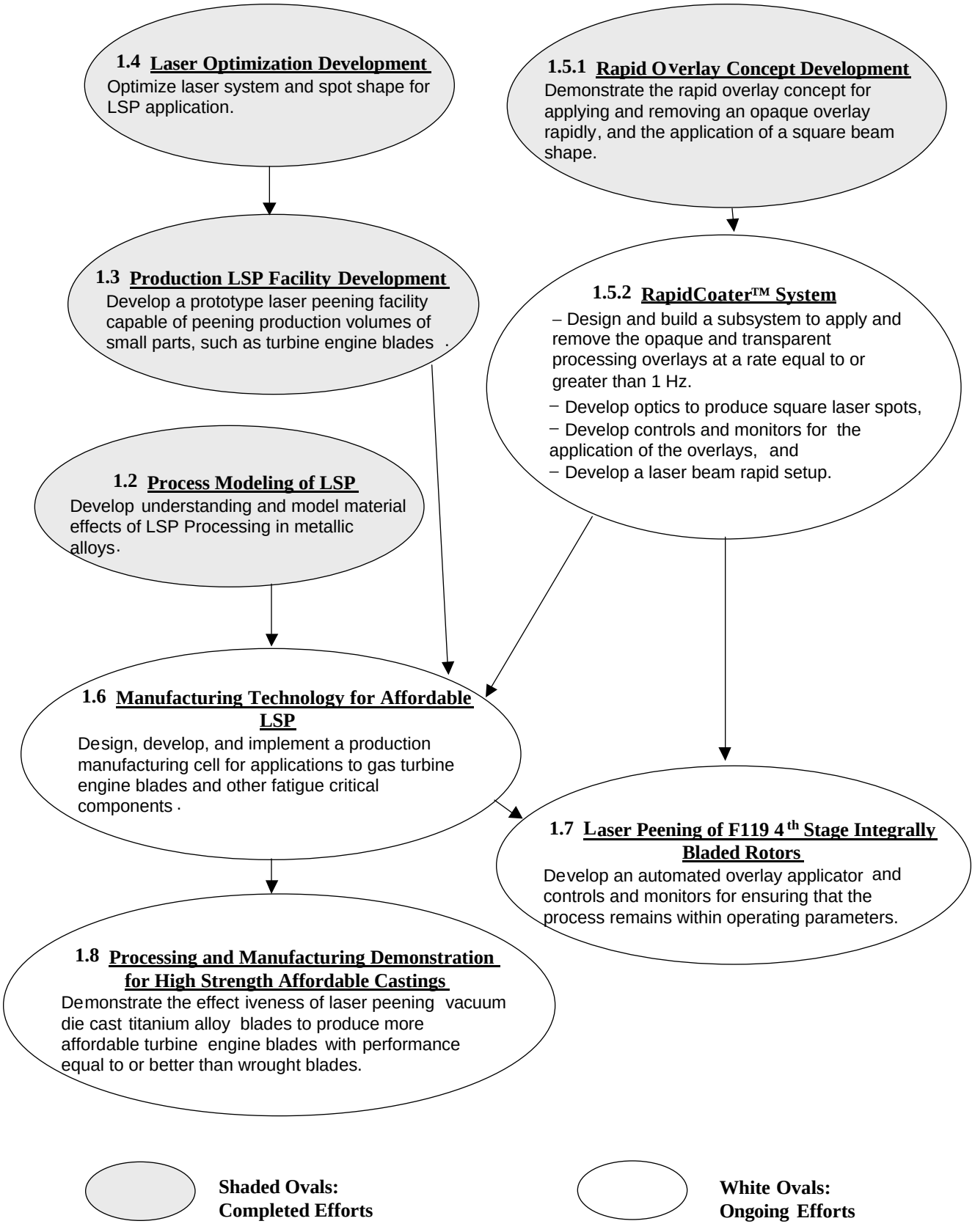

FIGURE 1.9 Interrelationship among LSP Programs

2.0 MATERIALS DAMAGE TOLERANCE

BACKGROUND

The Materials Damage Tolerance Research Action Team (Materials AT) is responsible for fostering collaboration among individual HCF materials damage tolerance research efforts, with the goal of reducing the uncertainty in the capability of damaged material by 50%. The Materials AT provides technical coordination and communication among active participants involved in HCF life prediction, damage nucleation and propagation modeling, fracture mechanics methodology development, residual fatigue capability modeling, and the evaluation of surface treatment technologies. The Chair, Co-Chair, and selected Materials AT members meet as required (estimated quarterly) to review technical activities, develop specific goals for materials damage tolerance research projects, and coordinate with the Technical Planning Team (TPT) and the Industry Advisory Panel (IAP). The Chairman (or Co-Chair) of the Materials AT will keep the TPT Secretary informed of AT activities on a frequent (at least monthly) basis. Annual technical workshops are organized and summaries of these workshops are disseminated to appropriate individuals and organizations. This AT includes members from government agencies, industry, and universities who are actively involved in materials damage tolerance technologies applicable to turbine engine HCF. The team is multidisciplinary with representatives from multiple organizations representing several component technologies as appropriate. The actual membership of the AT changes as individuals assume different roles in related programs.

ACTION TEAM CHAIRS

Chair
U.S. Air Force
Dr. Jeffery R. Calcaterra
AFRL/MLLMN, Bldg. 655
2230 Tenth St., Suite 1
Wright-Patterson AFB, OH 45433-7817
Phone: (937) 255-1305
Fax: (937) 656-4840

INTRODUCTION

Prior to this research program, no accurate techniques were available to determine the capability of materials subjected to variations in manufacturing, component handling, and usage. Such techniques are needed for accurate life prediction and optimized design to assure damage tolerance. The following pages summarize the schedules, backgrounds, and recent progress of the current and planned projects managed by this action team.

Figure 2.0 Materials Damage Tolerance Research Schedule

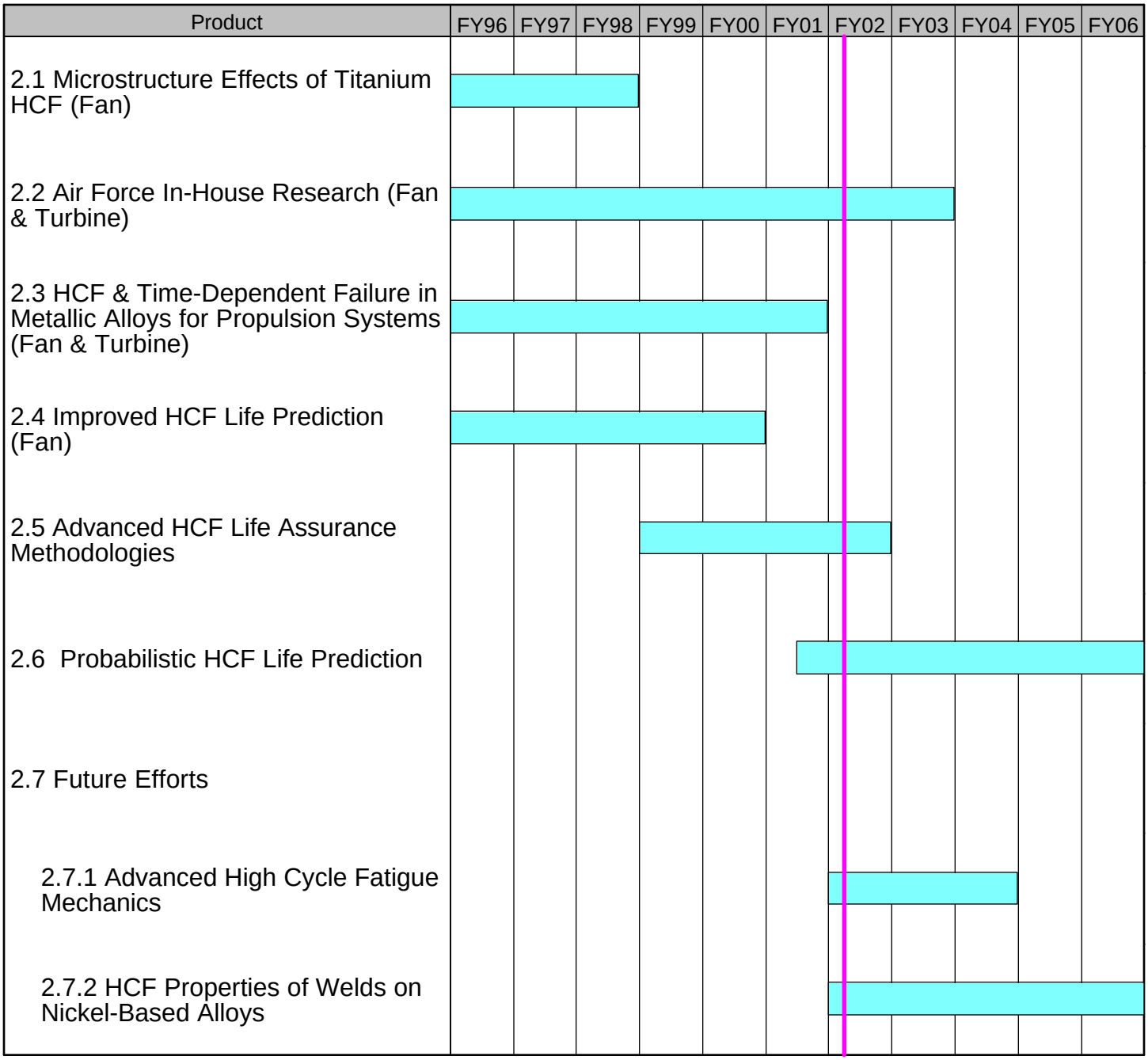

2.1 Microstructure Effects of Titanium HCF (Fan)

FY 96-98

Summary

The objective of this project was to determine the relationship between mean stresses and high cycle fatigue strength for Ti-6Al-4V by correlating the fatigue crack nucleation process with the cyclic deformation behavior of the alloy for different microstructures and crystallographic texture characteristics. An investigated hypothesis was that high mean stress fatigue life sensitivity is associated with cyclic softening of Ti-6Al-4V, which in turn results in the absence of an endurance limit. In addition to establishing such a correlation, the purpose of the investigation was also to study the crystal orientation influence on, and the microstructural features that affect, the cyclic deformation behavior. The specific factors that control crack nucleation were also studied. The focus was on the formation of dislocation substructure and the statistical nature of crack formation. Analytical procedures emphasized the use of quantitative physical models that could be used to predict the mean stress sensitivity in this class of titanium alloys. The results are also useful in the search for the best alloy/process for maximizing fatigue resistance in engineering structures.

Overall results of this program include:

- Cyclic strain tests did not reveal significant differences in cyclic deformation based on microstructure.
- Bimodal fine uni-rolled and lamellar cross-rolled microstructures exhibited the best fatigue properties in Ti-6Al-4V.
- This effort resulted in a model that allows the accurate prediction of high and low cycle fatigue curves for titanium alloys from microstructure and texture characteristics at different stress ratios ($\sigma_{min}/\sigma_{max}$).

A more detailed description of the program results can be found in the 2000 HCF annual report.

Participating Organizations: Air Force Office of Scientific Research (AFOSR), Worcester Polytechnic Institute, Pratt & Whitney

Points of Contact:

Government
Dr. Spencer Wu
U.S. Air Force, AFOSR/NA
110 Duncan Ave., Suite B115
Bolling AFB, DC 20332-8080
Phone: (202) 767-4989
Fax: (202) 767-4988

Contractor
Prof. Richard D. Sisson, Jr.
Worcester Polytechnic Institute
Mechanical Engineering Department
100 Institute Road
Worcester, MA 01609
Phone: (508) 831-5335
Fax: (508) 831-5178

2.2 Air Force In-House Research (Fan and Turbine)
FY 96-03

Background

The objectives of this program are as follows:

(1) Conduct breakout research on titanium and nickel-base superalloys.
(2) Explore high cycle fatigue related damage mechanisms, including the determination of the relative significance of specific damage mechanisms and the identification of specific areas requiring a concentrated research and development effort for incorporation into the HCF design system.
(3) Develop innovative test techniques and modeling concepts to guide the industry research program.
(4) Conduct research and evaluation to demonstrate and validate damage tolerance design methodologies for HCF.

Recent Progress

During the past year, progress has been made in all areas. The following paragraphs highlight specific accomplishments with regard to the approaches being taken in this task.

- ***Material Behavior for Modeling.*** Further testing has been accomplished to generate valid data for modeling the damage mechanisms associated with high cycle fatigue interaction with low cycle fatigue, fretting fatigue, and foreign object damage (FOD).

  - *High Cycle Fatigue / Low Cycle Fatigue Interaction.* Previously, load history effects on fatigue crack thresholds were evaluated using both load shed and step testing. Prior load history effects were investigated by measuring threshold values where overload LCF pre-cracking is used prior to step testing (Fig. 2.2.1).

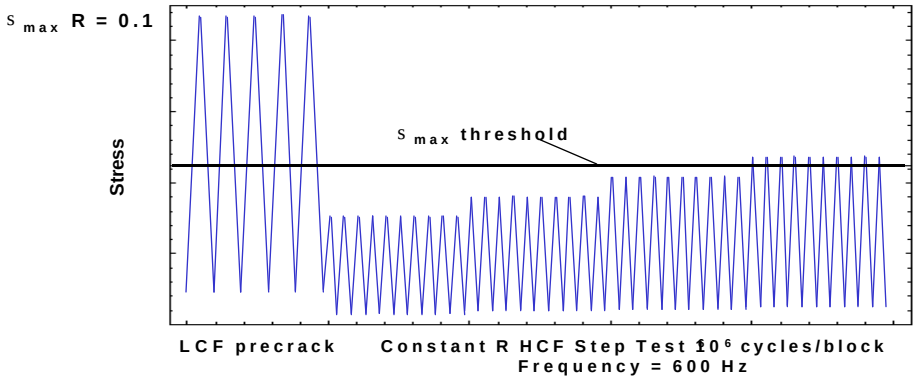

FIGURE 2.2.1 Pre-Crack and Step-Test Loading Technique Used to Determine LCF/HCF Thresholds

Additionally, a simple overload model was developed to formulate a relationship between ΔK_{th} and ΔK_{pc}. This model is described in the 2000 HCF Annual Report.

The current year activities focused on better understanding the effects of LCF damage on HCF properties. The load history shown in Figure 2.2.1 was used to initiate and grow damage in notched specimens. A schematic of the specimen is shown in Figure 2.2.2.

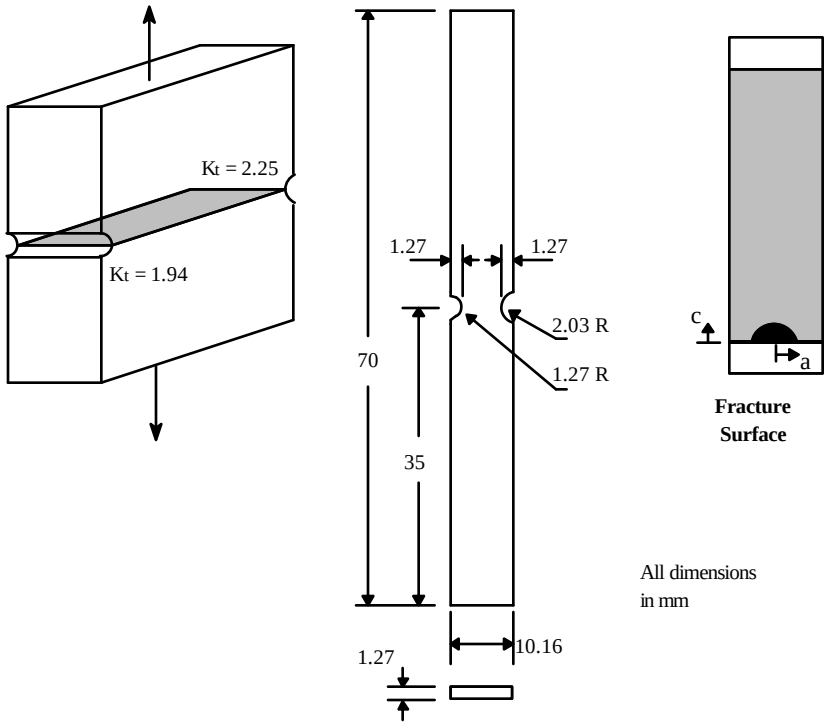

FIGURE 2.2.2 Schematic of Double Edge Notch (DEN) Specimens Used for HCF/LCF Interaction Study

As can be seen in this schematic, the specimen is not symmetric. One notch has a higher K_t than the other. This ensures that the crack initiates within that notch. Specimens were cycled using the LCF block, shown in Figure 2.2.2, until damage initiated. Damage was tracked using an infrared damage detection system. The resolution of this system enabled the control system to stop the LCF cycles when initial damage had reached a size of ~20-40μm. An SEM micrograph of typical damage identified using the infrared system is shown in Figure 2.2.3.

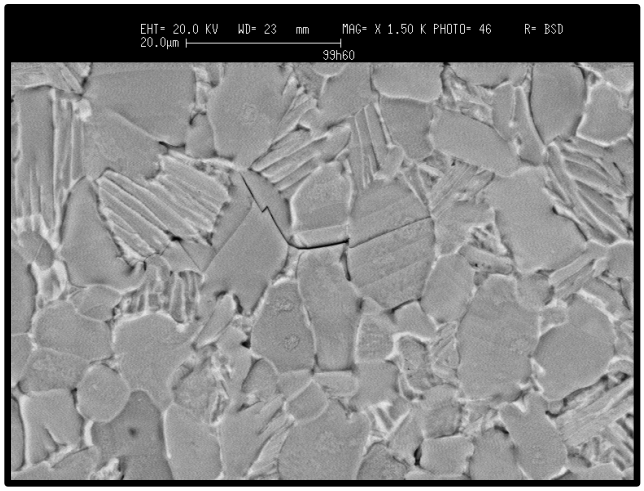

FIGURE 2.2.3 Micrograph of Typical Damage Identified by the Infrared Damage Detection System (IDDS)

The projected length of the crack shown in Figure 2.2.3 is approximately 20µm. This is well below the inspectable limit for all practical non-destructive evaluation procedures currently used by aircraft repair facilities. This damage is also small enough that it does not fall within the realm of standard linear elastic fracture mechanics. However, studies completed during the past year have shown the effects that this damage can have on component life. One effect of these small cracks on HCF life is shown in Figure 2.2.4.

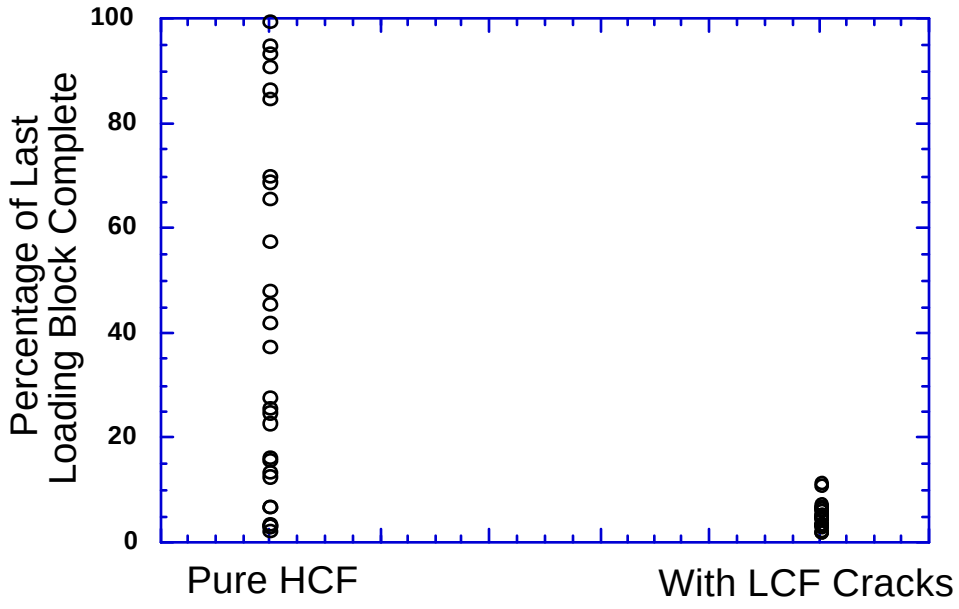

FIGURE 2.2.4 Comparison of Cycles to Failure in Last HCF Loading Block for Specimens with and Without Damage.

As described by Figure 2.2.1, the HCF fatigue threshold in the presence of HCF/LCF interaction was identified by first damaging the specimen under LCF conditions, then cycling the specimen under a given HCF load for 10^6 or 10^7 cycles. If a block of HCF cycles was completed, the load was raised by a small increment and a new HCF block was started. The HCF threshold was determined by a linear interpolation between the load level of the last completed block and the percentage that was completed of the final loading block. Figure 2.2.4 illustrates that in the absence of previous LCF damage, the specimen fails at a random point within the last load block. However, when there is LCF damage present, the specimen always fails within the first 20% of the final load block. In some cases, the load level during the final HCF block were the same, with and without damage, but there was a wide variation in the percentage of the last block that was completed. This suggests that crack initiation under pure HCF can occur over a wide range of cycles, but that once a crack is initiated the component can be expected to fail quickly if the load is above the threshold limit.

This result will have significant implications on engine design because it removes a large amount of uncertainty from the process of material failure due to HCF/LCF interaction. For example, the current version of ENSIP typically requires that damage tolerant parts have a detectable crack size that will not grow to a critical size within two inspection cycles. This statement is based on typical long crack linear elastic fracture mechanics. In light of this new analysis, these statements may be revised to charge that the crack should not grow to a point where it exceeds the HCF threshold within two inspection cycles. This new information could also have an impact in areas of turbine engines with large stress gradients such as the contact region. Using this information, new limits on damage depth can be determined such that the damage size and the stress state at the tip of the crack are below the HCF threshold values. Unfortunately, the relationship between damage depth and fatigue threshold stress can be complex. In order to handle the relationship, the data are plotted on a Kitagawa diagram that describes the behavior of damaged specimens with cracks of a given depth, c. This is shown in Figure 2.2.5

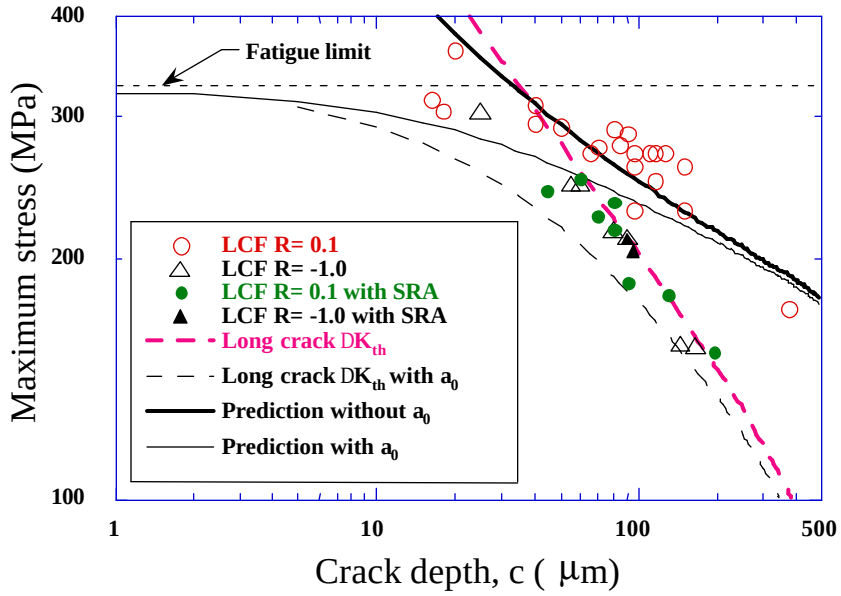

FIGURE 2.2.5 Kitagawa Diagram Showing the Relationship between Crack Depth and Failure Stress at 10^7 Cycles.

The Kitagawa diagram is used to show the failure stress for a given life. In the case of Figure 2.2.5, life is 10^7 cycles. Figure 2.2.6 illustrates the impact of damage caused by LCF on HCF lives. Nearly all of the data fall below the smooth bar fatigue limit. Using the fatigue limit, notch strength reduction factors (K_t) or standard long crack fracture mechanics all result in predictions that are at least partially non-conservative. The non-conservative nature of these predictions forces designers to apply factors of safety in order to meet the requirement that the part will not fail. These factors of safety, in turn, increase the weight of the overall engine. Fortunately, the long crack threshold prediction with a small crack correction seems to model the data well. In all cases, this results in a conservative prediction of the failure stresses. Although this model needs a more thorough investigation, it indicates that the design factor of safety, and thus material uncertainty, could be reduced in future engine designs using this method.

- *Effect of Mean Compressive Stress.* In addition to load history effects, a large effort was directed at understanding the effect of mean compressive stresses in the HCF regime. This understanding was necessitated by the common use of the Goodman, or Haigh, diagram in engine design. Similar to the Kitagawa diagram, the Goodman diagram plots data at a given cyclic life. The x-axis of the Goodman diagram is the mean stress and the y-axis is the alternating stress. Based on these quantities, the x-axis intercept is the ultimate strength of the material while the y-axis intercept is the value of R = -1 failure stress for the given cyclic life. A simple Goodman diagram simply uses a straight line to connect the points. This is shown in Figure 2.2.6.

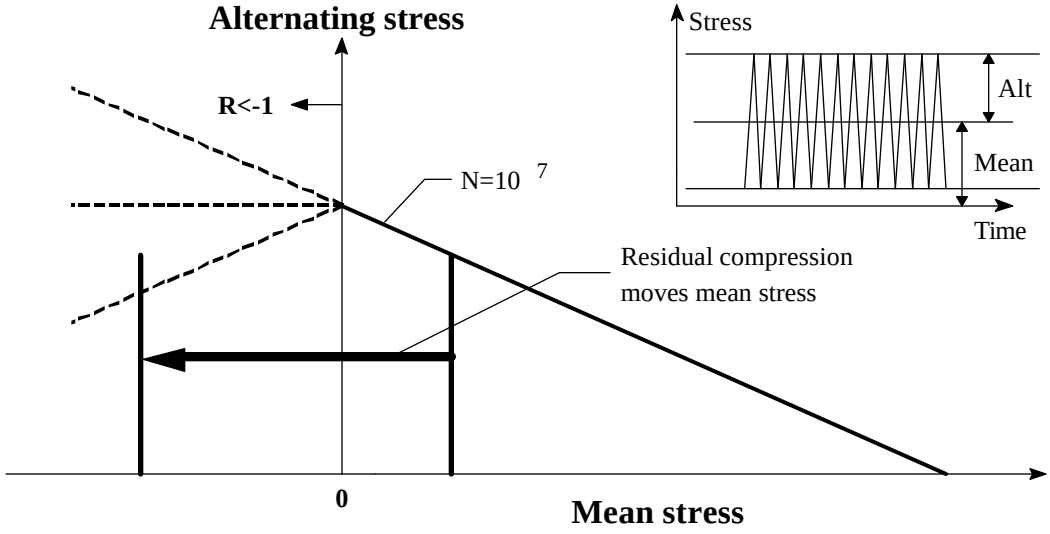

FIGURE 2.2.6. Notional Goodman Diagram

In the design process, a combination of alternating and mean stress that falls above this curve indicates the component or specimen will fail prior to the given life (10^7 for Figure 2.2.6). A combination that is below the line indicates a safe-life design for the indicated life. Unfortunately, there is a lack of data describing the behavior of the curve in the compressive mean stress regime.

Because of this, the prediction of cyclic life for these conditions was extrapolated from tensile mean stress data. The indication is that there is a continuous benefit from mean stress. To verify this assumption, numerous data were developed. The result is shown in Figure 2.2.7.

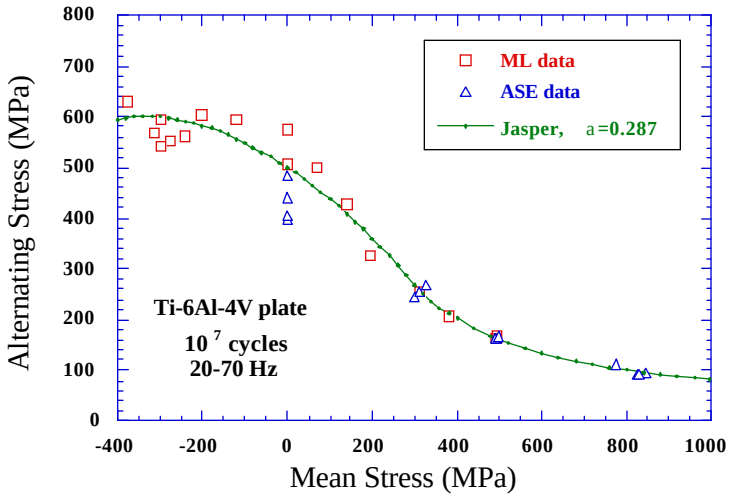

FIGURE 2.2.7 Goodman Diagram with Jasper Equation and Compressive Mean Stress Data

Figure 2.2.7 indicates that there is some benefit from a compressive mean stress at cyclic lives of 10^7. However, allowable alternating stress does not seem to continuously increase with increasing compressive mean stress. In fact, the increase in the allowable alternating stress range is only 100 MPa for a mean stress decrease of 400 MPa. This is significant in turbine engine design because of the widespread use of surface treatments such as shot-peening. Shot-peening is commonly applied to a wide array of turbine engine components as a way of enhancing fatigue life and damage tolerance. In applications, such as contact loads, that already have a significant compressive mean stress, the application of shot peening may not provide any significant benefit. This conclusion may allow engine maintenance facilities to remove time intensive shot-peening steps from the refurbishment process for turbine engine disks, decreasing workload and maintenance cost. In fact, the loads at the edge of contact can have very large negative stress ratios. The Jasper equation *(Jasper, T.M., "The Value of the Energy Relation in the Testing of Ferrous Metal at Varying Ranges of Stress and at Intermediate and High Temperatures," Philosophical Magazine, Series. 6, Vol. 46, Oct 1923, pp. 609-627)* suggests that the allowable alternating stress may start decreasing at these types of stress ratios. If this is truly the case, shot-peening a surface that already sees a significant compressive stress may decrease the life of the component. Unfortunately, test machine limitations precluded development of data in this regime, so the downward trend of the Jasper equation cannot be substantiated. This will be addressed during the upcoming year.

- *Attachment Fatigue.* The work on attachment fatigue, formerly described as fretting fatigue, continues along the same lines as last year. Some of the major results from this year's work are as follows:

- The fatigue limit stress corresponding to 10^7 cycles under fretting fatigue is only 20 to 40 percent of that of a smooth bar. Thus, fretting fatigue is highly detrimental to the fatigue properties of Ti-6Al-4V. (Illustrated in Figure 2.2.8.)

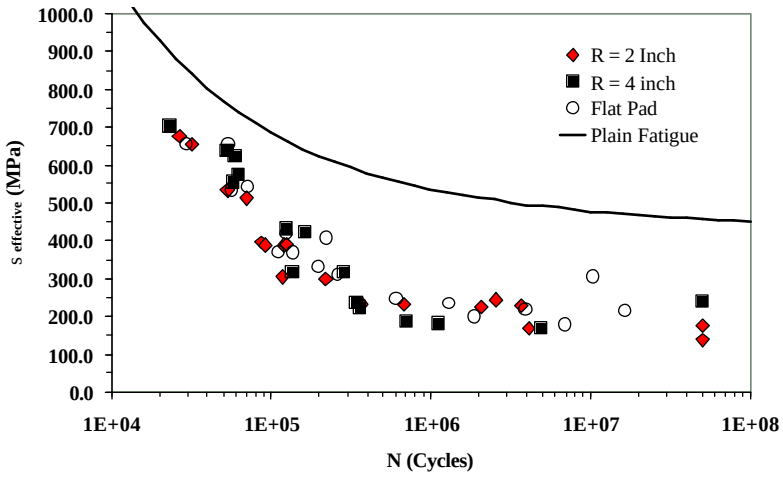

FIGURE 2.2.8 Fretting Fatigue SN Data Compared to Plain Fatigue Curve

- The debit in fatigue limit stress is relatively insensitive to the average shear stress or average normal stress, Figure 2.2.9.

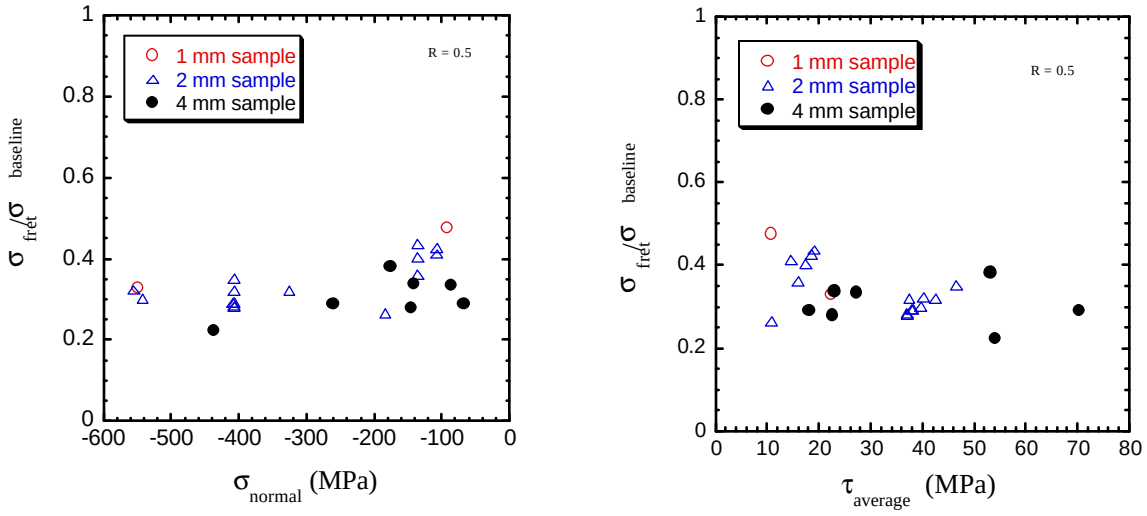

FIGURE 2.2.9 Insensitivity of Fretting Fatigue Debit to Normal and Shear Stress

- Coefficient of friction continues to play a major role in the determination of stress and displacement fields in the vicinity of the contact region.

In addition to experimental work, analysis of attachment stress fields in engines and laboratory specimens has also progressed. Finite Element Analyses (FEA) have progressed from simulations of two-dimensional models of experimental hardware to three-dimensional models of engine components. FEA models consisted of flat pads with rounded edges contacting flat plates, two-dimensional modeling of the dovetail fixture described in the 2000 HCF Annual Report and three-dimensional models of turbine engine compressor disks and blades. The majority of the analyses are purely elastic due to constraints on computational power. CAPRI has also been obtained from Purdue University in order to determine accurately the stress state at the edge of contact. Coefficient of friction has been varied from 0.3 to 1.0 in these studies and various life prediction methodologies have been used to correlate the data. However, no single stress-based or displacement-based parameter was found to be useful for predicting fretting fatigue lives under all conditions. Studies investigating the development of a useful fretting fatigue parameter are ongoing.

The 2000 HCF Annual report described a novel procedure used to characterize the threshold behavior of fretting fatigue cracks. The procedure involves machining fretting pads from fretting fatigue experiments into non-standard crack growth specimens, Figure 2.2.10.

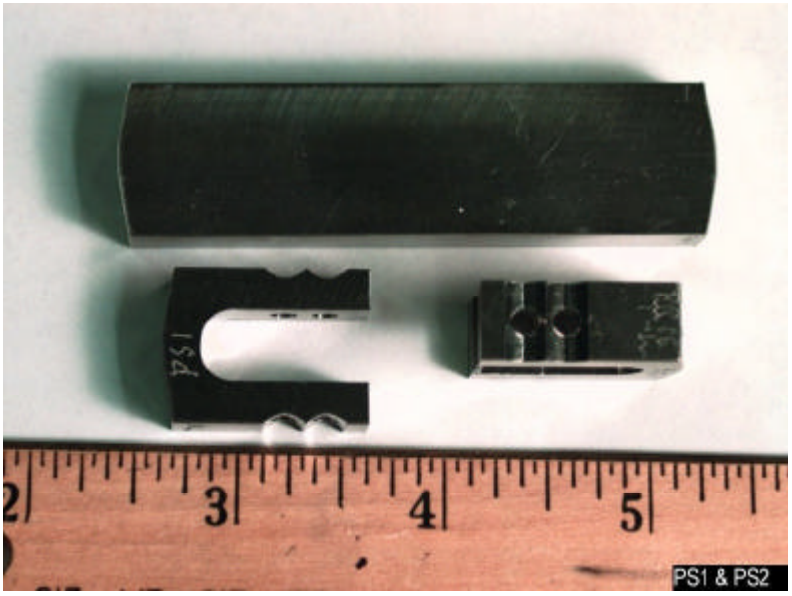

FIGURE 2.2.10 Fretting Pad (Top) and Non-Traditional "Golden Arch" Specimens (Bottom)

These pads are used to apply the normal contact pressure to the fretting specimen and therefore see the same contact loads over the life of the experiment. The difference between these pads and the specimen is that the specimen is also subjected to a bulk axial load. Examination of the fretted surface on the arch specimen provides significant insight into crack nucleation and growth due to full life contact loads. The surface of one of these arch specimens can be seen in Figure 2.2.11.

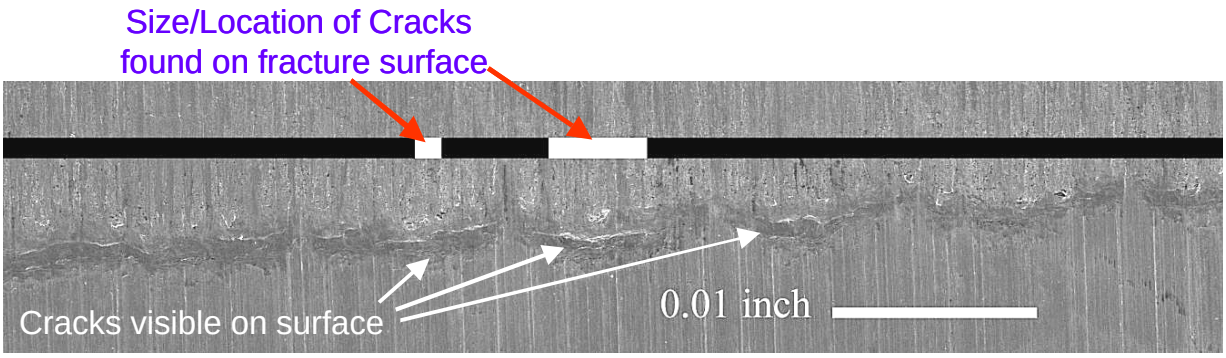

FIGURE 2.2.11 Micrograph of Arch Specimen Fretting Surface.

After the standard fretting fatigue test was completed, the surface of each arch specimen was examined to determine surface length. From heat tinting, the depth of the crack could also be determined but not until after the arch specimen fatigue test had been completed. Cracks were typically shallow with a depth that was normally less than one tenth of the surface length. The specimens were then fatigued using the step-test method described in Figure 2.2.1 without the initial LCF cycles. The geometry of the arch specimens was analyzed to determine the stress applied at the crack location. The resulting data was then plotted on a Kitagawa diagram, Figure 2.2.12.

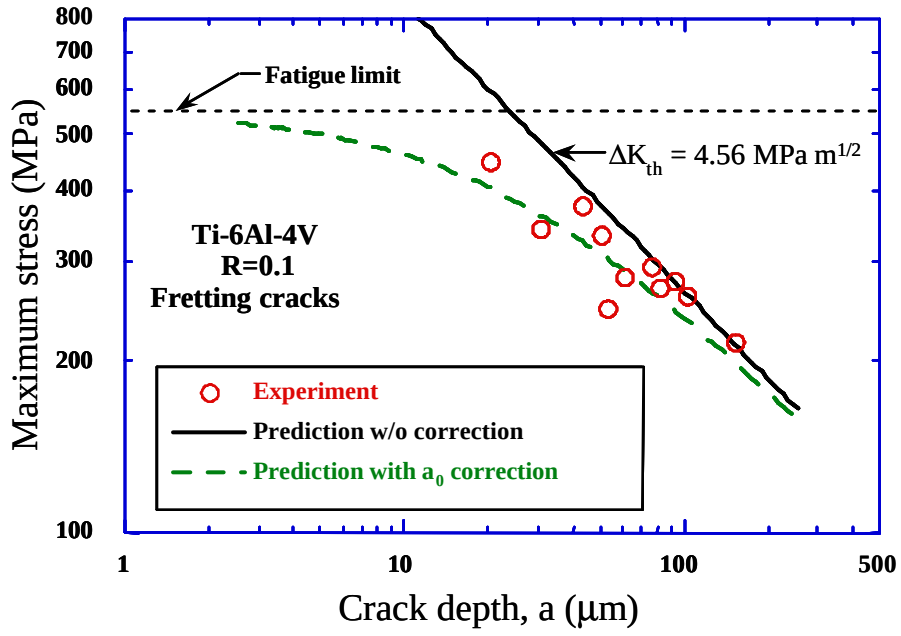

FIGURE 2.2.12 Kitagawa Diagram with Data from Fretted Arch Specimens

Similar to Figure 2.2.5, the data are best represented by long crack threshold data with a small crack correction. Unfortunately, this prediction is not completely conservative. This may be due to the fact that load history is not accounted for in the predictions. This aspect will be further investigated in the upcoming year.

The 2000 HCF Annual Report described an innovative test technique on dovetail specimens. The dovetail fixture, shown in Figure 2.2.13, differs from many typical fretting fatigue experiments because it enables a variation in normal and shear loads.

FIGURE 2.2.13 Overview of the Dovetail Fretting Fatigue Fixture

Fretting fatigue experiments on the dovetail fixture present a unique challenge because without prior knowledge of the coefficient of friction, the analysis of the stress states is statically indeterminate. The features of the dovetail fixture that make it statically indeterminate also make it difficult to complete a successful experiment, primarily due to alignment issues. Despite that, a study has been completed to determine the effect of contact geometry on fatigue failure stress at 10^6 cycles. Three different fretting pad geometries were tested. These geometries included a short flat pad with a flat region length of 0.040” and a taper angle of 11^o, a long flat pad with a flat region length of 0.250”, and a cylindrical pad with a 2” radius. The results of this study can be seen in Figure 2.2.14.

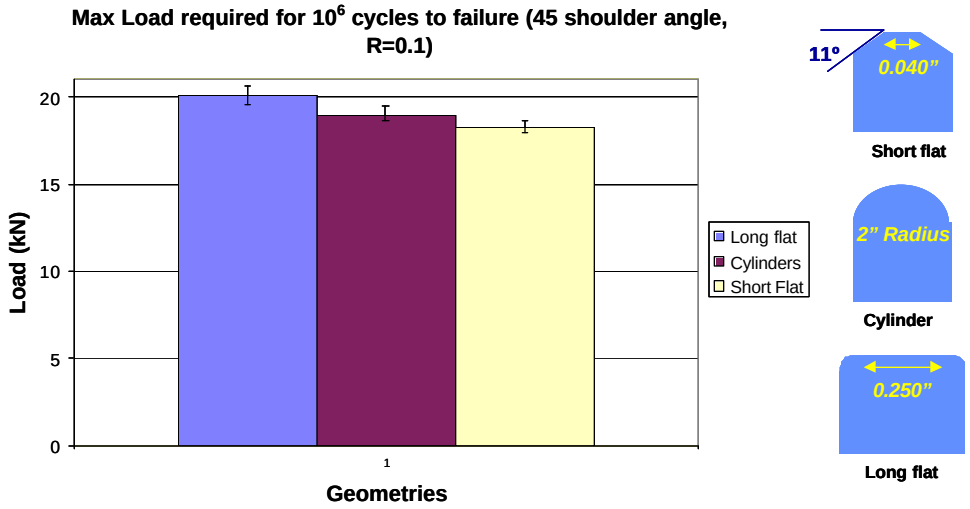

FIGURE 2.2.14 Variation of Fatigue Failure Loads for Three Different Fretting Pad Geometries

The bar chart represents the average of the failure loads that were completed for the indicated geometry while the error bar encompasses the entire range of the data. There is little variation in the failure loads for each of the tested geometries. This is surprising since the range of bulk contact loads varies widely over the range of contact geometries. In fact, the long flat bulk stress is approximately 6 times less than the short flat bearing load. Although bearing load has already been shown to be a poor correlating factor in fretting fatigue, the minimal difference in failure stress with such a large difference is still unexpected. Dovetail fixture experiments will continue in the upcoming year with emphasis on changing the shoulder angle of the fixture itself and refining the finite element analysis of the fixture in order to determine accurately the stresses at the edge of contact.

➢ *Effects of FOD.* Previous work dealing with the effect of FOD on HCF properties has focused on the effect s of tensile residual stresses on fatigue life. This work was well coordinated with the industry program (Section 2.5) in order to examine a number of specimen geometries ranging in complexity from standard flat bars up to actual airfoil specimens. Unfortunately, the emphasis on covering a range of specimen geometries resulted in several different impact methods, none of which was applied to the same specimen. This prevents a one-to-one comparison for most data. The current year activities are focused on determining differences in the impact process on a single specimen geometry.

The primary motivation for this study is to better understand the differences between ballistic impact and lower velocity impact types. It has been established that different impact velocities do not result in the same type of impact damage despite similar impact parameters. Unfortunately, ballistic impact, while representative of typical field damage, results in such a large range of scatter in the data that no single life prediction parameter has yet been identified. The solenoid gun results in less scatter but does not simulate accurately the damage of field impacts. The results of the study will be used to correlate ballistic and low-velocity impact types. The impact types being evaluated are:

- Ballistic impact with three different sizes of steel and glass spheres at constant velocity and constant energy

- Ballistic impact with steel cubes
- Pendulum impactor
- Solenoid gun impactor with two values of chisel sharpness
- Quasi-static indentation

Each of these impact types will be performed on the Diamond Cross-section Tension (DCT) specimens previously used for ballistic impact studies. The specimens will then be fatigued at 350Hz to determine the failure stress at 10^7 cycles. Details on the DCT specimen can be found in the 2000 HCF Annual Report.

❖ ***Innovative Test Technique Development.*** AFRL/MLLMN is currently working to develop a resonant test system capable of fatiguing specimens at 20 kHz. The system is capable of applying tensile mean loads in addition to the alternating load. This system builds upon previous work, adding improved provisions for alignment and automation using a personal computer. In addition, alternating load measurement is obtained through the use of an eddy current displacement gauge located at the end of the resonant section. Resonant excitation is produced through a commercially available ultrasonic oscillator and modified standard tooling.

Dynamic loads are applied to the specimen using a resonant piezoelectric device that can operate between 19.5 kHz and 20.5 kHz, and automatically shuts down if this range is exceeded. As a fatigue crack develops in the specimen during a test, the resonant frequency will shift and the test will stop, usually prior to the crack propagating completely through the specimen. A section view of the upper portion of the test system is shown in Figure 2.2.15.

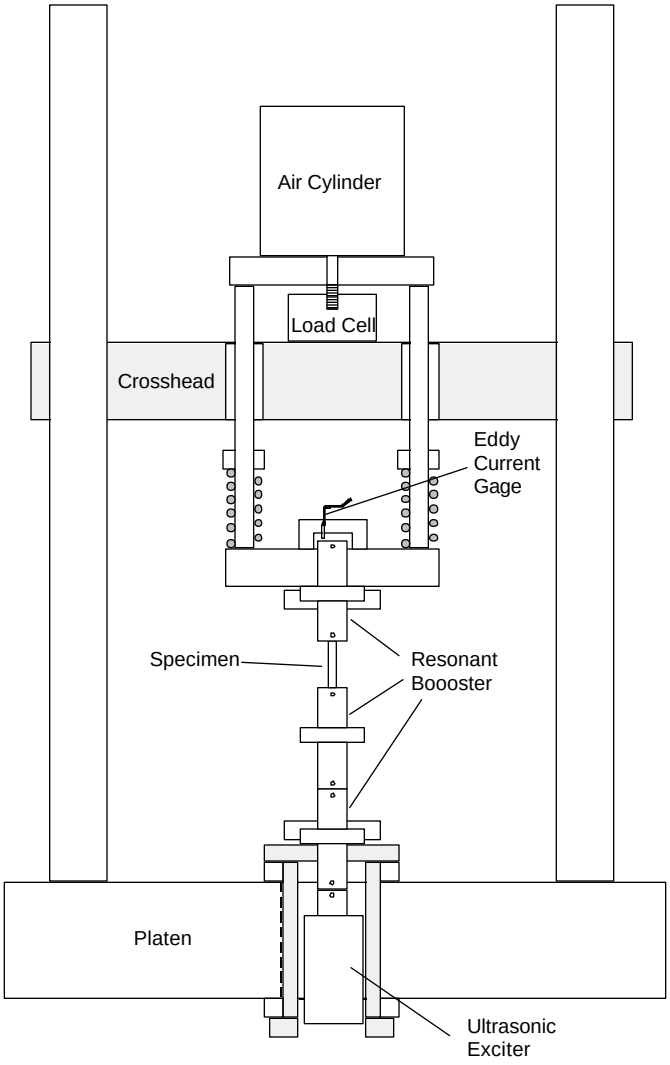

FIGURE 2.2.15 Section View of Ultrasonic Fatigue System

Development of this system will allow practical development of fatigue curves at cyclic lives of 10^9 and higher.

Participating Organizations: Air Force Research Laboratory (AFRL); University of Dayton Research Institute; Systran Corporation; Southern Ohio Council on Higher Education; University of Portsmouth, United Kingdom; Air Force Institute of Technology

Point of Contact:

Government
Dr. Theodore Nicholas
U.S. Air Force
AFRL/MLLMN, Bldg. 655
2230 Tenth St., Suite 1
Wright-Patterson AFB, OH 45433-7817
Phone: (937) 255-1305
Fax: (937) 656-4840

2.3 HCF & Time-Dependent Failure in Metallic Alloys for Propulsion Systems (Fan & Turbine)

FY 96-01

Background

This program is conducted under a Multi-University Research Initiative (MURI) led by the University of California at Berkeley. It is focused on the definition, microstructural characterization, and mechanism-based modeling of the limiting states of damage associated with the onset of high cycle fatigue failure in titanium and nickel-base alloys for propulsion systems. Experimental and theoretical studies were aimed at three principal areas: high cycle/low cycle fatigue interaction, foreign object damage, and fretting. The goal of this program was to provide quantitative physical/mechanism-based criteria for the evolution of critical states of HCF damage, enabling life prediction schemes to be formulated for fatigue-critical components of the turbine engine. The specific objectives are as follows:

(1) Perform systematic experimental studies to define crack formation and lower-bound fatigue thresholds for the growth of "small" and "large" cracks at high load ratios and high frequencies, in the presence of primary tensile and mixed-mode loading.

(2) Define lower-bound fatigue thresholds for crack formation in the presence of notches, fretting, or projectile damage on surfaces with and without surface treatment (e.g., shot or laser shock peened).

(3) Develop an understanding of the nature of projectile (foreign object) damage and its mechanistic and mechanical effect on initiating fatigue crack growth under high cycle fatigue conditions.

(4) Develop new three-dimensional computational and analytical modeling tools and detailed parametric analyses to identify the key variables responsible for fretting fatigue damage and failure in engine components, including the identification and optimization of microstructural parameters, geometrical factors and surface modification conditions to promote enhanced resistance to fretting fatigue.

(5) Develop mechanistic models of the initiation and early growth of small cracks to characterize their role in HCF failure, with specific emphasis on initiation at microstructural damage sites and on subsequent interaction of the crack with characteristic microstructural barriers; and correlate such models to experimental measurement.

The majority of work in this section has been accomplished on Ti-6Al-4V. Unless otherwise noted, the material used was a 6.30Al, 4.17V, 0.19Fe, 0.19O, 0.13N bal. Ti (wt%) alloy supplied as 20-mm thick forged plates after solution treating for 1 hour at 925^{o}C and vacuum annealing for 2 hours at 700^{o}C. This type of material is referred to as Solution Treated Over-Aged (STOA).

Recent Progress

This program was completed during the past year. The achievements of the program include:

- Worst-case fatigue threshold stress intensities have been measured in STOA Ti-6Al-4V using large (> 5 mm) cracks under representative HCF conditions (R > 0.95, 1000Hz). Values provide a

practical, frequency-independent (20 – 20,000 Hz) lower bound for the growth of naturally-initiated, physically-small (> 40 μm) cracks.

- Stress-intensity solutions have been developed for small, semi-elliptical, surface cracks under mixed-mode loading. Such solutions are (for the first time) being used to experimentally measure small-crack, mixed-mode thresholds in Ti-6Al-4V.

- Mixed-mode thresholds, at mixities of $K_{II}/K_I \sim 0.5$ to 8, for large, short and (for the first time) microstructurally-small cracks have been measured in Ti-6Al-4V, with both bimodal and lamellar microstructures. Mixed-mode short-crack and particularly small-crack thresholds are significantly lower than those for large cracks. Using a *G*-based approach, Mode I is found to be the worst-case threshold condition in the Ti-6Al-4V alloy.

- FOD, simulated with high velocity 200-300 m/s steel-shot impacts, has been found to severely reduce the smooth-bar fatigue life in Ti-6Al-4V microstructures. Whereas worst-case thresholds provide a lower-bound for high-cycle fatigue in the presence of continuum cracks, a modified Kitagawa-Takahashi is proposed where FOD-induced microstructurally small cracks are formed in damaged regions.

- The local residual stress gradients surrounding FOD regions have been analyzed using quasi-static and dynamic numerical models; predictions have been verified using synchronous x-ray micro-diffraction techniques. X-ray studies have also focused on the cycle-dependent relaxation of such stress fields. Dynamic finite element simulations of FOD damage have also been correlated to such measurements. Evidence for relaxation of such stresses on fatigue cycling has been modeled and directly observed by *in situ* x-ray diffraction measurements.

- Large-crack threshold behavior in a polycrystalline Ni-base disk alloy has been characterized at 100 and 1000 Hz at 25º, 550º and 650ºC, involving effects of microstructure, frequency load ratio and temperature. Values of the measured fatigue thresholds have been correlated to the fracture surface roughness.

- Theoretical solutions for the crack-tip opening and crack-shear displacements controlling the growth of small fatigue cracks have been developed.

- New computational (finite-element) methods for 3-D simulations of fretting fatigue (*Fretting Fatigue Simulator*) have been developed using a ring-element approach.

- Through an analogy between the asymptotic fields at contact edges and ahead of a crack, a crack-analogue approach to contact fatigue (*Crack Analogue*) has been developed, and validated by experiment in Al and Ti alloys.

- A continuum level mechanics model (*Adhesion Model*), incorporating interfacial adhesion, material properties and contact loads, for predicting contact fatigue crack initiation for a variety of loading states and contact geometry, has been developed. The effect of roundness of a nominally sharp contact geometry on fretting fatigue crack initiation was investigated analytically and validated with experimental results on Ti-6Al-4V.
- Palliatives to fretting fatigue such as surface modifications through shot-peening, laser shock-peening and coatings on fretting fatigue damage are being explored.

- ❖ The influence of contact and bulk stresses, contact geometry, material microstructure and surface finish on the fretting fatigue behavior of Ti-6Al-4V has been investigated through controlled experiments, using the MURI-developed fretting fatigue device.

- ❖ A new framework for understanding the fundamentals of foreign object damage has been developed within the context of dynamic indentation.

- ❖ A new theoretical model for the fretting of coated metal surfaces has been developed which specifically addresses the role of plastic deformation of the metal substrate.

The bulleted list above is taken directly from the MURI 2001 annual report. The report in its entirety, as well as other MURI reports, can be found at http://www.lbl.gov/Ritchie/Programs/URI/online.html.

Participating Organizations: Air Force Office of Scientific Research (AFOSR), University of California at Berkeley, Massachusetts Institute of Technology, Michigan Technological University, Harvard University, Southwest Research Institute, Imperial College, London University, Technische Universität Hamburg-Harburg, Universität für Bodenkultur (BOKU)

Points of Contact:

Government
Dr. Craig Hartley
U.S. Air Force, AFOSR/NA
801 North Randolph Street, Mail Room 732
Arlington VA, 22203-1977
Phone: (202) 767-8523
Fax: (202) 767-8451

Contractor
Prof. Robert O. Ritchie, Ph.D., Sc.D.
University of California at Berkeley
Dept. of Materials Science and Mineral Engineering
Berkeley, CA 94720-1760
Phone: (510) 486-5798
Fax: (510) 486-4995

2.4 Improved HCF Life Prediction (Fan)

FY 96-00

Summary

The focus of this program was the development of damage-tolerant design processes for gas turbine engines that substantially reduce the potential occurrence of high cycle fatigue failures in titanium (fan) structures. Specific objectives for this program were: (1) characterization of in-service damage associated with high-cycle fatigue loading of titanium fan blades; (2) development of techniques to generate in the laboratory damage states that are representative of in-service damage; (3) modeling of the nucleation and progression of damage in titanium fan blades; and (4) development of an improved damage-tolerant life prediction and design methodology for turbine engine rotating structures subjected to HCF and combined HCF/LCF loadings.

This program was accomplished through the development of a better understanding of the three primary damage mechanisms experienced in the fan section, and through the transitioning of that understanding into the development of improved damage tolerance life prediction methodologies. All experimental studies were performed on an $\alpha+\beta$ processed Ti-6Al-4V forged plate, specifically produced to provide a representative titanium alloy with consistent properties.

The results of this program can be found in the 2000 HCF Annual Report. Highlights of the program are described below:

- *HCF/LCF Interactions* research was aimed at developing a better understanding of the fatigue and crack growth damage accumulation processes due to the load interactions generated in HCF/LCF loading.

  - High-resolution studies of HCF/LCF crack growth found no significant, systematic effect of periodic LCF unloads on near-threshold fatigue crack growth rates under high-R HCF cycling.

  - The fatigue crack growth behavior of microstructurally short cracks, which have been known to propagate below conventional long-crack ΔK_{th} values, was evaluated.

- *Foreign Object Damage* research was aimed at developing a better understanding of the occurrence and levels of FOD in different sections of turbine engines and characterizing the relevant parameters for modeling FOD damage progression. Techniques for reproducing damage representative of in-service FOD were investigated, and specimens containing laboratory-induced FOD were tested to characterize the effects of FOD. Specific accomplishments in this area include:

  - Test results indicate that the presence of a large stressed area (unnotched FOD specimen) results in a predicted life similar to those of smooth specimens with a similarly highly stressed area. Yet, a relatively small notch (notched FOD specimens) can apparently result in a longer fatigue life for a given stress if the residual stress due to impact is not accounted for in the analysis.

  - FOD testing was performed on airfoil-shaped tension specimens and winged specimens.

  - Several un-impacted and impacted specimens were tested under axial-load-control HCF conditions for comparison to baseline smooth bar fatigue data. The data clearly indicate good agreement with the smooth-bar baseline for non-impacted tests, and the negative effect that FOD has on HCF life.

- *Fretting Fatigue* research was aimed at developing a better understanding of the occurrence and levels of fretting fatigue damage at the fan blade-root/disk-hub interface. Techniques for reproducing damage representative of in-service fretting fatigue were investigated, and specimens containing laboratory-induced fretting and fretting fatigue damage were tested to characterize the effects of fretting fatigue on the HCF behavior.

  - The stress invariant model that best predicted multi-axial results is based on the effective stress range and a modified Manson-McKnight mean stress.

  - Friction experiments were conducted by Purdue University to study the evolution of the coefficient of friction, μ, with the number of cycles in partial slip experiments in bare Ti-6-4 on Ti-6-4. Steady state values of μ ranged from 0.4 to 0.55.

  - Singular Integral Equation methods were shown to provide accurate predictions of edge of contact stress in simple geometries with minimal computational requirements.

❖ *Damage-tolerant Life Prediction Methodologies* have been developed or utilized as mentioned in the three damage state areas above and exit criteria were created.

Participating Organizations: University of Dayton Research Institute, General Electric Aircraft Engines, Pratt & Whitney, Rolls Royce Allison, Honeywell Engines and Systems, Southwest Research Institute, Purdue University, North Dakota State University, University of Illinois

Points of Contact:

Government
Dr. Theodore Nicholas
U.S. Air Force
AFRL/MLLMN, Bldg. 655
2230 Tenth St., Suite 1
WPAFB, OH 45433-7817
Phone: (937) 255-1305
Fax: (937) 656-4840

Contractor
Dr. Joseph P. Gallagher
Univ. of Dayton Research Institute
300 College Park
Dayton, OH 45469
Phone: (937) 229-2349
Fax: (937) 229-3712

2.5 Advanced HCF Life Assurance Methodologies (Fan and Turbine)
FY 99-02

Background

This program is a follow-on to Effort 2.4, "Improved HCF Life Prediction," and is focused on the extension and validation of the technologies developed in the earlier effort to other titanium alloys for use in the fan section, as well as to single crystal nickel-base superalloys for use in the turbine section. The objectives of this program are: (1) to extend the understanding of damage mechanisms in $\alpha+\beta$ processed Ti-6Al-4V blades and disks to other titanium alloys with varying microstructures, (2) to develop a better understanding of the underlying damage mechanisms to which single crystal nickel-base superalloy blades and disks are subjected, and (3) to extend and validate the damage-tolerant life prediction and design methodologies developed for $\alpha+\beta$ processed Ti-6Al-4V to other titanium alloys and to single crystal nickel-base superalloys.

Recent Progress

Results in the 2000 HCF Annual Report were presented in the main areas of fretting, FOD and HCF/LCF interaction. As the program nears completion, the development of these models has been extended to Ti-17β and PWA 1484 (single crystal). Because of this, the results from this year will be broken down by alloy.

❖ ***Ti-17b:***

- Room temperature crack growth tests at R=0.1 and 0.5 have been completed. The results are shown in Figure 2.5.1. Preliminary indications are that a Walker model with the sigmoidal fit will accurately describe the observed behavior.

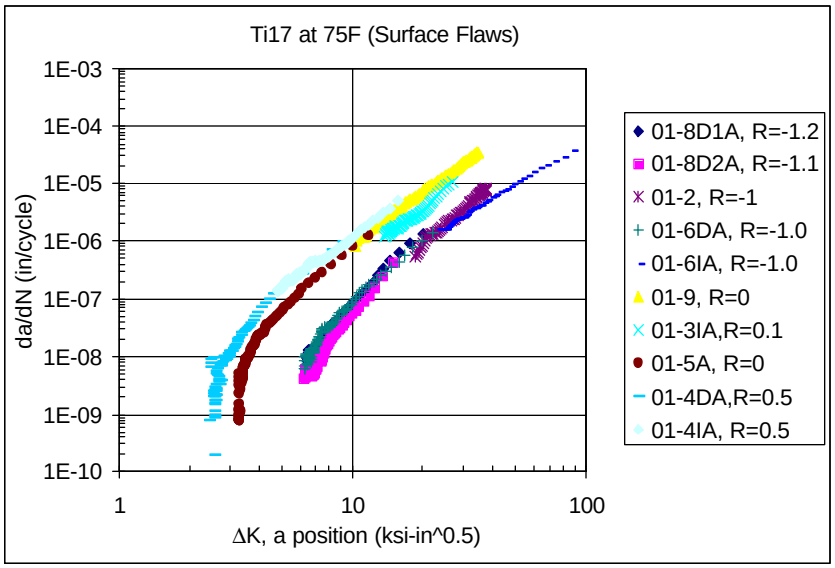

FIGURE 2.5.1 Room Temperature Crack Growth Rates for Ti-17β

- The stress capability determination of specimens with FOD has begun at room temperature and R= -1. Data from FOD in axial specimens are shown in Figure 2.5.2. Data from FOD in specimens representative of blade leading edges are shown in Figure 2.5.3. Preliminary data for the stress capability of these geometries are similar. Further data development must be completed before this conclusion is verified.

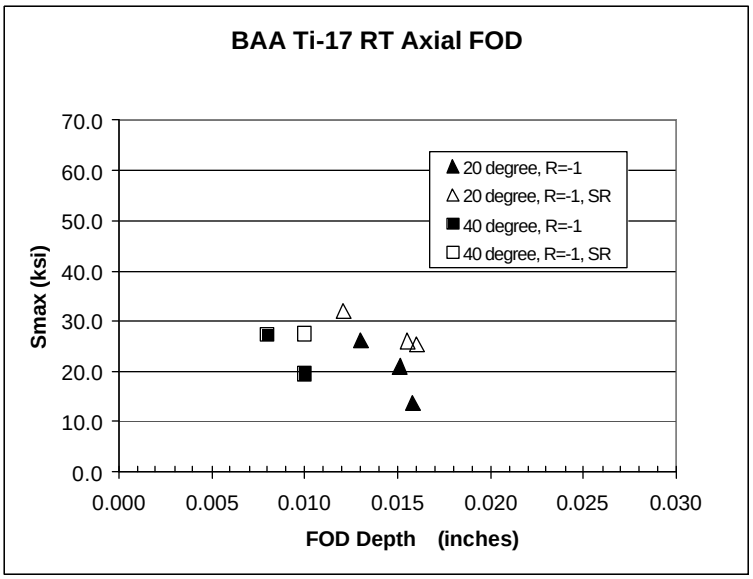

FIGURE 2.5.2 Fatigue Data at 10^7 Cycles for Axial FOD Specimens

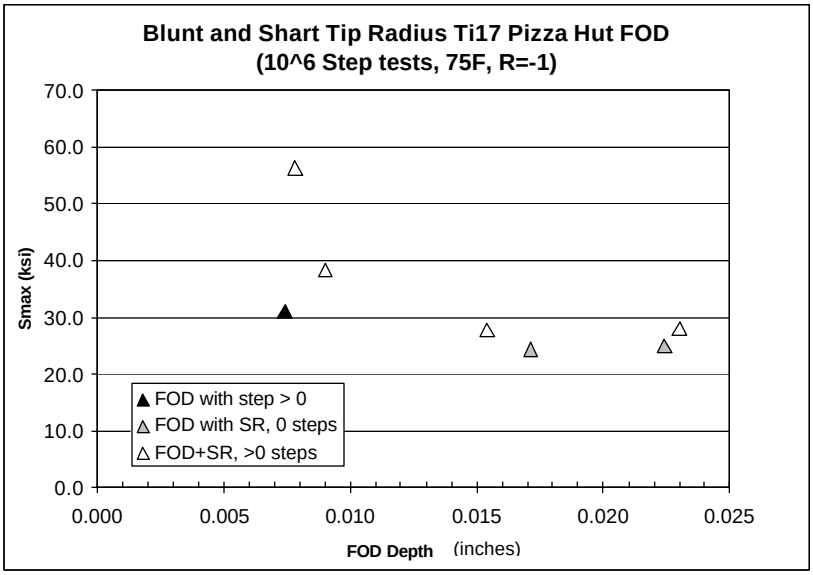

FIGURE 2.5.3 Fatigue Data at 10^7 Cycles for Leading Edge FOD Specimens

❖ ***PWA 1484:***

A large amount of this year's effort has concentrated on the application of previously developed HCF prediction methods to single crystal alloys. The material chosen for this transition was PWA 1484.

- Several of the life prediction parameters described in the 2000 HCF Annual Report were used to collapse the available data. All the calculations were performed using the following elastic constants, measured along the primary <001> orientations, for PWA 1484 at 1100°F: E = 15.69 msi, ν = 0.3995, G = 15.93 msi. The different parameters were evaluated by determining how well they were able to correlate the fatigue data for the different specimen orientations. Figure 2.5.4 graphically shows an S-N plot for different orientations of PWA 1484. This figure clearly indicates that the traditional S-N approach cannot be used to correlate the fatigue data for the different specimen and loading orientations. It underscores the need for a new paradigm for the fatigue analysis of single crystal materials.

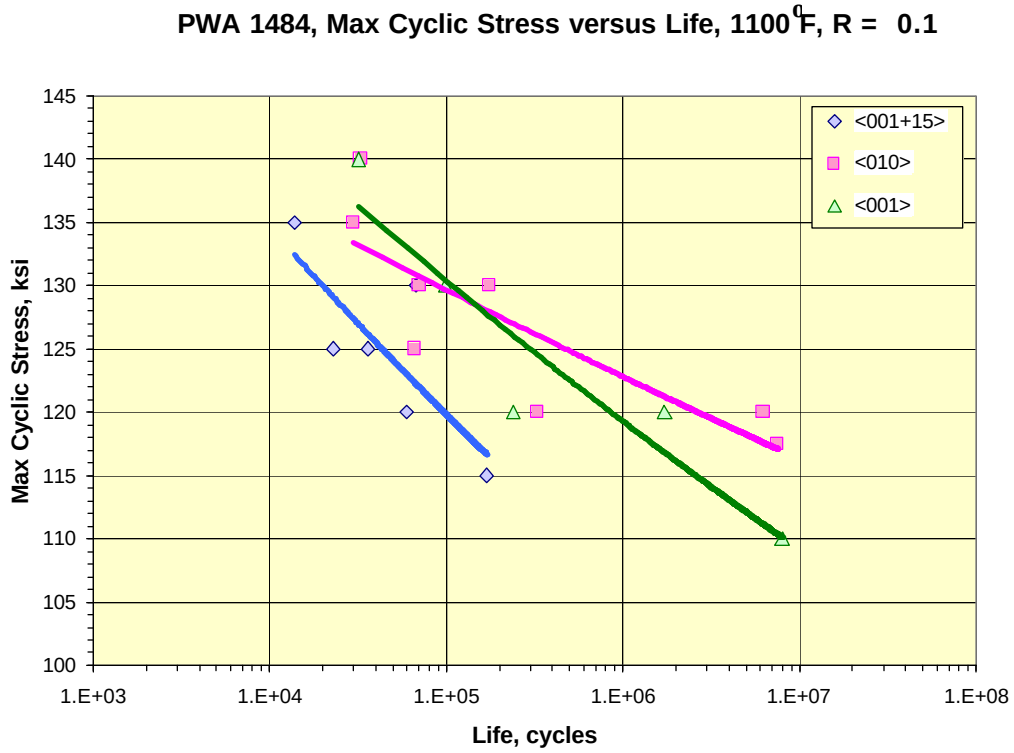

FIGURE 2.5.4 S-N Diagram for PWA 1484 at 1100°F

- Six models were applied to the test data in an effort to better correlate the data. Of these models, the maximum Shear Stress Range (SSR), the Walls parameter and the Chu Conle Bonnen (CCB) model appear to perform the best. Figure 2.5.5 shows the S-N data in Figure 2.5.4 after the Walls parameter has been applied.

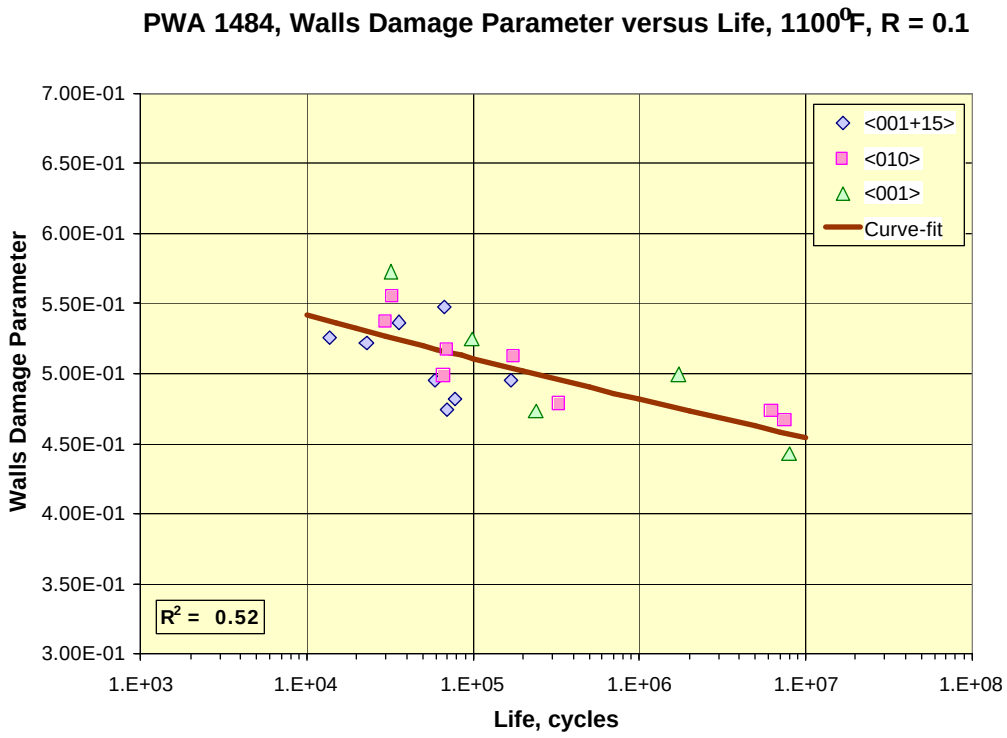

FIGURE 2.5.5 Application of Walls Parameter to S-N Data for PWA 1484 at 1100°F

- Considering the variability that is usually associated with single crystal fatigue data, R^2 values around 0.6 are assumed to indicate data correlations that are quite good. Based on how well the different damage parameters correlated with the observed critical planes and also how well the damage parameters correlated the fatigue data for the different specimen orientations, it appears that the SSR, Walls, and CCB damage parameters are well suited for the HCF analysis of single crystal materials.

- Fatigue crack growth testing was completed at 1900°F and 1100°F to define the effect of R-ratio on growth rate and threshold. Selected results are shown in Figures 2.5.6 and 2.5.7. There is a clear trend, as is normal in crack growth, of increased crack growth rate and lower threshold with increasing R-ratio (or mean stress). In addition, there is some indication that the crack arrest at threshold becomes less distinct at higher R.

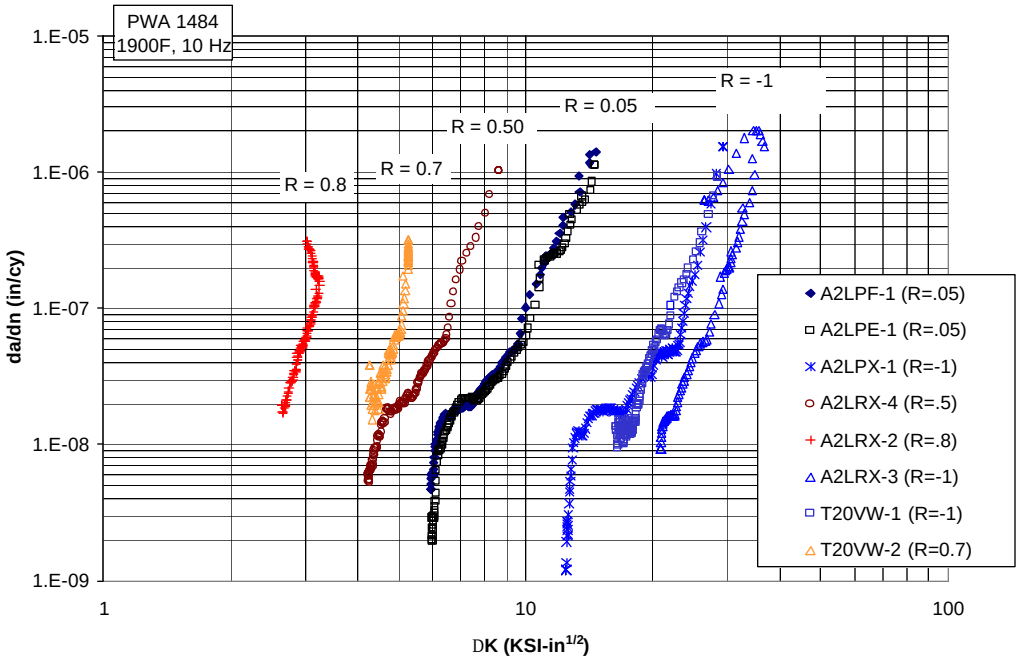

FIGURE 2.5.6 Crack Growth Rates for PWA 1484 at 1900°F

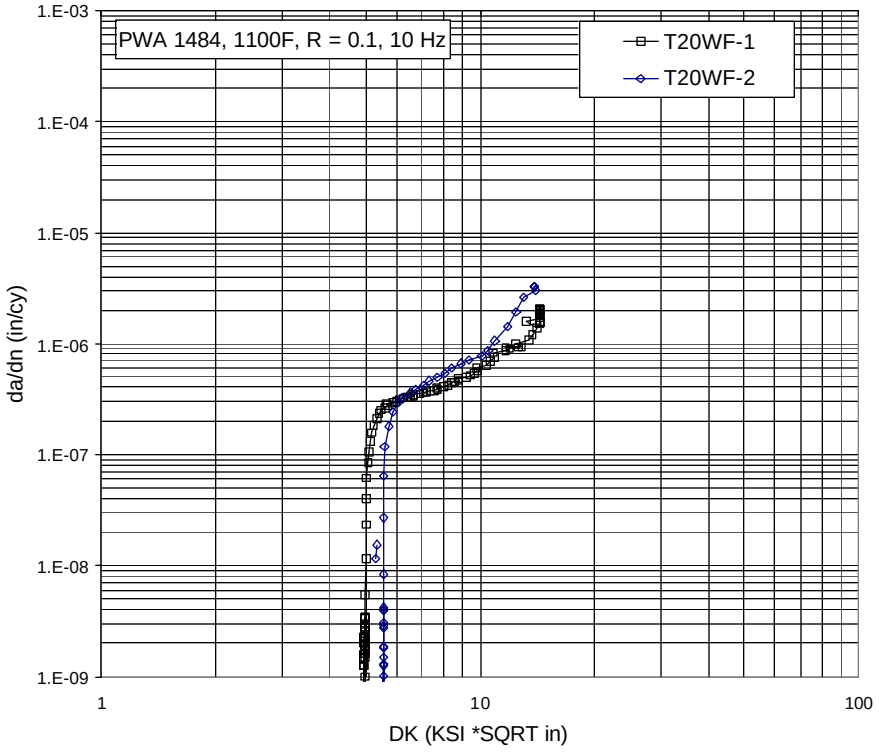

FIGURE 2.5.7 Crack Growth Rates for PWA 1484 at 1100°F

The crack growth rate data shown in Figure 2.5.6 were analyzed using the Walker Model for mean stress effects. This model takes the form:

$$da/dN = f(K_{eff}), \text{ where}$$
$$K_{eff} = \Delta K(1-R)^{(m-1)}$$

where K_{eff} is the Walker effective stress intensity at a given R-ratio and stress intensity range, ΔK. m is an empirical exponent found by fitting the data to the model. Generally the data are separated into two regimes, $R > 0$, and $R < 0$, since m usually has different values in these two regimes. The Walker exponents for PWA 1484 at 1900°F were determined to be 0.306 for $R \geq 0$ and $m = 0$ for $R < 0$. The value of zero for m implies that the crack is driven purely by tensile stress when there is compression present. A replot of the crack growth data using K_{eff} rather than ΔK is shown in Figure 2.5.8. This figure shows that the Walker K_{eff} model works reasonably well within the scatter of the results. The threshold for this model becomes: $K_{eff} = 6.5$ ksi$\sqrt{}$in.

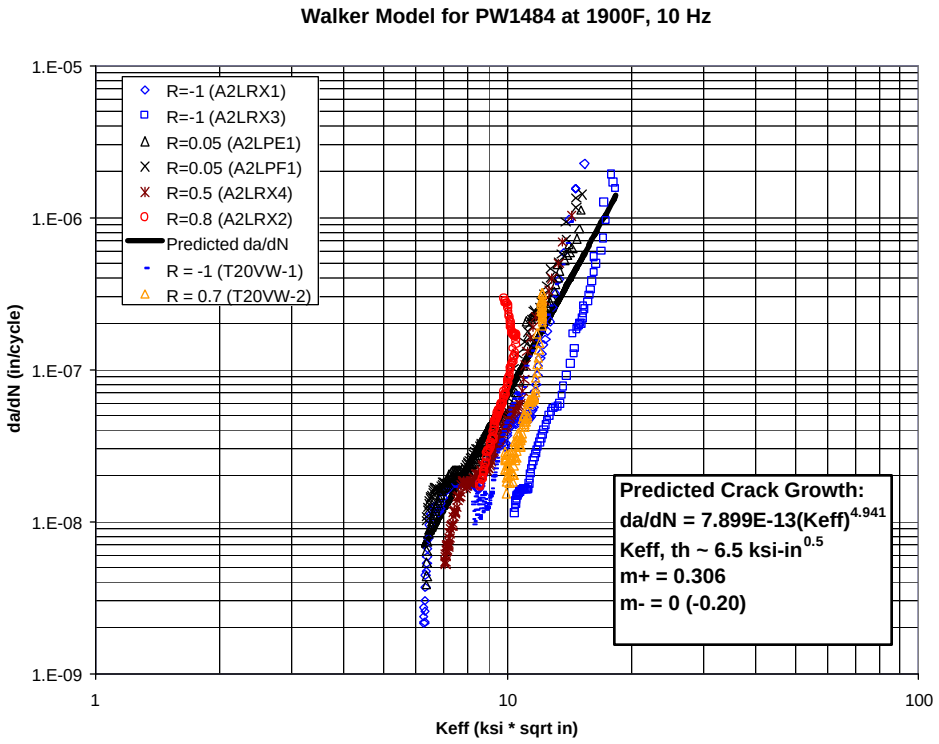

FIGURE 2.5.8 Walker Effective K Model for Fatigue Crack Growth of PWA 1484 at 1900°F, 10 Hz.

❖ ***General Modeling Developments:***

- In addition to the experimental work completed on PWA 1484 and Ti-17β, model development was continued. The results from this continued development are described here.

- The Random Fatigue Limit (RFL) model has been updated using two sets of room temperature fatigue test data, a Ti-6Al-4V dataset and a Ti-17 dataset. Both datasets include single load

specimen tests (LCF, staircase, or traditional S-N curve data) and step test data. RFL models were fit to the single load only data as well as the combined single load and step test data for the TI-6Al-4V data. Due to the small size dataset, only combined single load and step test data were fit for the Ti-17 specimens. Data for both materials were available spanning both the LCF and HCF regimes, which is an important consideration when fitting the RFL model. The results of the application of the RFL is shown in Figures 2.5.9 and 2.5.10.

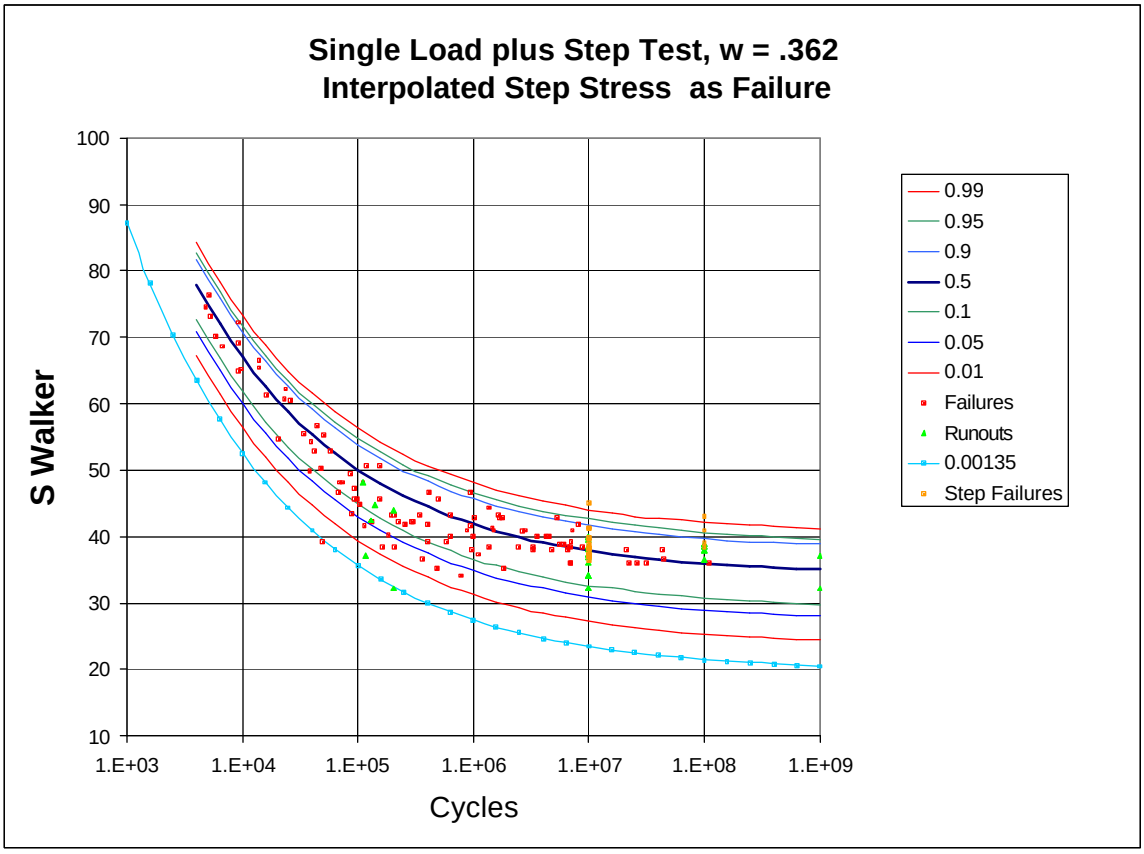

FIGURE 2.5.9 Ti-6Al-4V Single Load Plus Interpolated Step Test Failure Random Fatigue Limit Model Fit. Again, fatigue limit stress behavior is evident.

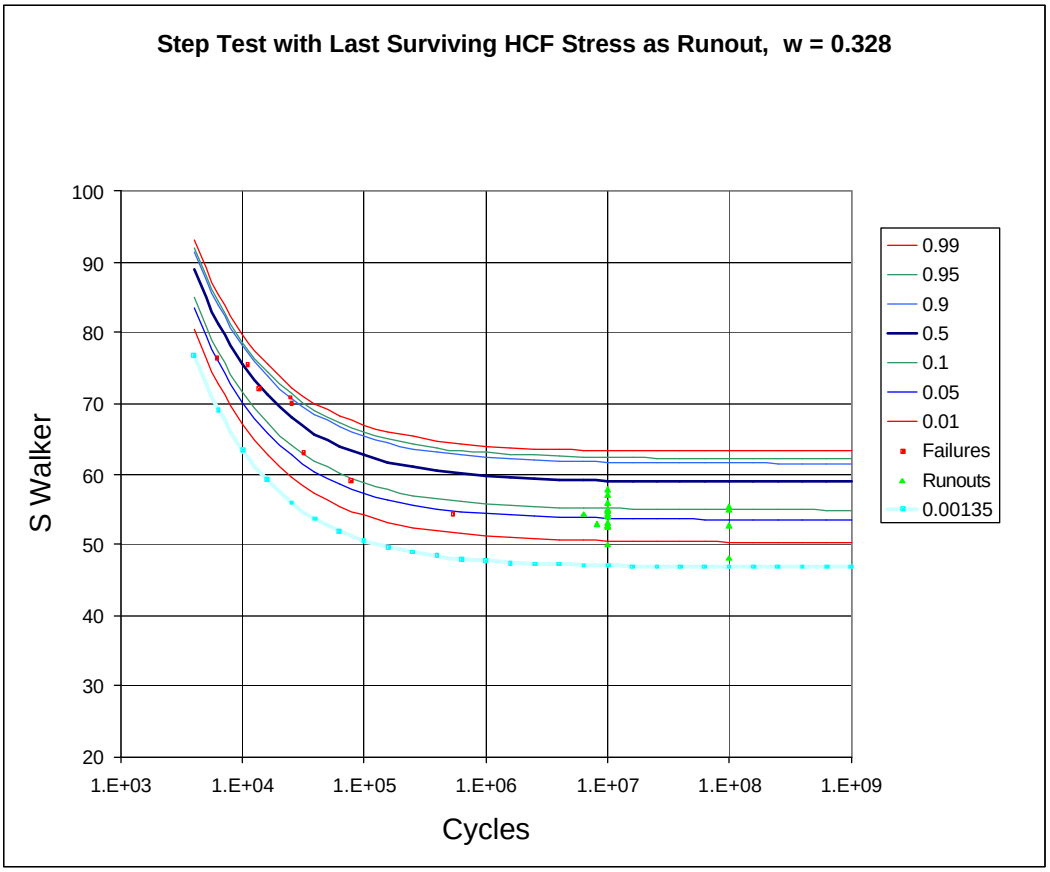

FIGURE 2.5.10 Ti-17 Step Test with Last Surviving Stress Level as Runout Random Fatigue Limit Model Fit. Note that this dataset results in a clear fatigue limit for the model.

- 1000 Hz baseline 10^7 step tests designed to validate the notch preparation procedures to be used for small, sharp notch testing have been completed and the results have been analyzed. The objective of these tests was to examine the possible influence of notch fabrication procedure on the small-notch endurance limit. The test results are summarized in Table 2.5. All data were generated at R = 0.5, since this is the R-value to be used in a majority of the planned small notch testing. For reference, the HCF Phase 1 data at 60 Hz generated by Metcut are also included in Table 2.5. Thus, three sets of data are provided:

  1) 60 Hz Metcut data on notches prepared by Low Stress Grinding plus Chem Milling (LSG + CM)

  2) 1000 Hz SwRI data on notches prepared by LSG + CM

  3) 1000 Hz SwRI data on notches prepared by Electrodischarge Machining plus Chem Milling (EDM + CM)

  Overall, good agreement was found among the data from the above three sets. Specifically, on average, the Max Stress was 49.1 with a standard deviation of plus or minus 1.65 (plus or minus 3.4%). On this basis, we can conclude that the notch preparation procedure did not significantly influence the measured endurance limits.

Table 2.5 Double-Edge-Notch 10^7 Step Test Data. Notch radius = 0.021in., b=0.047 in., k_t=2.5

Note: Values in Italics are suspensions.

Baseline Data from Phase 1 of HCF Program Set 1: Test freq: 60 Hz; Notch Fabrication: LSG + CM

Sample	Runs	Life	Max. Stress	R	Min. Stress	Mean Stress	Test Loc.	Interpolated Max. Stress at Failure
8606	*1*	*10,000,000*	*45.0*	*0.5*	*22.5*	*33.8*	*Metcut*	
8606	*2*	*10,000,000*	*47.3*	*0.5*	*23.7*	*35.5*	*Metcut*	
8606	*3*	*10,000,000*	*49.6*	*0.5*	*24.8*	*37.2*	*Metcut*	
8606	4	309,237	52.1	0.5	26.1	39.1	Metcut	**49.7**
123-21	*1*	*10,000,000*	*47.3*	*0.5*	*23.7*	*35.5*	*Metcut*	
123-21	2	2,388,074	49.6	0.5	24.8	37.2	Metcut	**47.8**
123-3	*1*	*10,000,000*	*47.3*	*0.5*	*23.7*	*35.5*	*Metcut*	
123-3	2	329,623	49.6	0.5	24.8	37.2	Metcut	**47.4**
							Average	**48.3**
							Std Dev	**1**
							Std Error	**2%**

Verification Data from Phase 2 of HCF Prog Set 2: Test Freq:1000 Hz; Notch Fabrication: LSG + CM

Sample	Runs	Life	Max. Stress	R	Min. Stress	Mean Stress	Test Loc.	Interpolated Max. Stress at Failure
153-3	*1*	*10,000,000*	*45.0*	*0.5*	*22.5*	*33.8*	*SwRI*	
153-3	*2*	*10,000,000*	*47.3*	*0.5*	*23.6*	*35.4*	*SwRI*	
153-3	*3*	*10,000,000*	*49.5*	*0.5*	*24.8*	*37.1*	*SwRI*	
153-3	*4*	*10,000,000*	*51.7*	*0.5*	*25.9*	*38.8*	*SwRI*	
153-3	5	1,132,047	54.0	0.5	27.0	40.5	SwRI	**52.0**
153-4	*1*	*10,000,000*	*45.0*	*0.5*	*22.5*	*33.8*	*SwRI*	
153-4	*2*	*10,000,000*	*47.3*	*0.5*	*23.6*	*35.4*	*SwRI*	
153-4	*3*	*10,000,000*	*49.5*	*0.5*	*24.8*	*37.1*	*SwRI*	
153-4	4	7,882,602	51.7	0.5	25.9	38.8	SwRI	**51.2**
153-2	*1*	*10,000,000*	*45.0*	*0.5*	*22.5*	*33.8*	*SwRI*	
153-2	*2*	*10,000,000*	*47.3*	*0.5*	*23.6*	*35.4*	*SwRI*	
153-2	*3*	*10,000,000*	*49.5*	*0.5*	*24.8*	*37.1*	*SwRI*	
153-2	4	275,938	51.7	0.5	25.9	38.8	SwRI	**49.6**
							Average	**50.9**
							Std Dev	**1**
							Std Error	**2%**

Verification Data - Phase 2 of HCF Prog Set 3: Test Freq:1000 Hz; Notch Fabrication: EDM + CM

Sample	Runs	Life	Max. Stress	R	Min. Stress	Mean Stress	Test Loc.	Interpolated Max. Stress at Failure
138-4	*1*	*10,000,000*	*45.0*	*0.5*	*22.5*	*33.8*	*SwRI*	
138-4	*2*	*10,000,000*	*47.3*	*0.5*	*23.6*	*35.4*	*SwRI*	
138-4	3	7,725,956	49.5	0.5	24.8	37.1	SwRI	**49.0**
138-6	*1*	*10,000,000*	*45.0*	*0.5*	*22.5*	*33.8*	*SwRI*	
138-6	*2*	*10,000,000*	*47.3*	*0.5*	*23.6*	*35.4*	*SwRI*	
138-6	3	3,813,460	49.5	0.5	24.8	37.1	SwRI	**48.1**
138-7	*1*	*10,000,000*	*45.0*	*0.5*	*22.5*	*33.8*	*SwRI*	
138-7	*2*	*10,000,000*	*47.3*	*0.5*	*23.6*	*35.4*	*SwRI*	
138-7	3	390,221	49.5	0.5	24.8	37.1	SwRI	**47.4**
							Average	**48.2**
							Std Dev	**0.65**
							Std Error	**1.30%**
							Grand Ave.	**49.1**
							Std Dev	**1.65**
							Std Error	**3.40%**

Key to Fabrication Processes
LSG = Low Stress Ground
CM = Chem Milled
EDM = Electro-discharge Machined

- Work continues to progress on the analysis of attachment fatigue. Building off of the success of the Singular Integral Equation methods for rapidly predicting contact stresses, these methods are currently being expanded to account for dissimilar contacts and plastic deformation. The utility of these models has repeatedly proven itself in industry design systems.

- The upcoming year will see the completion of the current program. The focus of the research this year will continue to be on transition of HCF tools developed for Ti-6Al-4V to different alloy systems.

Participating Organizations: Air Force Research Laboratory (AFRL), Air Force Office of Scientific Research (AFOSR), University of Dayton Research Institute, General Electric Aircraft Engines, Pratt & Whitney, Rolls Royce Allison, Honeywell Engines and Systems, Southwest Research Institute, Purdue University, University of Illinois, North Dakota State University, Rensselaer Polytechnic Institute

Points of Contact:

Government
Dr. Craig Hartley
U.S. Air Force, AFOSR/NA
801 North Randolph Street
Mail Room 732
Arlington VA, 22203-1977
Phone: (703) 696-8523
Fax: (703) 696-8451

Government
Dr. Jeffrey R. Calcaterra
U.S. Air Force
AFRL/MLLMN, Bldg. 655
2230 Tenth St., Suite 1
WPAFB, OH 45433-7817
Phone: (937) 255-1305
Fax: (937) 656-4840

Contractor
Dr. Joseph P. Gallagher
Univ. of Dayton Research Institute
300 College Park
Dayton, OH 45469
Phone: (937) 229-2349
Fax: (937) 229-3712

2.6 Probabilistic HCF Modeling of Titanium

FY 02-06

Background

HCF behavior is an inherently probabilistic process. The properties of a given material system can range widely based on a number of microstructural parameters including, but not limited to, grain size, texture, imperfections, inclusions and grain shape. The impact each of these parameters has on HCF life and endurance stress has not been explicitly identified. The purpose of the effort described in this section is to determine the statistical HCF properties of a material based on the probabilistic distribution of the microstructure. This will enable materials developers to concentrate on material and process improvements in areas that will have the greatest impact on HCF properties.

Progress

The probabilistic model of HCF material behavior is being developed under a phase II SBIR. The first phase of the SBIR developed a material model that can be used in conjunction with probabilistic analysis packages.

The phase II SBIR will use the statistical distribution of microstructural parameters from the Ti-6Al-4V alloy system used throughout this program to populate the phase I model. The results will then be used to predict the HCF response of Ti-6Al-4V specimens subjected to FOD. Current efforts have focused on the collection and analysis of existing FOD data in an effort to identify pertinent damage

mechanisms. Results from this study have concluded that the life debit cause by FOD is primarily due to the stress concentration caused by the sharp notches that are imparted. There is some evidence to suggest that there may be an underlying microstructural mechanism that also contributes to the life debit, but this is a secondary effect. Efforts during the upcoming year will focus on the application of the probabilistic model to specimens with FOD.

2.7 Future Efforts

FY 02-06

Background

As a result of previously described research, considerable insight has been gained in the area of thresholds for crack initiation and crack propagation under high cycle fatigue. Specifically, research on crack initiation under various mean loads and biaxial stress states and crack growth threshold investigations with different load histories has pointed the way to development of engineering solutions to relevant HCF design problems. This insight, on the other hand, has raised some fundamental questions about fatigue thresholds in general which, if answered, would enable the development of a more robust damage tolerant design system for HCF. Additionally, future turbine engines will have significant differences from those currently flying today. These engines will have components that must be fully characterized with respect to HCF. Some of the critical issues require continued basic research and are addressed below.

Planned Work

- ***Advanced High Cycle Fatigue Mechanics.*** FY 02-04.* This program will analyze the following areas of basic research:

  - Load history and spectrum loading effects
  - Multiaxial fatigue
  - Notch fatigue/stress gradients
  - Residual stress effects
  - Frequency and time-dependent effects

  All of these issues have to be addressed adequately in order to be able to establish fatigue thresholds for HCF. Most have been addressed partially or empirically under the present HCF program. The intent of this research is to establish methodologies that predict HCF behavior on a more fundamental basis. This will enable a more reliable basis for extrapolating behavior beyond the conditions under which a database is obtained and allows scale-up from laboratory specimens to components.

- ***HCF Properties of Welds on Nickel-Based Alloys.*** FY 02-06.* Future turbine engines will rely heavily on Integrally Bladed Rotors (IBRs). These have several structural advantages over traditional bladed disks including lower weight and better resistance to resonant stresses. However, a suitable maintenance procedure for IBRs must be developed in order to ensure that

whole assemblies are not discarded due to damage on one blade. One candidate for blade repair is welding a patch over the damaged region or welding on an entirely new airfoil. Both of these procedures are problematic because current welding methods do not reproduce the parent material microstructure. The proposed program will evaluate industry methods for weld repair, characterize the HCF life debit and suggest improvements to material microstructure and repair procedure. In addition, the program will evaluate other modern welding techniques in order to determine which repair maximizes HCF tolerance

(*) Dates are subject to change.

Point of Contact:

Government
Dr. Theodore Nicholas
U.S. Air Force
AFRL/MLLMN, Bldg. 655
2230 Tenth St., Suite 1
Wright-Patterson AFB, OH 45433-7817
Phone: (937) 255-1305
Fax: (937) 656-4840

2.8 Conclusion

The Materials Damage Tolerance Action Team dramatically increased the propulsion community's understanding of turbine engine high cycle fatigue. Specifically, this Team is helping to implement and validate foreign object damage life models and attachment design methodologies. The Materials Team also developed several unique HCF capabilities, including a realistic fretting bench test, a high-temperature fretting fatigue rig, and new models for life prediction in the presence of high stress gradients. Technologies used to predict material HCF behavior will be transitioned to industry design systems over the course of the upcoming year.

3.0 INSTRUMENTATION

BACKGROUND

The Instrumentation Action Team (Instrumentation AT) has the responsibility of fostering collaboration between individual HCF instrumentation efforts with the overall goal of combining with the Forced Response and Component Analysis ATs to better determine alternating stresses to within 20%. The Instrumentation AT provides technical coordination and communication between active participants involved in HCF measurement, sensor, data processing, and engine health monitoring technologies. Technical workshops have been organized on at least an annual basis and summaries of these workshops are disseminated to appropriate individuals and organizations. The Chair, Co-Chair, and selected Instrumentation AT members meet as required (estimated quarterly) to review technical activities, develop specific goals for instrumentation and engine health monitoring programs, and coordinate with the TPT and IAP. The Chairman (or Co-Chair) of the Instrumentation AT keeps the TPT Secretary informed of AT activities on a frequent (at least monthly) basis. This AT includes members from Government agencies, industry, and universities who are actively involved in instrumentation technologies applicable to engine HCF. The team is to be multidisciplinary with representatives from multiple organizations representing several component technologies as appropriate. The actual membership of the AT may change in time as individuals assume different roles in related projects.

ACTION TEAM CHAIRS

Chair
Charles Vining
AEDC/DOO
1099 Avenue C
Arnold AFB, TN 37389-9200
Phone: (931) 454-5115

Co-chair
1Lt Brian Beachkofski
U.S. Air Force, AFRL/PRTC
1950 Fifth Street, Bldg. 18D
Wright-Patterson AFB, OH 45433-7251
Phone: (937) 255-2611
Fax: (937) 255-2660

INTRODUCTION

The following pages summarize the schedules, backgrounds, and recent progress of the current and planned projects managed by this action team.

FIGURE 3.0.1 Instrumentation Research Schedule

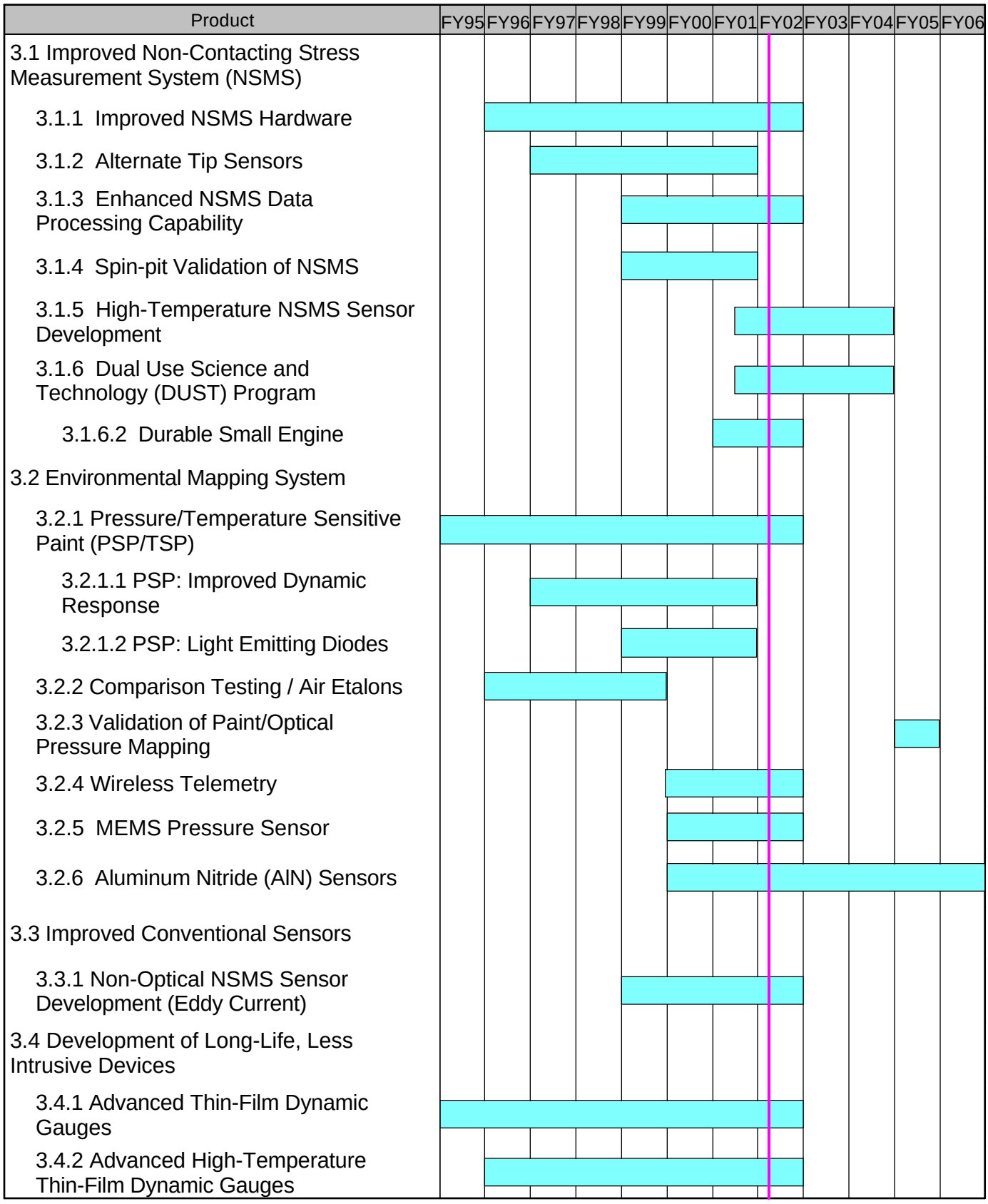

3.1 Improved Non-Contact Stress Measurement System (NSMS)

To date, prediction of aerodynamic forcing functions has been difficult or impossible due to lack of Computational Fluid Dynamics (CFD) fidelity, structural modeling accuracy, instrumentation effects, and insufficient characterization of instrumentation installation effects. The purpose of the projects described below is to develop an advanced generation NSMS (Figure 3.1) capable of detecting simultaneous integral-order modes with a 5X improvement in accuracy, and to provide the ability to accurately convert the measured tip deflection to a dynamic stress map.

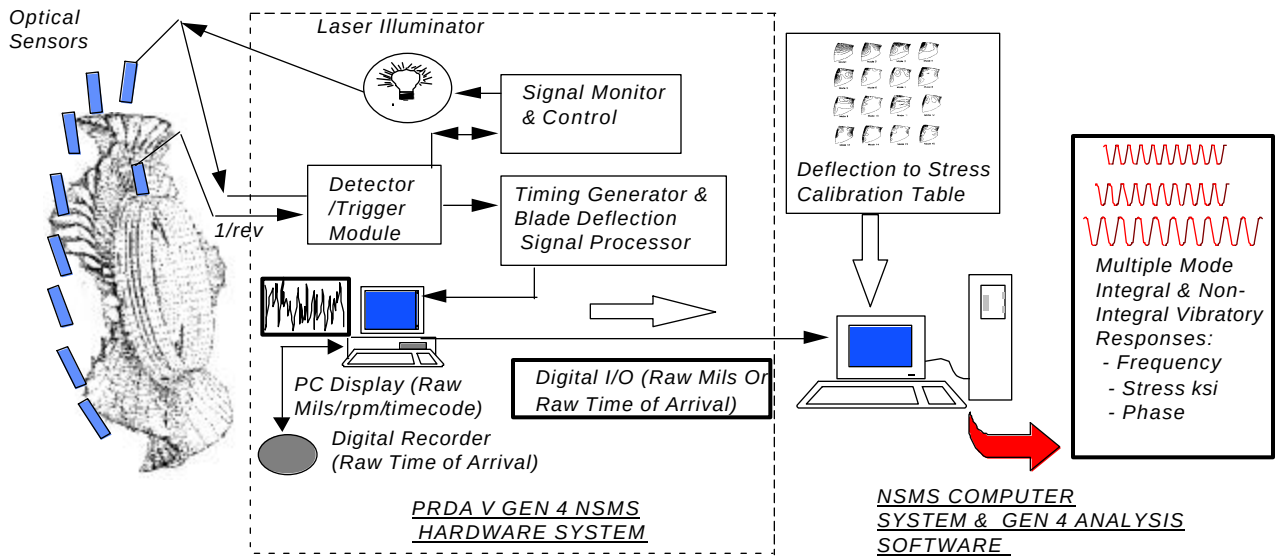

FIGURE 3.1 Next-Generation NSMS Overview

3.1.1 Improved Non-Intrusive Stress Measurement System (NSMS) Hardware (Generation 4)

FY 96-02

Recent Progress

The PRDA V contract has been completed. Partially operational subcomponents of a prototype Gen-4 Front End (G4F) were delivered to AEDC for subsystem evaluation, integration, and subsequently system-level assessment and evaluation in the laboratory followed by engine test validation. Post delivery, the system prototype subcomponents have been modified and the 24-channel system made partially operational (12 channels). Laboratory evaluations and assessments have been conducted on the12-channel configuration. The system is currently installed in the J1 engine-test area at AEDC awaiting validation testing on Pratt & Whitney's (P&W's) ATEGG engine XTC67/1, first quarter 2002.

Post delivery, AEDC modified and refined design shortfalls within all subsystems of the G4F including the Electro-Optics (E-O), Blade Timing Generator (BTG), and Blade Deflection Signal

Processor (BDSP). The G4F prototype system hardware is now operational with 12 channels (optical and alternate inputs) of the 24-channel design goal to meet the channel and bandwidth capacity requirements for validation testing on XTC67/1.

Extensive laboratory assessment and evaluations of the G4F, ATEGG Gen-4 probes and optical cables were conducted by AEDC and P&W personnel prior to installation into the test stand. Additional work is required to achieve a commercialized production-ready version of the prototype system.

The prototype G4F along with P&W's Data Acquisition Computer and a P&W Gen-3 Front end are currently installed in the J1 engine test area at AEDC. Integration of these systems is undergoing final checkout pursuant to XTC67/1 testing. The G4F is also interfaced to AEDC's developmental NSMS Gen-4 Monitor subsystem for assessment and evaluation of interface operation. Optical cables have been run between the stand and the Instrumentation Equipment room. Twelve Gen-4 optical line probes fabricated under the ATEGG contract have been installed into the 1st stage of XTC67/1's High Pressure Compressor (HPC) at P&W's Middletown, CT. facility. Engine testing is now scheduled for first quarter calendar year 2002.

P&W proprietary Gen-4 processing routines running on a Sun Workstation will be used to validate Generation 4 NSMS measurement and analysis capabilities. Data will also be acquired during the XTC67/1 testing from the G4F by AEDC's Gen 4 Monitor for subsequent analysis and comparisons when its G4P processing software/system is available (FY03-04).

Electro-Optic Development

AEDC performed hardware redesigns to correct noise problems associated with the power supply biasing of the avalanche photo-detectors, AC coupling, and back-plane probe-mapping wiring. Twelve prototype channels have been made operational to meet the needs and requirements of the XTC67/1 test. A vendor search for replacement of the laser-to-pigtail coupling is still underway.

Blade Timing Generator Development

The prototype subsystem has undergone some hardware and software modifications at AEDC in cooperation with Honeywell and is being prepared for validation testing on the ATEGG XTC67/1.

Blade Deflection Signal Processing (BDSP) Development

This prototype subsystem has also undergone some hardware and software modifications at AEDC in cooperation with Honeywell and is being prepared for validation testing on the ATEGG XTC67/1. Cooperation between Honeywell, AEDC, and P&W has continued to resolve operational and subsystem interfacing problems following completion of the PRDA V contract and delivery to AEDC. Various software bugs and shortfalls (such as data structure, windowing algorithms, and IRIG time stamping) are being corrected or greatly improved to satisfy operational requirements.

Optical Line Probe Development

One prototype Gen-4 probe was developed and delivered to AEDC for assessment and evaluation. The prototype probe was also used in preliminary assessment of the Gen-4 E-O subsystem.

Twelve probes were fabricated under the ATEGG contract for XTC67-1. Prior to engine installation, these probes were individually coupled to the G4F E-O system in the laboratory at AEDC and return signals from a small blisk of blades (similar to an F119 HPC R5 blade tip) were evaluated.

P&W is currently completing adaptive designs of the Gen-4 line probe assembled with conventional epoxy (lower temperature capability) for use in the first two stages of the HPC of JTDE engine XTE67/SE1. These designs may also be used in near term SDD (System Design and Development) programs if the ATEGG Gen-4 validation test confirms the predicted measurement improvements and appropriate G4F hardware can be funded. Additionally, some line probes for P&W commercial engine use are being produced with both Gen-3/Gen-4 capability by simply replacing one of the multiple transmit fibers with a single-mode fiber and a minor change in the lens-polishing procedure. This provides a very cost-effective way of providing Gen-4 line-probe capability prior to full validation.

Gen-4 Hardware Interface to Gen-4 Data Processing Systems

The G4F has been coupled to AEDC's Gen-4 diagnostics monitor via reflective memory, and the initial assessment and evaluation have been completed. AEDC has continued to work with Honeywell and Pratt & Whitney regarding the industry standard interface and data format. Additionally, reflective hardware and software needed to interface the G4F to P&W's on-stand NSMS Data Acquisition system are the final stage of check out.

Participating Organizations: Pratt & Whitney, Honeywell Engines and Systems, Arnold Engineering Development Center (AEDC)

Points of Contact:

Government
Lt Brian Beachkofski
U.S. Air Force, AFRL/PRTC
1950 Fifth Street, Bldg. 18D
Wright-Patterson AFB, OH 45433-7251
Phone: (937) 255-2611
Fax: (937) 255-2660

Contractor
Mr. Woodrow Robinson
Pratt & Whitney
M/S 403-39, P.O. Box 611
Aircraft Road
Middletown, CT, 06457
Phone: (860) 344-4364
Fax: (860) 557-7464

3.1.2 Alternate Tip Sensors

FY 97-01

Background

As part of the Fourth Generation NSMS development effort, a study of alternate (i.e., non-optical) NSMS sensors was initiated. The motivation for this study arises principally from problems associated with applying optical sensors, namely installation complexity and susceptibility, to optical contamination. These problems are of paramount importance in flight test and engine health monitoring applications (but are of less concern in ground-based engine testing). A sensor capability specification was prepared with input from the members of the Fourth Generation NSMS design team. This sensor specification defines the requisite characteristics of sensors to be used for engine health monitoring and Third and Fourth Generation NSMS applications. This sensor specification was used

as a basis for evaluating the suitability of alternative sensor technologies for Fourth Generation NSMS applications.

The alternate sensor feasibility study is a subtask of the PRDA-5-funded Fourth Generation NSMS development program. This subtask was accomplished by Rolls-Royce Corporation (Allison Advanced Development Company). The objective of the subtask was to define the necessary and desirable characteristics—such as spatial resolution, depth of field, sensitivity, temperature range, and bandwidth—that an NSMS blade passage sensor would need to possess in order to implement each of the four generations of NSMS systems. The NSMS generations are defined by functional capability and are shown in table 3.1.2.1.

Generation	Capabilities
1	- Multi-Probe Capable Flutter Monitor - Deflection Only - Analog Signal - Single Probe - No Algorithms for Stress, Frequency, and Amplitude of Non-Integral Order Modes - First Computer Based NSMS - Algorithms For Frequency and Modes.
2	- Multi-Probe Capability - Frequency and Amplitude of Non-Integral Order Modes - First Computer Based NSMS - Algorithms for Frequency and Modes
3	- Frequency and Amplitude Of Single Mode - Integral Order Blade Vibrations - Limited Algorithms For Stress
4	- Frequency and Amplitude of Multi-Mode Integral Order Blade Vibrations - Algorithms for Stress

Table 3.1.2.1 NSMS Generations as Defined by System Capability

The NSMS sensor capability specification integrated the input from all the participating organizations of the Propulsion Instrumentation Working Group (PIWG) NSMS team, drawing on the team's extensive NSMS experience. The key NSMS sensor capabilities are shown in Table 3.1.2.2 below. Noteworthy are the stringent bandwidth and spatial resolution specifications for Generation 4 HCF applications.

NSMS Generation	Bandwidth (Rise Time)	Effective Spatial Resolution
Basic LPC/Fan Health	88 kHz (4 microseconds)	5 mils (S) 10 mils (L) *
Gen 3	350 kHz (1 microseconds)	2 mils
Gen 4	12 MHz (30 nanoseconds)	0.1 mil
(*) "S" denotes "small engine." "L" denotes "large engine."		

TABLE 3.1.2.2 NSMS Sensor Capability Specification

Final Results

The above NSMS sensor capability specification was used as a benchmark against which the capabilities of candidate NSMS sensors were compared in order to objectively determine in which

NSMS generation (see Table 3.1.2.1) these candidate sensors would find application. This compilation of NSMS sensor requirements represents the consensus of the entire Propulsion Instrumentation Working Group (PIWG) NSMS team.

The principal characteristics that determine the "generational ranking" of a NSMS sensor are bandwidth (or equivalent rise time) and spatial "jitter." Another key sensor characteristic is the "sensor field geometry," which represents a specification of the geometry of the area of the blade "interrogated" by the NSMS sensor. The goal of the PRDA 5 funded NSMS development effort was to design an integrated optical line probe and NSMS front end capable of resolving the higher order vibration modes that result in blade high cycle fatigue. For measuring the blade tip deflections resulting from these higher order vibration modes, it is essential that the location on the blade being interrogated by the sensor (illuminated in the case of optical sensors) be well defined and of limited spatial extent. If the area of the blade tip being interrogated includes a substantial portion of a "spatial wavelength" of a vibration mode, then the NSMS sensor will, in effect, measure an average tip deflection, which might well be zero!

It is the inherent ability of optical NSMS probes to have a tightly focused spot (or line) of light to interrogate the blade tip that makes optical NSMS probes eminently suitable for Generation 4 (HCF) applications. It is the inherent inability of probes depending on non-propagating electric or magnetic fields to tightly focus the blade tip interrogation geometry (and for that matter to quantitatively specify that geometry) that makes them unsuitable for Generation 4 (HCF) applications. Examples of probes depending on a non-propagating electric or magnetic fields include capacitive and eddy current displacement/tip clearance probes.

The finding of the Alternate Sensor Feasibility Study is that, to date, no non-optical NSMS probe technology has been identified that is suitable for Generation 4 (i.e. HCF) applications.

Participating Organizations: Rolls-Royce

Points of Contact:

Government
Lt Brian Beachkofski
U.S. Air Force, AFRL/PRTC
1950 Fifth Street, Bldg. 18D
Wright-Patterson AFB, OH 45433-7251
Phone: (937) 255-2611
Fax: (937) 255-2660

Contractor
Mr. Thomas Bonsett
Rolls-Royce
Speed Code W03A, P.O. Box 420
Indianapolis, IN 46206-0420
Phone: (317) 230-3448
Fax: (317) 230-4246

3.1.3 Enhanced Data Processing Capability for Generation 4 and 5 NSMS Development

FY 99-02

There is no progress reported on this effort for CY2001.

3.1.4 Spin-Pit Validation of NSMS
FY 99-01

Background

The application of NSMS in engine testing requires a multiplicity of probes and sophisticated software to automate the reduction of data. The requirements for spin-testing are much simpler, and can best be met without the development of a standard arrangement of probes and packaged software.

Efforts prior to CY2001, are described in the 2000 High Cycle Fatigue Annual Report.

Recent Progress

In the 2001 project, the goal was to implement a system of commercially available probes and acquisition hardware to obtain unsteady stresses in an engine rotor excited to resonance in a spin pit. Following initial tests with small rotors excited with air-jets, oil jets and magnets (eddy-current excitation), in which eddy-current, capacitance and light probes were used, a light-probe system was used with magnet excitation of a partially bladed, second-stage turbine rotor.

The setup is shown in Figure 3.1.4.1. The reflected light signals were input to a PC computer through a Hood Technology Corporation (HTC) interface board. HTC software was used to acquire and analyze the probe data.

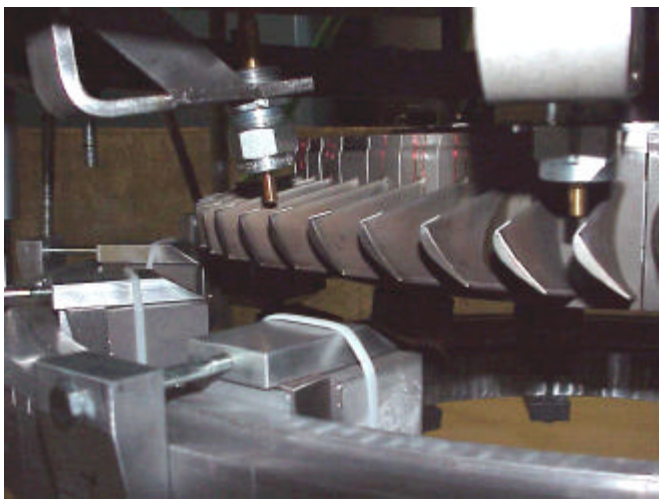

FIGURE 3.1.4.1 Turbine Rotor Spin Test with Magnet Excitation and 2-Light Probe NSMS System.

Figure 3.1.4.2. shows the measured behavior of one blade from the signal from one probe, as the rotor RPM was swept through resonance, with magnets raised to cover the blade tips. The amplitude of the blade oscillation and the Q of the resonance were deduced from a curve fit to the transient behavior. A linear and noise-free calibration of the NSMS measurements to strain measurements was obtained

using the measured deflections of strain-gauged blades. This calibration was applied to deduce the micro-strains produced in all blades during resonance, and to examine the repeatability of measurements from data sample to data sample without stopping, and from data sample to data sample after stopping.

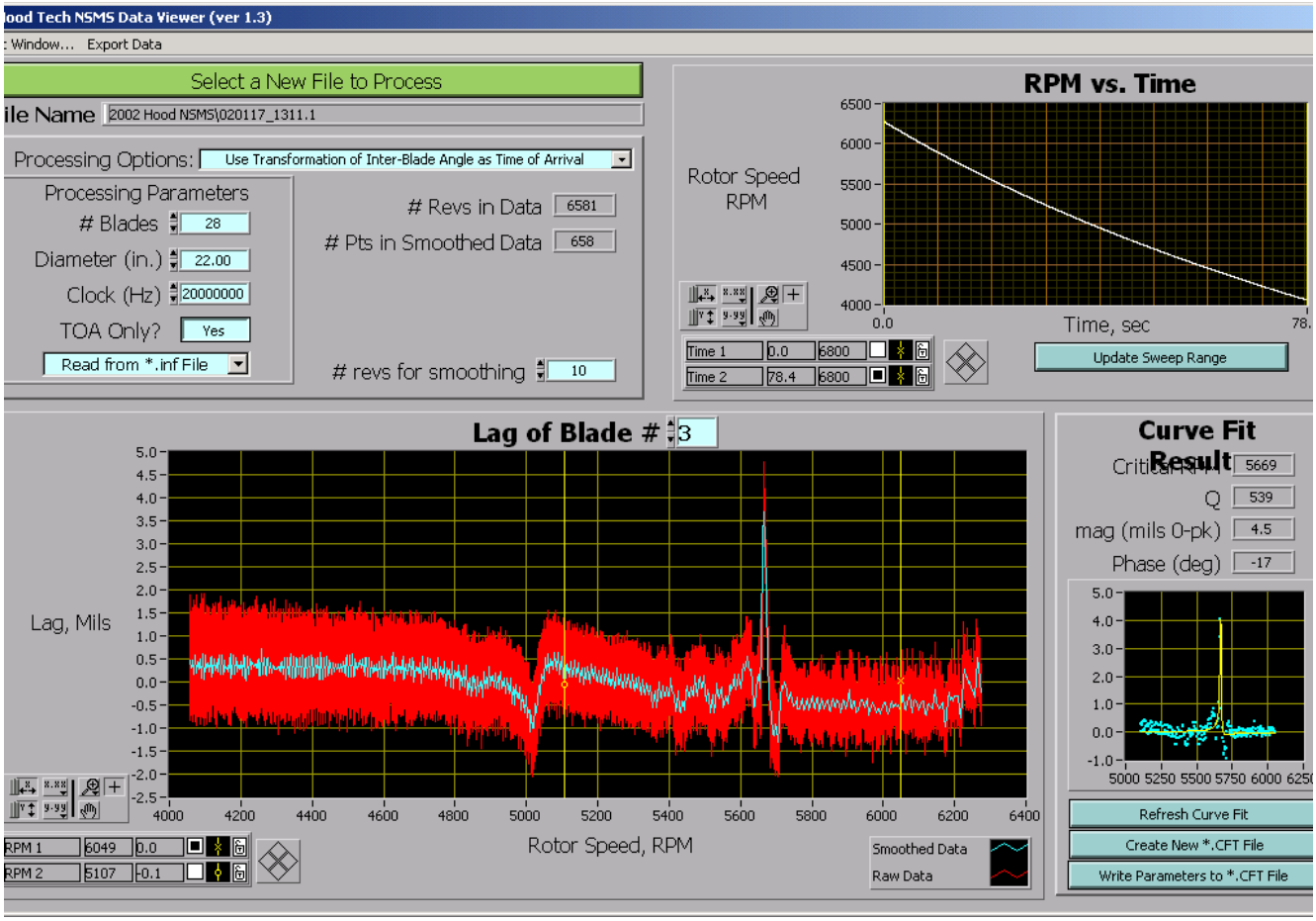

FIGURE 3.1.4.2 Example of Resonant Response of One Blade from One Light Probe Signal

Figure 3.1.4.3. shows the results obtained in five rotor starts and stops. Sweeps A and B were taken after each start. The results showed that after the first two starts, plastic inserts under the blades held the blades in their slots when the rotor was stopped. In the final three starts, the behavior of the separate blades around the rotor repeated. The degree of repeatability was excellent, since a separate curve-fit was made to the data for each blade (in 2 sets of 14, separated by blanks), for each probe (2), for each sweep (10).

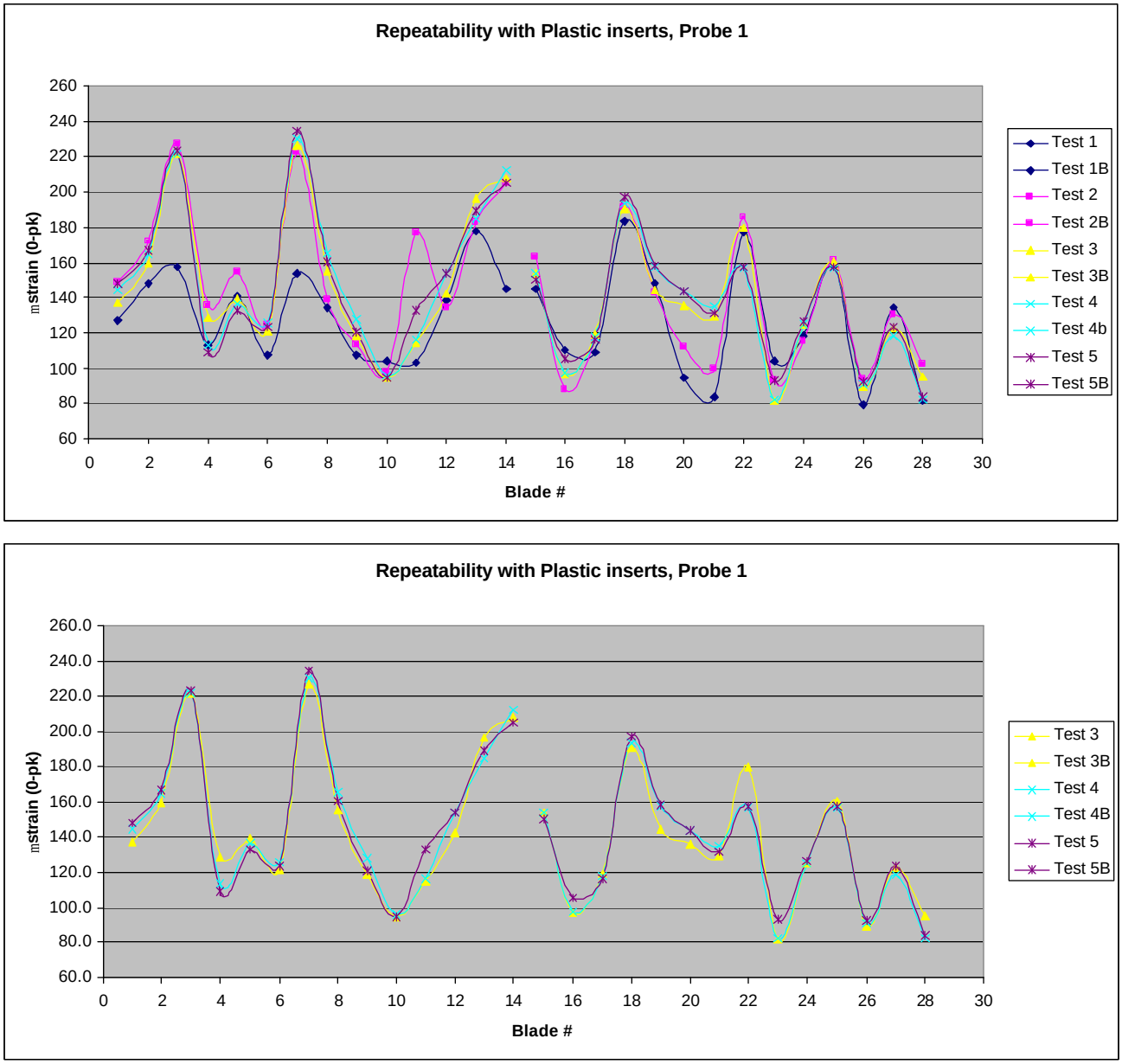

FIGURE 3.1.4.3 Micro-Strain in Each Blade Deduced from (Calibrated) Light Probe Measurements.

Complete results are reported in an Naval Postgraduate School Master's Thesis by M. Mansisdor (March 2002). It is noted that the latest version of the HTC software automates the curve fitting procedure, and tabulates the results.

Participating Organizations: Naval Postgraduate School Turbopropulsion Laboratory, Hood Technology Corp

Points of Contact:

Government
Mr. Ray Pickering
U.S.Navy
Propulsion & Power Engineering
Naval Air Warfare Center
Aircraft Division
22195 Elmer Rd.,
Patuxent River, MD 20670
Phone: 301-342-0865
Fax: 301-342-4781

Government
Dr. Ray Shreeve
U.S.Navy
Turbopropulsion Laboratory
Naval Postgraduate School
699 Dyer Road, Room 137
Monterey, CA 93943-5106
Phone: 831-656-2593
Fax: 831-656-2864

Contractor
Dr. Andy von-Flotow
Hood Technology Corporation
1750 Country Club rd.
Hood River, OR 97031
Phone: 541-387-2288
Fax: 541-387-2266

3.1.5 High-Temperature NSMS Sensor Development

FY 01-04

There is no progress reported on this effort for CY2001.

3.1.6 Dual Use Science and Technology (DUST)

FY 01-04

Two Dual Use Science and Technology (DUST) Programs have been awarded supporting this effort. The first DUST is with Honeywell/Excell, Inc. and the second effort is with Williams International/Hood Technologies, Inc.

3.1.6.1 Small Engine NSMS

There is no progress reported on this effort for CY2001.

3.1.6.2 Durable Small Engine NSMS

FY01-02

Background

PROGRAM OBJECTIVES

The objective of this 24-month program is to develop and demonstrate a non-intrusive strain monitoring system that is suitable for use in current and future generations of small gas turbine engines. The basis for the system design requirements will be a small axial compressor that is currently being developed for use in UAV engines.

Williams International is building upon Hood Technologies successful large engine test experience. Hood Technologies is expanding the sensor capability by decreasing the sensor size, improving the resolution, and raising the frequencies required for the extremely small airfoils, high shaft speeds, and high discharge temperatures of the small turbine engines. The small engine system will have to be capable of detecting damaging resonance and able to provide data that can be accurately related to blade stresses.

A further objective is to develop a system with a longer service life than the surface mounted strain gauges and slip rings used today. This system will be attractive because it could cover the entire service life for a typical UAV or UCAV application.

PROGRAM APPROACH

- Use existing engine residual hardware as test bed for NSMS system demonstration & development.
- Small engine NSMS will build upon Hood Technologies large engine test experience.
- Specification for the NSMS system are based on the HP compressor operating environment.
- System development will include two design, fabrication, and test cycles composed of an initial prototype and optimized NSMS system.

Validation of the system is to be based on previous experience and analytical predictions.

Recent Progress

The basis for defining the system operating requirements has been a small high-pressure compressor being evaluated for a UAV technology demonstrator engine. The last stage of the compressor represents the most challenging application for the non-intrusive stress measurement system because of the very small size of the airfoils and high rotational speeds.

The last stage of the HP compressor has the smallest blades and the highest operating temperatures and pressures. It is anticipated that if the system works on this stage it should be able to be applied to any of the larger stages.

Hood Technologies has been developing small fiber-optic, blade tip sensing probes. In development they have produced optical sensors less than 0.010" diameter and capacitance sensors approximately 0.060" in diameter.

The optic fibers are 0.005" in diameter and will be potted into 0.010" diameter holes electro-discharge machined into the compressor case. Sensors will be bonded with a silica adhesive then attached into a mounting block. Fibers will be routed out in bundles of seven in 0.040" diameter hypodermic tubing. Five tubes will be brought out of the engine case through an existing fitting modified with a custom designed sealing device, see Figure 3.1.6.2.1.

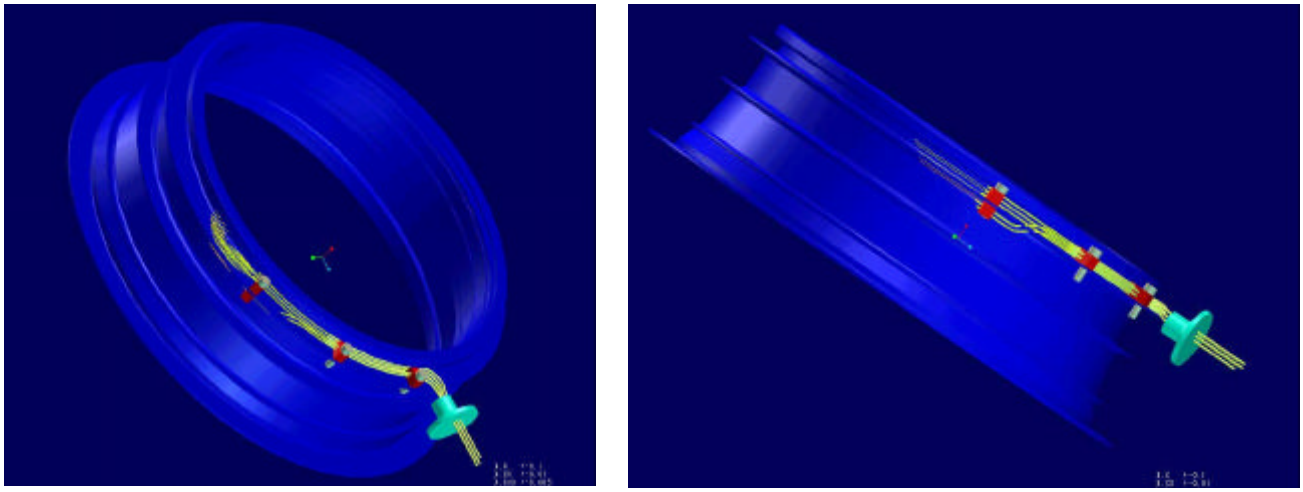

FIGURE 3.1.6.2.1 Installation of the Fiber-Optic Sensors in the Compressor Case

Plans for the sensor layout have 5 rows of 7 fibers. The first row is at the leading edge followed by a second row just behind it. The third row is located mid-chord and is followed by two rows one at the trailing edge and one just aft of the trailing edge. This cluster of sensors covers an area approximately 0.50" X 0.50", see Figure 3.1.6.2.2.

After installation of the sensors in the engine component, the fibers will be trimmed off close to the abradable surface. The ends of the fibers have to be polished to provide good signal to noise levels. The fibers will be polished into the abradable surface until they are about 0.001" below the abradable material.

Not all of the sensors will be used during the initial testing. Some of the sensors aft of both the leading and trailing edges will not have pre-amplifiers. During engine testing if the blades are found to shift fore or aft, or if sensor failure occurs, then other sensors will be fitted with pre-amps and used based on the initial engine test data.

A simulated high-pressure compressor case was fabricated and used for rig testing at Hood Technologies. This part has the same tip shroud abradable material and inside diameter as the actual engine hardware. Assembly, potting and polishing trials were conducted using this hardware. Spin testing was conducted using the test shroud along with a test rotor. Based upon the test results a maximum tip clearance of 0.010" was determined. Increasing the tip clearance more than 0.010" reduces the amplitude of the sensor return signal below a usable level. The tip clearance for the engine component is designed for a running clearance of 0.008".

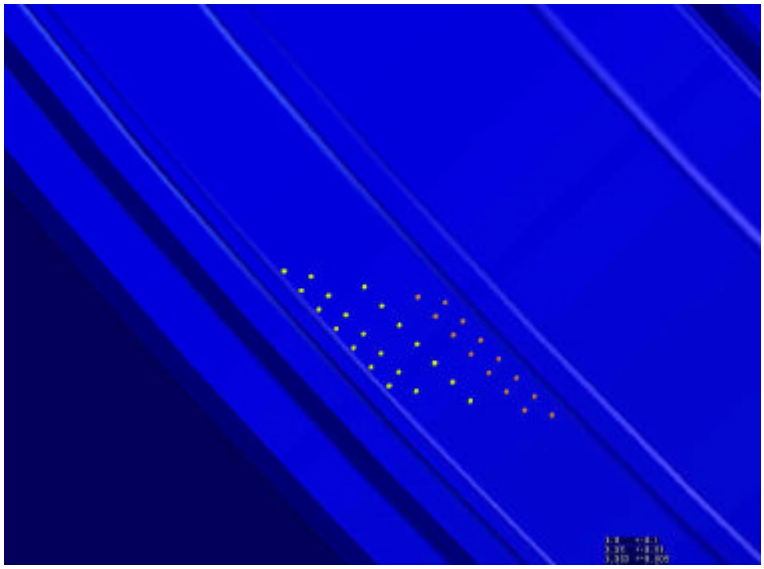

FIGURE 3.1.6.2.2 Fiber-Optic Sensor Installation Array Pattern

Oil was introduced into the spin pit testing to assess its effect on signal pickup. Oil had no adverse affect on the signal returned from the sensors. This is important since the first testing with the sensor system will be in a compressor rig that could have oil contamination.

Hardware will be modified in the near future with initial rig testing to be conducted in the first quarter of 2002. Engine testing is to follow after successful rig testing of the instrumentation.

Participating Organizations: Air Force Research Laboratory (AFRL)

Points of Contact:

Government
Lt Brian Beachkofski
U.S. Air Force, AFRL/PRTC
1950 Fifth Street, Bldg. 18D
Wright-Patterson AFB, OH 45433-7251
Phone: (937) 255-2611
Fax: (937) 255-2660

Contractor
William Fohey
Williams International
2280 West Maple Road, P.O. Box 200
Walled Lake, MI 48390-0200
Phone: (248) 624-5200
Fax: (937) 656-4652

3.2 Environmental Mapping System

To date, prediction of aerodynamic forcing functions has been difficult or impossible due to lack of Computational Fluid Dynamics (CFD) fidelity, lack of structural modeling accuracy, instrumentation effects, and insufficient characterization of instrumentation installation effects. The purpose of the tasks described below is to develop an optical pressure and temperature measurement system to non-intrusively measure the dynamic pressure and temperature distribution over the surface of the blade.

\

3.2.1 Pressure Sensitive Paint/Temperature Sensitive Paint (PSP/TSP)

FY 95-02

Background

The objective of this task is to shed light on critical issues required to ensure that pressure sensitive paints (PSPs) and thermographic phosphors (TPs) can be used in high cycle fatigue studies of turbomachinery. The critical issues to be addressed include probe miniaturization and paint/phosphor improvements.

Probe miniaturization requires the development of compact excitation and detection systems. Current excitation sources are heavier, bulkier, more labor-intensive, and costlier than those desired for certain Advanced Turbine Engine Gas Generator (ATEGG) and Joint Turbine Demonstrator Engine (JTDE) demonstrations. In this project, the use of high-power blue LEDs that hold promise for significant improvements in current methods of excitation for both PSPs and TPs will be investigated.

Pressure sensitive paint improvements in time response, survivability, and sensitivity at higher pressures and temperatures, and the use of thermographic phosphors as a means of temperature correction for the PSPs, are also being investigated.

Recent Progress

A measurement campaign was conducted at the Air Force Research Laboratory Compressor Research Facility. This state-of-the-art facility used no preconditioning of the air prior to entering the compressor section during this test. This proved to be a problem due to the high humidity of the air experienced during the summer test, which resulted in condensation (fogging) in the test section at speeds above 68% design speed.

To overcome this drawback, the facility was run at reduced inlet pressure (~ 10 psi). This greatly reduced fogging due to humidity condensation but caused seepage of lubricating oil into the test section. The effects of this contamination were reduced relative intensities, smearing of fiduciary marks, and stripping of the painted surface.

The main source of error in the temperature data was light scattering from the fluid particles in the flow. This resulted in a reduced relative intensity (offset) and erroneous temperature field. Two methods of determining a temperature distribution despite the contamination were investigated. Both approaches utilize CFD results to act as an *in-situ* reference. In the first method, a limited number of calculated pressure values are used in conjunction with the experimental pressure data to determine what temperatures would be necessary to give agreement. The temperature derived in this manner is then used to determine the scale factor needed to adjust the temperature data to achieve these values. This scale factor is then applied to the entire temperature data to determine the experimental temperature field distribution. The result of this method is shown in Figure 3.2.1.1. The blue line represents the spanwise temperature distribution derived in this manner at 10% chord.

The second method is to disregard the temperature measurement and utilize only the measured pressure data along with the CFD results to determine the temperature distribution. For example, along the 10% chord, the CFD analysis predicts that the pressure field is relatively constant (0.3 reduced pressure units). From this knowledge, the temperature distribution along the chord can be

calculated from the pressure data. This is represented in Figure 3.2.1.1 as the red line. The agreement between the two methods is quite good considering the contamination experienced in the test.

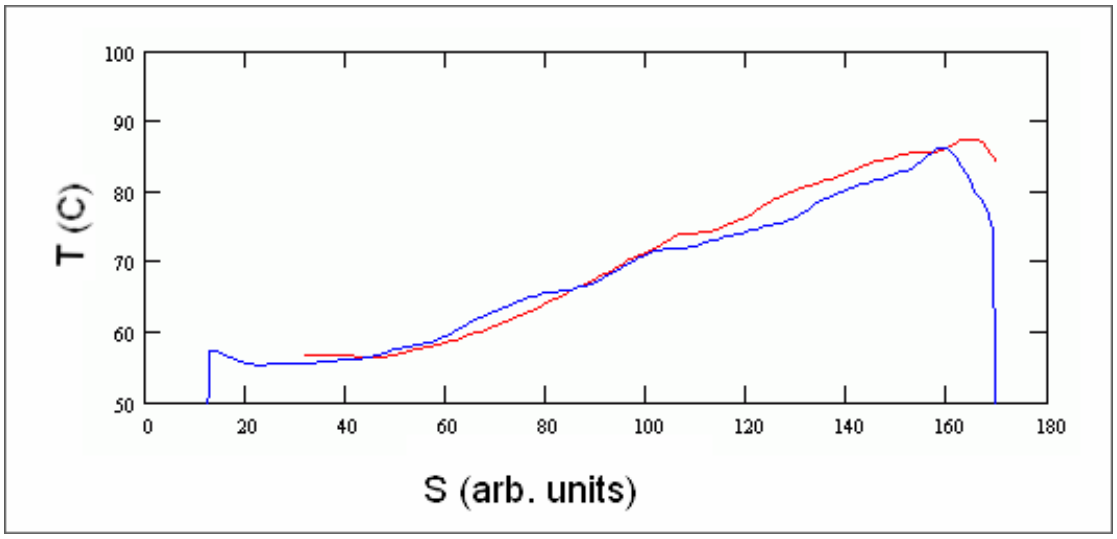

FIGURE 3.2.1.1 Spanwise Temperature Distribution at 10% Blade Chord. Blue – Using Scaled Temperature Data. Red – Using CFD Temperature Distribution and Experimental Pressure Data.

Both approaches can also be utilized to produce the full temperature field as shown in Figure 3.2.1.2. Here vertical and horizontal slices, inserts A-A and B-B, respectively, are plotted for quantitative comparison. While the temperature fields do not completely agree, the similarities give weight to using these approaches to determine temperature. It should be noted that the T/PSP coatings yield information about the surface temperature and pressure where the CFD code predicts the near-wall temperature and pressure. In some areas on the blade surface there could be substantial differences between these two conditions.

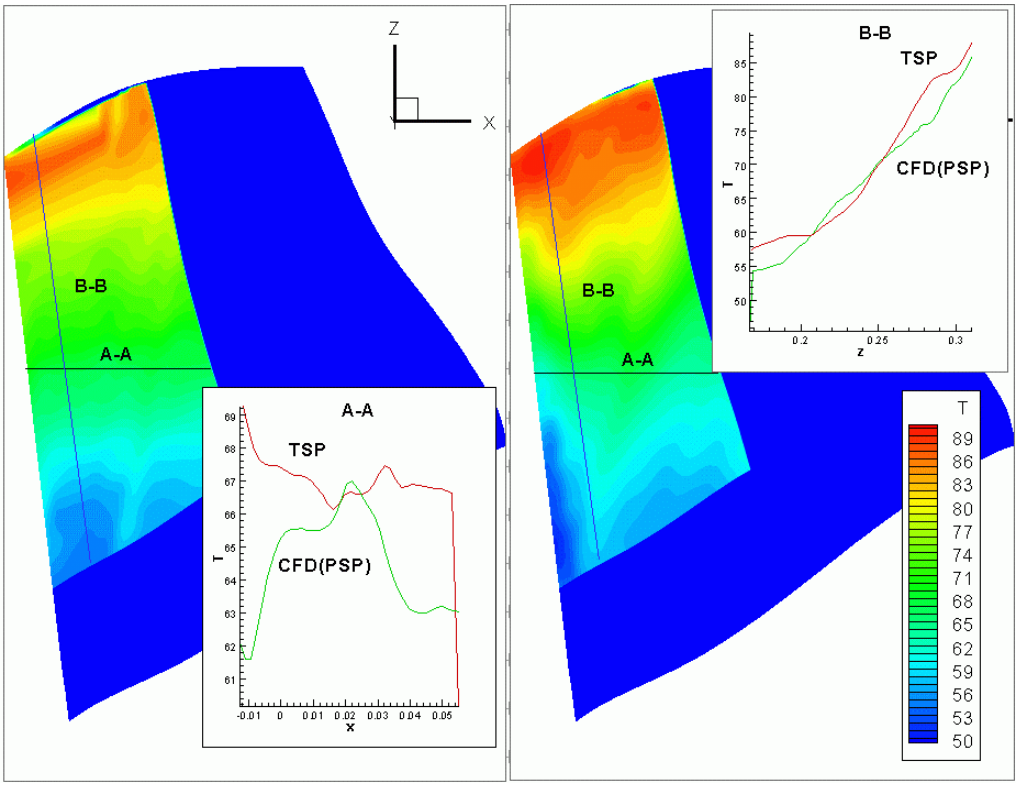

FIGURE 3.2.1.2 Temperature Fields Obtained From Scaled TSP Data and Temperature Fitting of the CFD Pressure and PSP Relative Intensity Distributions.

Once determined, the temperature field can be used to correct the experimental pressure measurement allowing the pressure field to be determined. Utilizing the scaled temperature field for this purpose, the experimental pressure field is plotted versus the CFD pressure in Figure 3.2.1.3. Note the general agreement between the measured and calculated pressure field is quite good considering the complexity of the flow field. Both approaches display the location and magnitude of the shock at the 85% near stall condition (see inserts A-A and B-B). The major differences occur at the leading edge and blade tip. Based upon examination of the blade surfaces after testing, these locations are the most susceptible to lubricating oil build up which would adversely affect the experimental pressure results. The more subtle differences (post-shock region shown in insert A-A) are likely due to temperature field inaccuracy. Considering the simplified approach to determining the temperature in this case and the high sensitivity of the pressure paint to temperature, the agreement is reasonable. Although past validation studies have indicated that the present CFD code calculates the pressure field very well, some discrepancies near the tip could be due to the shortcomings of the applied turbulence model. As previously mentioned, the CFD predicts the flow behavior near the wall while the T/PSP coatings measure these parameters within the paint layer. Heat transfer and other physical effects can contribute to the differences between the two results.

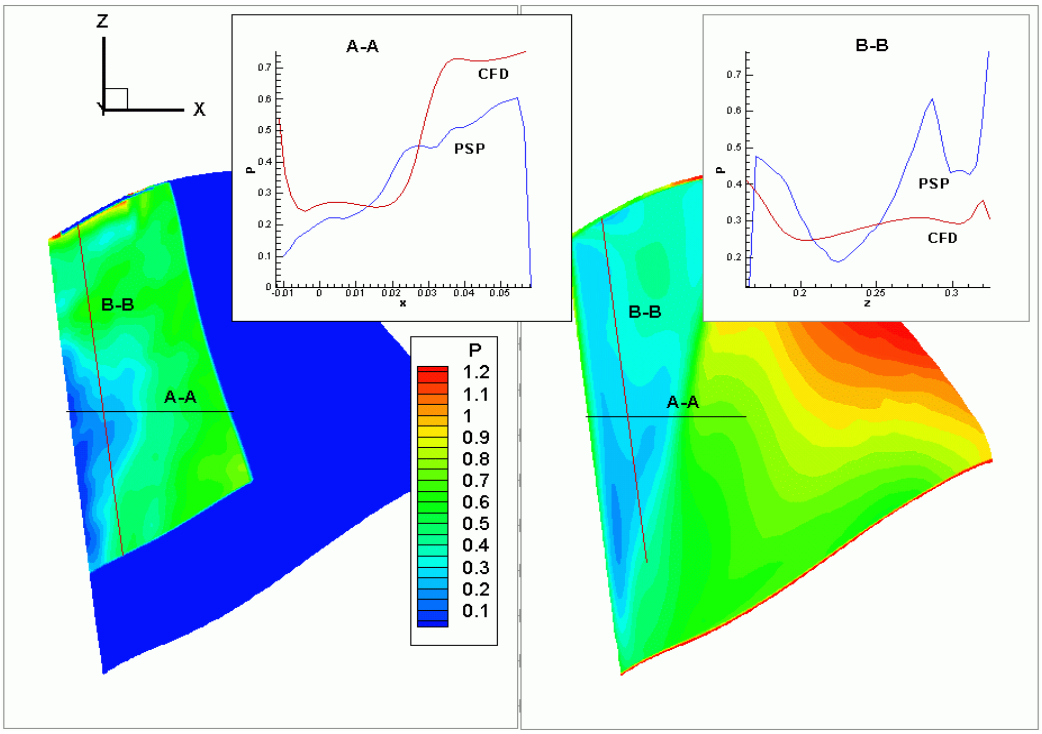

FIGURE 3.2.1.3 Pressure Fields Obtained from PSP (Left) and CFD (Right).

Overall, this research has demonstrated the potential of using T/PSP techniques to obtain static temperature and pressure measurements on the surface of advanced turbomachinery rotor blades. Through this work the steady-state data acquisition system has been optimized. This success was achieved despite contamination problems encountered with operating the facility at a reduced inlet pressure. The sol-gel-derived T/PSPs developed have been shown to exhibit higher output signal and improved pressure sensitivity as compared to the silicone-based systems demonstrated in the initial tests. More importantly, this work has demonstrated the ability to optimize the T/PSP for the desired need. An error analysis of the measurement approach indicates that a highly accurate temperature measurement is required to correct the pressure measurement. In particular at elevated temperatures above 80°C, the temperature measurement uncertainty must be better than 1°C to ensure a 1% error in the pressure measurement due to temperature. This proved to be a formidable requirement in this study due to the humidity and lubricating oil contamination encountered during the tests. *In-situ* calibration utilizing the CFD temperatures proved to be an adequate approach to correcting the experimental temperature data for interferences. The CFD-calculated overall three-dimensional shock location and the shock structure agreed fairly well with the T/PSP results. This good agreement indicates that the viscous blockage in the rotor passage is correctly modeled in the CFD simulation. However, the near-wall predictions of the CFD model can be expected to be different from the surface measurement results of the T/PSP coatings due to heat transfer and other physical effects. To this end, future efforts will be directed toward more accurate temperature measurements and towards the development of a heat transfer measurement technique for turbomachinery applications.

Participating Organizations: ISSI

Points of Contact:

Government
Lt Brian Beachkofski
U.S. Air Force, AFRL/PRTC
1950 Fifth Street, Bldg. 18D
Wright-Patterson AFB, OH 45433-7251
Phone: (937) 255-2611
Fax: (937) 255-2660

Contractor
Dr. Larry Goss
ISSI
2786 Indian Ripple Rd.
Dayton, OH 45440-3638
Phone: (937) 252-2706
Fax: (937) 656-4652

3.2.1.1 PSP-TSP: Improved Dynamic Response

FY 97-01

Recent Progress

- TSP. Thermally sensitive phosphors for potential use with pressure sensitive paint were selected and tested for the temperature range from ambient to 300º degrees C. Cerium-doped phospors appear to hold the most promise for very fast response requirements, particularly in hosts of rare-earth aluminum garnets or silicates. No one phosphor covers the entire temperature range but a combination can. The fluorescence decay times are 60 ns or less and the emission peaks are in the 500 nm region or less depending on material.

  - *Yttrium Garnets.* Figure 3.2.1.4 shows a plot of decay time versus temperature for Ce-doped garnet phosphors with varying gallium content as shown. The general formula is $Y_3(Ga_xAl_{1-x})_5O_{12}$:Ce and x varied from 0 to 0.75. All but one of the phosphors were procured from Phosphor Technology of Essex, England. (http://www.phosphor-technology.com/). The one exception is sample 1 for x = 0 which came from GTE Sylvania (now known as Osram Sylvania). From the plot it is seen that no one phosphor can cover the entire range from ambient to 300. The effect of the gallium is to shift the temperature dependence. High gallium content moves the calibration curve to lower temperatures. There are two exceptions to this trend. It is seen that there is little difference between the two Phosphor Technology samples, X = 0.25 (sample 1) and X = 0 (sample 2). There is a considerable difference between the X = 0 (sample 1, GTE Sylvania) and X = 0 (sample 2, Phosphor Technology). Our first conjecture is that cerium concentration may play a role. This could be addressed in future investigations. The garnets seem to exhibit most of the characteristics that are required, including the fact that they may be excited with blue light emitting diodes. An emission spectrum in relation to a pressure sensitive paint spectrum is depicted in "Fast Responding Pressure Sensitive Paints Based on High Concentration of Hard Particles in Polymer," (Ponomarev, S. and Gouterman, M., 6th Annual Pressure Sensitive Paint Workshop, 1998). The emission peaks at around 500 nm, but there is a tail that extends into the red. The degree to which this may interfere with PSP emission should be addressed. There appeared to be a small change in decay time with emission wavelength. All the data reported here for Yttrium Aluminum Garnet (YAG) materials and silicates (see below) were for fluorescence monitored at 510 nm.

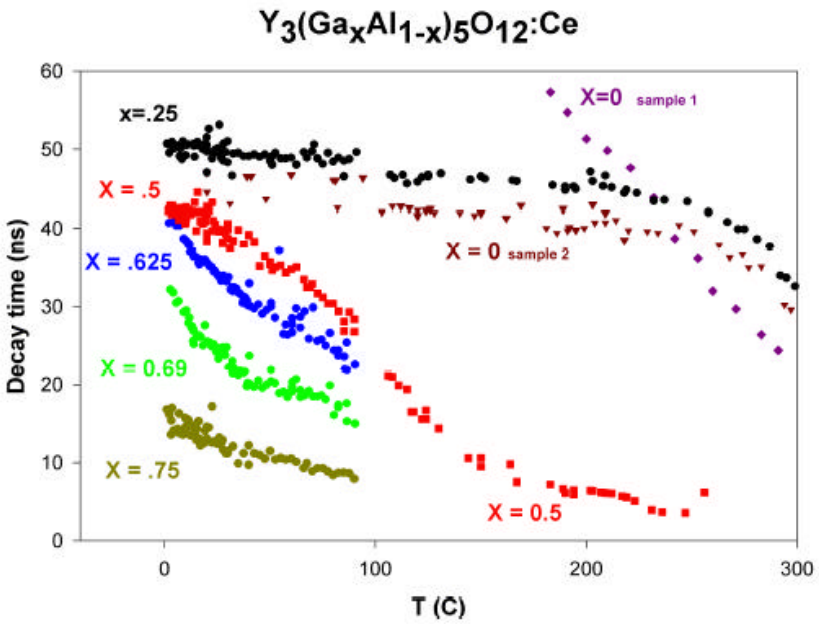

FIGURE 3.2.1.4 Decay Time Verses Temperature for Cerium-Doped Yttrium Garnets

- *Silicates.* Figure 3.2.1.5 shows results for several silicate phosphors that were tested. Last year it was noted that yttrium silicate exhibited a sharp temperature response in the middle of the region of interest, from about 50 to 150 degrees C. It is sometimes the case with thermal phosphors that substitution with lanthanum or gadolinium will shift the temperature response to lower temperatures. Thus lanthanum and gadolinium silicates were procured and tested. They exhibited some temperature dependence over the range. The lanthanum material ranged from about 20 to 5 ns from ambient to 300 degrees C. A greater change per degree would be desirable. The emission for these silicates peaks in the blue region of the spectrum.

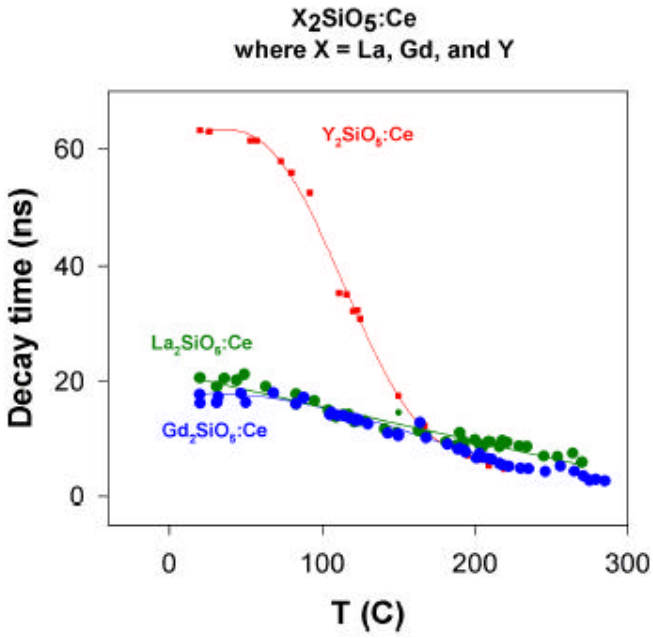

FIGURE 3.2.1.5 Decay Time Verses Temperature for Cerium-Doped Silicates.

The garnet materials hold much promise for fast response applications with pressure sensitive paints. Of course, testing and further development will be required to establish this. Some other garnet materials are on hand for further testing wherein the yttrium is replaced with lanthanum or gadolinium. These could be tested in the future. The yttrium silicate material showed the most striking temperature dependence and so may be the best material for the 50 to 150 degrees C range. The silicates cannot be excited with a blue LED but should be excitable with an ultraviolet LED, blue laser diode, nitrogen laser, or tripled YAG laser.

- PSP. The temporal-response characteristics of PSP have been studied by several groups over the past 10 years. It is generally recognized that a compromise must be made between the response time and the mechanical properties of the paint. While porous surfaces such as silica-gel plates (25 μs) and anodized aluminum (80 μs) have shown extremely fast response to pressure, these surfaces are not practical in many experimental circumstances. Polymer binders have the desirable mechanical properties but lack the necessary temporal response (> 20 ms) for time-resolved pressure measurements. Ponomorev combined Al_2O_3 /$AL(OH)_3$ particles and tetra-butyl methacrylate resin to produce a PSP with a temporal response of 1 ms [Ponomarev, S. and Gouterman, M., "Fast Responding Pressure Sensitive Paints Based on High Concentration of Hard Particles in Polymer," 6th Annual Pressure Sensitive Paint Workshop, 1998]. Scroggin created a PSP surface based on a combination of ceramic TiO_2 particles and an acrylic polymer binder [Scroggin, A., "Processing and Optimization of Doped Polymer/Ceramic Composite Films for Luminescence-Based Pressure and Temperature Measurement in Aerodynamic Applications," M.S. Thesis, Purdue University, 1999]. As part of this work, Scroggin performed a parametric study in which the ratio of the weight of the ceramic particles to that of the polymer binder was varied from 0 to 1. The temporal response of the resulting PSP was determined using a pressure step generated by a shock tube. Scroggin noted that as the weight ratio of the ceramic particles was increased above a critical value, the temporal response of the paints began to improve significantly (Figure 3.2.1.6). At the highest ceramic loading reported, the PSP maintained the desired mechanical properties of the binder and yielded a temporal response of 100 μs.

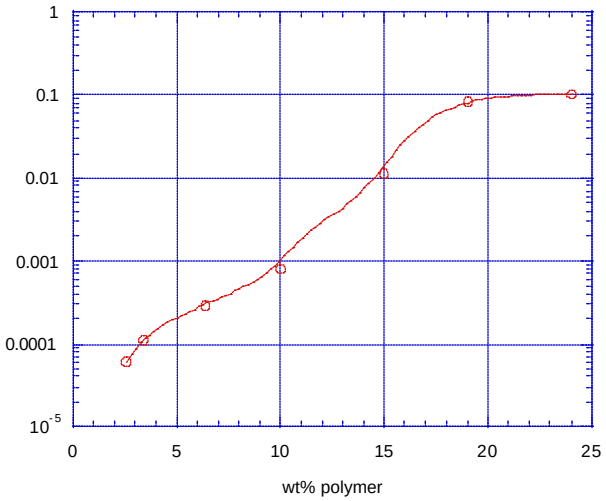

FIGURE 3.2.1.6 Response Time of the PSP to a Pressure Step Versus Weight Percent of Polymer (Scroggin).

Based on the information contained in the preceding discussion, a series of PSP samples were produced in which TiO_2 particles were introduced into the polymer binders of the PSP. Several binders were surveyed, and the ratio of the weight of the ceramic particles to that of the binder was varied from 0 to 0.95. The resulting PSP surfaces were screened for mechanical robustness, and the temporal response of the PSP was tested using the step-response rig shown in Figure 3.2.1.7. The temporal response of four PSPs to the pressure step is plotted in Figure 3.2.1.8. It should be noted that the upper limit of the step-response mechanism shown in Figure 3.2.1.7 is about 2 kHz; therefore, the temporal response of the FIB/TiO_2 paint shown in Figure 3.2.1.8 might be limited by the test mechanism. These results indicate that the use of ceramic particles to increase the porosity of existing PSP formulations should improve their temporal response while maintaining the necessary mechanical properties of the polymer binders.

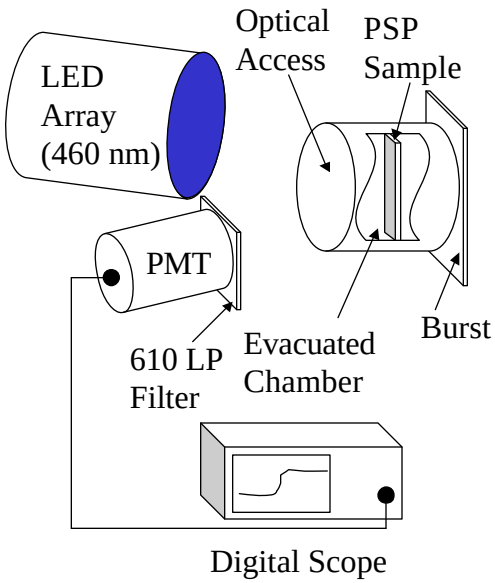

FIGURE 3.2.1.7 Experimental Setup for Response of PSP to Pressure Step.

The modifications necessary to obtain optical access to a shock tube have been completed, and the system has been test fired. The shock tube will serve as a test bed for evaluation of both the pressure- and the temperature-response characteristics of fast (>1 kHz) PSP's. New polymer/ceramic materials are being evaluated to improve the mechanical properties of the fast PSPs.

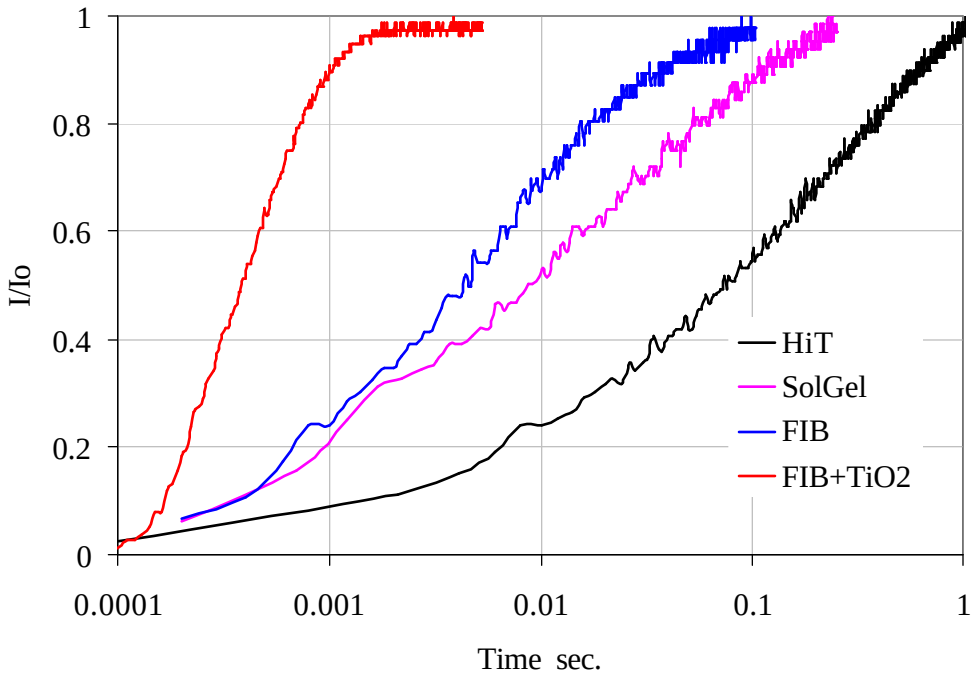

Figure 3.2.1.8 Temporal Response of Several PSPs to a Pressure Step.

Participating Organizations: ISSI

Points of Contact:

Government
Lt Brian Beachkofski
U.S. Air Force, AFRL/PRTC
1950 Fifth Street, Bldg. 18D
Wright-Patterson AFB, OH 45433-7251
Phone: (937) 255-2611
Fax: (937) 255-2660

Contractor
Dr. Larry Goss
ISSI
2786 Indian Ripple Rd.
Dayton, OH 45440-3638
Phone: (937) 252-2706
Fax: (937) 656-4652

3.2.1.2 PSP: Light Emitting Diodes (LEDs)

FY 99-01

Recent Progress

ISSI has developed a commercial product line based upon LED arrays. ISSI LED modules can operate in either a continuous wave or pulsed mode. Both 2" and 4" models are available with a broad selection of LED wavelengths. For turbomachinery applications, a pulsed system is recommended. The peak light output of the LED's can be increased to several times their normal continuous output level by increasing the drive current. This increase, however, requires a corresponding reduction of the duty cycle to ensure the average power dissipation is kept at or below the damage threshold.

The standard ISSI pulsed LED product provides a robust, long life light source with 6 times the light output of the continuous models. Figure 3.2.1.9 displays the drive pulse and corresponding light output for a 4" LED array. The rise times of the optical pulses are less than 0.5 microseconds (0.3 typical) and less than 1.0 microseconds (0.8 typical) for the 2" and 4" LEDs, respectively. The fall times are much faster, 0.15 and 0.2 microseconds respectively. Therefore, the shortest full strength pulse these units can deliver is slightly less than 1 microsecond for the 2", and slightly longer than 1 microsecond for the 4" model. This is sufficient to stop or minimize motion blurring on rotating machinery. Shorter duration pulses are possible at reduced output light levels.

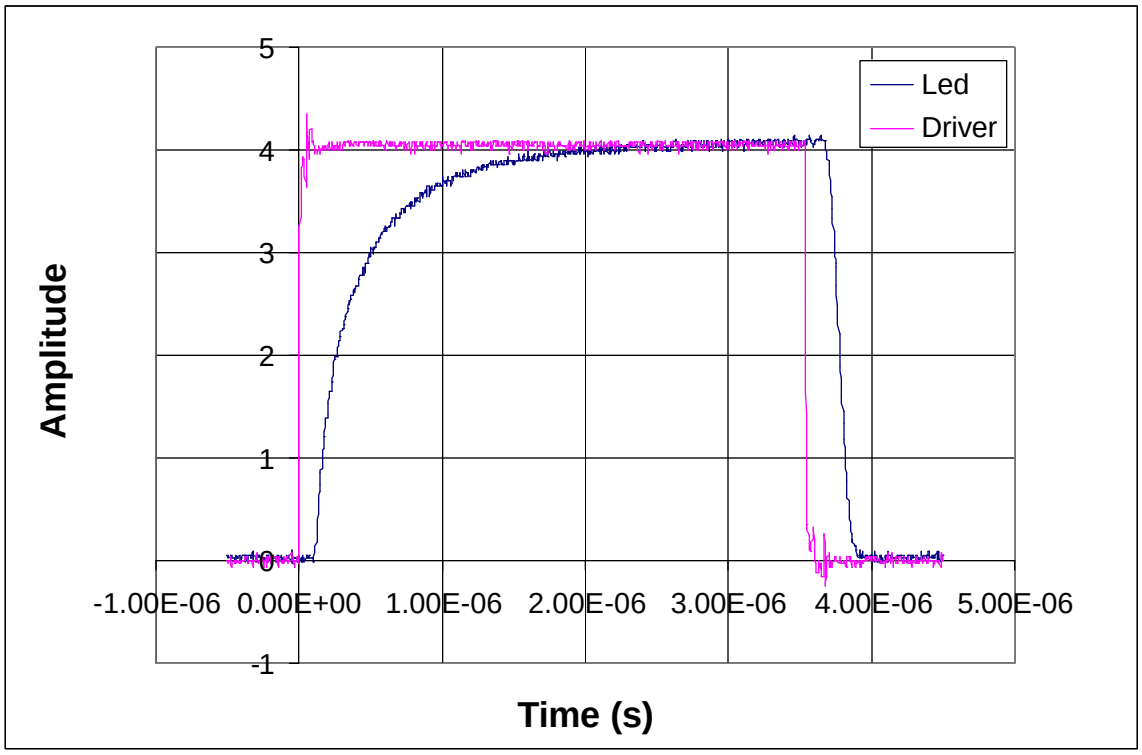

FIGURE 3.2.1.9 Driver Pulse and Corresponding LED Light Output for ISSI's 4" LED Array.

Participating Organizations: ISSI

Points of Contact:

Government
Lt Brian Beachkofski
U.S. Air Force, AFRL/PRTC
1950 Fifth Street, Bldg. 18D
Wright-Patterson AFB, OH 45433-7251
Phone: (937) 255-2611
Fax: (937) 255-2660

Contractor
Dr. Larry Goss
ISSI
2786 Indian Ripple Rd.
Dayton, OH 45440-3638
Phone: (937) 252-2706
Fax: (937) 656-4652

3.2.2 Comparison Testing/Air Etalons

FY 96-99

This effort has been completed. It is described in the 2000 High Cycle Fatigue Annual Report.

3.2.3 Validation of Paint/Optical Pressure Mapping
FY05

There is no progress reported on this effort for CY2001.

Participating Organizations: Rolls-Royce, ISSI

Points of Contact:

Government
Lt Brian Beachkofski
U.S. Air Force, AFRL/PRTC
1950 Fifth Street, Bldg. 18D
Wright-Patterson AFB, OH 45433-7251
Phone: (937) 255-2611
Fax: (937) 255-2660

Contractor
Mr. Thomas Bonsett
Rolls-Royce
Speed Code W03A, P.O. Box 420
Indianapolis, IN 46206-0420
Phone: (317) 230-3448
Fax: (317) 230-4246

3.2.4 Wireless Telemetry
FY 00-02

There is no progress reported on this effort for CY2001.

Participating Organizations: NASA Glenn Research Center

Point of Contact:

Government
Dr. Jih-Fen Lei
NASA Glenn
Cleveland, OH
Phone: 216-433-3922
Fax: 216-433-8643

3.2.5 MEMS Pressure Sensor
FY 00-02

There is no progress reported on this effort for CY2001.

3.2.6 Aluminum Nitride (AlN) Sensors
FY 00-06

There is no progress reported on this effort for CY2001.

3.3 Improved Conventional Sensors

To date, prediction of aerodynamic forcing functions has been difficult or impossible due to lack of Computational Fluid Dynamics (CFD) fidelity, structural modeling accuracy, instrumentation effects, and insufficient characterization of instrumentation installation effects. The purpose of the projects described below is to improve the lifetime and performance of conventional sensors (eddy current/strain gauges) for transition into engine health monitoring applications.

3.3.1 Non-Optical NSMS Sensor Development (Eddy Current)
FY 99-02

Effort prior to 2001 is described in the 2000 High Cycle Fatigue Annual Report.

Recent Progress

Eddy Current Sensor System Development for 2001

In 2001, General Dynamics Advanced Technology Systems (GDATS) completed a new eddy current sensor (ECS) system. The new system, referred to as Build 5, has most of the characteristics of Build 4 sensor, i.e. it utilizes a ceramic core with a larger 0.5-inch diameter to achieve a single pass, single blade clearance resolution of 0.005 inch at a stand-off distance of 0.300 inch. An impedance matching circuit, which was previously housed outside the sensor, is now included in the sensor body providing a lower profile for the sensor. Key components of the system are shown in Figure 3.3.1.1.

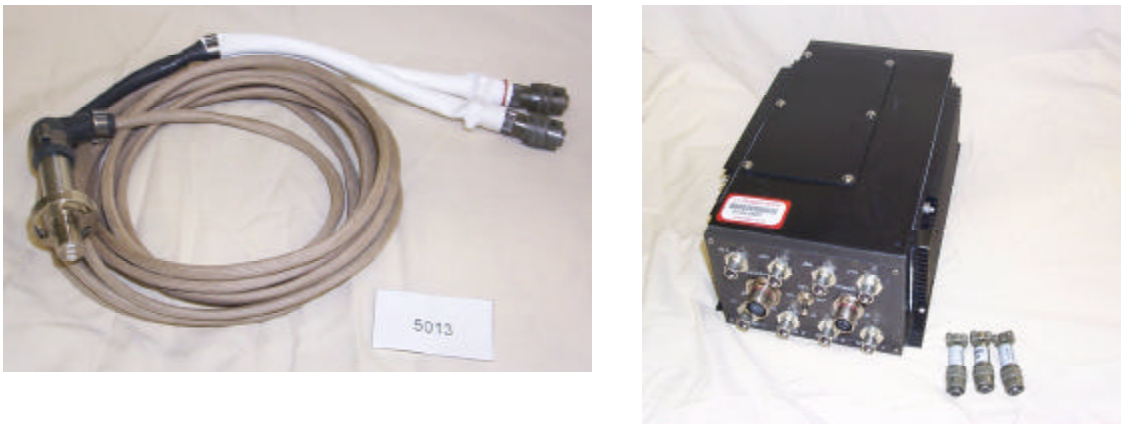

(a) (b)

FIGURE 3.3.1.1 a) Sensor and Cabling b) Signal Processor

In addition, the groundwork for a digital signal processor (DSP)-based real-time signal processing system was completed, proving that a single DSP chip (TI C6701) coded in machine language can monitor and extract critical ECS waveform parameters from up to 4 sensors at a sampling rate of 1 MHz. Currently the DSP platform contains two DSP modules and a multi-channel sampling module programmed to extract these parameters in real-time, format the data into large packets, and pass these packets to the host PC for storage on hard disk. Data bandwidths in excess of 2 Mbytes/sec to disk

have been achieved, simulating capability to maintain real-time processing and data storage for 4 sensors mounted on a jet engine with 50 blades spinning at 10,000 RPM. Figure 3.3.1.2 below provides details of the platform in development. A simple graphical user interface will enable the system to be used at engine test sites.

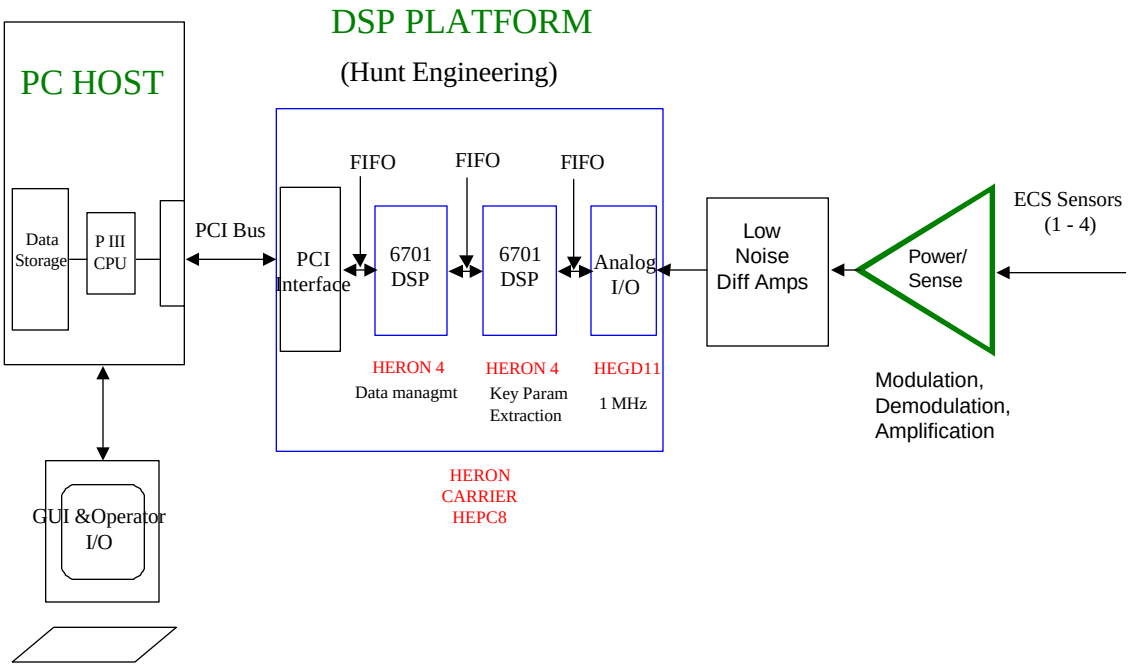

Figure 3.3.1.2 Eddy Current Sensor Signal Processing System

Participating Organizations: Pratt & Whitney

Points of Contact:

Government
Lt Brian Beachkofski
U.S. Air Force, AFRL/PRTC
1950 Fifth Street, Bldg. 18D
Wright-Patterson AFB, OH 45433-7251
Phone: (937) 255-2611
Fax: (937) 255-2660

Contractor
Mr. Robert Morris
Pratt & Whitney
M/S 707-22, P.O. Box 109600
West Palm Beach, FL 33410
Phone: (561) 796-5981
Fax: (561) 796-7454

3.4 Development of Long-Life, Less-Intrusive Strain Gauges

The following sections describe NASA's efforts to develop long-life, less-intrusive strain gauges.

3.4.1 Advanced Thin-Film Dynamic Gauges

FY 95-02

Background

The objective of this program is to develop and utilize the already successful NASA PdCr static strain gauges in a thin-film form for dynamic strain measurement. Thin-film sensors are fabricated directly onto the test surface using vapor deposition and lithography techniques. They do not require additional bonding agents, such as adhesive or cements, and are in direct contact with the test surface. Thin-film sensors in general have a thickness on the order of a few micrometers (μm) and are much thinner than the commonly used sensor wires. They have fast response times (in milliseconds), add negligible mass to the test surface, and create minimal disturbance of the gas flow over the surface. Consequently, thin-film sensors have minimal impact on the thermal, strain, and vibration patterns that exist in the operating environment, and they provide a minimally intrusive means of accurate measurement of surface parameters.

Recent Progress

During calendar year 2000, the PdCr thin-film strain gauges were fabricated and dynamically evaluated on a nickel-base superalloy at NASA Glenn. The dynamic response of these gauges was characterized in a newly-set-up shaker facility under ±2000 microstrain, 1,100 Hz to 700C. The lifetime of this PdCr-based thin-film gauge was compared to the conventional foil strain gauges at room temperature. Only two of the six commercial foil gauges (33%) survived after only 3.5 minutes dwell at 1,100 Hz, while all four PdCr gauges remained functional after a 50 minutes dwell exposure. The test at high temperature was postponed because the test bar cracked and broke; no gauge delamination was observed. Meanwhile, NASA Glenn provided funding to Honeywell (AlliedSignal Engine) to apply nine thin-film strain gauges, three per stage, on the stages 2, 3 and 4 gamma blades of a Pratt & Whitney engine XTC67/1 compressor. However, due to the surface imperfection of the compressor blades, which required additional time to redo the thin-film gauges, Pratt & Whitney decided not to apply thin-film sensor technologies for validation.

The engine test effort has not yet been completed to demonstrate and document the increased durability that comes with using thin film strain gauges over conventional stain gauges. Honeywell has sputtered the strain gauges and Pratt & Whitney will run the test in Connecticut and then report the results back through NASA Glenn. This effort is expected to be completed in 2002.

Participating Organizations: NASA Glenn Research Center, Honeywell Engines and Systems, Pratt & Whitney

Points of Contact:

Government
Dr. Jih-Fen Lei
NASA Glenn
Cleveland, OH
Phone: 216-433-3922
Fax: 216-433-8643
Email: jih-fen.lei@grc.nasa.gov

Contractor
Harvey Niska
Honeywell Engines and Systems
Phoenix, AZ
Phone: 602-231-7584
Fax: 602-231-2018
Email: h.niska@alliedsignal.com

3.4.2 Advanced High-Temperature Thin-Film Dynamic Gauges
FY 96-02

There is no progress reported on this effort for CY2001.

3.5 Conclusion

Much progress has been made in establishing the Generation 4 NSMS capability at Arnold Engineering Development Center (AEDC). Twelve of the twenty-four channels are operational and will be use to validate Generation 4 capabilities during the testing of XTC67/1 in CY2002. Software development for the AEDC capability continues, while in the meantime Pratt & Whitney proprietary software will be used for the XTC67/1 testing.

Use of NSMS in spin pit testing has been successfully demonstrated, and progress has been made on extending this instrumentation capability to small engines as well. In addition, the exploration of eddy current sensors for use in NSMS is continuing.

Progress has been made with pressure and temperature sensitive paints; however, issues remain with the level of accuracy that can be achieved because of the influence of both pressure and temperature on the paint's response. The need to know pressure to determine temperature or temperature to determine pressure from the paint's response may limit its accuracy sufficiently to also limit the usefulness of this instrumentation technique for HCF-related testing.

MEMS and thin film devices will require further development before their promise can be realized.

4.0 COMPONENT ANALYSIS

BACKGROUND

The Component Analysis Action Team (Component Analysis AT) is responsible for fostering collaboration among individual HCF component analysis efforts, with the overall goal of combining with the Instrumentation and Forced Response ATs to better determine alternating stresses to within 20%. The Component Analysis AT provides technical coordination and communication among active participants involved in HCF component analysis technologies. Annual technical workshops have been organized and summaries of these workshops are disseminated to appropriate individuals and organizations. The Chair, Co-Chair, and selected Component Analysis AT members meet as required (estimated quarterly) to review technical activities, develop specific goals for component analysis projects, and coordinate with the TPT and IAP. The Chairman (or Co-Chair) of the Component Analysis AT keeps the TPT Secretary informed of AT activities on a frequent (at least monthly) basis. This AT includes members from government agencies, industry, and universities who are actively involved in component analysis technologies applicable to engine HCF. The team is to be multidisciplinary with representatives from multiple organizations representing several component technologies as appropriate. The actual membership of the AT may change in time as individuals assume different roles in related projects.

ACTION TEAM CHAIRS

Chair
Mr. Jeff Brown
U.S. Air Force, AFRL/PRTC
1950 Fifth Street, Bldg. 18D
Wright Patterson AFB, OH 45433-7251
Phone: (937) 255-2611
Fax: (937) 255-2660

Co-Chair

Naval Air Systems Command
AIR 4.4.7.2 Bldg. 106
22195 Elmer Road, Unit #4
Patuxent River, MD 20670-1534
Phone: (301) 757-0500
Fax: (301) 757-0562

INTRODUCTION

The following pages summarize the schedules, backgrounds, and recent progress of the current and planned projects managed by this action team.

FIGURE 4.0 Component Analysis Research Schedule

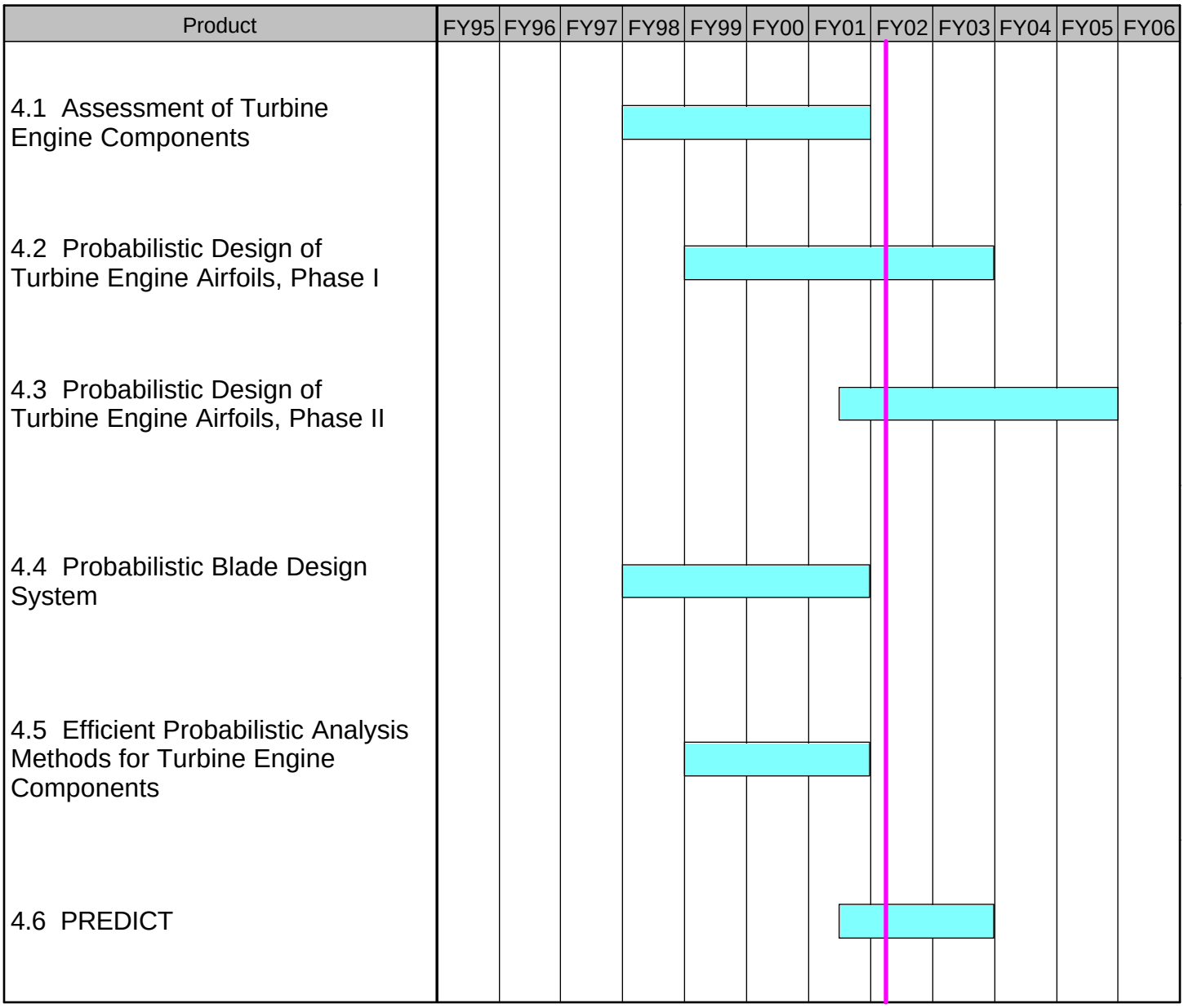

4.1 Assessment of Turbine Engine Components
FY 98-01

Background

Activities on this program are focused on analytical models of the complex behavior encountered in turbine engine design, including improvements in both model physics and computational efficiency.

This effort is now complete. Over its lifespan it addressed many areas critical to the HCF prediction, such as the blade frequency prediction accuracy, FOD damage modeling, new dynamic material models, mistuning, and support for the Turbine Engine Fatigue Facility.

Recent Progress

An effort was aimed at providing tools for estimating errors in finite element natural frequency predictions. This effort was successfully completed and a capability now exists that can bound the frequency prediction error based on the mesh density of model. This capability will be used as a design tool to estimate and include model error as a factor in future designs.

UDRI conducted an effort to determine if Selective Laser Sintering (SLS) could be utilized as a cost-effective means to generate hardware for limited performance testing. If successful, SLS would allow more experimental validation earlier in the design cycle, which should result in performance improvements, reduced programmatic risks, and ultimately, improved design codes, because of the more abundant experimental data. It was determined, however, that current state-of-the-art SLS materials were inappropriate for realistic HCF testing. Advancements in SLS material capabilities will be monitored, and at such a time that improved material capabilities are available, this approach will be reassessed.

Simulations of the XTE-66/SE TiAl compressor blade performed as part of this program have clarified the role of foreign object damage in design using more brittle high-temperature materials and have identified the need for improved models of nonlinear material response and failure. A preliminary version of such a model has been developed and is being tested currently. To investigate the influence of typical FOD events on high cycle fatigue of advanced materials, impact damage was inflicted on several TiAl and nickel compressor blades, which next will be tested under HCF loading conditions. This research has given an improved capability to assess the life of TiAl components.

This program recently completed a comparison of several three-dimensional contact analysis approaches. The investigation showed that contact stress analyses from ABAQUS, Capri, and an in-house contact code all correlated well with analytical solutions for cylindrical contact problems on basic geometry.

Participating Organizations: University of Dayton Research Institute

Points of Contact:

Government
U.S. Air Force, AFRL/PRTC
1950 Fifth Street, Bldg. 18D
Wright Patterson AFB, OH 45433-7251
Phone: (937) 255-2611
Fax: (937) 255-2660

Contractor
University of Dayton Research Institute
300 College Park
Dayton, OH 45469-0110
Phone: (937) 229-3484
Fax: (937) 229-4251

4.2 Probabilistic Design of Turbine Engine Airfoils, Phase I

FY 99-03

Background

The objective of this effort is to establish the best practices for HCF probabilistic risk assessment, life prediction, and design procedures. STI Technologies, Inc. is the prime contractor, but all major engine companies (P&W, GEAE, Allison, and Honeywell) are actively participating in the contract.

The proposed probabilistic methods and approaches are intended to improve the overall engine design system. Probabilistic design methods will assist the turbine engine industry and responsible government agencies by reducing HCF-related costs and by improving safety by: (1) providing a better engine design "out of box," (2) providing a methodology to develop bench, rig, and engine testing plans that identify and characterize potential HCF problems, (3) providing a methodology to track HCF "life" in the field, and (4) enabling the PPGM to schedule regular HCF maintenance intervals and to accurately assess future needs for spare parts. Probabilistic models will be developed that incorporate refinements to the design process of gas turbine fan blades through the use of advanced stochastic modeling of the HCF-related phenomena, with a special focus on blade forced response, including unsteady aero-forcing, damping and flutter, mistuning, manufacturing effects, and other critical aspects. Finally, an integrated probabilistic HCF prediction system capable of incorporating the rapid technological developments and new information from test and field data will be implemented.

These best practices will: (1) significantly improve the fundamental engineering process for interpreting the complex, random phenomena involved in blade design, (2) develop more efficient tools for probabilistic modeling using advanced stochastic concepts and models, (3) apply probabilistic approaches to evaluate existing or fielded designs, (4) develop methods for updating probabilistic assessments with information from both experimental and analytical data sources, (5) identify requirements for blade and specimen data and conduct testing where appropriate, and (6) identify requirements for component, rig, and engine testing.

Recent Progress

Over the last year, substantial progress has been made towards the development of a probabilistic blade analysis and design process. Strides were made in the area of stochastic field modeling of spatial data, integration with Test Protocol development, and development of a probabilistic design framework.

Development of stochastic field modeling capabilities enables simulation of complex spatial data that is relevant to significant mechanisms of HCF response. These mechanism include blade frequency, mode shape, forcing function and forced response. Each of these mechanisms is strongly influenced by spatial variations such as geometry and pressure fields that must be modeled with stochastic fields. During the last year, stochastic field methods were developed and validated with test data. These methods will enable future prediction of the distribution of response.

An integration with the Test and Evaluation team developing the Test Protocol was initiated in the last year. It began with a white paper describing how many tests are required to validate a probabilistic design and led to a joint meeting between the Test and Evaluation Team and the Component Analysis Action Team. Now, both teams have a better understanding of the goals and progress each has made, and plans for more joint work are being pursued. Part of this joint work will include the integration of both test and analysis capabilities in an overall design framework.

The design framework is based upon tracking and documenting uncertainty throughout the development process. The contract for this effort will build on a design process developed by Los Alamos National Labs, called Information Integration Technology, and advance it to meet the needs of the engine industry. The process combines expert opinion, historical experience, analysis and testing to determine the current capability of a design along with an uncertainty bound to quantify the knowledge, or lack of it, about the design in question.

Together, these three areas of progress have built a firm foundation for further developments under this program.

Participating Organizations: STI Technologies, General Electric, Pratt & Whitney, Allison Advanced Development Co., GE Aircraft Engines, Honeywell Engines and Systems, Virginia Tech.

Points of Contact:

Government
U.S. Air Force, AFRL/PRTC
1950 Fifth Street, Bldg. 18D
Wright Patterson AFB, OH 45433-7251
Phone: (937) 255-2611
Fax: (937) 255-2660

Contractor
STI Technologies, Inc.
1800 Brighton-Henrietta Town Line Rd.
Rochester, NY 14623-2572
Phone: (716) 424-2010
Fax: (716) 272-7201

4.3 Probabilistic Design of Turbine Engine Airfoils, Phase II

FY 01-05

Background

Phase II will make any required improvements to the probabilistic forced response approaches developed in Phase I, enhance the probabilistic material modeling, and work towards validating probabilistic predictions and designs.

Recent Progress

The phase II effort was funded as a PRDA VII program, scheduled to be on contract in February 2002. Under this program, further work toward probabilistic blade analysis and design will be conducted. Highlights of this effort include continuation of the development of the analysis and design processes, validation of these processes in demonstrator engine tests, and "mining" of existing data at AEDC. The data mining effort will produce a database of engine test results, conditions, and instrumentation that can be used as basic inputs to probabilistic analysis.

Participating Organizations: Pratt & Whitney, GE Aircraft Engines, Honeywell, AADC

Points of Contact:

Government
U.S. Air Force, AFRL/PRTC
1950 Fifth Street, Bldg. 18D
Wright Patterson AFB, OH 45433-7251
Phone: (937) 255-2611
Fax: (937) 255-2660

Contractor
STI Technologies, Inc.
1800 Brighton-Henrietta Town Line Rd.
Rochester, NY 14623-2572
Phone: (716) 424-2010
Fax: (716) 272-7201

4.4 Probabilistic Blade Design System

FY 98-01

Background

Probabilistic analysis capabilities are being investigated in the areas of response variability due to blade mistuning, fracture screening, and manufacturing geometry variation. Application of these techniques to several blades will provide guidance for the incorporation of such capability into a mainstream blade design system.

Recent Progress

Investigation of blade-to-blade response variability due to mistuning continued, using the REDUCE computer code developed at the University of Michigan. Two military fan blades were used in this study: one that has exhibited a substantial amount of response variation and another that has shown low variability. Analysis showed that REDUCE was able to predict the level of variation of blade maximum amplitudes relatively well but was not able to accurately predict the response of individual

blades. It provided correct trend information to differentiate rotors with the potential for relatively higher or lower blade-to-blade variation. This work indicates that REDUCE provides worthwhile guidance and insight in predicting potential harmful blade-to-blade response variation.

Fracture Screening to consider the effects of surface damage due to foreign object damage (FOD) has been worked using the Probabilistic Design Analysis System (PDAS) analysis environment, which was developed under the Probabilistic Rotor Design System (PRDS) contract. The basic infrastructure developed for PRDS has been extended for blade applications to assess the probability of exceeding the crack growth threshold, using probabilistic fracture mechanics with the capability of considering distributions of material data, leading edge (LE) damage, strain distribution, and amplitude variability. PDAS was used to link several computational modules to determine the overall failure probability of a front stage military fan. Static and modal finite element stress solutions were developed to consider airfoil geometric variations; blade-to-blade variability in rotor builds was predicted using REDUCE; and probabilistic fracture mechanics was used to predict the impact of randomly placed surface defects. This aspect of the study successfully demonstrated the mechanics of linking together the various modules. However, there is uncertainty about which fracture mechanics modeling and damage distributions should be applied. Additionally, reliable predictions of absolute forced response levels are inherently difficult. These aspects combine to yield failure probabilities having less certainty than the prior disk work.

The ability to simulate response variability due to manufacturing variations has also been studied through adaptation of a conventional design/analysis toolkit used routinely for deterministic blade finite element analysis. Airfoil manufacturing inspection data from a military fan were analyzed to determine the fundamental geometric variations exhibited by the manufacturing process. These patterns were characterized by a reduced set of "manufacturing modes" consisting of correlations of traditional airfoil design parameters. The design/analysis toolkit was adapted to apply such correlated variables in response simulations. The toolkit was further extended to provide direct access to probabilistic analysis services including Design of Experiments, Response Surface determination, and Monte Carlo simulation. Application of the tool to simulate modal response variation of a population of fan blades, constructed according to the patterns of variation exhibited by the manufacturing variations, yielded reasonable predictions of frequency variation that were consistent with typical design experience.

This GEAE developed system conducted preliminary work towards the development of a probabilistic blade design system. The work is now complete and has provided a solid beginning toward the development of a probabilistic blade design system.

Participating Organizations: GE Aircraft Engines

Points of Contact:

Government
U.S. Air Force, AFRL/PRTC
1950 Fifth Street, Bldg. 18D
Wright Patterson AFB, OH 45433-7251
Phone: (937) 255-2734
Fax: (937) 255-2660

Contractor
GE Aircraft Engines
1 Neumann Way
Mail Drop A405
Cincinnati, OH 45215
Phone: (513) 243-3337
Fax: (513) 243-1343

4.5 Efficient Probabilistic Analysis Methods for Turbine Engine Components

FY 99-01

Background

Development of efficient and accurate methods for the reliability analysis of large-scale engine component models is the main goal of the project. For practical engine components, there are potentially dozens of uncertain variables, and the designers need to use robust techniques that can accurately predict the failure probability with a minimum number of simulations. Under this research effort, methods are being developed that use high-quality function approximations to reduce the computational cost of simulations. The simulations are typically carried out using finite element methods and computational fluid dynamics procedures. The project team developed methods based on Fast Fourier Transformation (FFT) techniques for accurately predicting the failure probability for highly nonlinear limit-states and non-normal distributions. To validate the concepts, several highly nonlinear analytical functions and structures modeled with truss and plate members were considered with normal, log-normal, and Weibull distributions. The results obtained using FFT were compared with the Monte Carlo simulations.

Recent Progress

Currently, emphasis is being placed on instances involving multiple failure modes, such as the uncertain natural frequencies and critical stresses. In these cases, the formulation needs to consider the system reliability instead of just the individual failure mode. Techniques are being developed based on multi-point function approximations to construct a representation for the physical behavior of multiple functions. Once a representative model is developed, the designers will be able to use a Monte Carlo simulation on this analytical representation and compute the system failure probability. This work is in progress and will be demonstrated on turbine engine components. A schematic of airfoil stochastic analysis is shown in Figure 4.5.

This effort is now complete. The program developed advanced probabilistic integration algorithms that increase the computational efficiency for approximate solutions. These tools are available for the industry as probabilistic methods.

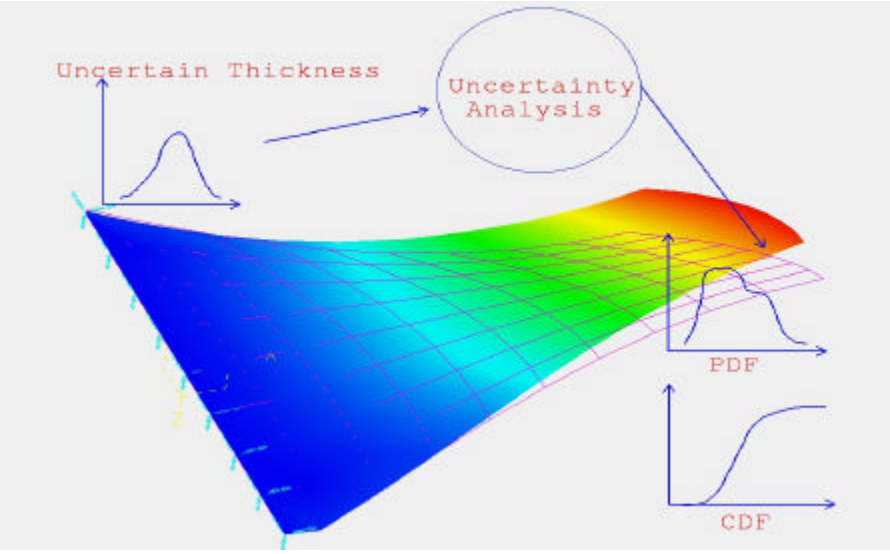

FIGURE 4.5 Airfoil Stochastic Analysis

Participating Organizations: Wright State University

Points of Contact:

Government
U.S. Air Force, AFRL/PRTC
1950 Fifth Street, Bldg. 18D
Wright Patterson AFB, OH 45433-7251
Phone: (937) 256-5530
Fax: (937) 255-2660

Contractor
Wright State University
3640 Colonel Glenn Hwy
Dayton, OH 45435-0001
Phone: (937) 775-5090
Fax: (937) 775-5147

4.6 PREDICT

FY 01-03

Background

PREDICT is a process that assesses a component's failure probability throughout its design, test, and field experience. It has been used with great success in the nuclear and manufacturing industries. The process creates the framework for the implementation of the probabilistic design system. PREDICT combines physics-based distributional models of critical contributors into a model for overall blade HCF failure probability estimation. The process also guides the development of initial design parameter assessments that capture expert opinion and similarity to previous designs in a structured manner to remove bias.

Recent Progress

This effort is being done in collaboration with the blade design contracts, and its objective is to demonstrate the techniques of a new design process. This process integrates expert opinion, historical data, analysis, and test data to quantify the capability of a design and the uncertainty in the capability assessment. Over the last year, meetings were held with the Forced Response Action Team and individually with each industry partner. These meetings have led to the identification of a detailed process that leads to blade frequency prediction and estimates of the parameters' variations that are critical to that process.

Participating Organizations: Pratt & Whitney, GE Aircraft Engines, Honeywell, AADC, LANL, NASA

Points of Contact:

Government
U.S. Air Force, AFRL/PRTC
1950 Fifth Street, Bldg. 18D
Wright Patterson AFB, OH 45433-7251
Phone: (937) 255-2611
Fax: (937) 255-2660

Contractor
Statistical Sciences Group, D-1
Los Alamos National Laboratory
MS F600
Los Alamos, NM 87545
Phone: 505-667-1479
Fax: 505-667-4470

4.7 Conclusion

The Component Analysis Action Team continued the government/industry/university team activities, making substantial progress towards the development of a process for probabilistic analysis and design. Key accomplishments have been made on some fundamental needs for probabilistics for blade analysis, including stochastic field modeling, test protocol integration, and development of a framework for the process.

5.0 FORCED RESPONSE PREDICTION

BACKGROUND

The responsibility of the Forced Response Prediction Action Team (FRAT) is to foster collaboration between individual HCF forced response efforts and the Instrumentation and Component Analysis ATs in order to determine alternating stresses to within 20%. The Forced Response AT provides a means for technical coordination and communication between active participants involved in HCF unsteady aerodynamics and blade response technologies. Annual technical workshops have been organized and workshop summaries are disseminated to appropriate individuals and organizations. The Chair, Co-Chair, and selected Forced Response AT members meet as required to review technical activities, develop specific goals for forced response programs, and coordinate with the TPT and IAP. The Chairman (or Co-Chair) of the Forced Response AT keeps the TPT Secretary informed of AT activities on a frequent basis. This AT includes members from government agencies, industry, and universities who are actively involved in forced response technologies applicable to engine HCF. The team is to be multidisciplinary with representatives from multiple organizations representing several component technologies as appropriate.

ACTION TEAM CHAIRS

Chair
Dr. Charles J Cross
U.S. Air Force, AFRL/PRTC
1950 Fifth Street, Bldg. 18D
Wright Patterson AFB, OH 45433-7251
Phone: (937) 656-5530
Fax: (937) 656-5532

Co-Chair
Mr. George Stefko
NASA Glenn Research Center
Mail Stop 49-8
21000 Brookpark Road
Cleveland, OH 44135-3191
Phone: (216) 433-3920
Fax: (216) 977-7051

Co-Chair
1Lt Chris Blackwell
U.S. Air Force, AFRL/PRTF
1950 Fifth Street, Bldg. 18D
Wright Patterson AFB, OH 45433-7251
Phone: (937) 255-4738

INTRODUCTION

The following pages summarize the schedules, descriptions, and progress of the current and planned projects managed by this action team.

FIGURE 5.0.1 Forced Response Research Schedule

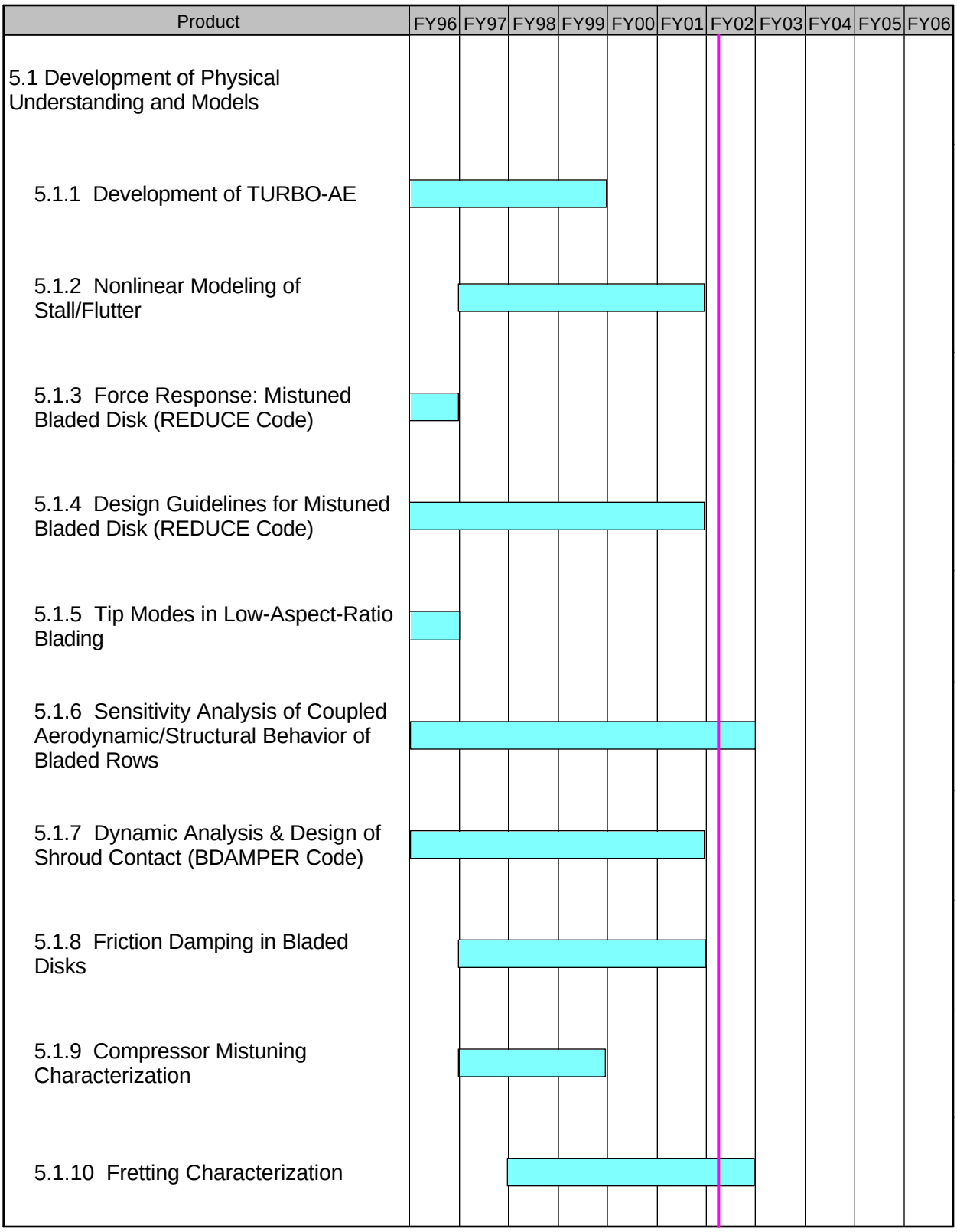

FIGURE 5.0.2 Forced Response Research Schedule (2)

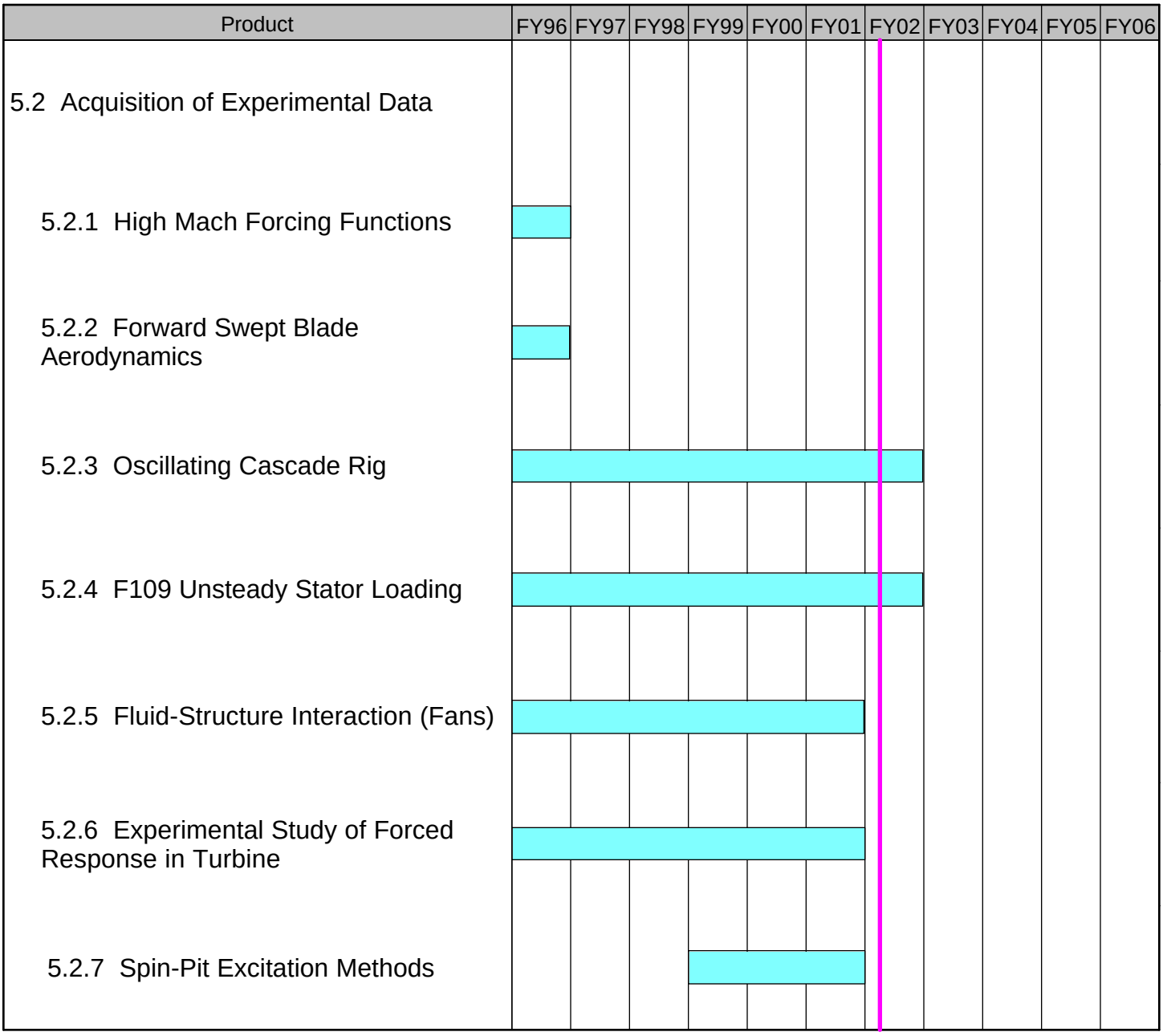

FIGURE 5.0.3 Forced Response Research Schedule (3)

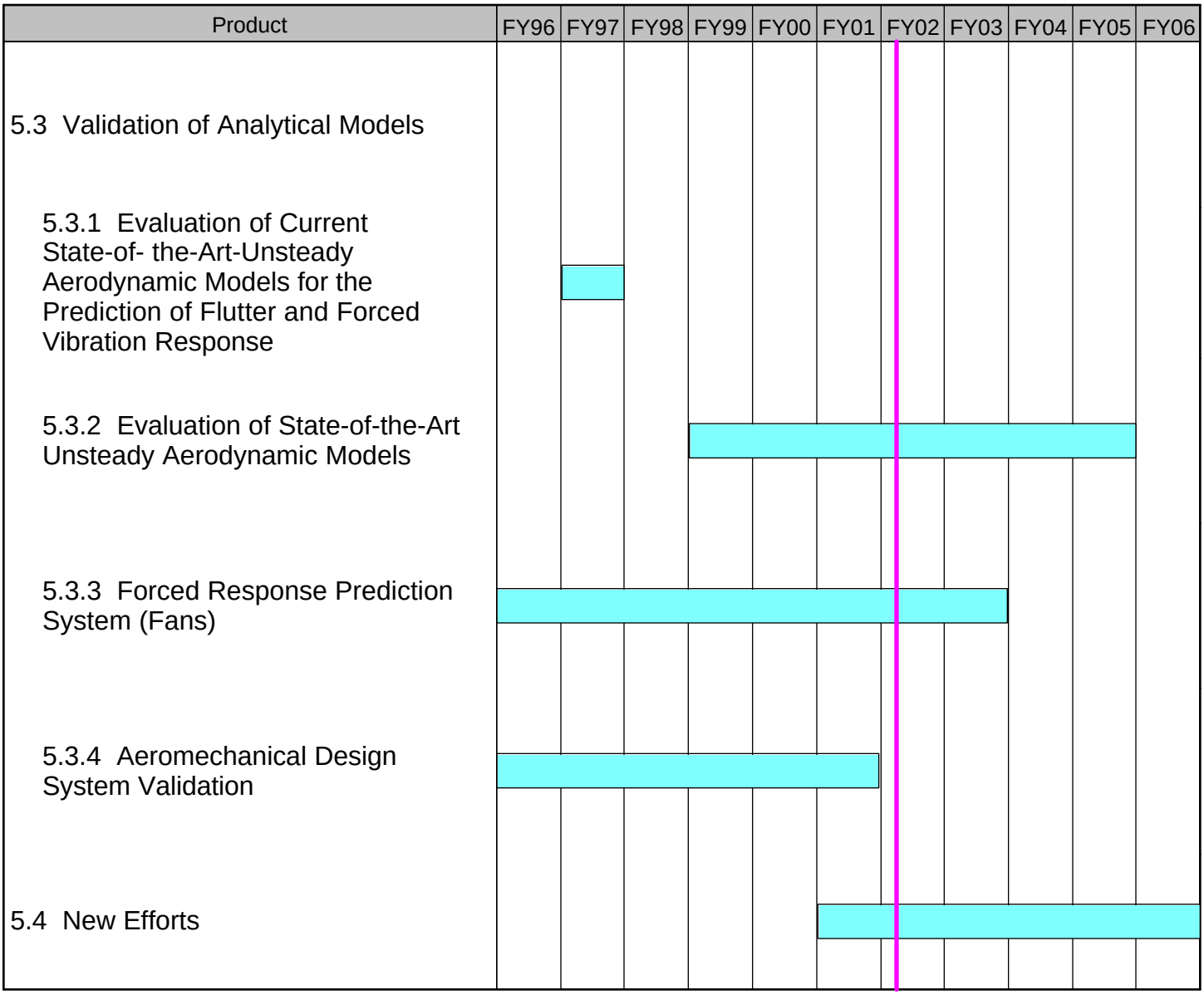

5.1 Development of Physical Understanding and Models

Predicting forced response is difficult due to the lack of Computational Fluid Dynamics (CFD) fidelity and structural modeling accuracy. Improvements in both structural response modeling and the development of increased fidelity CFD have greatly improved the ability to predict forced response. With each increase in capability, new challenges are identified and efforts are developed to enhance the knowledge of the underlying physics of the aerodynamic forcing functions and the structural system response. The emphasis of the following projects is to develop the necessary modules for improved forced response prediction.

5.1.1 Development of TURBO-AE

FY 96-99

(This effort has been completed. Reference 2000 HCF Annual Report, Section 5.1.1 for more details.)

5.1.2 Nonlinear Modeling of Stall/Flutter

FY 97-01

Background

The objective of this project is to investigate the use of reduced-order modeling (ROM) techniques to simulate linear and nonlinear stall flutter in cascades. Research will be conducted in three main areas: (1) the development of a time-domain, linearized Navier-Stokes analysis; (2) the development of an efficient eigenmode extraction code for large systems of equations; and (3) the development of reduced-order modeling techniques to model nonlinear unsteady flows, especially phenomena such as hard flutter boundaries and limit cycle behavior.

Final Results

Research has been conducted in two main areas: (1) the use of proper orthogonal decomposition (POD) techniques, and (2) the use of a novel harmonic balance technique for computing periodic but nonlinear unsteady flows in turbomachinery. Of these two techniques, the harmonic balance technique has proven to be the most useful for turbomachinery applications. Using this approach, the unsteady flow is assumed to be composed of harmonics of the excitation frequency—blade-passing frequency in the case of wake/rotor interaction; blade vibratory frequency in the case of flutter. Borrowing from the structural dynamics community, the harmonic balance technique was then used to write a set of coupled partial differential equations for the unknown flow solution at each harmonic. Finally, after introducing a pseudo-time term into the harmonic balance equations so that they may be solved by time marching, these equations are solved using conventional CFD techniques.

The method has a number of distinct advantages over the more conventional time-domain solutions. First, because the solutions are computed in the frequency domain, the time-marching algorithm is only used to converge the solution to steady state. Thus, acceleration techniques, including pseudo-

time time marching with multiple-grid acceleration, can be used. Second, complex periodicity conditions may be applied for each harmonic, so that the computational domain may be reduced to a single blade passage. Finally, for many applications where "engineering accuracy" is required, the harmonic balance series can be truncated to just a few harmonics. The result is that the present method is potentially two orders-of-magnitude faster than conventional time-marching methods. Recently, the method has been applied to the Navier-Stokes equations with turbulence models. We have been able to predict both the onset of flutter and limit cycle behavior in a front stage compressor.

Participating Organizations: GUIde*, Air Force Research Laboratory (AFRL), NASA

> ***(*) About GUIde:*** *The GUIde Consortium was formed in 1991 when a number of companies joined with Carnegie Mellon University and Purdue University to form a partnership that would result in improved technology for understanding the problem of forced response in turbine engines. The "GUIde" acronym stands for "Government, Universities, and Industry" working together for a specific goal. The consortium is a precursor to the current national HCF program. The consortium consists of members from the US Air Force (Air Force Research Laboratory and the Air Force Academy), NASA, all four major engine manufacturers (GE, Pratt & Whitney, Allison and Honeywell Engines and Systems) and academia (Ohio State, University of California at Davis, Purdue, Carnegie Mellon, University of Michigan, Duke, and Notre Dame). Together, the consortium works to address shortfalls in alternating stress prediction capability with the academic and industrial members developing or validating new codes funded by the government and industry. Some of GUIde's early codes are currently being integrated into the design systems of the engine manufacturers.*

Points of Contact:

Government
Dr. Antole Kurkov
NASA Glenn Research Center
NASA Glenn Research Park
21000 Brookpark Rd., M/S 49-8
Cleveland, OH 44135-3191
Phone: (216) 433-5695
Fax: (216) 977-7051

Contractor
Dr. Kenneth C. Hall
Duke University
Dept. of Mechanical Engineering & Materials Science
School of Engineering
P.O. Box 90300
Duke University
Durham, NC 27708-0300
Phone: (919) 660-5328
Fax: (919) 660-8963

5.1.3 Forced Response: Mistuned Bladed Disk (REDUCE Code)
FY 92-96

(This effort has been completed. Reference 2000 HCF Annual Report, Section 5.1.3 for more details.)

5.1.4 Design Guidelines for Mistuned Bladed Disks (REDUCE Code)
FY 96-01

Background

The objective of this project is to develop a program for analysis and design of mistuned bladed disks based on REDUCE (first developed under GUIde I).

Recent Progress

Version 3.0 of REDUCE has been released to the GUIde Consortium. This is the final version of the REDUCE code. The main improvement since the previous version is that the code has been made compatible with the Fortran compilers on Silicon Graphics and IBM UNIX workstations, which are used by the Air Force, NASA, and other organizations. In fact, REDUCE 3.0 has been compiled successfully on all major UNIX platforms, on Linux, and on Windows-based PCs.

In addition, a more powerful, accurate, and efficient reduced order modeling technique has recently been developed. Based on this method, a new code called Turbo-Reduce has been written. The second version of this code, Turbo-Reduce 2001, has been delivered to the members of the GUIde Consortium. Turbo-Reduce has superior accuracy and efficiency compared to REDUCE. Furthermore, improvements have been made so that the new code can handle large finite element models, aerodynamic coupling, and simple modeling of shrouds (full-slip or full-stick condition at shroud interfaces). As with REDUCE, Turbo-Reduce can be used to analyze the effect of a particular mistuning pattern on the free and forced response of a bladed disk, or it can be used to run statistical simulations to predict the effects of various levels of mistuning and various cases of engine order excitation. There is even an option in the code to automatically run a sweep through these parameters.

Further, both Turbo-Reduce and REDUCE allow the inclusion of intentional mistuning, which means that the nominal rotor design is changed in such a way that the blades are intended to be different. Numerical simulations performed with both the REDUCE and Turbo-Reduce codes have determined that this design strategy shows great promise for reducing the harmful effects of unintended, random mistuning. Finally, initial work in a complementary experimental investigation has confirmed Turbo-Reduce predictions for the effectiveness of intentional mistuning in reducing the forced response blade amplitudes for an experimental rotor. Further validation work is underway.

Participating Organizations: GUIde

Points of Contact:

Government
Dr. Charles Cross
U.S. Air Force, AFRL/PRTC
1950 Fifth Street, Bldg. 18D
Wright-Patterson AFB, OH 45433-7253
Phone: (937) 656-5530
Fax: (937) 656-5532

Contractor
Dr. Christophe Pierre
University of Michigan
2250 G. G. Brown Bldg.
2350 Hayward Street
Department of Mechanical Engineering
The University of Michigan
Ann Arbor, MI 48109-2125
Phone: (734) 936-0401
Fax: (734) 647-3170

5.1.5 Tip Modes in Low-Aspect-Ratio Blading

FY 95-96

(This effort has been completed. Reference 2000 HCF Annual Report, Section 5.1.5 for more details.)

5.1.6 Development of Aeroelastic Capability for the TURBO Code

FY 96-02

Background

TURBO is a three-dimensional unsteady aerodynamic Navier-Stokes turbomachinery code for propulsion applications. Mississippi State University developed the TURBO code under a grant from Glenn Research Center. For aeroelastic calculations with TURBO, the structural dynamics model of the blade is based on a normal mode representation. For flutter calculations, a pre-processor is used to interpolate modal displacements onto the TURBO grid and to generate the deformed grid. Then, a prescribed harmonic blade vibration with a work-per-cycle calculation is used to determine flutter stability. For forced response calculations with TURBO, the aerodynamic interaction between adjacent blade rows is modeled either as (1) a rotor-stator interaction with multiple passages per blade row, (2) a rotor-stator interaction with phase-lag boundary conditions which requires modeling only one passage per blade row, or (3) a wake-blade interaction with the influence of the upstream row represented as an unsteady inlet excitation.

Recent Progress

Additional verification and validation of the aeroelastic analysis capability of the TURBO code have been done. Fan flutter data from NASA Glenn Research Center's wind tunnel tests have been used for validation of the flutter analysis capability of the TURBO code. Benchmark turbine data acquired under NASA funding have been used to validate the forced response capability of TURBO. The aeroelastic capability present in the current sequential (serial) version of the TURBO code (v4.2) is being transferred to the parallel version of the TURBO code. After the transfer of the relevant coding, all the benefits of the parallel version will be available for aeroelastic analyses.

Participating Organizations: NASA Glenn

Points of Contact:

Government
Oral Mehmed
NASA Glenn Research Center MS 49-8
21000 Brookpark Road
Cleveland, OH 45135-3191
Phone: (216) 433-6036
Fax: (216) 977-7051

Contractor
Dr. Milind A. Bakhle and Dr. Rakesh Srivastava University of Toledo
NASA Glenn Research Center MS 49-8
21000 Brookpark Road
Cleveland, OH 45135-3191
Phone: (216) 433-6037 (Bakhle)
(216) 433-6045 (Srivastava)
Fax: (216) 977-7051

5.1.7 Dynamic Analysis and Design of Shroud Contact

FY 92-01

Background

The objective of this project is to develop 3D friction contact models and computer codes to predict blade vibration for rotors having shrouds and/or platform dampers (friction dampers). The completed GUIde I effort was instrumental in the development of BDAMPER, which facilitates analysis of blade-to-ground dampers, blade-to-blade dampers, shroud contact interfaces, and wedge dampers. The GUIde II effort focuses on the stick-slip-separation transition for 3D relative motion of the shroud-contact interface.

Final Results

Under this effort, 3D contact kinematics, including stick-slip-separation transition, in a shrouded blade system was developed. In the developed model, the assumed blade motion has three components, namely axial, tangential, and radial components, which result in a 3D relative motion at the shroud contact. The resulting relative motion has an in-plane component and another component perpendicular to the contact plane. The in-plane tangential relative motion can have an elliptical trajectory, and it induces stick-slip friction. On the other hand, the normal relative motion can cause variation of the contact normal load and, in extreme circumstances, separation of the two contacting surfaces.

Three major tasks were accomplished. In the first task, based on the developed 3D contact kinematics, a 3D friction contact model was developed and an impedance module was implemented to calculate the resulting constrained forces at 3D friction constraints. In the second task, the developed impedance module was employed to predict the resonant response of blades having 3D shroud constraints. By using the Harmonic Balance Method along with Fast Fourier Transform, the constrained force can be integrated with the receptance of the bladed system to allow calculation of the forced response of the system. In the third task, the concept of constrained mode shapes was employed to predict the resonant response of a frictionally constrained blade system. For a tuned blade system, the constrained mode shapes can be calculated using a finite element model of a single blade along with the cyclic symmetry constraint that simulates a fully stuck friction contact. The newly developed modules were integrated into BDAMPER. BDAMPER 8.0 was transitioned to industrial GUIde members.

Participating Organizations: GUIde

Points of Contact:

Government
Dr. Charles Cross
U.S. Air Force, AFRL/PRTC
1950 Fifth St, Bldg. 18D
Wright-Patterson AFB, OH 45433-7251
Phone: (937) 656-5530
Fax: (937) 656.5532

Contractor
Dr. Chia-Hsiang Menq
Ohio State University
Department of Mechanical Engineering
The Ohio State University
206 18th Avenue
Columbus, OH 43210-1107
Phone: (614) 292-4232
Fax: (614) 292-3163

5.1.8 Friction Damping in Bladed Disks

FY 97-01

Background

The goals of the research in this project were twofold:

1. To develop methods for predicting friction damping in shrouded bladed disk assemblies and

2. To develop an understanding of what might cause shrouded systems to exhibit highly variable response from one build to the next (i.e., to investigate the extreme sensitivity of shrouded bladed disk systems to small changes in the input variables).

In the past, Carnegie Mellon University (CMU) had developed a linear mistuning code, LMCC, for NASA Marshall. The intent was to extend LMCC's component mode approach to include nonlinearities. However, this was found to be too unwieldy, i.e. it required too much preprocessing and introduced too many nonlinear degrees of freedom. A more efficient representation of the linear mistuning problem needed to be developed prior to solving the nonlinear one.

Final Results

Linear Mistuning Analysis

A new reduced order modeling approach was developed, called the subset of nominal modes (SNM). The model is based on two simple concepts. First, the mode shapes of the tuned system and the mistuned system span the same displacement space. As a result, the mistuned modes can be determined as a weighted sum of the nominal tuned modes, which are generated efficiently using a cyclic symmetric finite element model. Second, only the modes with natural frequencies near that of the mode of interest, or of the excitation, contribute significantly to the response. Thus, only a relatively small subset of the nominal tuned system modes is needed to accurately calculate the forced response.

The SNM approach had a number of features that made it significantly more useful that the older component mode synthesis approach (LMCC). Specifically:

1. The input data are relatively easy to generate. For example, only a finite element analysis of a single blade, disk sector is needed to generate the tuned system modes as input to SNM. In addition, since only nominal modes are used as a basis for the representation, it is necessary to determine the motion dependent aeroelastic forces only for these modes. In contrast, in LMCC the aerodynamic influence coefficients also have to be calculated for rigid body blade motions since they are also used to represent the system's response.

2. The mathematical formulation exactly yields the finite element solution as the amount of mistuning goes to zero. This is especially important when frequency veering occurs since other reduced order models can have difficulty in predicting the tuned system modes and natural frequencies in this case.

3. As the number of degrees of freedom in the SNM model increases, the results from a mistuned system calculation converges to the exact solution. Consequently, the accuracy of the SNM model can be checked by observing how the results converge as more degrees of freedom are used in the SNM model. This is especially important in bladed disks with a large number of degrees of freedom in the finite element model since it is difficult to run a finite element analysis of a full mistuned bladed disk as a benchmark.

4. The SNM approach first solves for the eigenvalues and modes of the mistuned system. This has several advantages:

   It provides a very natural formulation for solving the mistuned aerodynamic eigenvalue problem to determine how mistuning affects flutter.

   It is easy to calculate the stresses in the bladed disk, because the mistuned modes are calculated as a weighted sum of nominal system modes. The modal stresses of the mistuned modes are the same as the weighted sum of the nominal system's modal stresses.

   It is computationally very efficient, since the forced response is expressed as a sum of mistuned modes that are independent of the excitation frequency (at least over the limited speed range associated with a particular engine order crossing). The SNM approach automatically captures the deformation at the base of the blade and the manner in which it transfers dynamic forces to neighboring blades. In contrast, LMCC imposes rigid interfaces between the blades and disk that only transmit non-self equilibrated forces and moments. This increase in accuracy should be important when analyzing the effect of mistuning on the response of higher frequency blade mode families in which the dynamic forces tend to be more self equilibrated.

5. The SNM approach uses "nominal modes" to represent the response, and the nominal system modes do not have to be tuned modes. For example, the system could have some type of imposed periodicity which may be taken into account in defining the nominal modes. The periodicity could be from periodic boundary constraints or imposed manufacturing variations. In this case, the nominal modes would be calculated from a single periodic sector that could include multiple blades. In fact, the modes of a completely mistuned system could be used as nominal modes and SNM used to determine the effect of additional random mistuning on the system's response. In this case the nominal modes would have to be calculated once from a finite element model of the full, mistuned stage.

The theory underlying SNM approach was documented in an ASME paper, "A Reduced Order Model of Mistuning Using a Subset of Nominal System Modes," by M.-T. Yang and J.H. Griffin (presented at the 1999 International Gas Turbine and Aeroengine Congress and Exposition, June 1999, Indianapolis, IN, Paper No. 99-GT-288. Accepted for publication in the *ASME Journal of Engineering for Gas Turbines and Power*, in Press).

Nonlinear Mistuning Analysis

A nonlinear version of the SNM code was developed that could solve for the mistuned response of frictionally damped shrouded blades. The code and its documentation were delivered to NAVAIR in August, 2001. It has also been distributed to the Air Force, NASA, and the GUIde Industrial Partners (which include GE, RR, PWA, Honeywell and Siemens Westinghouse).

The theory underlying the nonlinear code was documented in a paper, "A State Space Approach for the Nonlinear Analysis of Frictionally Damped Turbines," by N.E. Kim and J.H. Griffin (presented at the Fifth National Turbine Engine High Cycle Fatigue Conference, Chandler, AZ, March 2000).

Physical Causes of High Sensitivity

It was determined that a shrouded bladed disk can be very sensitive to small variations in the slip load if the number of blades on the disk is approximately equal to five times the engine order of the excitation. In addition, it was shown that high sensitivity can also occur in disks with randomly varying slip loads, and that the predictive criteria developed for alternate mistuning also apply to randomly mistuned disks. This work is documented in the final report to the Navy.

Deliverables

The first implementation of the new method and the corresponding computer code (SNM V1) for solving the linear mistuning problem that was released to the US Government and the industrial members of the GUIde Consortium in the Fall of 2000. A nonlinear version (SNM V2) that solves for the mistuned response of bladed disks that have friction constraints was released at the completion of the contract in September 2001. Copies of the SNM Computing Code and a User Manual describing its use was distributed to the US Navy, Air Force, NASA and the affiliated GUIde Industrial Partners on a CD titled, *SNM v2.0 Reduced Order Modeling*. Interested parties can contact Dr. M. Klein of NAVAIR by email at Kleinma@navair.navy.mil for additional information.

Additional Related Research

The SNM methodology has spawned some additional research in related fields of study at CMU.

System Identification Based on SNM Theory

The Air Force has agreed to fund a research project on system identification using SNM as part of a GUIde III initiative. In the mistuning prediction system, SNM develops a reduced order model to calculate the modes, natural frequencies and forced response of mistuned disks. Because it is a reduced order model the algorithm is very fast, yet is still as accurate as a full FEM analysis. Given the standard deviation in the blades' frequencies it can be readily used in a Monte Carlo simulation to calculate the statistical response of the fleet.

The plan is to use the theory in a reverse manner, i.e. use the mistuned response to determine the mistuning. Specifically, a scanning laser vibrometer will be used to measure the modes in a non-rotating test in the laboratory, then centrifugal stiffening, temperature and gas loading effects will be analytically added to the model so that we can predict the IBR's response when it is in the engine. Because SNM results in a reduced order model, the theory yields a relatively small set of key parameters that are needed to characterize mistuning. These parameters represent mode shape as well as frequency mistuning and provide a fundamentally sound, yet compact, method of characterizing mistuning in these systems.

The Effect of Centrifugal Stiffening on Frequency and Mode Shape

A further goal of the system identification work is to measure the mistuned response of the IBR in the laboratory and project the mistuning to engine operating conditions, ie. add in centrifugal stiffening,

temperature effects, etc., analytically. Centrifugal stiffening effects can be accounted for using the SNM theory, as described in the paper, "A Reduced Order Model for Evaluating the Effect of Rotational Speed on the Natural Frequencies and Mode Shapes of Blades," by P. Marugabandhu and J.H. Griffin (presented at the 2000 International Gas Turbine and Aeroengine Congress and Exposition, May 2000, Munich, Germany, Paper No. 2000-GT-611, and accepted for publication in the *ASME Journal of Engineering for Gas Turbines and Power*).

Participating Organizations: GUIde

Points of Contact:

Government
Dr. Charles Cross
U.S. Air Force, AFRL/PRTC
1950 Fifth St, Bldg. 18D
Wright-Patterson AFB, OH 45433-7251
Phone: (937) 656-5530
Fax: (937) 656.5532

Contractor
Dr. Jerry Griffin
Carnegie Mellon University
Department of Mechanical Engineering
Room 414/Scale Hall/5000 Forbes
Carnegie Mellon University
Pittsburgh, PA 15213
Phone: (412) 268-3860
Fax: (412) 268-3348

5.1.9 Compressor Mistuning Characterization

FY97-99

(This effort has been completed. Reference 2000 HCF Annual Report, Section 8.1 for more details.)

5.1.10 Fretting Characterization

FY98-02

Background

The objective of this task is to develop an understanding of the mechanical drivers in fretting fatigue and develop techniques to minimize their impact on material behavior. In particular the metal-to-metal dovetail attachment of blade and disk attachments will be studied. Fretting fatigue is approximately 6 percent of all HCF failures. The elimination of this problem correlates to six million dollars ($6,000,000) per annum saved in maintenance costs.

The primary mechanical life drivers will be established through a systematic variation of various contacting bodies, the first of which will be "dog bone" specimens placed into contact by cylindrical pads. Different contact loads will be applied to determine the effect of the applied loads on fretting fatigue. Fatigue parameters will be evaluated as to their ability to predict the number of cycles to crack initiation, crack location, and crack orientation along the contact surface. The evaluation process will provide the basic mechanisms for fretting fatigue crack initiation for metal-to-metal contact. The

second phase of the program will concentrate on real blade-disk geometry. Simulated contact surfaces will be loaded in a manner similar to those experienced in a turbine engine environment. The fatigue parameters developed for fundamental surfaces will be evaluated and modified as necessary to predict fretting fatigue on the real blade-disk geometry. Subsequent programs will then explore techniques to minimize the detrimental effects of fretting fatigue in turbine engines.

The first efforts in this research were completed in early 2000. Through thesis work at AFIT, 96 "dog bone" specimens had been fabricated and tested to failure. Fatigue parameter evaluation had been completed on the simplified geometry. A single fir tree specimen, which is symbolic of the real part, was being modeled via finite element analysis. A fretting fatigue parameter had been developed based on the interaction between a plain fatigue specimen and a simplified pad geometry. It had been determined that fretting fatigue crack initiation occurred on the plane of maximum shear stress amplitude and that it was dependent on the amount of slip at the crack location. A simulated blade dovetail and disk slot (single fir tree component) had been modeled and CAD drawings had been developed for machining.

The simulated blade-dovetail and disk slot were to be tested in order to assess the accuracy of the fretting fatigue mechanisms determined through the simplified geometry approach. The robustness of the predictive model were to be evaluated by considering the crack initiation behavior on the single fir tree component. The final phase of fretting fatigue research would involve employing methods such as coatings and compressive residual stresses in order to alleviate the fretting damage induced at the blade-disk interface.

Recent Progress

Due to the departure of the primary research scientist in this area, fretting fatigue research was put on hold from early 2000 until September of 2001. This past fall, a new effort was initiated with AFIT to investigate time dependant contact of fretting surfaces. At this time, mounting hardware has been designed to cycle fretting specimens on the multi-axial fatigue frame. Testing of components will initiate in early 2002.

Participating Organizations: Air Force Research Laboratory, Air Force Institute of Technology, Pratt & Whitney

Point Of Contact

Government
Dr. Charles J. Cross
U.S. Air Force, AFRL/PRTC
1950 Fifth St., Bldg. 18D
Wright-Patterson AFB, OH 45433-7251
Phone: (937) 656-5530
Fax: (937) 656-5532

5.2 Acquisition of Experimental Data

New models and computational capabilities must be compared against experimental data. Through this comparison, either the model will be validated and transitioned to industry, or new weaknesses and shortfalls will be identified. In either case, a quantitative assessment of the models capability will be achieved. The objective of the following projects is to obtain the high fidelity data necessary to validate modules for improved forced response prediction.

5.2.1 High Mach Forcing Functions

FY 92-96

(This effort has been completed. Reference 2000 HCF Annual Report, Section 5.2.1 for more details.)

5.2.2 Forward Swept Blade Aeromechanics

FY 95-96

(This effort has been completed. Reference 2000 HCF Annual Report, Section 5.2.2 for more details.)

5.2.3 Oscillating Cascade Rig

FY 95-02

Background

The NASA linear oscillating cascade is one of a very few test facilities dedicated to unsteady aerodynamics of oscillating airfoils. The facility is used to investigate unsteady aerodynamic phenomena in an oscillating row of airfoils modeling self-induced cascade flutter. Experimental data acquired in this facility serve as benchmark sets to validate CFD codes for predictions applicable to real turbomachines, so that the data must be of the highest quality and reliability with characteristics sufficiently close to those encountered in annular cascades of real machines.

(Reference 2000 HCF Annual Report, Section 5.2.3 for details of work done prior to CY 2001.)

Recent Progress

A study was conducted in the NASA Glenn Research Center linear cascade on the intermittent flow on the suction surface of an airfoil section from the tip region of a modern low aspect ratio fan blade. Experimental results revealed that, at a large incidence angle, a range of transonic inlet Mach numbers exist where the leading-edge shock-wave pattern was unstable. Flush mounted high frequency response pressure transducers indicated large local jumps in the pressure in the leading edge area, a condition which generates large intermittent loading on the blade leading edge. These measurements suggest that for an inlet Mach number between 0.9 and 1.0 the flow is bi-stable, randomly switching between subsonic and supersonic flows. Hence, it appears that the change in overall flow conditions in the transonic region is based on the frequency of switching between two stable flow states rather than on the continuous increase of the flow velocity. To date, this flow behavior has only been observed in a

linear transonic cascade. Further research is necessary to confirm this phenomenon occurs in actual transonic fans and is not the byproduct of an endwall restricted linear cascade. The results are shown in Figure 5.2.3.

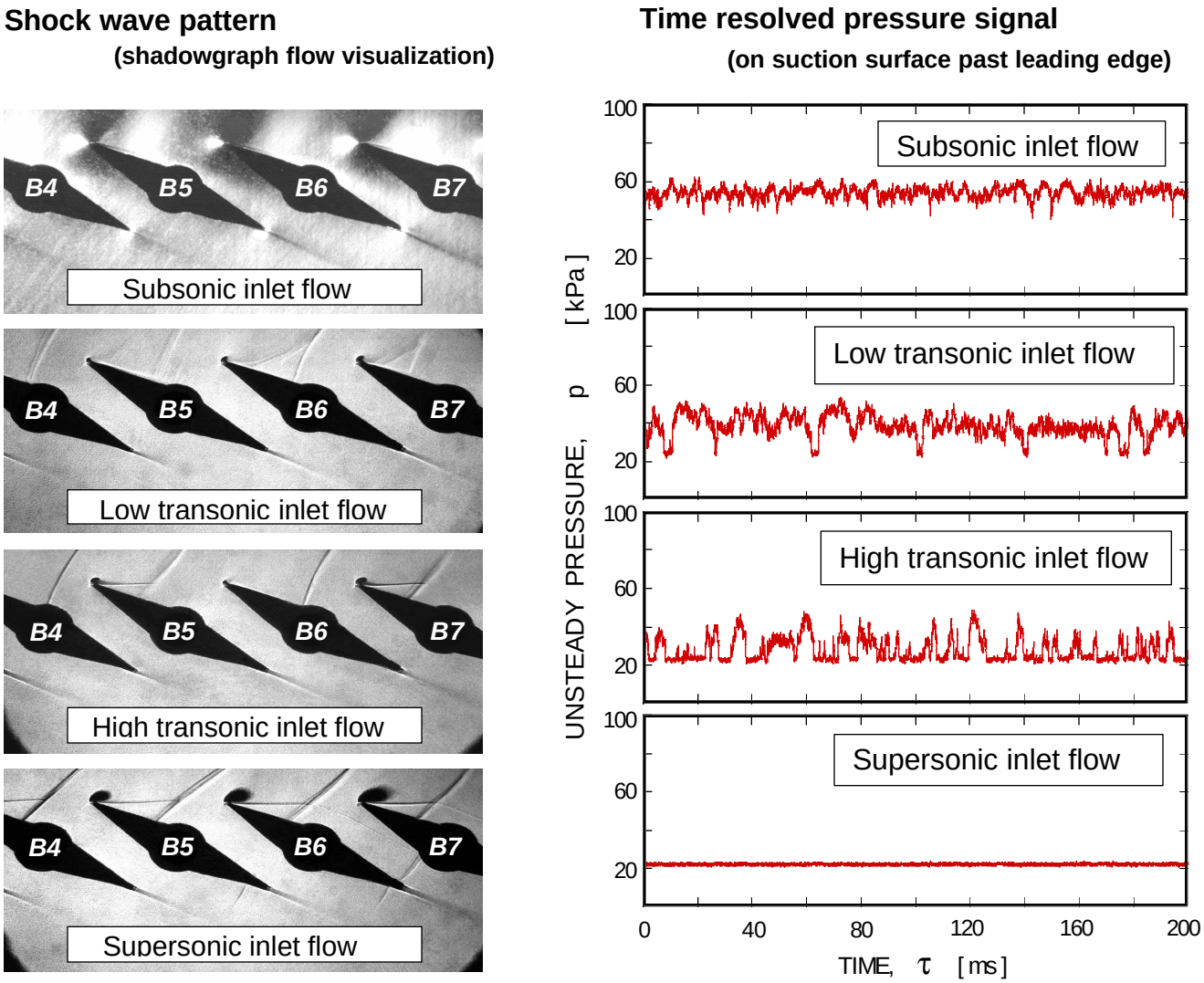

FIGURE 5.2.3 Oscillating Cascade Rig Test Results

Participating Organizations: NASA Glenn, Pratt & Whitney

Points of Contact:

Government
Dr. Jan Lepicovsky
Dynamics Engineering Co. / NASA Glenn
2001 Aerospace Parkway
Brookpark, Ohio 44142-1002
Phone: (216) 977-1402 or (216) 433-6207
Fax: (216) 977-1269

Contractor
Dr. Yehia El-Aini
Pratt & Whitney
P.O. Box 109600
West Palm Beach, FL 33410-9600
Phone: (561) 796-5911
Fax: (561) 796-3637

5.2.4 F109 Unsteady Stator Loading

FY 95-02

Background

The objective of this work is to use the Honeywell F109 high bypass ratio turbofan engine to investigate the presence and subsequent effect of potential velocity disturbances on closely coupled engine hardware. Cascade and F109 fan section research from FY95 to FY00 revealed the presence of a relatively large radiating potential disturbance. In the region upstream of the F109's single stage fan, a two-wire hot wire anemometer measured unsteady velocities as high as 50% of the mean axial flow in the azimuthal direction and on the order of 20% of the mean axial flow in the axial direction. These disturbances were found to decay rapidly with both increased distance from the fan and decreased engine RPM. Downstream of the fan, potential disturbances were also detected by hot wire measurements in the flowpath between the fan rotor and downstream stator and by pressure measurements using Kulite ultraminiature pressure transducers located very close to the surface of several downstream stators. From FY00 to FY01, research has focused on measuring the pressure response due to the fluctuating potential field upstream of the F109 fan. A single airfoil probe (hereafter referred to as the "vane") was instrumented with eight 15 psi differential Kulite pressure transducers. The vane was positioned 0.6 fan chords upstream of the fan as shown in Figure 5.2.4.1. The results of the forced pressure response on this vane were a factor of two greater than expected based on the previously measured velocity field. Near the trailing edge of the vane, significant unsteady peak-to-peak pressure amplitudes were recorded from 5 to 6 psi on one side of the vane with approximately 2 psi recorded at the same axial location on the opposite side of the vane. This potential unsteady loading on the vane of 8 psi was recorded under test conditions where the approaching flow's total pressure was 11.4 psia.

Recent Progress

The latest experiments involved investigating the effect of the vane's trailing edge geometry on the pressure response near the trailing edge of the vane. Two additional vane configurations were tested in the F109 engine in addition to the previous sharp trailing edge vane studies: semi-bluff trailing edge and bluff trailing edge configurations. All three vane configurations were identical from the leading edge to the mid-chord point. The sharp trailing edge vane was a baseline NACA 16-012 configuration with a chord length equal to the F109's fan chord, 2.625 inches. The semi-bluff trailing edge vane was designed such that the back half of the vane was a mirror image of the front half. This created a vane where the leading and trailing edges had the same radius of curvature. The bluff trailing edge vane consisted of a section of uniform thickness from the 50% chord location to the 95% chord location. Beyond the 95% location, the trailing edge became a semi-circle with a diameter equal to the maximum vane thickness. The reason for investigating the different trailing edge configurations was to see if what looked like a trailing edge singularity (large unsteady pressure differential at the trailing edge) for the sharp trailing edge vane would disappear if the "sharpness" was reduced.

Results of the semi-bluff and bluff trailing edge vanes, as seen in Figure 5.2.4.2, show that the RMS amplitude of differential pressure for the sharp trailing edge vane is approximately 1.5 times larger than that for the other bluffer configurations. This may suggest that the sharp trailing edge creates some kind of singularity that contributes to the differential pressure at the trailing edge, or that the difference in the wake associated with different trailing edge configurations strongly influences the pressure response. It can also be seen that the pressure across all the vanes shows no sign of dropping

to zero at the trailing edge as "required" by the Kutta condition. These trends in the data appear to be in conflict with the presumed Kutta condition and therefore demand a closer look at the physics of the flow near the trailing edge.

Future work involves continued data reduction for the semi-bluff and bluff trailing edge vanes to more definitively characterize the propagation phenomena. In addition, the use of Particle Image Velocimetry (PIV) will be investigated for use upstream of the F109 fan and near the trailing edge of the vane. This will involve addressing issues such as optical access paths, flow seeding, phase locking of PIV system with engine RPM, etc. Preliminary testing of a PIV setup is scheduled for summer of 2002.

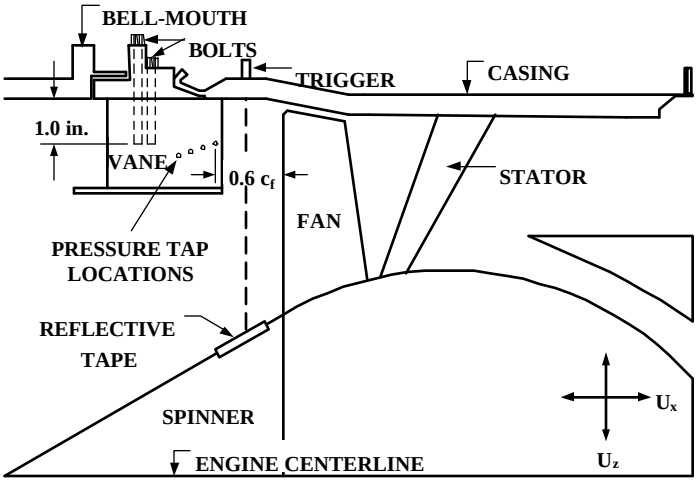

FIGURE 5.2.4.1 F109 Fan and Vane Configuration

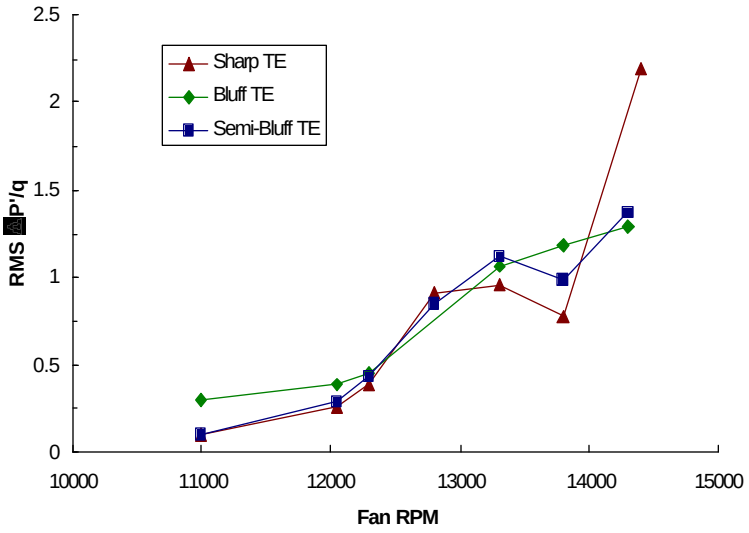

FIGURE 5.2.4.2 Normalized, RMS Unsteady Pressure vs. Fan RPM

Participating Organizations: U.S. Air Force Academy, Air Force Research Laboratory (AFRL), Air Force Officer of Scientific Research (AFOSR), University of Notre Dame

Points of Contact:

Government
Lt Col Brenda A. Haven/Dr. Aaron Byerley
U.S. Air Force Academy
Headquarters USAFA/DFAN
2354 Fairchild Dr., Suite 6H22
United States Air Force Academy
Colorado Springs, CO 80840-6222
Phone: (719) 333-4010
Fax: (719) 333-4013

Contractor
Dr. Eric Jumper
University of Notre Dame
Aerospace and Mechanical Engineering
Hessert Center for Aerospace Research
Notre Dame, IN 46556
Phone: (219) 631-7680
Fax: (219) 631-8355

5.2.5 Fluid-Structure Interaction (Fans)

FY 96-01

Background

The overall research objective is to develop the technology needed to predict significant blade row forced response in a multistage environment, thereby providing accurate predictions of HCF. Specific objectives include the following: (1) development of a benchmark standard multistage transonic research compressor; (2) a quantitative understanding and predictive capability for multi-stage blade row forced response; (3) addressing the inherently small damping of complex higher order modes, investigating techniques to control the flow induced vibrations; (4) considering the issue of robustness including the role of such issues as variability and flight maneuvers, nonlinearities, and fluid-structure interactions.

A transonic rotor operates with a supersonic relative velocity with a subsonic axial component. Shocks thus form near the leading edges that propagate upstream and are a significant forcing function to the upstream vane row. The rotor also generates an unsteady forcing function to the downstream stator row. The reduction in the relative velocity in the wake causes a decrease in the absolute velocity as well as a change in incidence to the downstream stators. This produces a fluctuating lift and moment that can result in large vibratory stress.

Recent Progress

The advanced-design inlet guide vane (IGV), rotor and stator rows have controlled diffusion airfoil (CDA) profiles and have been fabricated, with the IGVs and stators instrumented.

The new IGVs and stator vanes and the existing rotor were used in the investigation of IGV-rotor and rotor-stator interactions. Detailed benchmark unsteady aerodynamic rotor-stator interaction data were acquired at both design and part-speed compressor operating conditions. These detailed data include measurements of the rotor wake generated unsteady aerodynamic forcing function to the downstream stator, the resultant stator vane steady and unsteady aerodynamic response, and Particle Image Velocimetry (PIV) measurements of the time-variant stator mid-span vane-to-vane flow field.

The rotor wakes are the primary source of unsteady aerodynamic excitation to the downstream stator. The subsonic rotor wakes are narrow compared to the rotor pitch, while the transonic rotor wakes are very broad and deep, with their circumferential extent spanning almost the entire rotor pitch. The wake velocity deficits generated by transonic rotor operation are significantly deeper than those at the subsonic rotor speed. Significant static pressure fluctuations attributed to the spinning acoustic modes generated by rotor-IGV and rotor-stator interactions are also present for both rotor speeds, with the transonic static pressure fluctuations nearly 4x larger.

The low momentum rotor wake fluid has a slip velocity relative to the free stream that causes it to drift across the vane passage and accumulate on the vane pressure surface as the chopped rotor wake segments are transported downstream. This condition results in a local broadening of the wake segment near the pressure surface and a thinning near the suction surface due to “negative jet” effects. As the low momentum rotor wake fluid accumulates on the vane pressure surface, it interacts with the boundary layer and eventually appears in the stator wake regions.

The subsonic rotor wakes decay very rapidly after they are chopped and ingested into the stator passage. As the chopped wake segment disperses, both the wake width increases and the vorticity decreases considerably by the time it exits the stator passage 2.5 blade-passing periods after being initially cut. Note however, that even though the subsonic rotor wakes decay considerably as they are chopped and transported through the stator, the chopped wake segments are still clearly evident downstream of the stator trailing edge.

The chopped rotor wakes disperse much more rapidly at the transonic rotor speed and are not evident downstream of the stator trailing edge. This result is surprising, considering that the transonic rotor wakes are much larger than those generated by subsonic flow. Thus, it might be expected that the transonic rotor wakes would persist for longer downstream distances. However, the more rapid decay of the rotor wakes at the transonic speed is due to unsteady flow effects. Specifically, the rotor wake slip velocity causes low momentum fluid to drift across the stator passage as the chopped wake segments are transported downstream, with this rotor wake fluid accumulating on the vane pressure surface and thus appearing in the stator wake regions during the transport process. This unsteady intra-stator wake transport process is more significant at the transonic rotor speed due to the much deeper and broader rotor wakes generated by transonic compressor operation.

The development of a computational analysis of unsteady multistage flows in turbomachinery was continued. For a given multistage fan or compressor, a computational mesh for each blade row is first generated. The steady multistage flow is then computed using conventional CFD techniques, with "mixing planes" used to couple together the solutions computed in the individual blade rows. Several unsteady time-linearized (frequency domain) problems on each computational grid are then solved. Each solution is identified with one of a set of discrete "spinning modes," each with a different frequency and interblade phase angle. These unsteady flow problems are solved in parallel, using time-linearized CFD techniques developed for isolated blade rows. At each iteration, information is exchanged among the various spinning mode solutions at the inter-row computational boundaries. This iteration procedure is continued until a converged solution is obtained. The three-dimensional analysis technique has been considerably refined. Specifically, the aerodynamic damping of a rotor embedded in a multistage machine can now be computed.

Coupled fluid-structure prediction for high cycle fatigue (HCF) in a multi-stage environment is addressed, with particular emphasis on aerodynamic detuning strategies for HCF minimization. This is accomplished utilizing TAM-ALE3D, a finite element model that solves the three-dimensional Euler equations to simulate the blade-row-interaction-generated unsteady flow and vibration phenomena in

the inlet guide vane (IGV) row of the Purdue Transonic Compressor. The IGV's experienced cracking during operation at 15,000 rpm. These cracks are due to excitation of the trailing edge flapping mode, with the 4,750 Hz excitation from the downstream 19-bladed rotor potential field. The frequency of this flapping mode is 4,200 Hz, close enough to the excitation frequency to cause HCF problems. This case is ideal for the application and evaluation of HCF passive detuning techniques that reduce aerodynamically induced unsteady stresses while minimally impacting performance and reliability. The IGV-spacing detuning decreased the stress amplitude from the baseline by a factor of approximately six, thus validating that IGV-spacing detuning is an excellent strategy for alleviating the large HCF stresses in the IGV's at the 15,000-rpm operating condition.

Research under this initiative will include continued analytical development of multistage effects as well as fluid-structure interactions. Continued experimental research includes the investigation of the IGV response at off-design conditions, the study of the effect of steady loading on the unsteady aerodynamics of the downstream stator, the measurement of the vibratory stress in the IGVs and stators, as well as the study of airfoil-to-airfoil unsteady aerodynamic variability. Structural mistuning of the new rotor will be quantified, with investigations into rotor-stator and rotor-IGV interactions initiated, and the airfoil response for each airfoil row measured.

Participating Organizations: AFOSR, Purdue University, Duke University, Pratt & Whitney

Points of Contact:

Government
Dr. Thomas Beutner
U.S. Air Force, AFOSR/NA
801 N. Randolph Street
Arlington VA 22203-1977
Phone: (703) 696-6961
Fax: (703) 696-8451

Contractor
Dr. Sanford Fleeter
Purdue University
Thermal Sciences & Propulsion Center
1003 Chaffee Hall
West Lafayette, IN 47907-1003
Phone: (317) 494-1504
Fax: (317) 494-0530

5.2.6 Experimental Study of Forced Response in Turbine Blades
FY 97-01

Background

The purpose of this project was to develop an understanding of the forcing function, aerodynamic damping, and structural damping at actual engine conditions for high-frequency vibration of turbine blades. A Honeywell TFE731-2 high-pressure turbine stage was fully instrumented and a measurement/analysis program was conducted at the Gas Turbine Laboratory of the Ohio State University. The original blades had a high-frequency vibration problem. Unsteady surface pressure and blade response were measured as part of the effort. The result of this research project will be a database that can be used to validate future predictive codes. Because of significant reductions in funding, the original test plan, which included operating the turbine at actual engine conditions, had to be scaled down such that the measurements were performed for corrected engine conditions.

Final Results

The research program has been completed and funding has been exhausted. A final report titled "Experimental and Numerical Study of Blade Forced Response in a Full-Scale Rotating Turbine" describing the effort and including the database was distributed to all members of the government, industry, and university partners of the GUIde Consortium on September 18, 2000. A brief abstract of the contents of the report follows.

Abstract of Report:
The forced response of aircraft engine turbine blades has been studied with a careful combination of numerical predictions and experimentation to provide a data set and accompanying analysis of the coupled unsteady aerodynamics and structural response. The unsteady aerodynamics through the stage are modeled using the Quasi-3D Reynolds-averaged Navier-Stokes CFD solver (UNSFLO), and the structural response of the blade is modeled with the 3D finite element commercial code ANSYS. The measurement program utilized full-stage rotating engine hardware operating at design corrected conditions that had experienced previous forced response difficulties while in service. Two different vane/blade spacings were used in the measurement program in order to investigate the influence of this variable on the resulting forcing function. The rotating blade was instrumented with flush-mounted miniature pressure transducers, strain gauges, and piezoelectric crystals. Both aerodynamic and piezoelectric excitation techniques were used to study the blade vibratory response with and without aerodynamic loading. In this way, it was possible to measure the total damping and to obtain an accurate estimate of the contributions from structural and aerodynamic sources.

The results provide, for the first time, the coupled measurement of unsteady pressure and vibratory response of a high-pressure turbine blade due to vane/blade interaction. Comparison of the predictions and time-averaged surface pressure data demonstrated good agreement. Similar comparisons of the pressure harmonic amplitudes showed good agreement at midspan and moderate agreement near the tip. The results indicate a significant decrease in the amplitude of the pressure harmonic when the vane/blade spacing is increased.

The unsteady pressure field was analyzed prior to and during resonance. Vibration acts as a destructive interference with the vane wake forcing function during resonance. For this particular turbine, aerodynamic damping was found to be a large component of the total damping. Successful completion of this database provided a needed data set for the study of turbine blade forced response.

Participating Organizations: GUIde, NASA

Points of Contact:

Government
Dr. Antole Kurkov
NASA Glenn Research Center
NASA Glenn Research Park
21000 Brookpark Rd., M/S 49-8
Cleveland, OH 44135-3191
Phone: (216) 433-5695
Fax: (216) 977-7051

Government
Dr. Charles Cross
U.S. Air Force, AFRL/PRTC
1950 Fifth St, Bldg. 18D
WPAFB, OH 45433-7251
Phone: (937) 255-2611
Fax: (937) 656-5532

Contractor
Dr. Michael Dunn
Ohio State University
328 Bowlz Hall
2036 Neil Ave.
Columbus, OH 43210-1276
Phone: (614) 292-8453
Fax: (614) 292-8290

5.2.7 Spin-Pit Excitation Methods

FY99-01

See section 8.3 of the 2000 HCF Annual Report. There was no detailed progress report provided for inclusion in this report for this effort in CY2001.

5.2.8 Inlet Distortion Characterization

FY 99-01

Background

The objective of this project is to develop a technique to produce inlet flows that simulate conditions experienced in-flight. This technique will improve the fan system development process for aeromechanical evaluation of blade vibrations due to inlet flow distortions. As a result of this effort, aeromechanical risks to fan systems will be reduced by implementing a proper test and evaluation technique to simulate appropriate inlet flow field conditions, which are similar to those experienced in flight. The outcome of this program will be incorporated in the HCF test protocol. The technical challenge is to accurately predict the inlet flow distortion and the resulting unsteady forces experienced by a fan. In particular, key modeling requirements need to be determined for defining the excitation types on the fan's vibratory response. The approach is to use data analysis and computational analysis methods of flight, ground, and model tests of the F-16/F110, and the model test data of a bifurcated Advanced Compact Inlet System (ACIS).

Recent Progress

Extensive computational fluid dynamics (CFD) analyses have been performed for the F-16 airframe and the companion first-stage fan of the F110-GE-129 engine. Also, CFD analyses have been performed for the airframe for the Advanced Compact Inlet System (ACIS). The intent of the airframe analyses was to quantify the circumferential variations in the flow fields for evaluating the resulting fan vibratory response in the engine.

Figure 5.2.8.1 shows the variation in total and static pressure in the engine inlet section of the airframe for one of the cases where the fan's first-stage vibrations were the highest during the flight test program. Namely, the aircraft is in a maneuver termed an erect, climb departure, wherein the angle-of-attack and side-slip is high (roughly 45 degrees) and the speed is low (Mach number = 0.1). For this condition, the total pressure variations are dominant when compared to those of the static pressure, i.e., static pressures are approximately 5% of those of the total pressure. This implies that the flow in the inlet section of the F-16 is nearly parallel and thus has negligible flow angularity or circumferential components.

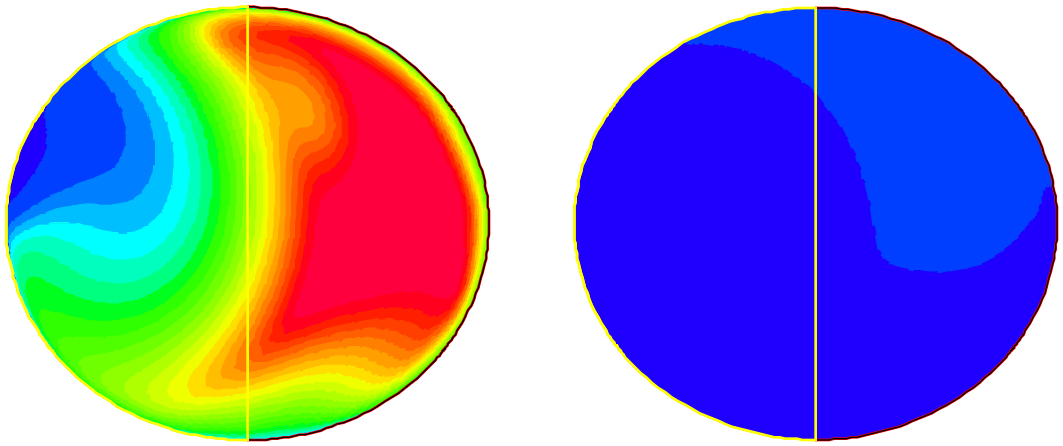

Total Pressure **Static Pressure**

FIGURE 5.2.8.1 CFD Solutions at an Axial Plane in the Inlet Section of the F-16

Figure 5.2.8.2 shows the CFD solutions for the total and static pressures in the ACIS airframe at a condition similar to that of the F-16, a high angle-of-attack, low speed operation. The interrogation plane for these contour plots is just aft of the bifurcation of the two inlets. With this calculation not being a side-slip condition the CFD model used a symmetry line to reduce the calculation domain to only half the aircraft, and, thus the plots show only half the inlet flow field. When comparing the static pressure to the total pressure variations, the static pressure is now a larger percentage, roughly 15%, but is still small. Thus, even for this shorter, bifurcated, turning inlet the flow is predominantly parallel near the entrance to the engine. Similarly to the F-16, the flow angularity has a small impact on the flow distortions entering into the engine, and, thus, it will have minimal impact on the fan's vibratory response.

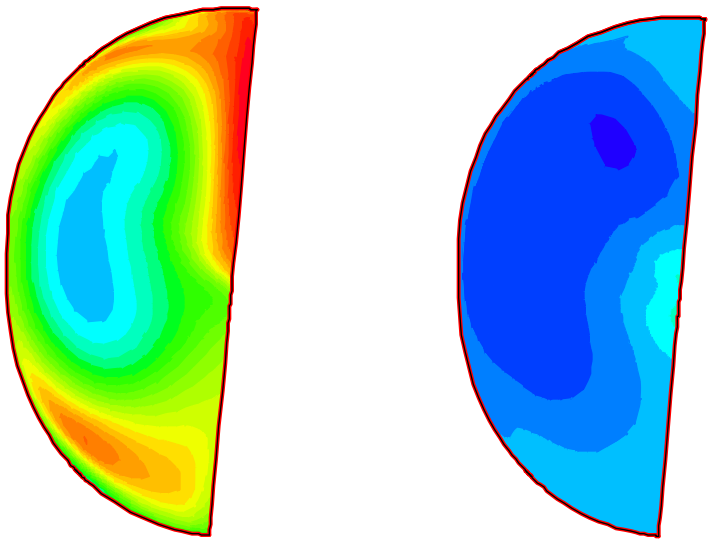

Total Pressure **Static Pressure**

FIGURE 5.2.8.2 CFD Solutions at an Axial Plane in the Inlet Section of the ACIS

Similar CFD analyses were performed for other conditions for the F-16 and the ACIS. These solutions were analyzed using the Modal Excitation Indices (MEI) technique of using a weighted, integration of the third harmonic of the pressure variations of the distorted flow, where the weighting is from the leading edge deflections of the first-flex mode of the first-stage fan blade for the F110-GE-129. Figure 5.2.8.3 shows the ratio of the MEI based on total pressure versus the MEI based on static pressure for ten conditions covering the flight test of the F-16 and three conditions for the ACIS. For all conditions except two, the total pressure excitation indices are at least five times higher than that for the static pressure. For the two other conditions the fan response due to the three-per-revolution excitation of the first-flex mode was small, thus implying that the total pressure variation has diminished to levels approaching the values of the static pressure variation.

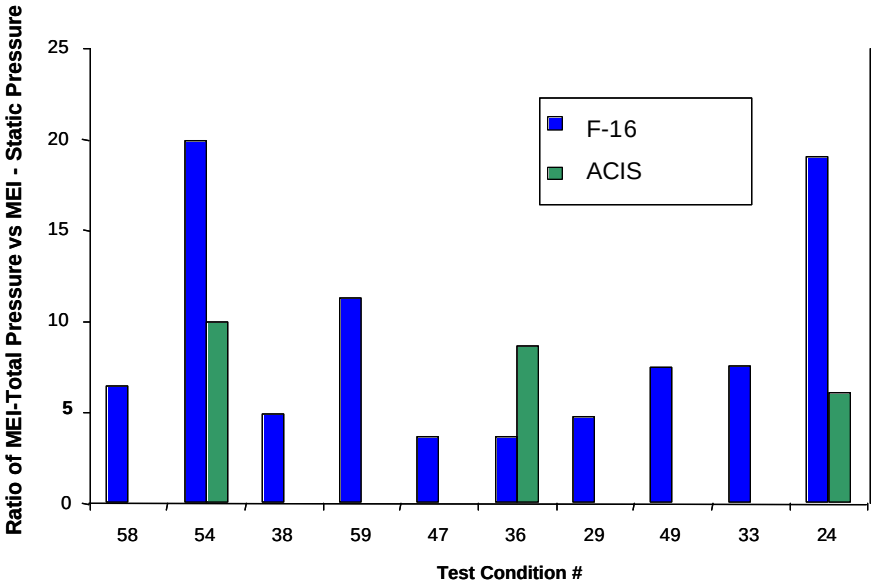

FIGURE 5.2.8.3 Total Versus Static Pressure Excitations across Spectrum of Conditions.

Participating Organizations: Aeromechanics Technology

Points of Contact:

Government
Dr. Charles Cross
U.S. Air Force, AFRL/PRTC
1950 Fifth St., Bldg. 18D
Wright-Patterson AFB, OH 45433-7251
Phone: (937) 255-2611
Fax: (937) 255-2660

Contractor
Dr. Steven Manwaring
Aeromechanics Technology
Address:
GE Aircraft Engines
One Neumann Way MD-A413
Cincinnati, OH 45215
Phone: (513) 243-3428
Fax: (513) 243-8091

5.3 Validation of Analytical Models

Once advanced codes have been developed and data sets have been obtained, the predictions must be compared to the experimental data. The objective of the following projects is to utilize existing experimental data to validate models for improved forced response prediction.

5.3.1 Evaluation of Current State-of-the-Art Unsteady Aerodynamic Models for the Prediction of Flutter and Forced Vibration Response

FY 97

(This effort has been completed. Reference 2000 HCF Annual Report, Section 5.3.1 for more details.)

5.3.2 Evaluation of State-of-the-Art Unsteady Aerodynamic Models

FY 99-05

Background

The objective of this project is to evaluate the capabilities of current state-of-the-art unsteady aerodynamic models that attempt to predict the gust and oscillating airfoil response of compressor and turbine airfoils over a range of realistic frequencies and loading levels. Additionally, the effect of the aerodynamic forcing function on gust response and the effects of three-dimensional flow on airfoil oscillation will be investigated. Codes currently under evaluation are TURBO, ADPAC, and 3DVBI.

Recent Progress

This project has been extended for three years by the AF. The various CFD codes are still being evaluated. The AF recently acquired a detailed unsteady pressure data set for the Compressor Aero Research Lab (CARL) Stage Matching Investigation (SMI) rig which is a transonic highly loaded compression stage. The project is currently in the process of both modeling the SMI rig with several CFD codes and reducing the experimental data for comparison and evaluation.

Participating Organizations: Air Force Research Laboratory (AFRL), Wright State University

Points of Contact:

Government
Dr. Charles Cross
U.S. Air Force, AFRL/PRTC
1950 Fifth Street, Bldg. 18D
Wright-Patterson AFB, OH 45433-7253
Phone: (937) 656-5530
Fax: (937) 656-5532

Contractor
Dr. Mitch Wolff
Department of Mechanical Engineering
Wright State University
Dayton OH 45435
Phone: (937) 775-5141
Fax: (937) 775-5009

5.3.3 Forced Response Prediction System (Fans)

FY 95-03

Background

The objective of this project is to develop and validate NASA's new Forced Response Prediction System design tools. Three codes are being developed for forced response predictions: FREPS, FREED, and TURBO. FREPS uses two-dimensional linearized potential unsteady aerodynamics and is the fastest running of the codes. The development and validation of FREPS is complete and is being followed by the development of FREED. FREED uses steady Euler aerodynamics from the TURBO code, and linearized three-dimensional unsteady Euler aerodynamics from LINFLUX. LINFLUX is a turbomachinery code developed under a contract from NASA Glenn Research Center (formerly Lewis Research Center). The linearized code FREED and the fully non-linear code TURBO (with aeroelastic capability) are complementary. Both codes are based on the same algorithm, but each provides a different level of physics modeling and has different computational requirements. The TURBO code, described elsewhere in this report, is the longest running of the three codes but includes the most physics modeling. The structural dynamic model of the blade for the three codes is based on a normal mode representation.

Recent Progress

A new version of LINFLUX was implemented on a Silicon Graphics Inc. workstation. The new version has the capability to model vortical gusts in addition to the downstream and upstream acoustic gusts. LINFLUX was exercised for acoustic and vortical gusts for a helical fan configuration with flat plate geometry. The LINFLUX results were compared with those obtained from linear theory. Good correlation was obtained for the grids considered, although the results for the vortical gust showed some differences, which are attributed to the coarseness of the grid. A finite element structural model was developed for the helical fan using ANSYS structural analysis software. The response amplitudes calculated from FREED compared well with those obtained from ANSYS using calculated unsteady pressures from LINFLUX.

Future plans include further verification and validation of FREED code forced response calculations for actual engine blade geometries, and developing a new interface code to work with the most recent versions of TURBO. In addition, the plans include improvement of the steady solver to obtain faster convergence and to obtain solutions with reduced numerical losses.

Participating Organizations: NASA Glenn

Points of Contact:

Government
Oral Mehmed
NASA Glenn Research Center
NASA Glenn Research Park
21000 Brookpark Rd., M/S 49-8
Cleveland, OH 44135-3191
Phone: (216) 433-6036
Fax: (216) 977-7051

Contractor
Dr. T. S. R. Reddy and Dr. Milind A. Bakhle
University of Toledo
NASA Glenn Research Center
M/S 49-8, 21000 Brookpark Road
Cleveland, OH 44135-3191
Phone: (216) 433-6083 (Reddy)
(216) 433-6037 (Bakhle)
Fax: (216) 977-7051 (both)

5.3.4 Aeromechanical Design System Validation

FY 96-01

Background

This contracted effort, performed by Pratt & Whitney, was completed in 2001. The objective of the effort was to validate a forced response prediction system for turbomachinery fan blades excited by inlet excitation. The overall process is shown in Figure 5.3.4.1.

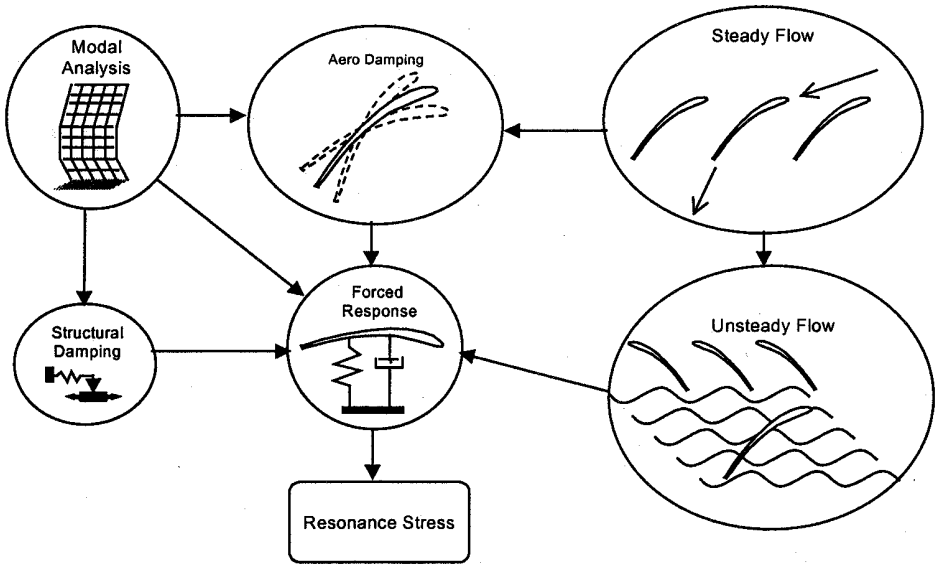

FIGURE 5.3.4.1 Forced Response Prediction Process

Final Results

The approach used a resonance stress prediction system to calculate the resonant stresses for an integrally bladed fan rotor. The initial calculation used the nominal blade geometry and the analysis compared to actual test measurements. Subsequent analysis was based on the actual geometry of the individual blades. A total of 62,720 measurements were made on the test rotor. The data were used to build finite element models of each individual blade (Figures 5.3.4.2 and 5.3.4.3). The data were also used to compare the actual blades to the design intent and identify significant variations. Small variations in overall thickness distributions produce significant variations at the leading and trailing edges that in turn produce larger frequency variations in the higher order modes.

The forced response analysis of the design intent blade was run with the CFD-generated unsteady loads from an inlet guide vane system. Vibratory stresses were compared with engine test data for the modes that responded. The agreement among results was mixed, with some modes showing large variations between predicted and test data.

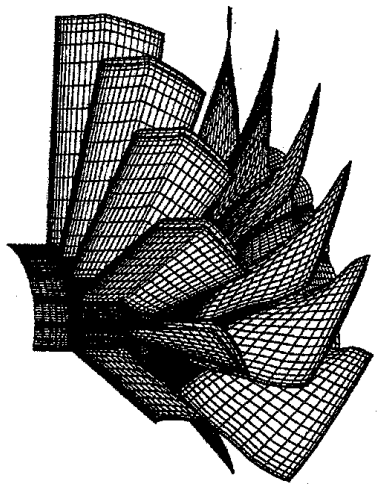

FIGURE 5.3.4.2 CFD Model of Inlet Guide Vane and Rotor

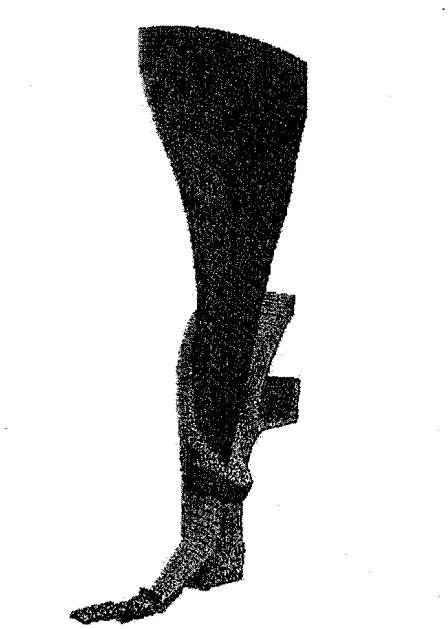

FIGURE 5.3.4.3 Rotor Blade Sector Finite Element Model Used in Tuned Analysis

Using the measured blade data in the forced response prediction reduced the variation between predicted and tested response for all modes (Figure 5.3.4.4). The improvement in correlation indicates that the HCF goal for vibratory stress prediction is not unrealistic for the limited number of modes and excitations studied.

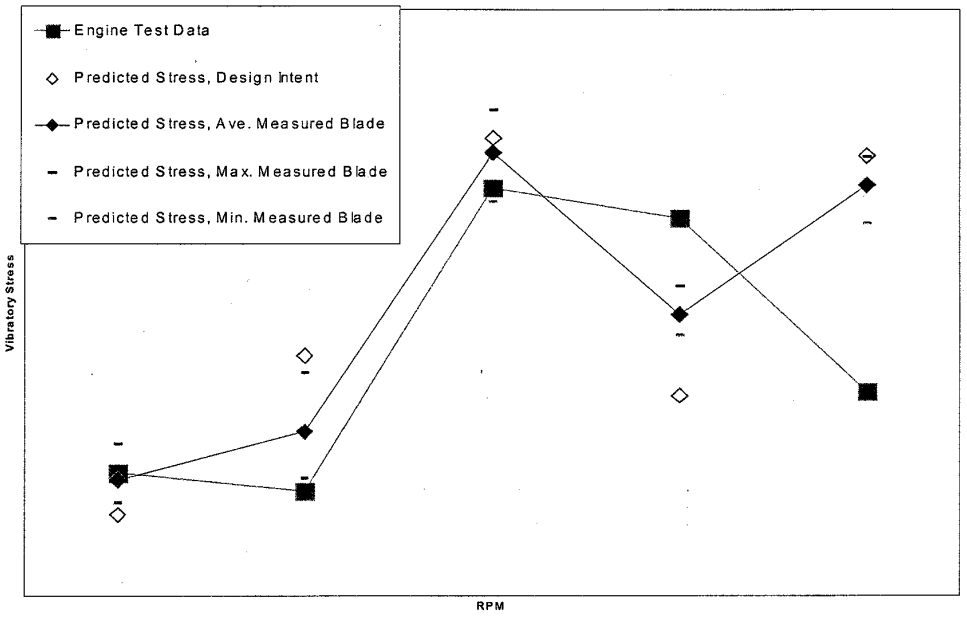

FIGURE 5.3.4.4 Comparison of Predicted and Measured Vibratory Stresses

A mistuned forced response analysis was conducted using measured blade geometry in a full rotor finite element model. The unsteady CFD analysis did not use the measured blade geometry in calculating the unsteady blade loading. This is believed to be responsible for under-predicting the actual individual blade responses.

Participating Organizations: Air Force Research Laboratory (AFRL), Pratt & Whitney

Point of Contact:

Government
John Lueke
U.S. Air Force, AFRL/PRTF
1950 Fifth Street, Bldg. 18D
Wright-Patterson AFB, OH 45433-7251
Phone: (937) 255-8210
Fax: (937) 255-2077

5.4 New Efforts

FY 01-06

With the extension of the HCF program through FY06, additional research in the Forced Response area is planned to further improve the ability to determine forced response. To enhance the efforts described in Section 5.1, Development of Physical Understanding and Models, new efforts in the areas of mistuning and friction damping will be initiated. Friction Damping research performed through the GUIde Consortiums in the development of the BDAMPER series of codes will be continued and microslip capability added. A new modeling technique to incorporate microslip into Finite Element

Models will also be initiated. For mistuning, prediction and characterization capabilities transitioned to industry through REDUCE and SNM, will continue and be enhanced. Additionally, the efforts will investigate system identification and optimization. In the world of centrifugal compressors, efforts to develop an understanding of the parameters which drive aeromechanical response in radial flow machines will begin. Section 5.2 will be enhanced through efforts which will develop the techniques to measure flow characteristic in complex flows including centrifugal impeller-diffuser interactions. Rig tests which employ the advanced mistuning algorithms of SNM and REDUCE will be run to develop a new database for mistuning investigations. New investigations in section 5.3 will include the development of fully integrated, versus coupled, forced response prediction systems and more in-depth investigations of fluid-structure interactions.

5.5 Conclusion

The Forced Response Action Team has successfully developed models to understand and predict friction and mistuning in gas turbine engine disks. Updates of models were transitioned to industry in this past year. An updated version of BDAMPER, a code developed through the GUIde Forced Response Consortium, is successfully predicting resonant responses of frictionally constrained blades. New versions of REDUCE and SNM, bladed disk mistuning codes, are being utilized by several turbine engine companies, and are successfully predicting response trends in bladed disk assemblies. Additionally, the government and industry are jointly pursuing new codes for flutter and resonant stress prediction. Many efforts have been coordinated and developed through the GUIde consortium of government, engine contractors, and universities, with validation performed through basic research, component rig testing, technology demonstrator engine testing, and production engine operation.

6.0 PASSIVE DAMPING TECHNOLOGY

BACKGROUND

The Passive Damping Technology Action Team (Damping AT) has the responsibility of fostering collaboration among individual HCF passive damping efforts with the overall goal of damping component resonant stress by 60% for fans and 25% for turbines. The Damping AT provides technical coordination and communication among active participants involved in HCF passive damping technology. Annual technical workshops have been organized and summaries of these workshops are disseminated to appropriate individuals and organizations. The Chair, Co-Chair and selected Damping AT members meet as required (estimated semi-annually) to review damping activities, develop specific goals for passive damping programs, and coordinate with the TPT and IAP. The Chair (or Co-Chair) of the Damping AT keeps the TPT Secretary informed of AT activities on a frequent (at least monthly) basis. This AT includes members from government agencies, industry, and universities who are actively involved in damping technologies applicable to engine HCF. The team is to be multidisciplinary with representatives from multiple organizations representing several component technologies as appropriate. The actual membership of the AT may change in time as individuals assume different roles in related projects.

ACTION TEAM CHAIRS

Chair
Mr. Frank Lieghley, Jr.
U.S. Air Force, AFRL/PRTC
1950 Fifth Street, Bldg. 18D
WPAFB, OH 45433-7251
Phone: (937) 255-2611
Fax: (937) 255-2660

Co-Chair
Mr. Ray Pickering
NAVAIR/NAWCAD
Propulsion & Power Engineering
Building 1461
48298 Shaw Road Unit 4
Patuxent River, MD 20670-1900
Phone 301-342-0873
FAX 301-342-4781

INTRODUCTION:

The following pages contain tables, schedules, backgrounds, and summaries of the recent progress of current and planned tasks managed by this action team.

FIGURE 6.0.1 Passive Damping Research Schedule

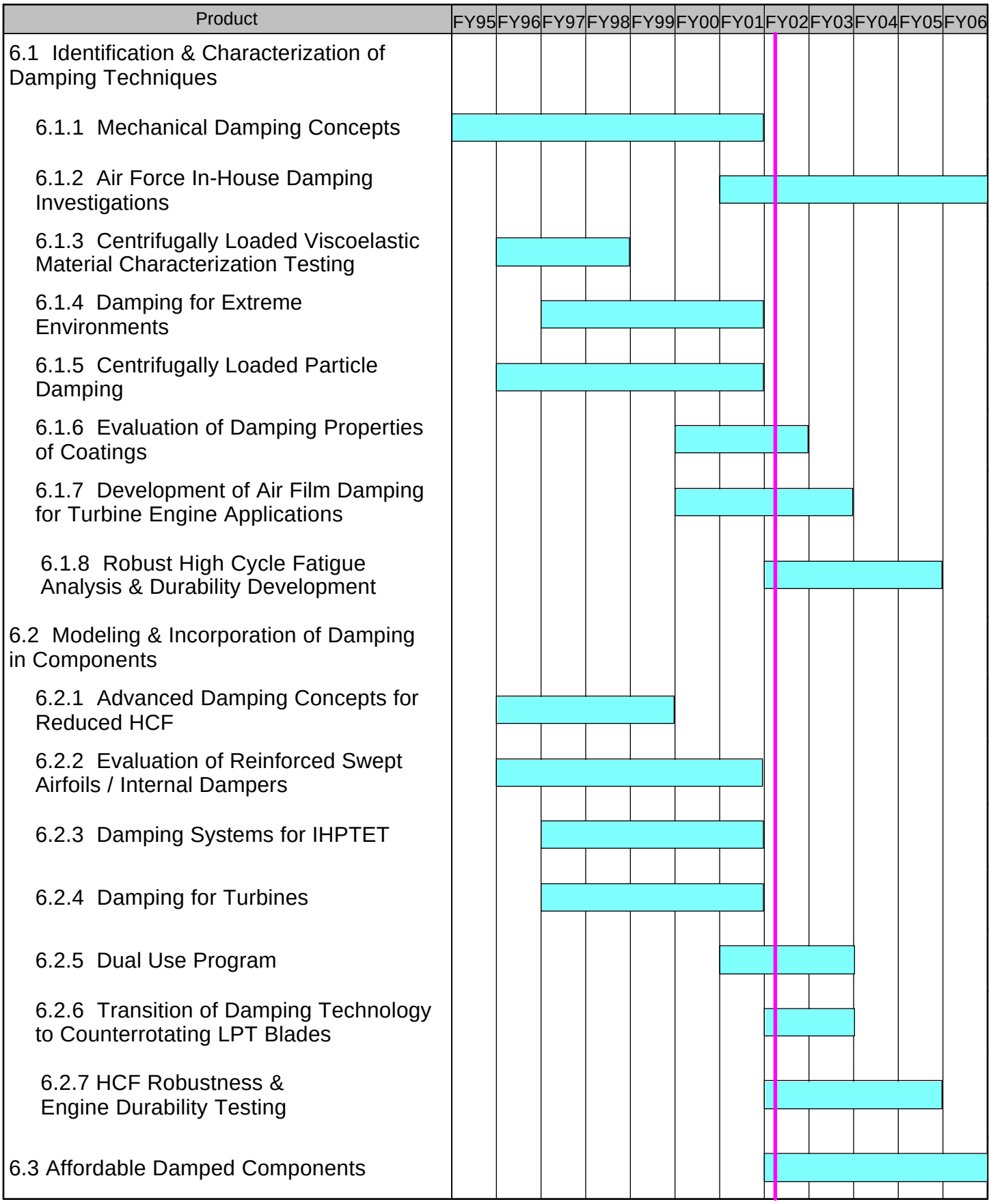

6.1 Identification and Characterization of Damping Techniques

Four types of passive damping systems, judged to have a reasonable chance of effectively damping rotating engine components, are being investigated: (1) friction damping systems, which have been used in platform and shroud applications and now show promise as devices internal to blades, (2) viscoelastic material systems, which have mature design optimization procedures and are now being designed to function under high centrifugal loads, (3) particle damping systems, which have the potential of providing damping independent of temperature, but require a lot of effort in characterization and design optimization, and (4) powder damping systems, which are an extension of the tribology of dry film lubricants, have temperature independent damping, and require the most work in the development of acceptable systems.

6.1.1 Mechanical Damping Concepts

FY 95-01

This effort has been completed. It is reported in more detail in section 6.1.1 of the 2000 HCF Annual Report.

6.1.2 Air Force In-House Damping Investigations

FY 01-06

Background

From 1995, when the National High Cycle Fatigue (HCF) Initiative was started, until 1999, any significant AFRL in-house work on damping was accomplished by the damping experts at the Acoustic and Sonic Fatigue Branch at the Flight Vehicle Directorate, AFRL/VASS. In 1998, the Propulsion Directorate (AFRL/PR) determined that it would be advantageous to develop its own research testing capability, specifically focused on engine hardware. Since that time, over 4 million dollars has been spent to establish that capability in a facility called the Turbine Engine Fatigue Facility (TEFF). Figure 6.2.1.1 is a drawing of its layout.

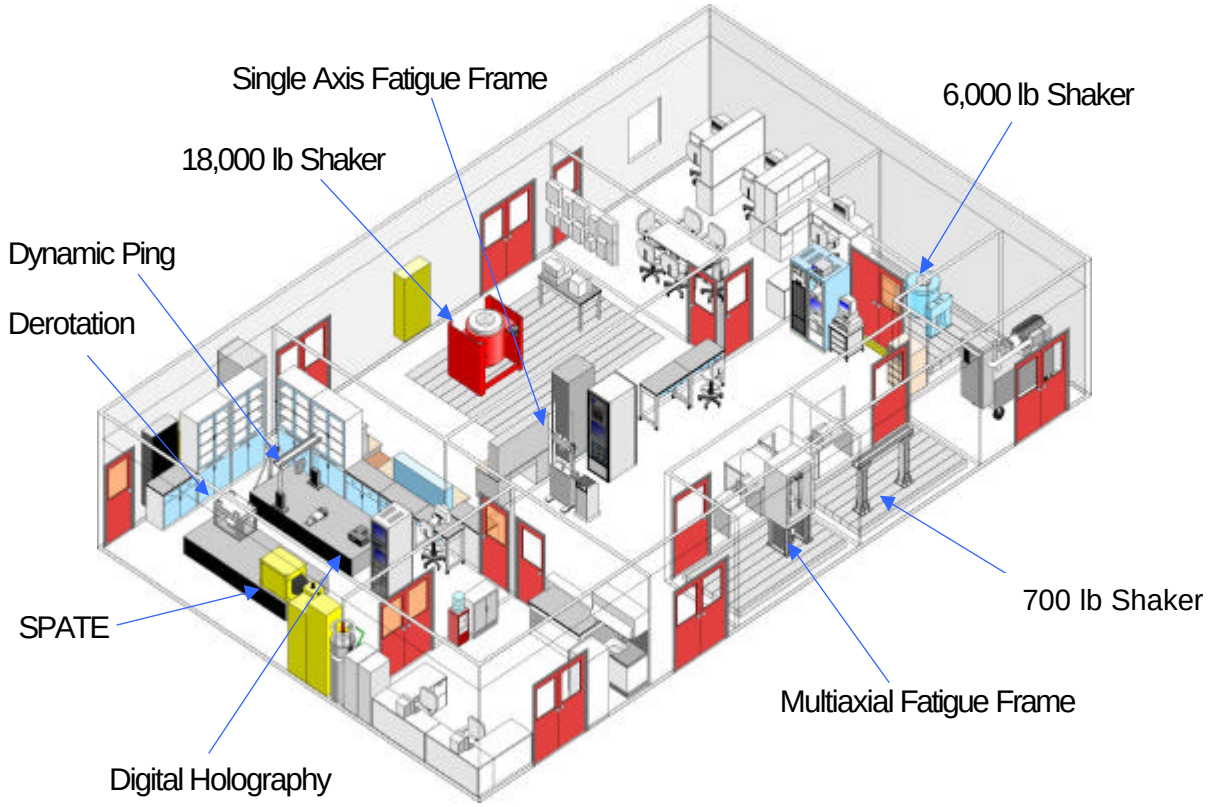

FIGURE 6.1.2.1 Turbine Engine Fatigue Facility

Some of the key test equipment for damping testing at the TEFF include;

a. 700 lb, 6000 lb. and 18000 lb. shakers (Figure 6.2.1.2)
b. High frequency piezo shaker
c. Holographic capability
d. Two laser vibrometers (Figure 6.2.1.3)
e. Intermediate (500°F) and high (2200°F) temperature furnaces
f. Ping test equipment and analysis systems
g. Bruel & Kjaur signal analyzer

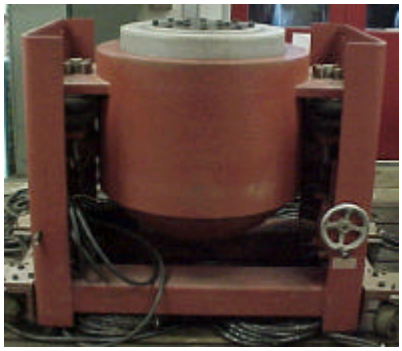

(a) (b) (c)

FIGURE 6.1.2.2 (a) 700 lb, (b) 6,000 lb and (c) 18,000 lb Shakers

FIGURE 6.1.2.3 Single Point Laser Vibrometer

Over the next several years additional equipment and upgrades to the current equipment are planned. Some of these include;

1. Function generators
2. Controllers for the shakers, so that each shaker will have a stand alone capability
3. Optical pyrometer

Currently, the TEFF has the capability of testing specimens or components up to frequencies of 20,000 Hz and up to temperatures of 2200°F.

Test Procedures:

For most damping projects there is a standard process in place to perform testing. When the specimen or component arrives, a fixture is designed to hold the specimen for testing. For simple flat specimens, a vise may be all that is required. The specimen is then tested using a broad-band sweep to determine where the modes are located in the frequency band. The specimen or component is then taken to holographic imaging. There the test article is tested to determine what the modes and mode shapes are that have been identified during the broad-band sweep. This is also helpful in identifying the nodal

lines, whose locations must be known to properly locate instrumentation. Once modes have been characterized, the test article is prepared for the damping test. The test setup will be determined by the test objectives and by the required test environment. At the completion of the test, the data are put in a format that is acceptable to the customer.

Recent Progress

Test Programs

AE3007 Fan Blade Fixture

The AFRL Propulsion Directorate (PR) sponsored a program that was investigating the feasibility of using viscoelastic materials as part of a damping system for fan blades. As part of this program a series of damping bench tests were performed on damped and undamped AE3007 fan blades. It was hoped that the Q values would be between 800 and 900, as they had been in other similar bench test programs. The test results are shown in Figure 6.2.1.4. From this figure it can be seen that for the undamped blade, Number 823, the Q value throughout the temperature range is approximately 300. Also, in the figure, it shows that damped blade, Number 809, is showing less damping than the undamped blade.

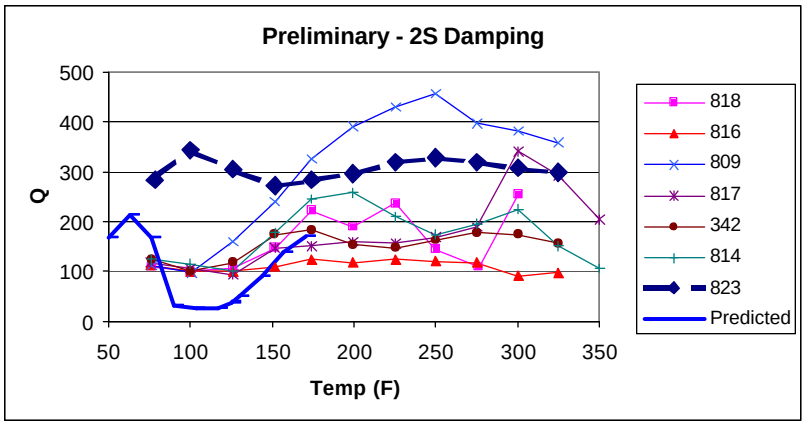

FIGURE 6.1.2.4 AE3007 Blade Bench Test Results

Given these results, it was necessary to modify the fixture, so that higher Qs could be obtained, and retest AE3007 blade 809. There were three modifications performed on the blade fixture. They were as follows:

1. The fixture was modified to allow a magnetic transducer be attached to the fixture, rather than have it mounted on a separate stand.
2. The shim used to force the blade dovetail against the fixture breach block was enlarged and changed from aluminum to stainless steel.
3. The number of set screws used to clamp the shim was increased from one to three and the size of the set screws was increased.

A picture of a blade and the bench test fixture is shown in Figure 6.2.1.5.

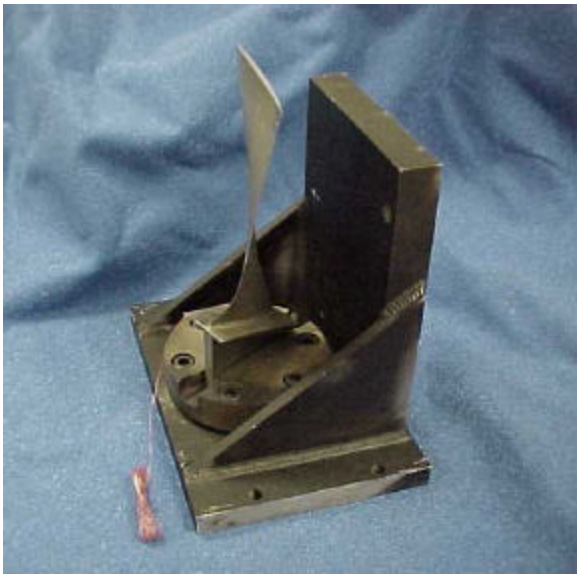

FIGURE 6.1.2.5 AE3007 Blade and Test Fixture

After these modifications were made, an undamped blade was tested up to 300°F at the TEFF. The results showed that Qs increased into the range of 800 to well over 1000. They are shown in Figure 6.1.2.6.

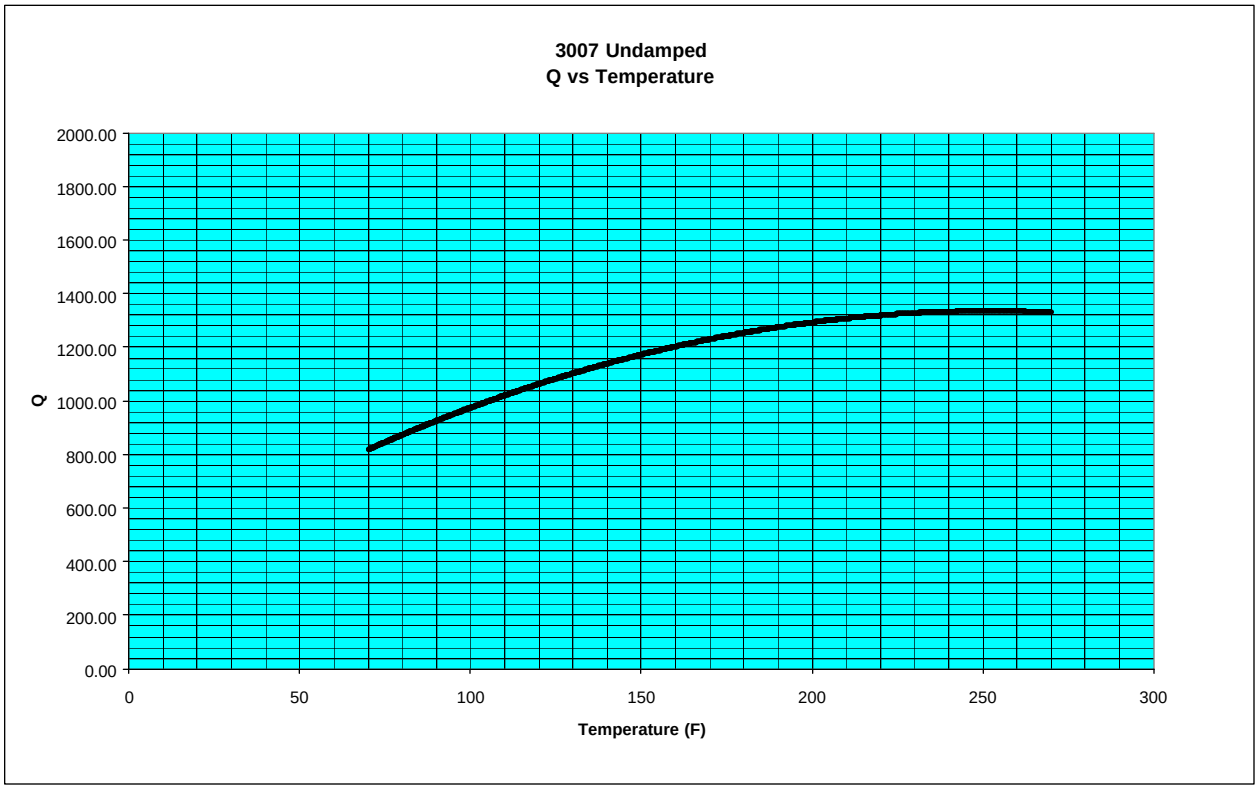

FIGURE 6.1.2.6 Undamped AE3007 Blade Bench Test

It is probable that the placement of the magnetic transducer on the fixture had little to do with the improvement, but it simplified the test setup. The key to the improvement was more likely the improvement of the boundary conditions of the test. The stiffer shim and the three set screws verses one, in conjunction with control of the torque on the set screws, provided a more uniform load distribution that was more representative of what would be seen in an engine.

After the undamped blade had been successfully tested, damped blade 809 was placed in the fixture under the same loading and tested at the same temperatures. The test results, Figure 6.2.1.7, show that the blade response was similar to that shown in the previous damped-blade test. It has its maximum damping at approximately 100°F, where the design intended it and shows approximately 75% reduction in the amplitude of Q.

These consistent results provide confidence that future tests on AE3007 fan blades in this fixture will provide good results.

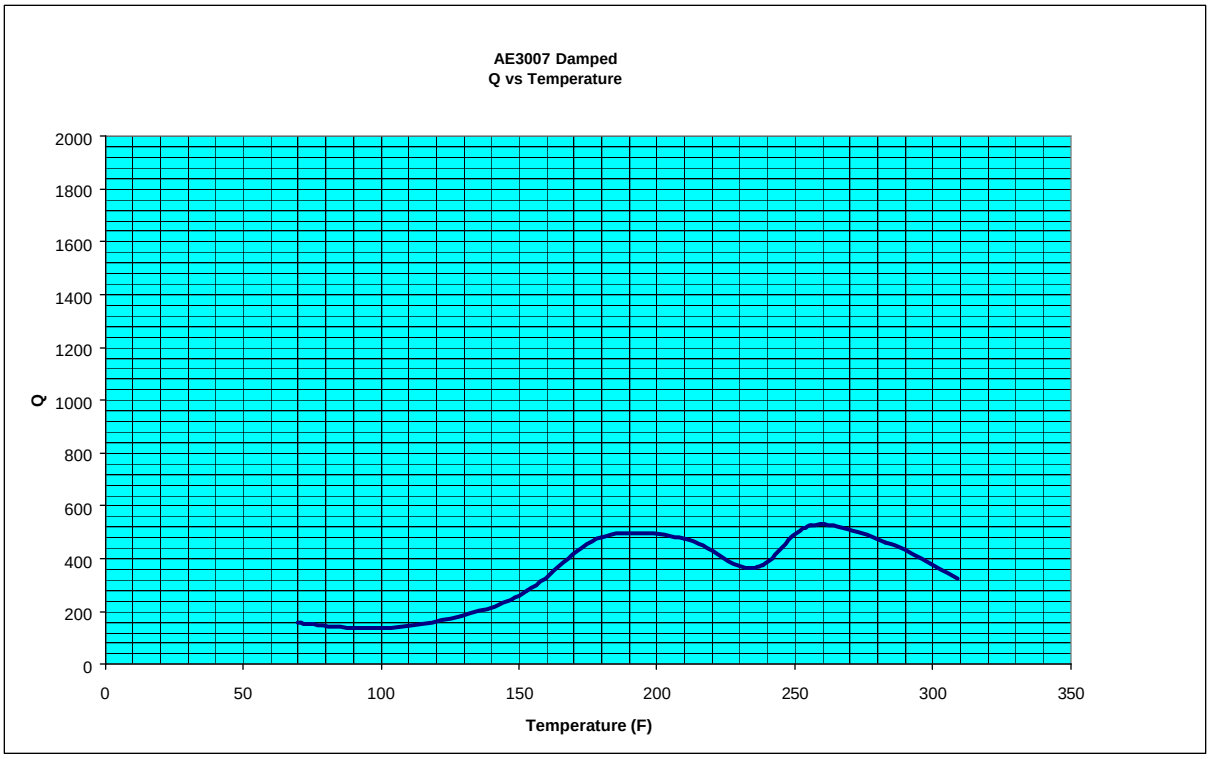

FIGURE 6.1.2.7 AE3007 Damped Blade #809 Test Results

Very Thin Constrained Layer Viscoelastic Damping

This project will attempt to demonstrate the damping effectiveness of a multi-layered thin viscoelastic constrained layer damping treatment on a simulated blade configuration. The blade specimens are made of industrial pure titanium. The constraining layers will be made out of 0.002" industrial pure titanium. The viscoelastic material will be 0.0002" thick. There will be a total of ten constraining layers and nine viscoelastic layers in the viscoelastic constraining layer "sandwich." A 0.028" pocket will be machined into the blade specimen. The viscoelastic sandwich then will be bonded into the machined pocket with AF191 adhesive. Figure 6.2.1.8 shows the blade specimen that was fabricated for this test.

FIGURE 6.1.2.8 Simulated Blade Specimen

The baseline specimen's characteristics have been analytically determined using finite element analysis. It has also been tested. A broad-band sweep has been performed on the baseline specimen. A typical broad-band sweep is shown in Figure 6.2.1.9. The specimen was then taken to the holographic imaging equipment and was scanned to better define each of the modes identified on the broad-band sweep. The test fixture and the blade were then placed into the intermediate temperature furnace (shown in Figure 6.2.1.10) and tested up to 450°F at 25°F increments. The test results are shown in Figure 6.2.1.11. These results will be compared with the test results of the damped specimens. The results of these tests will be presented in a paper at the 7th HCF Conference.

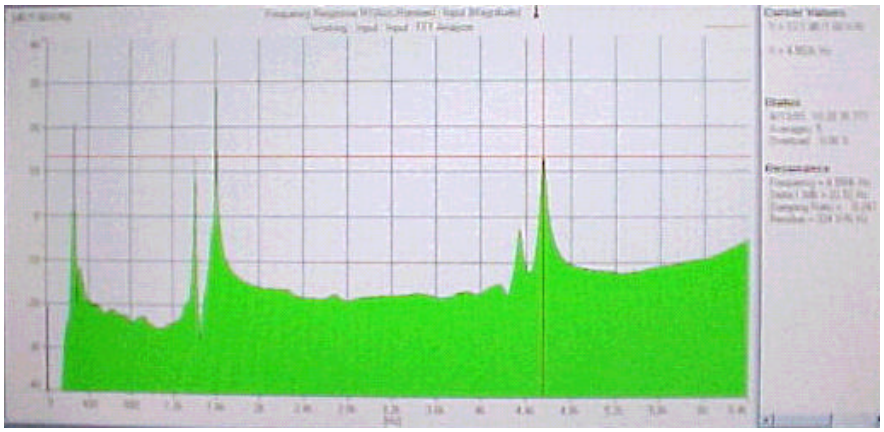

FIGURE 6.1.2.9 Typical Broad Band Sweep

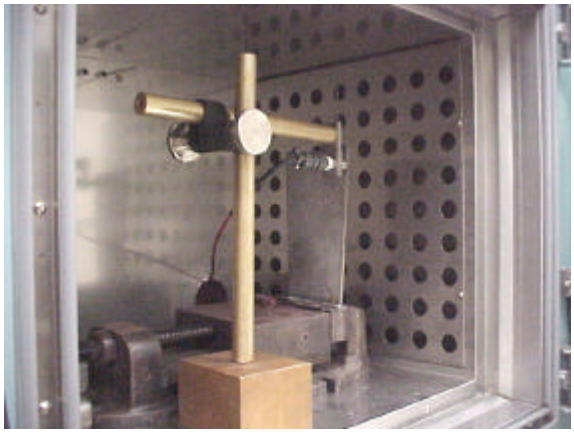

FIGURE 6.1.2.10 Specimen Baseline Test Setup in the Intermediate Temperature Furnace

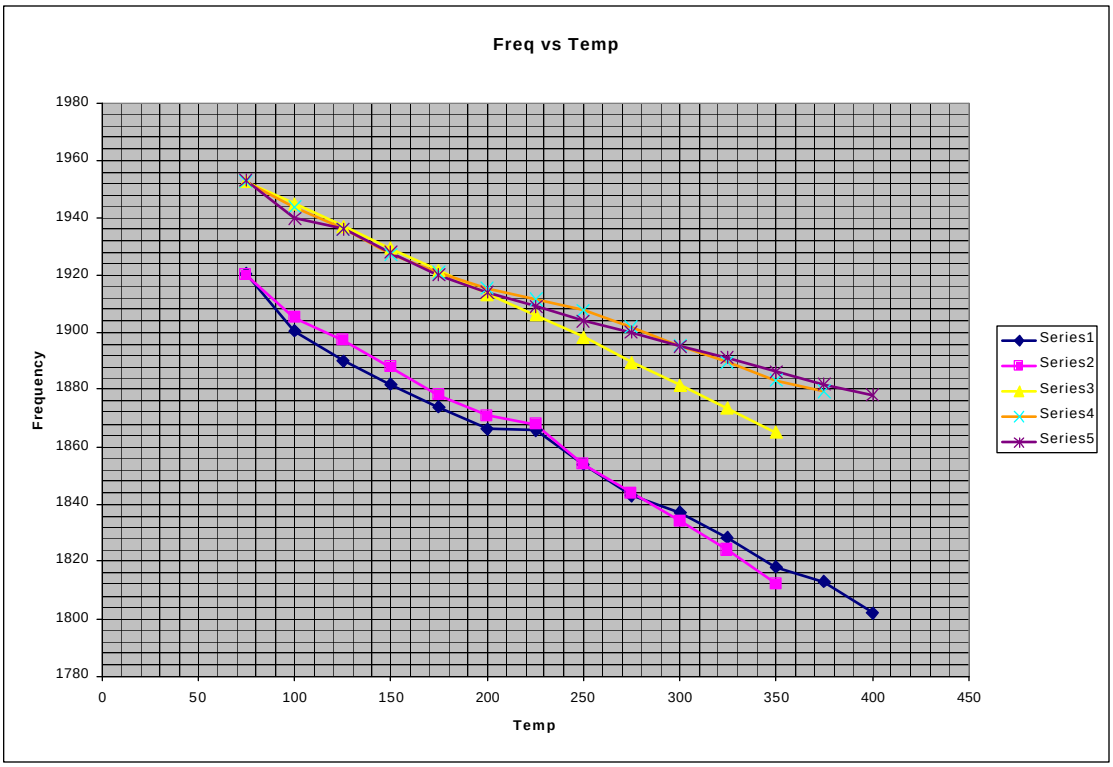

FIGURE 6.1.2.11 Baseline Test Results

Low Temperature Damping Coatings

This project supports the hard coating damping testing that has been performed at Roush Anatrol.

In designs that do not have a considerable interaction between a blade and a disk, where a rim damper would not be effective, available options for damping the rear stages of the compressor are very limited. Hard coatings on the blades offer one means of damping of such stages.

The primary coating being investigated is MagSpinel. Specimen baseline tests were performed at Roush Anatrol on eighteen uncoated beams before testing with a coating was performed. Specimens # 1-9 were coated with the MagSpinel coating. Coated specimens #1 and #4 were tested at Roush Anatrol and specimen #3 was tested at Ohio State University (OSU) and at the TEFF.

The tests at Roush Anatrol have produced some unexpected results. There were significant differences between the sets of test data. In the Roush Anatrol and the OSU data there were indications that the level of damping is a function of the strain in the coating. It was decided that the TEFF would run a test on one of the specimens (Specimen # 1) tested at Roush Anatrol. Since the TEFF was still developing testing capabilities above 500°F, room temperature testing only would be accomplished.

Figure 6.1.2.12 shows one of the test specimens. They are 10" long with a 2" base, 0.75" wide and 0.095" thick. A 0.5" hole is drilled through the center of the base. The TEFF test setup is shown in Figure 6.2.1.13.

Further TEFF testing of these beams is planned in order to verify which set of data is closer to being correct and to actually define the relationship between strain and damping. These tests will be run in CY2002.

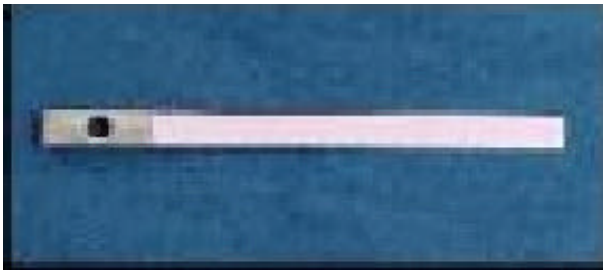

FIGURE 6.1.2.12 Low Temperature Coating Test Specimen

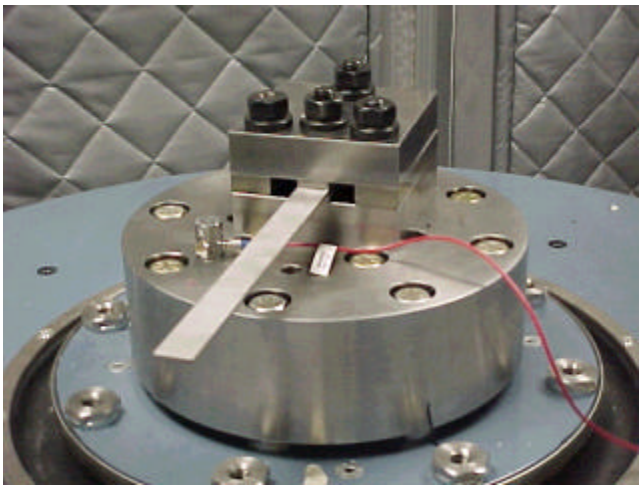

FIGURE 6.1.2.13 Low Temperature Coating Test Specimen in the Test Setup

High Temperature Turbine Blade Damping Coating

In conjunction with an AFRL/ PR contract the Air Force agreed to test a series of specimens that are both coated and uncoated. The uncoated specimens will be baseline specimens for the six coated specimens. Figure 6.1.2.14 shows one coated and one uncoated specimen.

Broad-band sweeps performed on one uncoated specimen and on one coated specimen revealed significant differences in the mode shapes and node locations on these test specimens. These specimens and the other six were tested holographically to specifically determine the modes and nodes of interest. The testing showed that there were two groups of specimens with a difference of almost 800 Hz between the two groups for the same room temperature mode. Consultation with the customer revealed that the specimens had been cut out of two different blocks of single crystal material with different crystal orientations. Analysis showed that the properties of single crystal material vary significantly with orientation. Review of the crystallographic orientation test data for the material showed that those test results agreed reasonably well with the analysis that had been performed.

A fixture for the shaker tests has been designed and analyzed to ensure that no fixture modes would interact with the specimen modes. The finite element model showed that there were no problems. The fixture is now ready to support the testing at temperatures up to 2200°F planned for CY2002.

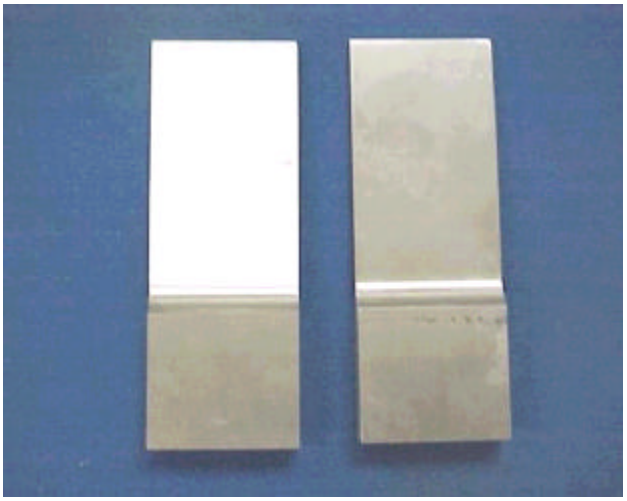

FIGURE 6.1.2.14 High Temperature Damping Coating Specimens

Participating Organizations: Air Force Research Laboratory (AFRL), Universal Technology Corporation, Ohio State University and Wright State University

Points of Contact:

Government
Dr. Charles Cross
U.S. Air Force AFRL/PRTC
1950 Fifth Street, Bldg 18D
Wright-Patterson AFB, OH 45433-7253
Phone: (937) 656-5530
Fax: (937) 656-5532

Contractor
Mr. Don Zabierek
Universal Technology Corporation
1270 N. Fairfield Road
Beavercreek, OH 45432-2600
Phone: (937) 255-5416
Fax: (937) 656-9004

6.1.3 Centrifugally Loaded Viscoelastic Material Characterization Testing

FY 96-98

This effort has been completed. It is reported in more detail in section 6.1.3 of the 2000 HCF Annual Report.

6.1.4 Damping for Extreme Environments

FY 97-01

No progress was reported for this effort for CY2001.

6.1.5 Centrifugally Loaded Particle Damping

FY 96-01

Background

This work was targeted at determining if particle damping can be a viable damping treatment for military aircraft engine blades despite their high centrifugal loads. Research has focused on three primary areas:

(1) Development of accurate predictive algorithms of particle damping behavior that can account for the centrifugal loads
(2) Performance of laboratory-based testing of particle damping characteristics of specific interest to the understanding of behavior under centrifugal loads
(3) Testing of potential candidate damping treatments under centrifugal loads

Final Results

Technical effort concluded in this reporting period. The majority of the effort in this period concentrated on the third task described above based on the results of the first two tasks. Numerous experimental results demonstrated that particle damping can work under ratios of centrifugal load and dynamic excitation that are comparable to aircraft engine blade applications. Over a thousand different tests on 25+ particle damping configurations were performed at different RPM and excitation levels. A previously described stand-alone laboratory based Centrifugally Loaded Dynamic Excitation Facility (CLDEF) was used to generate this data (see section 6.1.5 of the 2000 HCF Annual Report). Tested configurations consisted primarily of traditional multiple particles in one cavity, multiple particles in slots, and multiple individual particles (MIP) each in their own smaller cavities. Examples of trial cavities are shown in Figure 6.1.5.1.

FIGURE 6.1.5.1 Examples of Damper Trial Inserts

While most screening tests were performed at centrifugal load levels from 180 to 4500 G's, tests of the best damping configurations were also performed at centrifugal loads of up to 6000 G's. For these tests, particle damping effectiveness was still observable at dynamic excitation levels of ±150 G's to ±280 G's (which was the limit of the CLDEF excitation system). Significant levels of attenuation were seen for multiple configurations at acceleration ratios levels as low as about 0.016, which is well below the peak acceleration ratio levels typical in turbine engines. Damping was demonstrated for two different modes (first and second bending) ranging from 300 Hz to 1400 Hz. Damped results equivalent to traditional modes with Q's of 30 to 50 were typically achieved.

Tests were primarily performed at various consistent fixed dynamic acceleration amplitudes using dwell sine sweep excitation at a constant RPM/centrifugal load level. Representative results are shown in Figure 6.1.5.2. These results illustrate a common feature of particle damping in that achieved damping generally increases with increasing excitation levels (to a certain point). The "flattened" mode shape of the well-damped configuration at higher excitation amplitudes is also typical.

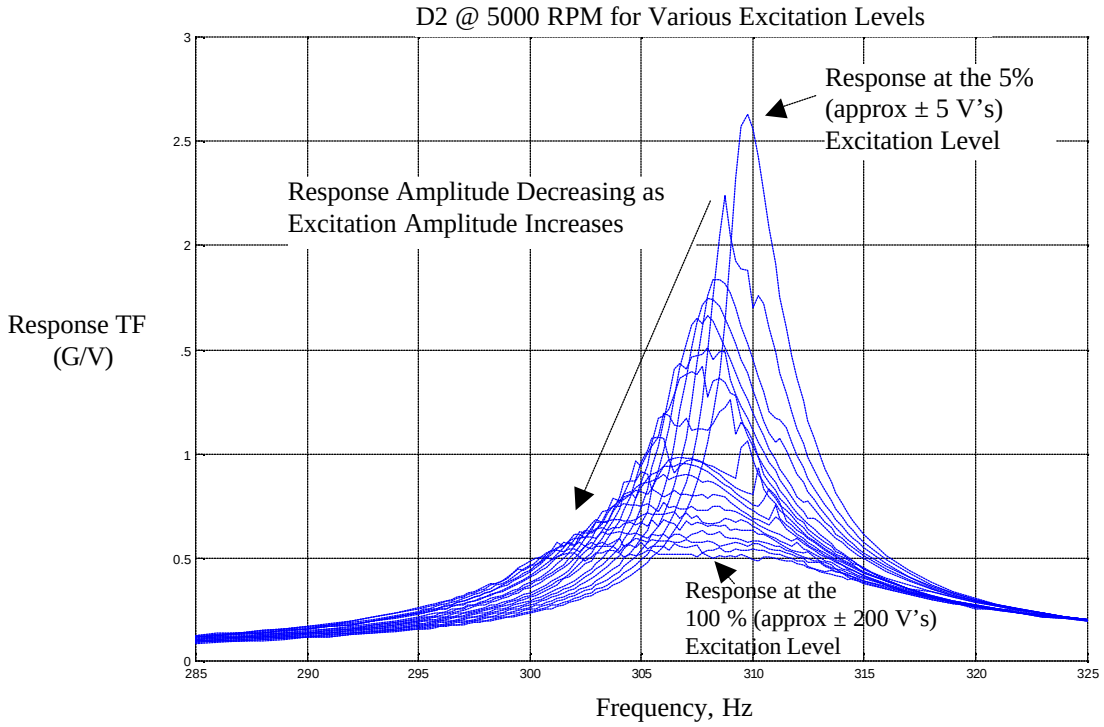

FIGURE 6.1.5.2 Examples of Results of Particle Damping Behavior at 4500 G's Centrifugal Load at Increasing Out-of-Plane Dynamic Excitation Levels

Examples of damping levels (for comparable excitation levels) at various RPMs are shown in Figure 6.1.5.3. These RPM settings correspond to centrifugal loads of 180 to 4500 G's. For ease of reference, damped cases and baseline cases are shown in the same color for each RPM setting. As is clear from the data, there is a small but clear decrease in damping effectiveness with increasing centrifugal load. In order to reduce the amount of data shown, and provide quick comparisons of effectiveness, a peak reduction factor was calculated for every test performed. Peak reduction was estimated by forming the ratio of the peak value of the baseline response, divided by the peak value of the damped response. Higher values are thus better. The rough method used is illustrated in Figure 6.1.5.3. Examples of results using this metric for two different damping configurations are shown in Figure 6.1.5.4. Each surface plot is built from the peak reduction response for 50 individual sine sweep measurements of the types shown in Figure 6.1.5.2 or Figure 6.1.5.3 plus a matching number of baseline tests. Peak reductions of about a factor of 2 to 3 were typically achieved. The damped results corresponded to effective Q's of 30 to 50.

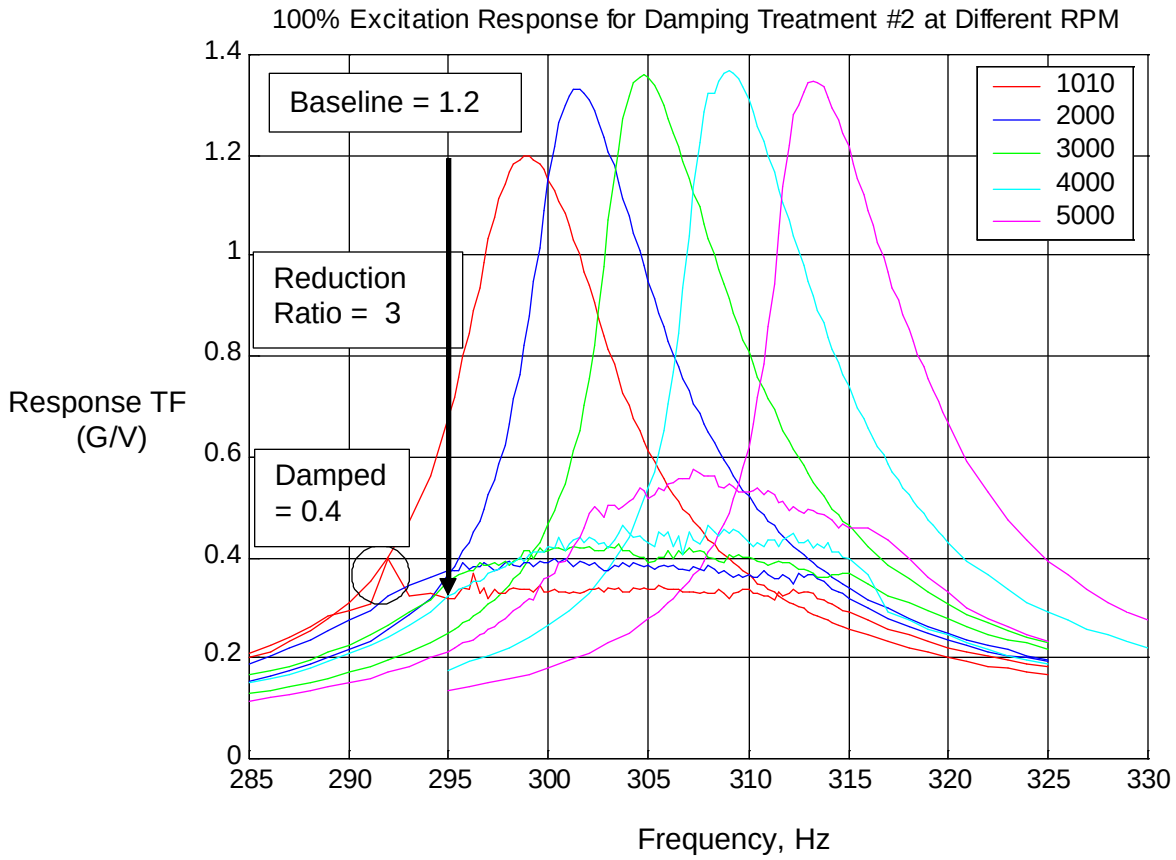

FIGURE 6.1.5.3 Representative Results Comparing First Mode Results for the Baseline (Undamped) Versus a Particle Damped Configuration at a Variety of RPM's Corresponding to 180 to 4500 G's Centrifugal Load. Full Scale Excitation Was 200V

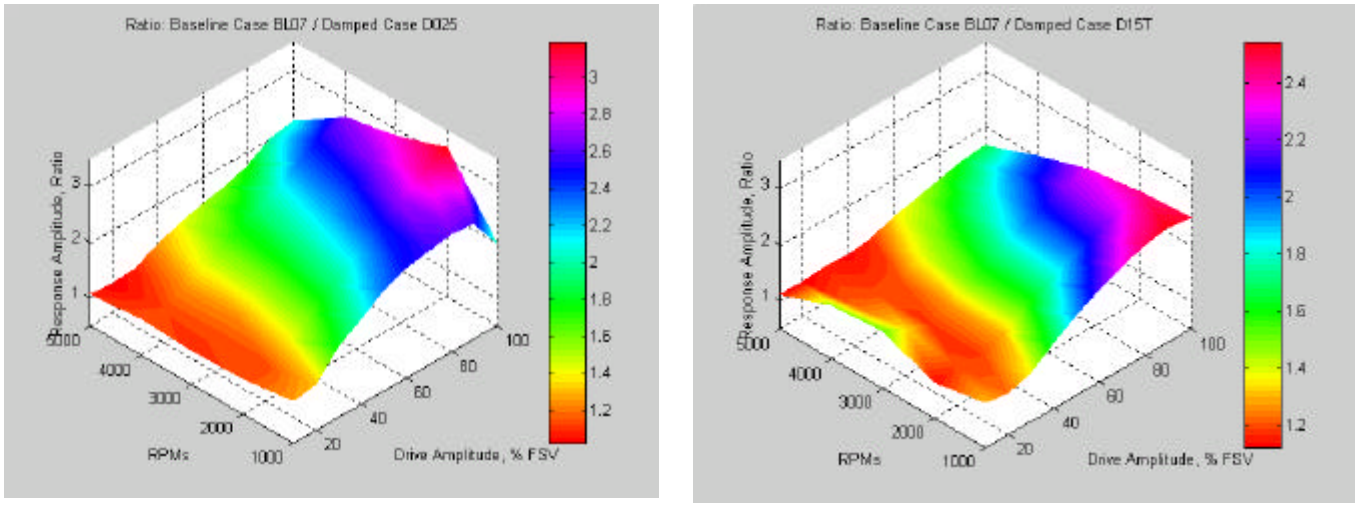

FIGURE 6.1.5.4 Comparison of Peak Reduction Versus Centrifugal Load and Dynamic Excitation Amplitude for Two Different Damping Configurations.

Technical effort in this project was concluded in August 2001. No further effort is currently planned.

Participating Organizations: CSA Engineering, Inc., University of Dayton Research Institute (UDRI)

Points of Contact:

Government
Mr. Frank Lieghley, Jr.
U.S. Air Force, AFRL/PRTC
1950 Fifth Street, Bldg. 18D
WPAFB, OH 45433-7251
Phone: (937) 255-2611
Fax: (937) 255-2660

Contractor
Mr. Eric Flint
CSA Engineering, Inc.
2565 Leghorn St.
Mountain View, CA 94043
Phone: (650) 210-9000
Fax: (650) 210-9001

6.1.6 Evaluation of Damping Properties of Coatings

FY 00-02

Background

While coatings have been reported as being effective in some cases in reducing the amplitude of resonant vibrations in blades, other studies have raised questions as to their effectiveness. In consequence, this work was undertaken to provide a fundamental study of the ability of coatings to reduce the amplitude of resonant vibration in blade-like structures.

Recent Progress

Prior work has suggested the probability of nonlinear damping. As the extraction of material damping properties from system response data in such cases requires a well-characterized stress distribution within the dissipating component, a cantilever-mounted rectangular beam was chosen as the test article. Beams were made of Hastelloy X, 0.095 inches thick, 0.75 inches wide and 8 inches of unsupported length, coated on each side by a plasma-sprayed layer of magnesium spinel, 0.015 inches in thickness. Results obtained to date are limited to room temperature properties. The damping at elevated temperatures will be determined during CY2002.

Vibration testing equipment in the Turbine Engine Fatigue Facility (TEFF) at WPAFB was used for most of the testing. The specimen was driven with a large Unholtz-Dickie shaker with sine controller at frequencies near resonance. Velocities were measured at a point 2 inches from the fixed end and elementary theory was used to evaluate strains. Acceleration at the root of the beam was also observed. Response curves in the vicinity of the resonances of the 2^{nd}, 3^{rd} and 4^{th} bending modes were obtained at several levels of constant amplitude of base acceleration. For the primary test series, a damping determination was made at 16 levels of amplitudes up to 511 micro-inches per inch (units) of strain in the 2^{nd} bending mode; at 17 levels, up to 336 strain units in the 3^{rd} bending mode; and at 24 levels, up to 166 strain units in the 4^{th} bending mode. For each run, at least two methods of determining the damping were used, with satisfactory agreement obtained between the two. System loss factors did not vary significantly between modes. A system Q = 900 at 10 micro-strain units, Q = 200 at 100 units, and Q = 120 at 400 units are typical of results obtained.

Data from a series of tests in the same facility (the same three modes, with a total of 12 amplitudes) at comparable ranges of strain were used to estimate the extent of dissipation due to the bare beam, the mounting system, and the environment. Using these results, together with data from the primary series, the contribution of the coating alone was determined, and from this, the inherent damping properties of the material were found. For the range of interest (100-500 micro-strain), material loss factors in the range of 0.018 to 0.04 were observed. Amplitude dependence was noted, with loss factors increasing (approximately) as the square root of strain. The storage modulus for the magnesium spinel was found to be 6 Mpsi. The loss modulus of the magnesium spinel was determined to be in the range of 200 to 300 Ksi at a representative strain of 300 micro-inches per inch.

Damping values were extracted from response functions measured in two other series of tests. Response curves were developed from data obtained by Dr. Lazreq, at Roush Anatrol under UTC contract. Strains were computed by observing the peak velocities and applying classical beam theory. This produced results at 5 amplitudes, to 216 micro-strain units in the 2^{nd} bending mode and at 4 amplitudes to 74 units in the 3^{rd} bending on the same beam, but in a different facility. When reduced by the same methodology, this data indicated a loss modulus of 250 ksi at 200 micro-inches of strain. This is taken as satisfactory confirmation of the results obtained with the primary data series. (See Section 6.1.6.1 for a description of the Roush Anatrol testing.) Damping values were also extracted from data taken by Dr. Shen, of the Ohio State University under UTC contract, at the TEFF (at 7 amplitudes to 741 micro-strain units in the 2^{nd} bending mode; at 9 amplitudes to 415 units in 3^{rd} bending, and at 8 amplitudes to 241 micro-units in 4^{th} bending). After applying the same techniques of analyses, the material loss modulus was determined from these tests to be about 400 ksi in the range of interest. However, indications were found that this specimen had been subjected to significant overload. This suggests that mechanical damage may increase the damping of coatings materials such as these.

The material properties, as determined above, were used to estimate the damping such a coating would add to that of an actual blade. A cantilever beam having thickness, frequency, and wavelength characteristic of the two-stripe mode was identified. Using the above data and a methodology developed through this effort, a system amplification factor (Q) of 160 at 500 micro-inches of strain was predicted. The addition of this amount of damping to a blade would be extremely useful in the control of engine vibrations.

Participating Organizations: Air Force Research Laboratory (AFRL), Universal Technology Corporation, Roush-Anatrol, and Ohio State University

Points of Contact:

Government
Mr. Frank Lieghley, Jr.
U.S. Air Force, AFRL/PRTC
1950 Fifth Street, Bldg. 18D
WPAFB, OH 45433-7251
Phone: (937) 255-2611
Fax: (937) 255-2660

Contractor
Peter J. Torvik, Consultant
Universal Technology Corporation
1270 North Fairfield Road
Dayton, OH 45432-2600
Phone: (937) 426-2808

6.1.6.1 Damping Testing of Simple Coated Beams
FY 01

Following successful design modifications of the test apparatus, a test matrix was defined that includes four strain levels at three temperatures for both the 2nd and 3rd bending, and four strain levels at room temperature for the 4th bending as illustrated in Table 6.1.6.1.1.

Mode	Room Temp.	500 °F	1000 °F
2B	120, 180, 270, 400 *me*	120, 180, 270, 400 *me*	120, 180, 270, 400 *me*
3B	95, 135, 200, 300 *me*	95, 135, 200, 300 *me*	95, 135, 200, 300 *me*
4B	95, 135, 200, 300 *me*	--	--

TABLE 6.1.6.1.1 Test Matrix

The uncoated specimen baseline testing was completed. For each of the 18 bare beams, the damping ratio, the force input, the maximum tip velocity, as well as the maximum strain level were measured and documented per the test matrix parameters shown above.

The bare beams were then returned for coating. A total of four coatings were selected from three engine companies (General Electric, Pratt and Whitney, and Rolls Royce). These coatings were as follows:

1. Thermal barrier coating
2. UTRC Hard coating
3. Magspinel (old version)
4. Magspinel (new version)

Only the magspinel beams were coated and returned for testing, thus far. The old version Magspinel was coated 15 mils thick while the new version was coated in two thicknesses: 15 mils and 25 mils. Initial evaluation of these coated beams showed a non-linear jump phenomenon. This is particularly obvious when comparing a sweep-up measurement to a sweep down. In a non-linear case, both the period and the shape of the frequency response will vary with the amplitude of the excitation force. The location of the peak response for a slowly sweeping input frequency is not the same for an upward sweep as it is for a downward sweep as shown in Figure 6.1.6.1.1.

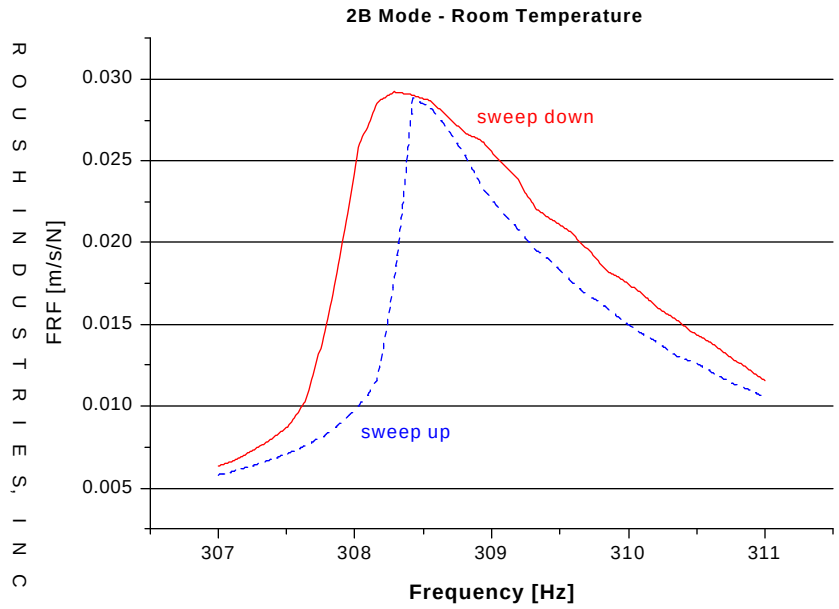

FIGURE 6.1.6.1.1 Frequency Response Function for Sweep-Up and Down Excitation of the Coated Beam.

The initial evaluation of this phenomenon was that this particular ceramic coating would considerably stiffen the beam while adding very little damping to the system, resulting in a non-linear jump phenomenon. In order to verify this, a series of tests were conducted and the findings are summarized in Table 6.1.6.1.2.

Beam Configuration	Test Conditions	Result
A. Bare beam	Different force levels Different modes	Linear
B. Beam with CLDT	Different force levels Different modes Different damping ratios	*Linear*
C. Thicker beam	Different force levels Different modes	*Linear*
D. Bare beam with increased stiffness	Different force levels Different modes	*Linear*
E. Coated beam	Different force levels Different temperatures Different modes Different coating thickness Old and new Magspinel	*Non-linear*

TABLE 6.1.6.1.2 Test Conditions to Check for Non-Linearity

The thicker bare beam in configuration C was made with the same dimensions as the baseline beam but with an increased thickness from 95 mils to 105 mils. In beam configuration D, 5 mils shim stock was super glued on one side of the bare beam for an estimated 20% to 30% increase in stiffness.

The results of Table 6.1.6.1.2 clearly show that the test setup is not the reason this non-linearity phenomenon was observed, but rather, they confirm that the increase in stiffness coming from the coating material is the main cause.

To further validate this assumption, more tests were conducted using a ring-down approach. The response of the beam was measured in the time domain instead of the frequency domain. The beam clamping fixture was removed from the shaker and mounted firmly to a bedplate. A "padded" pluck mechanism was built with a hook over the tip of the beam to enforce a static tip displacement. The beam tip was then deflected by ¼", the hook let-off, and the time history of the beam tip velocity recorded for 18 seconds. A portion of this time history is shown in Figure 6.1.6.1.2.

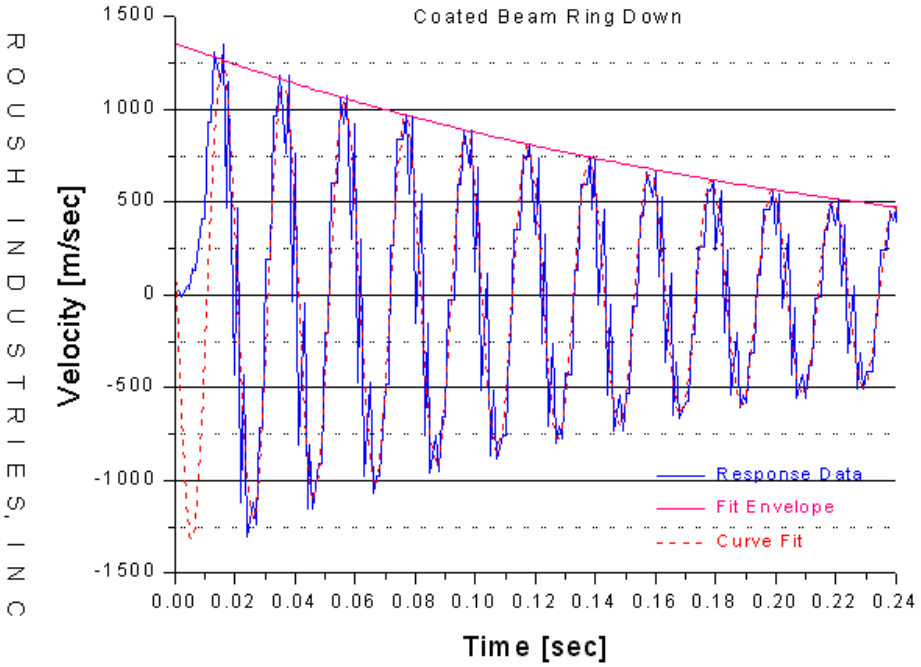

FIGURE 6.1.6.1.2 Time History of Beam Tip Velocity in a Ring-Down Approach for a Coated Beam

The time history data for both a bare beam and a coated beam were measured using this approach. The tip velocity time response was curve-fitted with two exponentials that account for ring-down of the two dominant frequencies observed in the data. For the coated beam, the curve-fitting process had to be achieved over several short time segments of the beam response. The curve fitting used ideal decaying sinusoids over the time data of interest.

Good linearity is again observed for the bare beam. As for the coated beam, a frequency increase was noticed with a decrease in amplitude, confirming our assumption of a softening spring and therefore the non-linear jump phenomenon measured in the frequency response functions. Moreover, a decrease in damping was measured with decreasing amplitudes.

After it was confirmed that the test setup is still adequate to perform this experiment, two coated beams (Magspinel old and new version) were tested per a modified test matrix. Attention was paid to the parameters affecting the damping properties of these coating materials to refine the matrix. In addition, because the coating material had significantly increased the system stiffness, the highest strain levels of the test matrix of Table 6.1.6.1 could be not reached anymore. Table 6.1.6.1.3 shows the refined test matrix where the highest strain level is exchanged for a lower level, and a very low strain level is added to the test matrix.

Mode	Room Temp.	500 °F	1000 °F
2B	0.5, 80, 120, 180, 270 *me*	0.5, 80, 120, 180, 270 *me*	0.5, 80, 120, 180, 270 *me*
3B	0.2, 45, 95, 135, 200 *me*	0.2, 45, 95, 135, 200 *me*	0.2, 45, 95, 135, 200 *me*
4B	0.1, 50, 95, 135, 200 *me*	--	--

TABLE 6.1.6.1.3 Refined Test Matrix

Again, as was done for the bare beams, the damping ratio, the force input, the maximum tip velocity, as well as the maximum strain level were measured and documented. Typical results are shown in Figures 6.1.6.1.3 and 6.1.6.1.4 for the coated beams testing.

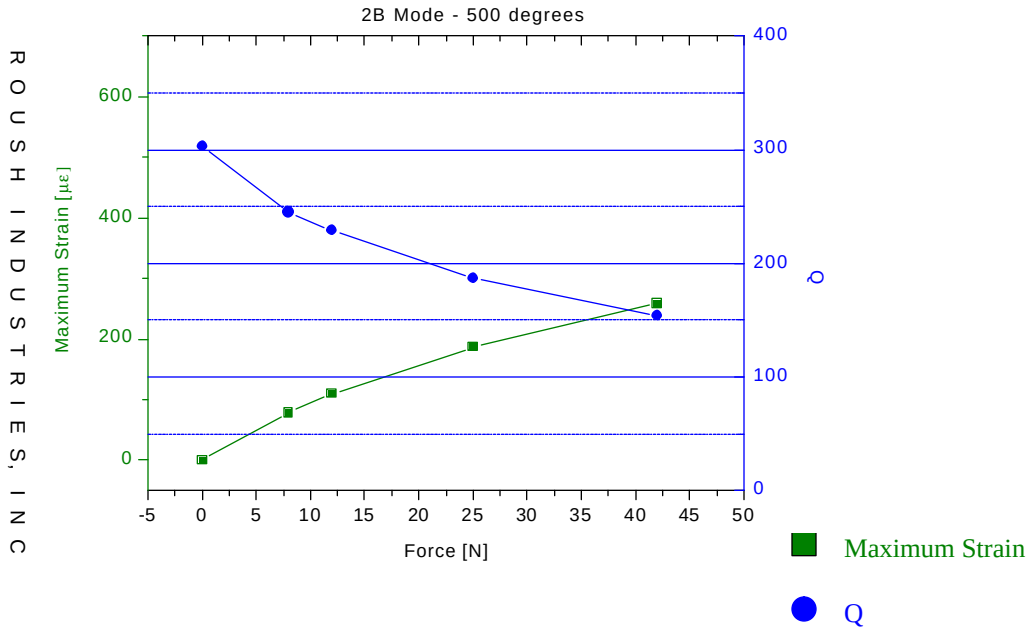

FIGURE 6.1.6.1.3 Strain and Q vs. Forces for the Coated Beam

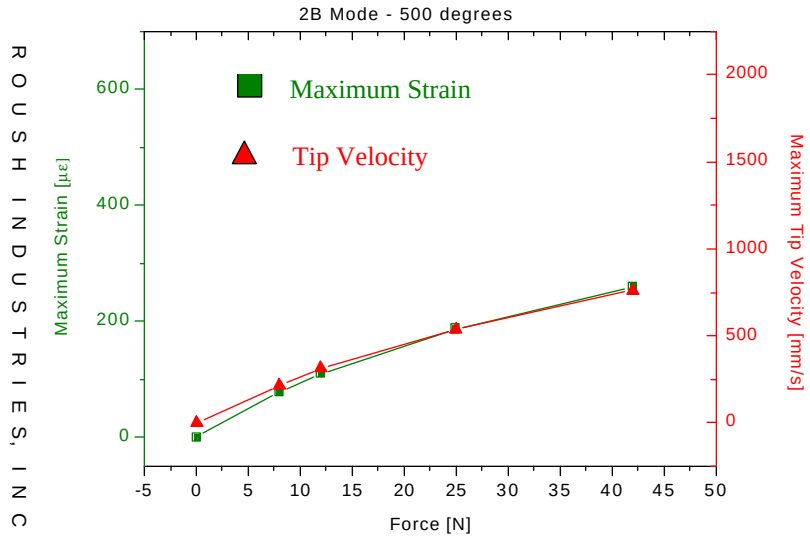

FIGURE 6.1.6.1.4 Strain and Maximum Tip Velocity vs. Force for the Coated Beam

These coated beams will be thermally cycled to induce micro-cracking in the coating and will be re-tested per the same test matrix of Table 6.1.6.1.3 to evaluate the effect of the micro-cracking on the damping performance of the coated beam. An analytical model will also be developed to investigate the presence of non-linear damping and/or non-linear stiffness. Finally, since these beams respond in a non-linear manner to sinusoidal force excitation, the data needs to be fitted to an appropriate model for an accurate determination of damping properties of these coating materials.

6.1.7 Development of Air Film Damping for Turbine Engine Applications

FY 00-03

Background

The basic premise of the *Damping Technologies, Inc., (DTI) Air Film Damping* System (AFDS) concept involves integrating an air gap into a given structure such that, during vibration of the structure, relative motion of the surfaces of the AFDS results in movement or "pumping" of the air in the gap. The flow in the air film gap appears to be viscous and results in high internal cyclic pressure differences, acting in opposite phase to the local modal velocity, much as occurs with squeeze film dampers in rotating turbo-machinery. The difference is that no rotation is involved here, and no special means are needed to maintain the film. Since air is the damping medium, there are no temperature survival limitations or effective temperature range concerns. The properties of air, which are pertinent to AFDS, are reasonably constant across the (-50^{o} F) to ($2{,}000^{o}$ F) temperature range. Since air has little mass, it will be impervious to centrifugal loads. This is very promising technology relative to solving HCF issues in rotating and non-rotating turbine engine structures.

Recent Progress

Work completed in the first quarter of 2001 was related to completion of the SBIR Phase I Contract F33615-00-2025. The goal of this particular program was to develop design tools for application of AFDS and also to demonstrate the use of the tools to design, fabricate, and test an AFDS applied to an actual turbine engine fan blade. The work was limited to prediction and bench test measurement of the attenuation associated with given AFDS designs.

FIGURE 6.1.7.1 AFDS Integrated into a Fan Blade

Techniques were developed during the program to model AFDS using FEA and to do some limited optimization work using the model. Two separate AFDS designs were generated. Hardware was fabricated according to the designs. The hardware was tested and the resulting attenuation performance associated with each AFDS was documented. Results were very impressive. $Q < 20$ was achieved in the target two-stripe mode for one design. Correlation to the FEA predictions was excellent. Figure 6.1.7.1 shows one of the AFDS designs. In essence, a pocket is milled in the fan blade. A separate cover platelet is attached via structural adhesive or metallic bond. A specific air film gap is maintained between the AFDS platelet and the fan blade. Figure 6.1.7.2 describes predicted frequency response on the fan blade for a particular AFDS configuration. Figure 6.1.7.3 describes an experimental frequency response measurement acquired on the hardware built according to the design of Figure 6.1.7.2. Correlation between model and experiment was very good, with the FEA model being slightly conservative. Experimentally, $Q < 20$ was again obtained for the target two-stripe mode.

Work completed in the third and fourth quarters of 2001 was related to SBIR Phase II Contract F33615-01-C-2125. This program is a continuation of the previous work, but includes significantly more design detail and optimization work related to AFDS performance and durability, as well as model methodology development, hardware fabrication, bench durability testing, and spin rig durability test work. Significant effort has been ongoing in the third and fourth quarters to develop methodologies for convenient integration of AFDS technologies into existing fan blade FEA models and geometries. This task has not been at all trivial. However, various sensitivity studies have been conveniently carried out using these methodologies to characterize the effects of AFDS gap thickness, AFDS platelet thickness, and AFDS area coverage issues in relation to the two-stripe mode of vibration of a particular fan blade. This information is being used to design several optimized AFDS configurations that will be fabricated and tested in 2002 work.

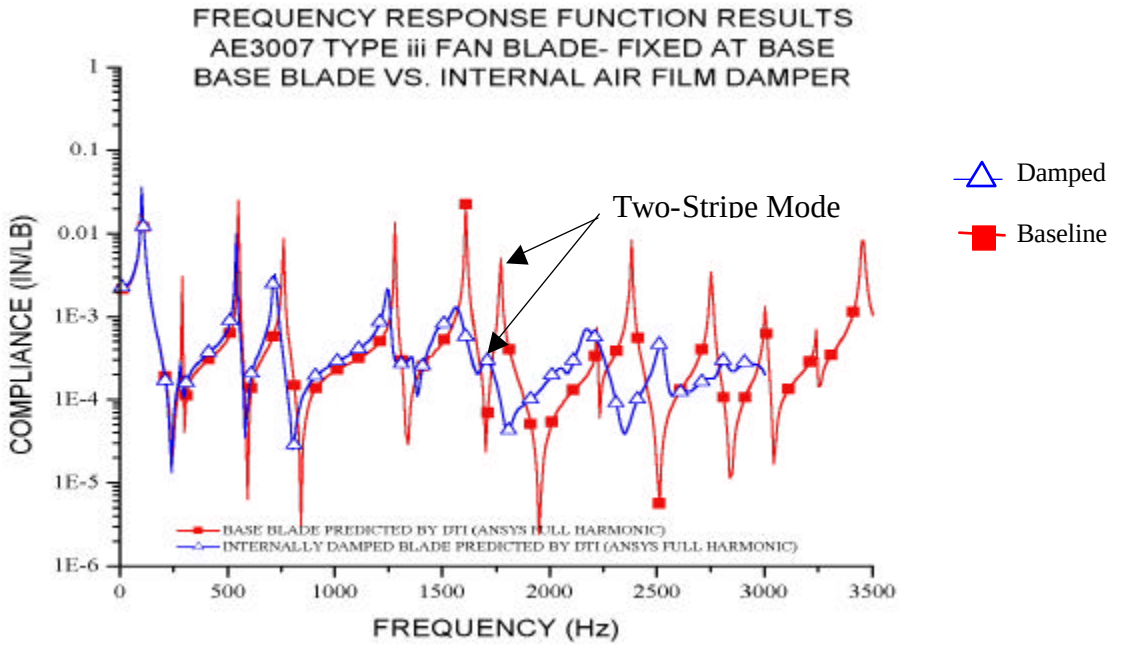

FIGURE 6.1.7.2 FEA Prediction of AFDS Performance

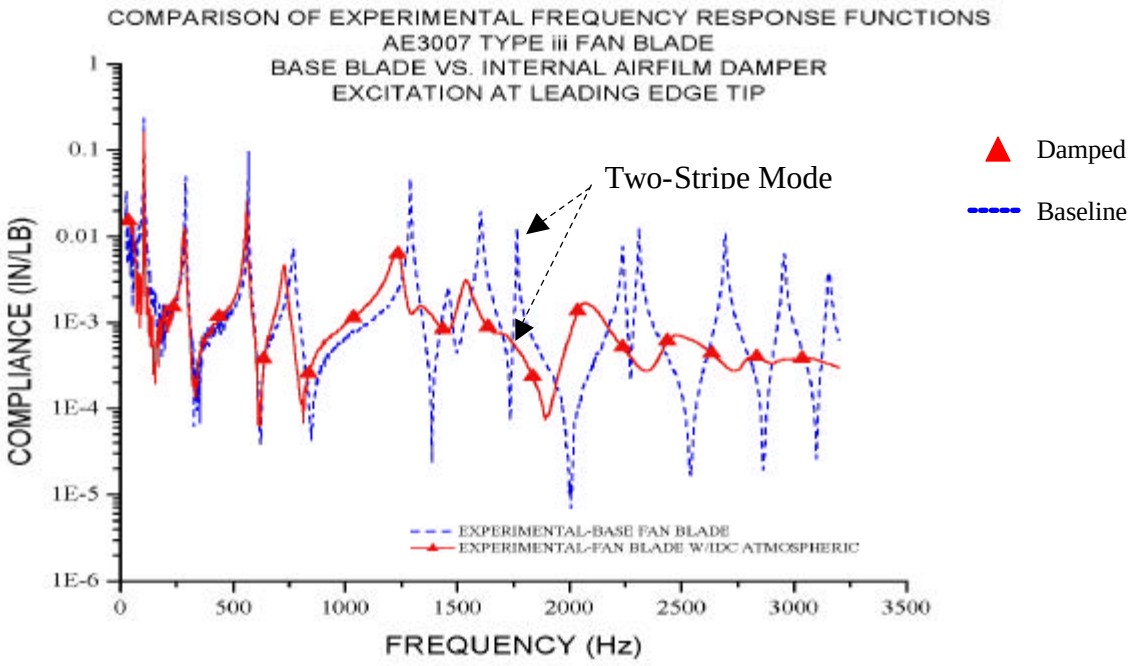

FIGURE 6.1.7.3 Measured AFDS Performance

Figure 6.1.7.4 describes an optimized AFDS designed to attenuate the 2-stripe mode of a particular fan blade. The AFDS has been located on the high pressure side of the fan blade with one inch remaining untreated at the leading edge and one-half inch left untreated at the tip and trailing edges, for FOD concerns. A titanium AFDS platelet is utilized. Predicted attenuation performance (via FEA) associated with this AFDS is described in Figure 6.1.7.5. Attenuation of over a factor of 10.0, compared to engine baseline (Q = 200) is anticipated for the 2-stripe mode of vibration. Q = 20 is anticipated for the design.

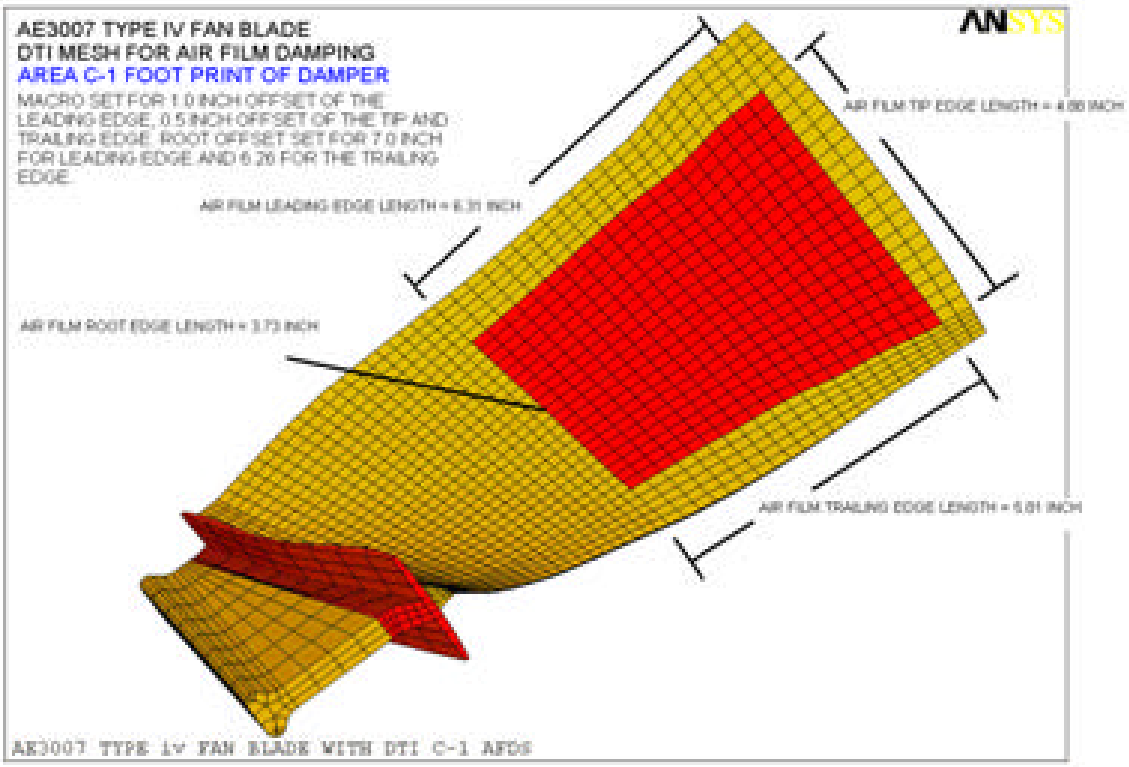

FIGURE 6.1.7.4 AFDS Optimization via FEA

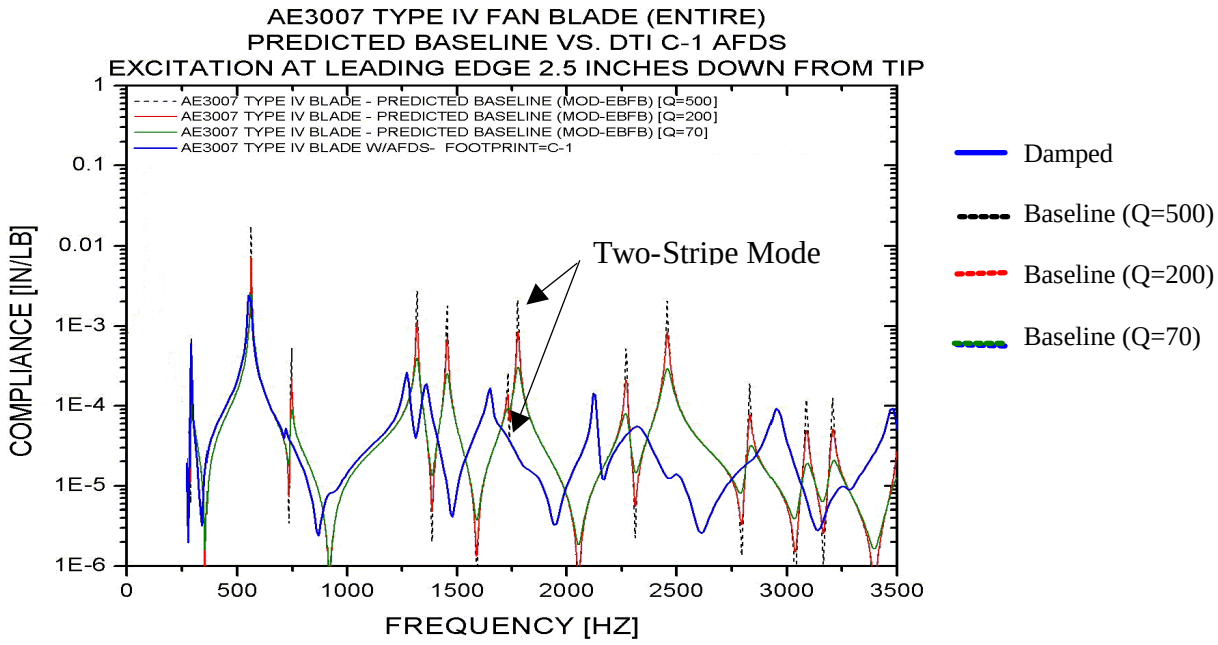

FIGURE 6.1.7.5 FEA Prediction of C-1 AFDS Performance

Participating Organizations: Damping Technologies, Inc.

Points of Contact:

Government
Mr. Frank Lieghley, Jr.
U.S. Air Force, AFRL/PRTC
1950 Fifth Street, Bldg. 18D
Wright Patterson AFB, OH 45433-7251
Phone: (937) 255-2611
Fax: (937) 255-2660

Contractor
Mr. Tom Lewis
Damping Technologies, Inc.
12970 McKinley Hwy.
Unit IX
Mishawaka, IN 46545-7518
Phone: (513) 779-2237

6.1.8 Robust High Cycle Fatigue Analysis and Durability Development

FY 02-05

Background

The USAF and all major designers and manufacturers of gas turbine engines have been addressing and working to develop new solutions to the High Cycle Fatigue problem which constrains development of performance-improved engine configurations and causes expenditure of huge O&S costs to support existing engines in the USAF global fleet.

In particular, blisks (Figure 6.1.8.1) provide a unique challenge for robust design, because of their inherent lack of structural damping. Conventional bladed disk assemblies have significant damping provided by the blade-to-disk dovetail connection which is absent for the blisk construction. For

blisks, ring sleeve dampers provide some structural (frictional) damping for the low order modes. However, there are no dampers in production for the higher order blade-only modes such as the stripe (chordwise bending) modes.

FIGURE 6.1.8.1 Typical Solid Blisk Design

The planned effort will build on the successful demonstration of the constrained viscoelastic (VE) layer damping system (CLDS) recently completed in the PRDA V Advanced Damping Systems for Fan and Compressor Blades Program. That program developed the VE CLDS and spin tested it on fan blades (Figure 6.1.8.2). The objective of the current effort is to demonstrate (in a durability spin test) the effectiveness (4:1 stress-reduction for target modes) and durability (non-life-limiting) of a VE CLDS on a military fan blisk element. This application will push the CLDS technology developed in PRDA V to new levels; for example, "g" levels will be doubled while operating temperatures will increase by 70 degrees F. Follow-on work to task will build on this successful program and adapt/test a CDLS on the XTE77/SE2. The goal is to deliver a near production damping system ready for transition to a ManTech Program.

FIGURE 6.1.8.2 PRDA V Constrained Layer Damping System Viscoelastic Damper Successfully Tested on an AE3007 Fan Blade (1999)

Recent Progress

This Program is scheduled to be underway in mid 2002; the period of Performance is through 2003/2004 into 2005.

Participating Organizations: Air Force Research Laboratory (AFRL), Allison Advanced Development Company (AADC)

Points of Contact:

Government
Mr. Frank Lieghley, Jr.
U.S. Air Force, AFRL/PRTC
1950 Fifth Street, Bldg. 18D
Wright Patterson AFB, OH 45433-7251
Phone: (937) 255-2611
Fax: (937) 255-2660

Contractor
Mr. Dick Horan
Allison Advanced Development Company
P.O. Box 7162 Speed Code X-12A
Indianapolis IN 46206-7162
Phone: (317) 230-8211
Fax: (317) 230-6100

6.2 Modeling and Incorporation of Damping in Components

Of the four types of damping systems (friction dampers, viscoelastic damping systems, particle dampers, and powder damping systems), two were ready for use in the design of rotating components: friction and viscoelastic damping systems. A program was initiated to use friction dampers for lower-order modes and to establish their ability to damp higher-order modes. Although there were some concerns with using viscoelastic materials, it was decided that a design program should be started while final characterization of viscoelastic materials was pursued. Component design work for particle and powder damping systems was considered premature, due to a lack of knowledge and a lack of confidence as to the likely performance of either system in a centrifugal environment. Design and testing of components with these systems will occur in the future.

6.2.1 Advanced Damping Concepts for Reduced HCF
FY 96-99

This effort has been completed. The results are reported in the 2000 HCF Annual Report.

6.2.2 Evaluation of Reinforced Swept Airfoils / Internal Dampers
FY 96-01

No progress was reported for this effort in CY2001.

6.2.3 Damping System for the Integrated High Performance Turbine Engine Technology (IHPTET) Program

FY 97-01

No progress was reported for this effort in CY2001.

6.2.4 Damping for Turbines

FY 97-01

Background

The objective of this project is to develop alternate friction damping systems for turbine blades. The program will also be used to evaluate the potential for advanced blade excitation systems to provide durability data on advanced damping configurations. This will be achieved by spin testing at the Naval Postgraduate School Turbopropulsion laboratory.

Advanced program requirements dictate alternative solutions to damping of turbine blades. Improvements in platform damping and internal damping are being pursued to allow higher aspect ratio blading. These approaches to damping will provide increased design space, providing more-optimal blade and turbine stage designs. The design and calibration of advanced codes is key to the introduction of these advanced concepts into tomorrow's engines.

Vital to the insertion of these technologies into advanced configurations is providing a means not only to evaluate the effectiveness of various damping configurations in a spin environment, but also, and almost equally as important, to establish a configuration's durability limits. What is needed is a means to provide a first look at a new system, which will test at resonance dwells with blade and damper configurations. This will establish engine life limits and ultimately reduce risk of insertion of new configurations.

Recent Progress

Testing was accomplished at the Naval Post Graduate school to assess low order damping and conduct an evaluation of eddy current excitation as a means of providing sustained resonant data for durability testing. Testing was successful in providing an understanding of the ability of eddy current systems to drive high frequency and low frequency fundamental mode responses. It was determined that this system is inadequate as a means of providing extended operation for damper durability testing. Air jets were also successfully tested to produce lower speed first bending data for the advanced internal damper; however, an air jet system produces considerable heating if used for the longer duration durability testing. Based on these results, the technology focus for simulated mission testing of advanced rotors should be on methods either with oil jets or with piezo-electric crystals which are either directly on the blades or built into the spin arbor.

Participating Organizations: Pratt & Whitney, Naval Postgraduate School (NPS)

Points of Contact:

Government
Mr. John Warren
Naval Air Warfare Center
Bldg. 106, Unit #4
22195 Elmer Rd.
Patuxent River, MD 20670-1534
Phone: (301) 757-0466
Fax: (301) 757-0562

Contractor
Mr. Al Stoner
Pratt & Whitney
M/S Ave. C
1306 Ave. C
Arnold AFB, TN 37389-4700
Phone: (931) 454-7591
Fax: (931) 454-0504

6.2.5 Dual Use Program
FY 01-03

Background

This program will provide damping improvements required to support advanced engine configurations. This will be accomplished by using rapid casting hardware fabrication techniques to generate rig hardware. The development of a verification method relying on rapid prototyping will reduce technology development cycle times. By providing designs rapidly, technology and innovation can be more readily proved out. This will allow marked progress toward improving damping, and delivering designs that meet program goals or requirements. It is not enough to develop new concepts, but these must be fully integrated into advanced cooled turbine blades. The key to developing advanced damping approaches is marrying the damper and blade design to the manufacturing process.

Recent Progress

This program is focused on damper verification and development and ultimately on developing an approach for spin testing of components. A major goal is to develop technology readiness level equivalency with engine AMT testing. In concert with this goal, the efforts obtained under the last phase of the enhanced turbine damping program augment and are very useful in establishing program direction for simulated mission testing. Based on these results, the technology focus for simulated mission testing of advanced rotors should be on methods either with oil jets or with piezo-electric crystals which are either directly on the blades or built into the spin arbor. These systems have all been proven.

During 2001, verification testing was conducted on two damping concepts by rig testing and bench testing. These two internal damper concepts were the tuned impact damper and the paddle damper. In addition, a rig was built up to evaluate the advanced platform wedge damper.

The tuned impact damper was tested at NASA GRC in their spin facility, with a subscale disk holding two blades. This test successfully demonstrated the feasibility of this concept on a modified advanced LPT configuration. These results showed stress reductions up to 40 per cent at maximum deflection.

The internal paddle damper was tested in conjunction with Patuxent River NAVAIR Dynamics test facility. This was done with bench testing to evaluate the advanced internal damper concept. The damper was determined to be ineffective and potentially locked up. Testing was conducted to simulate centrifugal loads. Also, testing was conducted with lubrication. All tests showed very little success

for first mode bending for the advanced LPT blade application. This concept will be evaluated further for its applicability to higher frequency modes.

Participating Organizations: Air Force Research Laboratory (AFRL), Pratt & Whitney Aircraft

Points of Contact:

Government
Mr. Frank Lieghley, Jr.
U.S. Air Force, AFRL/PRTC
1950 Fifth Street, Bldg. 18D
Wright Patterson AFB, OH 45433-7251
Phone: (937) 255-2611
Fax: (937) 255-2660

Contractor
Mr. Al Stoner
Pratt & Whitney
M/S Ave. C
1306 Ave. C
Arnold AFB, TN 37389-4700
Phone: (931) 454-7591
Fax: (931) 454-0504

6.2.6 Transition of Damping Technology to Counterrotating Low-Pressure Turbine Blades

FY 01-02

Background

Counterrotating turbine designs subject the low-pressure turbine (LPT) blades to high-frequency excitation from the high-pressure turbine blades immediately upstream. The vibratory response of the LPT blades is in a high-order airfoil mode for which typical platform friction dampers used for lower modes are less effective. Damping performance of some high temperature coatings will be determined to identify potential treatments for these higher-order modes.

The contract consists of two tasks. In Task 1, simple test specimens with two different damping treatments are being provided to the Air Force for elevated temperature testing. The Turbine Engine Fatigue Facility (TEFF) at the U.S. Air Force Research Laboratory will contrast damping performance of the two treatments for selected airfoil modes of vibration with untreated baseline specimens. In Task 2, a preferred damping treatment will be selected, based on the Task 1 test results, and applied to prototype LPT blades. These blades will then be tested at elevated temperature at the U.S. Air Force TEFF.

Recent Progress

Two coatings were selected for test on simple plate geometry specimens in Task 1. The first coating is a GE thermal barrier coating (TBC). The purpose of this selection is to characterize the inherent damping properties of the TBC placed on LP turbine blades for thermal design reasons rather than damping per se. The second coating selected is a hard coating from Allison Advanced Development Company (AADC). Three specimens with each coating and two uncoated baseline specimens were provided to the Air Force for testing in TEFF. In addition, bend test specimens are being prepared to support intrinsic damping property measurements of the TBC coating under another USAF funded effort.

Participating Organizations: GE Aircraft Engines, Allison Advanced Development Company (AADC), Roush Anatrol

Points of Contact:

Government
Mr. Frank Lieghley, Jr.
U.S. Air Force, AFRL/PRTC
1950 Fifth Street, Bldg. 18D
Wright Patterson AFB, OH 45433-7251
Phone: (937) 255-2611
Fax: (937) 255-2660

Contractor
Mr. James A. Griffiths
General Electric Aircraft Engines
One Neumann Way, M/D A413
Cincinnati, OH 45215-6301
Phone: (513) 243-2770
Fax: (513) 243-8091

6.2.7 High Cycle Fatigue Robustness and Engine Durability Testing

FY02-05

Background

The USAF and all major designers and manufacturers of gas turbine engines have been addressing and working to develop new solutions to the High Cycle Fatigue problem. That problem constrains development of performance improved engine configurations and causes expenditure of huge O&S costs to support existing engines in the USAF global fleet.

In addressing the problem, it is important to perform engine durability testing of different potential technical solutions, because spin rig testing rarely can achieve the conditions, and time at those conditions, necessary to determine whether the damping effectiveness of a particular HCF solution deteriorates with exposure to long hours and other outside effects found in the engine environment. Engine testing is also a necessary precondition for transitioning to ManTech Programs for the same reason.

This project consists of two development activities which address the HCF challenge from two different perspectives in separate tasks. Both these tasks culminate in a separately contracted 200 – 400 hour AE3007 engine durability test of these technologies and other HCF experimental treatments (Figure 6.2.7.1). The durability test program and development of the additional damping and health monitoring technologies will be underwrittem by RRplc (UK) and the British Ministry of Defense in this cooperative Program. Development of two other HCF mitigation technologies will be carried out under the USAF Program. This Program is described in the following paragraph.

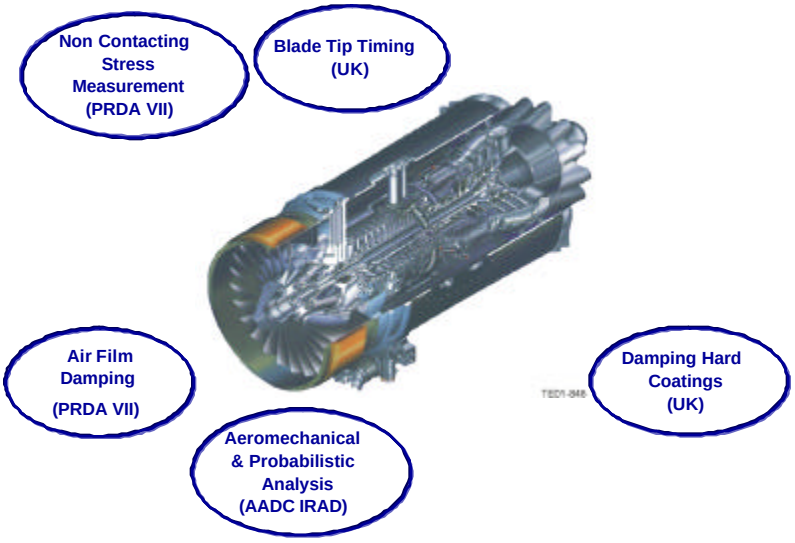

FIGURE 6.2.7.1 Planned AE3007 Engine Testing

Task 1 develops Air Film Damping (AFD) technology from its current status of a laboratory concept and adapts an engine ready design to an AE3007 Fan Blade. The preliminary conceptual work on Air Film Damping was accomplished in SBIR Phase I and Phase II Programs. Air Film Damping achieves significant damping of higher modes such as 2S by means of the viscous action of air entrained in an air pocket incorporated in the pressure surface of the blade; no additional hardware or devices are incorporated in the air pocket/system (Figure 6.2.7.2). Significant reductions in both amplitudes and stresses (Q<15) have already been demonstrated in bench testing; however, the hardware design is not acceptable or proven for engine incorporation at this time. The next contract development transitions the basic design to engine level standards and rig tests it prior to incorporating in a development engine for > 200 hours. Task 1 will build on this successful program and adapt and engine test AFD treated blades in an endurance test.

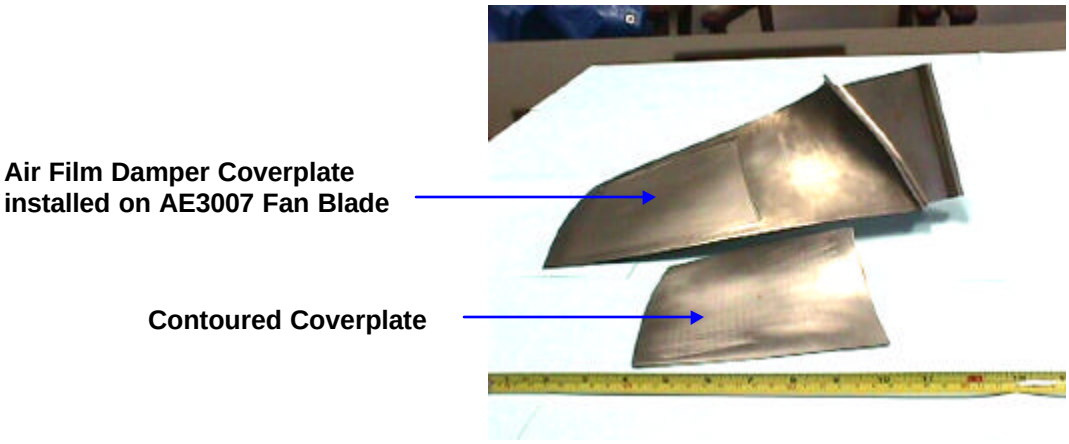

FIGURE 6.2.7.2 SBIR Phase 1 Damping Installed on an AE3007 Fan Blade

Task 2 adapts a USAF provided and developed NSMS (Non-intrusive Stress Measurement System – Figure 6.2.7.3) to the 200-hour durability test engine and correlates its output to fan strain gauge measurements in a pre-endurance baseline test. The NSMS System measurements will be vital to measuring the change in damping effectiveness of the various treatments/technologies (including Air Film Damping) as a function of hours accumulated in the durability test, since it is not possible to incorporate strain gauges and slip ring or telemetry hardware in an extended test. The 200-hour test will also provide a substantiation of the durability of the NSMS system mechanical and electrical components themselves.

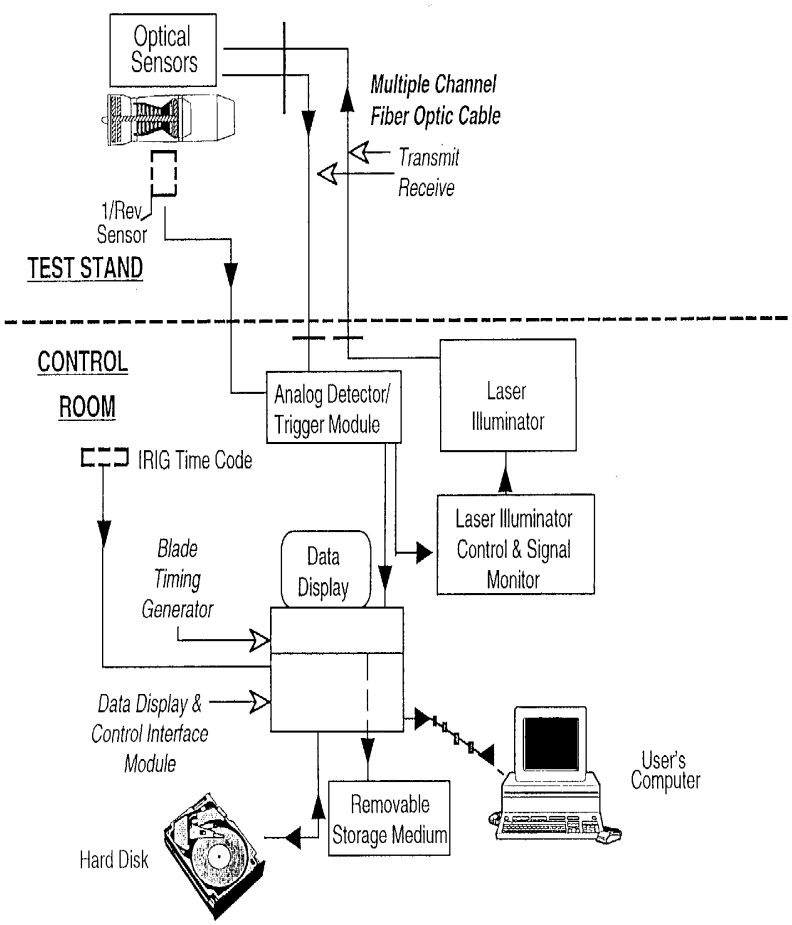

FIGURE 6.2.7.3 Gen IV NSMS System

Recent Progress

This Program is scheduled to be underway in mid 2002; the periods of performance for both tasks are through 2003/2004 into 2005.

Participating Organizations: Air Force Research Laboratory (AFRL), Allison Advanced Development Company (AADC)

Points of Contact:

Government
Mr Frank Leighley
USAF, AFRL/PRTC
1950 Fifth Street, Bldg. 18D
Wright Patterson AFB, OH 45433-7251
Phone: (937) 255-1867
Fax: (937)255-2660

Contractor
Mr. Dick Horan
AADC
P.O.Box 7162 Speed Code X-12A
Indianapolis IN 46206-7162
Phone: (317) 230-8211
Fax: (317) 230 6100

6.3 Affordable Damped Components

FY 02 - 06

A manufacturing technology program has been developed to bring the cost of demonstrated damped components down to affordable levels. Toll gates have been setup, which each damping system must pass before they will be considered for this program. Exit criteria have also been established. The program will start in late fiscal year 2002.

Participating Organizations: AFRL/MLMP and AFRL/PRTC

Points of Contact:

Government
Dr. Carl M. Lombard
U.S. Air Force
AFRL/MLMP Bldg 653
2977 P Street, Suite 6
Wright Patterson AFB OH 45433-7739
Phone: 937-255-7279
Fax: 937-656-4420

Contractor
Mr. Al Stoner
Pratt & Whitney
M/S Ave. C
1306 Ave. C
Arnold AFB, TN 37389-4700
Phone: (931) 454-7591
Fax: (931) 454-0504

6.4 Conclusion

By conducting rig, component, and engine tests, and by developing very successful modeling techniques, the Passive Damping Technology Action Team has evaluated numerous damping schemes with great potential. The Team has demonstrated that the historically-based "rainbow" or mixed wheel concept is not an acceptable test protocol for HCF modal damping investigation. The team has demonstrated the feasibility of applying viscoelastic damping to the rim of a bladed rotor rather than to the blade surface. Doing so could effect an 80% reduction in blade stresses, and further work on this concept is underway. The turbine friction damping effort has been a major success, with test results showing vibratory reductions much greater than predicted. The turbine damper is currently being applied in an advanced engine development program. The use of coatings for damping has become an area of significant interest. Developing an understanding of the physical mechanisms associated with damping coatings and modeling the damping behavior of coatings are major challenges that are currently being addressed. Great strides have been made in the modeling of particle damping systems. A redesign of a VEM damping system has been successfully demonstrated in spin pit testing. Air film damping also shows great promise. These damping systems are being further developed for future demonstration in engine testing. Manufacturability of damping solutions is becoming a major area of future emphasis, given the need to implement these technologies in a cost-effective way. Programs are planned to develop cost-competitive manufacturing methods for the most promising of the damping concepts.

7.0 ENGINE DEMONSTRATION

BACKGROUND

The Engine Demonstration Action Team (Engine Demo AT) has the responsibility of coordinating all the emerging HCF technologies with planned engine demonstrator targets. The engine demonstrations are responsible for acquiring the necessary data to establish or update the design space for the specific emerging HCF technologies so that the technology can then transition to meet user mission-specific requirements. The technology action teams will develop their specific HCF technologies to an acceptable level of risk to run on a demonstrator engine. Initial engine demonstrator planning was based on the original set of HCF technologies that was approved, and is constantly being updated as the budget and technologies change. The Demo AT has been concentrating on the turbojet/turbofan fighter engine class, which includes IHPTET demonstrator engines, and advanced operational engines currently in development. Planning for the F110-129, F100-229 and other engines in the operational inventory is in process. Detail is only given on the IHPTET demonstrators because of the competitive and proprietary issues associated with the product engines.

ACTION TEAM CHAIRS

Chair
Mr. Michael Barga
U.S. Air Force,
AFRL/PRTP, Bldg. 18 Room D201
1950 Fifth Street
Wright-Patterson AFB, OH 45433-7251
Phone: (937) 255-2767
Fax: (937) 656-4179

Co-Chair
Mr. Dan Popgoshev
Naval Air Systems Command
AIR 4.4T Bldg. 106
22195 Elmer Road
Patuxent River, MD 20670-1534
Phone: (301) 757-0453
Fax: (301) 757-0534

INTRODUCTION

The following pages contain descriptions of objectives, HCF technologies validated, and results of current and planned HCF engine demonstrations. In general, the engine demonstrations are planned to provide the required data to validate the HCF technology performance and to update the design codes. The action teams develop technologies, then identify them as ready for engine demonstration. These technologies are then planned for incorporation into a core or engine test. Once successfully demonstrated in a core or engine, a given technology is ready for transition into a fielded engine (F100, F110, etc.) or a development engine program (F119, etc.). Core or engine demonstration of HCF technologies will continue through 2006.

FIGURE 7.0 HCF Demonstrator Engine Plan

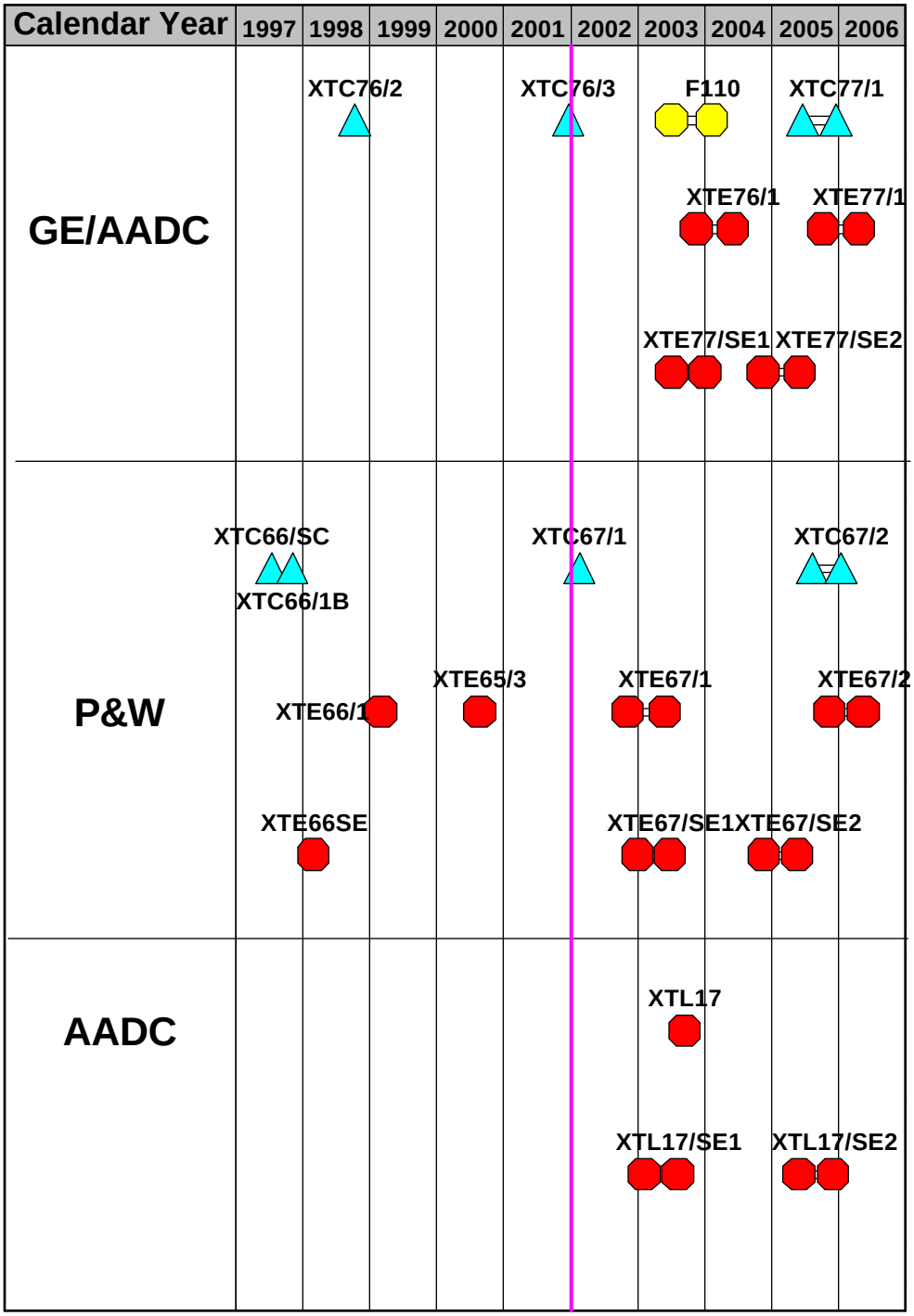

7.1 General Electric / Allison Advanced Development Company

The main focus of the GE/AADC demonstrator programs is to provide the test beds for the evaluation of Integrated High Performance Turbine Engine Technology (IHPTET) Program technologies and new HCF technologies. These critical core an engine demonstrations assess the performance and mechanical characteristics of HCF technologies in a realistic engine environment and provide the data necessary to validate and update advanced HCF prediction tools.

7.1.1 XTC76/2

FY 99 (1st Qtr)

Objectives: Demonstrate technologies to achieve the Integrated High Performance Turbine Engine Technology (IHPTET) Program Phase II T41 objective, variable cycle engine concept, and advanced core technologies required to meet the IHPTET Phase II thrust-weight goals.

HCF Technologies Demonstrated: The need for compressor flutter design and test methods was demonstrated.

Final Results: This test demonstrated the importance of advanced unsteady design methods for use on modern low-aspect-ratio compressor airfoils, which have stability properties outside traditional experience.

Participating Organizations: Air Force Research Laboratory (AFRL), GE Aircraft Engines / Allison Advanced Development Company (AADC)

Points of Contact:

Government
Mr. Michael Barga
U.S. Air Force, AFRL/PRTP
1950 Fifth St., Bldg. 18D
Wright-Patterson AFB, OH 45433-7251
Phone: (937) 255-2767
Fax: (937) 656-4179

Contractor
Dr. Dennis Corbly / Mr. Durell Wildman, Bernie Rezy
GE Aircraft Engines/AADC
Allison Advanced Development Co.
2056 South Tibbs Ave.
Indianapolis, IN 46207
Phone: (317) 230-5670
Fax: (317) 230-6100

7.1.2 XTC76/3

FY 02 (1st Qtr)

Objectives: Demonstrate the core technologies required to meet the IHPTET Phase II thrust-to-weight goal and the structural durability of the advanced technologies.

HCF Technologies Demonstrated: This core included demonstrations of unsteady aerodynamics and forced response flutter prediction, friction and coating damping, Non-Intrusive Stress Measurement System (NSMS), and CADDMAS, as well as the application of elements of the recommended HCF Test Protocol.

Details/Progress: Flutter analysis was done with fully-coupled 2D and 3D nonlinear unsteady codes. REDUCE has been used to investigate mistuning in Stage 2 compressor blades. Hard damping coatings and ring dampers were designed for this compressor. The effectiveness of these damping treatments was demonstrated on the bench and in engine testing. The recommended Test Protocol was used to validate bench and core test results.

Participating Organizations: Air Force Research Laboratory (AFRL), Naval Air Warfare Center (NAWC), GE Aircraft Engines / Allison Advanced Development Company (AADC)

Points of Contact:

Government
Mr. Michael Barga
U.S. Air Force, AFRL/PRTP
1950 Fifth St., Bldg. 18D
Wright-Patterson AFB, OH 45433-7251
Phone: (937) 255-2767
Fax: (937) 656-4179

Contractor
Dr. Dennis Corbly / Mr. Durell Wildman, Bernie Rezy
GE Aircraft Engines/ Allison Advanced Development Co.
2056 South Tibbs Ave.
Indianapolis, IN 46207
Phone: (317) 230-5670
Fax: (317) 230-6100

7.1.3 XTE76/1

FY 04 (1st to 3rd Qtr)

Objectives: Demonstrate the core technologies required to meet the IHPTET Phase II thrust-to-weight goal and the structural durability of the advanced technologies. HCF technologies to be validated in this core include unsteady aerodynamics, damping, and the Non-Intrusive Stress Measurement System (NSMS).

Details/Progress: Flutter analysis will be done with a fully-coupled 3D nonlinear unsteady code. REDUCE has been used to investigate mistuning in Stage 2 compressor blades. Hard damping coatings and ring dampers have been designed for this compressor. The effectiveness of these damping treatments will be evaluated on the bench and in engine testing. NSMS instrumentation will be used to gather blade response data for correlation with predictions.

Participating Organizations: Air Force Research Laboratory (AFRL), Naval Air Warfare Center (NAWC), GE Aircraft Engines / Allison Advanced Development Company (AADC)

Points of Contact:

Government
Mr. Michael Barga
U.S. Air Force, AFRL/PRTP
1950 Fifth St., Bldg. 18D
Wright-Patterson AFB, OH 45433-7251
Phone: (937) 255-2767
Fax: (937) 656-4179

Contractor
Dr. Dennis Corbly / Mr. Durell Wildman, Bernie Rezy
GE Aircraft Engines/Allison Advanced Development Co.
2056 South Tibbs Ave.
Indianapolis, IN 46207
Phone: (317) 230-5670
Fax: (317) 230-6100

7.1.4 XTE77/SE1
FY 03 (4th Qtr)

Objectives: Demonstrate the integration of advanced fan and turbine technologies into an engine system; provide an early risk reduction evaluation of Phase III technologies.

HCF Technologies to Be Demonstrated: Flutter and forced response predictions; correlation with strain gauges and Non-Intrusive Stress Measurement System (NSMS); friction damper predictions, mistuning codes, and application of probabilistic assessment methods.

Details/Progress: The HPC hardware is being fabricated, bench data and instrumentation requirements have been set.

Participating Organizations: Air Force Research Laboratory (AFRL), GE Aircraft Engines / Allison Advanced Development Company (AADC)

Points of Contact:

Government
Mr. Dan Popgoshev
Naval Air Systems Command
AIR 4.4T Bldg. 106
22195 Elmer Road
Patuxent River, MD 20670-1534
Phone: (301) 757-0453
Fax: (301) 757-0534

Contractor
Dr. Dennis Corbly
GE Aircraft Engines
1 Neumann Way
A413
Cincinnati, OH 45215-1988
Phone: (513) 243-5832
Fax: (513) 243-8091

7.1.5 XTE77/SE2
FY 05 (1st Qtr)

Objectives: Demonstrate the integration of advanced fan and turbine technologies into an engine system; provide a test bed to demonstrate and transition HCF Technologies and durability validation.

HCF Technologies to Be Demonstrated: Application of Laser Shock Peening (LSP) to forward-swept fans; damage tolerance assessments; unsteady aero predictions with a variety of codes; correlation with the Non-Intrusive Stress Measurement System (NSMS) and other monitoring sensors; the impact of low-excitation features in front frames; application of probabilistic assessment methods; viscoelastic damping treatment to the fan.

Details/Progress: The advanced, forward swept fan for this engine will be tested at the Compressor Research Facility (CRF) in fourth quarter of FY02. This fan will be mated with SE1 components.

Participating Organizations: Air Force Research Laboratory (AFRL), GE Aircraft Engines / Allison Advanced Development Company (AADC)

Points of Contact:

Government
Mr. Dan Popgoshev
Naval Air Systems Command
AIR 4.4T Bldg. 106
22195 Elmer Road
Patuxent River, MD 20670-1534
Phone: (301) 757-0453
Fax: (301) 757-0534

Contractor
Dr. Dennis Corbly
GE Aircraft Engines
1 Neumann Way
A413
Cincinnati, OH 45215-1988
Phone: (513) 243-5832
Fax: (513) 243-8091

7.1.6 XTC77/1

FY 05 (4th Qtr)

Objectives: Demonstrate the technologies required to achieve the Integrated High Performance Turbine Engine Technology (IHPTET) Program Phase III thrust-to-weight goal.

HCF Technologies to Be Demonstrated: Advanced technologies in the areas of damping, instrumentation, and design methods, including probabilistics and unsteady aerodynamics.

Details/Progress: This effort is in the preliminary design phase.

Participating Organizations: Air Force Research Laboratory (AFRL), GE Aircraft Engines / Allison Advanced Development Company (AADC)

Points of Contact:

Government
Mr. Michael Barga
U.S. Air Force, AFRL/PRTP
1950 Fifth St., Bldg. 18D
Wright-Patterson AFB, OH 45433-7251
Phone: (937) 255-2767
Fax: (937) 656-4179

Contractor
Dr. Dennis Corbly / Mr. Durell Wildman, Bernie Rezy
GE Aircraft Engines/Allison Advanced Development Co.
1 Neumann Way
A413
Cincinnati, OH 45215-1988
Phone: (513) 243-5832
Fax: (513) 243-8091

7.1.7 XTE77/1

FY 06 (1st Qtr)

Objectives: Demonstrate the integration of advanced fan and low-pressure turbine technologies into an engine system.

HCF Technologies to Be Demonstrated: Application of advanced unsteady design methods on advanced high pressure (HP) and low-pressure (LP) turbine systems will be demonstrated; HCF Test Protocol will be applied; flutter and forced response tools used in design; advanced low excitation features incorporated into fan module.

Details/Progress: Initial preliminary design effort has begun.

Participating Organizations: Air Force Research Laboratory (AFRL), GE Aircraft Engines / Allison Advanced Development Company (AADC)

Points of Contact:

Government
Mr. Michael Barga
U.S. Air Force, AFRL/PRTP
1950 Fifth St., Bldg. 18D
Wright-Patterson AFB, OH 45433-7251
Phone: (937) 255-2767
Fax: (937) 656-4531

Contractor
Dr. Dennis Corbly / Mr. Durell Wildman
GE Aircraft Engines/Allison Advanced Development Co.
1 Neumann Way
A413
Cincinnati, OH 45215-1988
Phone: (513) 243-5832
Fax: (513) 243-8091

7.2 Pratt & Whitney

The main benefit of the P&W demonstrator programs to the HCF Initiative is to provide the test beds for the initial evaluation of new HCF technologies. These critical core and engine demonstrations, in addition to demonstrating improved thrust-to-weight and providing a validation for technology transition candidates, assess the performance and mechanical characteristics of HCF technologies in a realistic engine environment and provide the data necessary to validate and update advanced HCF prediction tools.

7.2.1 XTE66/A1

FY 95 (4th Qtr)

Objectives: Validate the F119 Hollow Fan Blade integrally bladed rotor (IBR) in an engine environment.

HCF Technologies Demonstrated: Unsteady aerodynamic and forced response (FLARES) codes, first-generation eddy current sensor.

Final Results: HCF tools correctly identified root cause and fix for unacceptable rotor response. Demonstration of the eddy current sensor to measure blade tip response was successfully completed.

Participating Organizations: Air Force Research Laboratory (AFRL), Pratt & Whitney Independent Research and Development (P&W IR&D)

Points of Contact:

Government
Capt Anthony Cerminaro
U.S. Air Force, AFRL/PRTP
1950 Fifth St., Bldg. 18D
Wright-Patterson AFB, OH 45433-7251
Phone: (937) 255-2767
Fax: (937) 255-2278

Contractor
Mr. Bill Doehnert
Pratt & Whitney M/S 715-01
P. O. Box 109600
West Palm Beach, FL 33410-9600
Phone: (561) 796-6639
Fax: (561) 796-4901

7.2.2 XTC66/SC

FY 97 (3rd Qtr)

Objectives: Demonstrate and evaluate F119 technology transition, technology maturation risk reduction for advanced engines currently in development, and Integrated High Performance Turbine Engine Technology Program (IHPTET) technologies.

HCF Technologies Demonstrated: Robustness of gamma-TiAl high-pressure compressor (HPC) blades; supercooled high-pressure turbine (HPT) blades.

Final Results: Testing demonstrated the HCF robustness of gamma-TiAl blades and supercooling technologies.

Participating Organizations: Air Force Research Laboratory (AFRL), Naval Air Warfare Center (NAWC), Pratt & Whitney

Points of Contact:

Government
Mr. Marty Huffman
U.S. Air Force, AFRL/PRTP
1950 Fifth St., Bldg. 18D
Wright-Patterson AFB, OH 45433-7251
Phone: (937) 255-2767
Fax: (937) 255-2278

Contractor
Mr. Bill Campbell
Pratt & Whitney
M/S 715-01
P. O. Box 109600
West Palm Beach, FL 33410-9600
Phone: (561)796-5179

7.2.3 XTC66/1B

FY 98 (1st Qtr)

Objectives: Demonstrate temperature, speed, and structural capability of the core to run Integrated High Performance Turbine Engine Technology Program (IHPTET) Phase II conditions and evaluate the aerodynamic and thermodynamic performance of the high-pressure compressor (HPC), Diffuser/ Combustor, and high-pressure turbine (HPT).

HCF Technologies Demonstrated: Unsteady aerodynamic (NASTAR V3.0) and forced response (FLARES V1.0) codes.

Final Results: Testing provided benchmark data for analytical tool calibration and validation. Data have been used to establish code performance against Action Team metrics.

Participating Organizations: Air Force Research Laboratory (AFRL), Pratt & Whitney

Points of Contact:

Government
Mr. David Jay
U.S. Air Force, AFRL/PRTP
1950 Fifth St., Bldg. 18D
Wright-Patterson AFB, OH 45433-7251
Phone: (937) 255-2767
Fax: (937) 255-2278

Contractor
Mr. Bill Campbell
Pratt & Whitney
M/S 715-01
P. O. Box 109600
West Palm Beach, FL 33410-9600
Phone: (561)796-5179

7.2.4 XTE66/1

FY 99 (2nd Qtr)

Objectives: (1) Demonstrate the Integrated High Performance Turbine Engine Technology Program (IHPTET) Phase II thrust-to-weight goal. (2) Provide initial engine demonstration of a vaneless counter-rotating turbine and microwave augmentor.

HCF Technologies Demonstrated: Internal low-pressure turbine (LPT) dampers for control of high-frequency excitation.

Final Results: A counter-rotating vaneless turbine was successfully demonstrated. Low turbine (LPT2) blade stresses were low in higher-order modes. The configuration was evaluated with FLARES for comparison to Action Team metrics. Durability testing of these advanced dampers will be conducted in an HCF spin test at Pratt & Whitney in the Summer of 2002.

Participating Organizations: Air Force Research Laboratory (AFRL), Pratt & Whitney

Points of Contact:

Government
Capt Tony Cerminaro
U.S. Air Force, AFRL/PRTP
1950 Fifth St., Bldg. 18D
Wright-Patterson AFB, OH 45433-7251
Phone: (937) 255-2767
Fax: (937) 255-2278

Contractor
Mr. Bob Morris
Pratt & Whitney M/S 163-07
400 Main Street
East Hartford, CT 06108
Phone: (860) 565-8653

7.2.5 XTC67/1

FY 02 (2nd Qtr)

Objectives: Demonstrate the temperature, speed, and structural capability of the core to run Integrated High Performance Turbine Engine Technology Program (IHPTET) Phase II and some early Phase III conditions and to evaluate the high-pressure compressor (HPC), Diffuser/Combustor, and high-pressure turbine (HPT) aerodynamic and thermodynamic performance.

HCF Technologies to be Demonstrated: Generation 4 Non-Interference Stress Measurement System (NSMS), Advanced Pyrometry, Finite Element Modeling (FEM) Enhancements, the FLARES (V2.0) Code, Asymmetric high-pressure compressor (HPC) Stators, Comprehensive Engine Condition Management (CECM), improved platform dampers in the high-pressure turbine (HPT)

Progress to Date: Hardware fabrication is in final stages of completion, and core instrumentation and assembly are in progress. Testing has been delayed into March 2002.

Participating Organizations: Air Force Research Laboratory (AFRL), Pratt & Whitney

Points of Contact:

Government
Mr. David Jay
U.S. Air Force, AFRL/PRTP
1950 Fifth St., Bldg. 18D
Wright-Patterson AFB, OH 45433-7251
Phone: (937) 255-2767
Fax: (937) 255-2278

Contractor
Mr. Howard Gregory
Pratt & Whitney M/S 165-21
400 Main Street
East Hartford, CT 06180
Phone: (860) 565-4682
Fax: (860) 755-1976

7.2.6 XTE66/SE

FY 98 (2st Qtr)

Objectives: Demonstrate the structural durability of Integrated High Performance Turbine Engine Technology Program (IHPTET) technologies in an F119 engine and transition some of those technologies to the F119 for the F-22 or and other advanced systems. The demonstration was an accelerated mission test (AMT) using an F-22 IFR mission.

HCF Technologies Demonstrated: Robustness of gamma-Ti Compressor Blades, Supervanes and Superblades.

Final Results: The engine completed 1505 AMT TACs and most of the technology component hardware met durability predictions.

Participating Organizations: Air Force Research Laboratory (AFRL), Naval Air Warfare Center (NAWC), Pratt & Whitney

Points of Contact:

Government
Mr. Marty Huffman
U.S. Air Force, AFRL/PRTP
1950 Fifth St., Bldg. 18D
Wright-Patterson AFB, OH 45433-7251
Phone: (937) 255-2767
Fax: (937) 255-2278

Contractor
Mr. John S. Anderson
Pratt & Whitney M/S 715-01
P. O. Box 109600
West Palm Beach, FL 33410-9600
Phone: (561) 796-4621
Fax: (561) 796-4901

7.2.7 XTE67/1

FY 03 (1st Qtr)

Objectives: Demonstrate the temperature, speed, and structural capability of the engine to run early Integrated High Performance Turbine Engine Technology Program (IHPTET) Phase III conditions and evaluate the low spool and integrated aerodynamic and thermodynamic performance.

HCF Technologies to be Demonstrated: Integrally bladed rotors (IBRs) designed for low resonant stress and flutter response, IBR damping, lightweight turbine dampers, and high-temperature eddy current sensors will be validated. Analytical tools to be applied during the XTE67/1 design include unsteady aerodynamics, FLARES (V2.0), MDA, BDAMPER (V7.0), and CDAMP (V2.0).

Progress to Date: The final design review for XTE67/1 was held in November 1999. Hardware fabrication is in progress. Testing has been delayed to the third quarter of CY 2002.

Participating Organizations: Air Force Research Laboratory (AFRL), Naval Air Warfare Center (NAWC), Pratt & Whitney

Points of Contact:

Government
Capt Anthony Cerminaro
U.S. Air Force, AFRL/PRTP
1950 Fifth St., Bldg. 18D
Wright-Patterson AFB, OH 45433-7251
Phone: (937) 255-2767
Fax: (937) 255-4179

Contractor
Mr. Willard Pospisil
Pratt & Whitney M/S 165-21
400 Main Street
East Hartford, CT 06180
Phone: (860) 565-0028
Fax: (860) 565-1323

7.2.8 XTE65/3

FY 00 (4th Qtr)

Objectives/HCF Technologies to be Demonstrated: (1) Demonstrate the utility and accuracy of new fan blade damage tolerance HCF tools during engine testing of damaged blades. (2) Evaluate benefits of laser shock peening of titanium integrally bladed rotors (IBRs) to mitigate damage-induced fatigue debits.

Progress to Date: Instrumentation and assembly of the engine was completed. F119 first fan blade component testing was in progress to evaluate the new FOD methods prior to engine test. An "event" on August 2, 2000, during initial check-out of the engine resulted in significant damage to the engine. An XTE65/3 recovery plan involving bench level FOD testing followed by HCF spin testing at NAVAIR is planned. Testing should be completed during CY02.

Participating Organizations: Air Force Research Laboratory (AFRL), Pratt & Whitney Independent Research and Development (P&W IR&D)

Points of Contact:

Government
Mr. Ray Pickering
Naval Air Warfare Center Aircraft Division (NAWCAD)
Propulsion and Power Engineering, Bldg 106, Unit 4
22195 Elmer Rd.
Patuxent River MD 20670-1534
Phone: 301-342-0865

Contractor
Mr. Willard Pospisil
Pratt & Whitney M/S 161-22
400 Main Street
East Hartford, CT 06180
Phone: (860) 565-0028
Fax: (860) 755-4293

7.2.9 XTE67/SE1

FY 03 (2nd Qtr)

Objectives/HCF Technologies to be Demonstrated: (1) Demonstrate new HCF instrumentation technologies in an engine environment. (2) Gather aeromechanical and aerothermal data to validate and update analytical tools.

Progress to Date: The engine to support the first build of the structural engine (SE1) has been purchased. Delivery of the engine hardware for HCF instrumentation is ongoing. The application of the new HCF Test Protocol is being supported by Dr. Kurt Nichol of EDAS.

Participating Organizations: Air Force Research Laboratory (AFRL), Pratt & Whitney Independent Research and Development (P&W IR&D)

Points of Contact:

Government
Major Steven Rose
AFRL/PRTP
1950 Fifth Street
Building 18 Room D201
Wright Patterson, OH 45433-7251
Phone: (937) 255-2767
Fax: (937) 255-4179

Contractor
Mr. Mark Whitten
Pratt & Whitney M/S 161-22
400 Main Street
East Hartford, CT 06180
Phone: (860)557-0474
Fax: (860) 755-0795

7.2.10 XTE67/SE2

FY 05 (1st Qtr)

Objectives/HCF Technologies to be Demonstrated: (1.) Provide a vehicle for demonstration and transition of new technologies from the National High Cycle Fatigue and Turbine Engine Durability Initiatives to programs for advanced fighter engines currently in development. (2.) Validate durability of new component technologies through accelerated testing and implementation of new HCF test protocols.

Progress to Date: The proposal for this activity is scheduled for delivery March 2002. A complementary program for "High Cycle Fatigue Tools Application" is under negotiation. A candidate list of technologies for the SE2 engine has been identified.

Participating Organizations: Air Force Research Laboratory (AFRL), Pratt & Whitney Independent Research and Development (P&W IR&D)

Points of Contact:

Government
Mr. Mark Dale
U.S. Air Force, AFRL/PRTP
1950 Fifth St., Bldg. 18D
Wright-Patterson AFB, OH 45433-7251
Phone: (937) 255-2767
Fax: (937) 656-4179

Contractor
Mr. Mark Whitten
Pratt & Whitney M/S 161-22
400 Main Street
East Hartford, CT 06180
Phone: (860)557-0474
Fax: (860) 755-0795

7.2.11 XTC67/2

FY 05 (4th Qtr)

Objectives: Demonstrate the temperature, speed, and structural capability of the core to run Integrated High Performance Turbine Engine Technology Program (IHPTET) Phase conditions.

HCF Technologies to be Demonstrated: Incorporate new HCF tools in the core final design activities. These tools (FLARES et al.) are part of the P&W Standard Work process.

Progress to Date: IBR friction rim damping under a Structural Enhancement Option has been successfully demonstrated in an HCF spin test.

Participating Organizations: Air Force Research Laboratory (AFRL), Pratt & Whitney

Points of Contact:

Government
Mr. David Jay
U.S. Air Force, AFRL/PRTP
1950 Fifth St., Bldg. 18D
Wright-Patterson AFB, OH 45433-7251
Phone: (937) 255-2767
Fax: (937) 656-4179

Contractor
Mr. Howard Gregory
Pratt & Whitney M/S 165-21
400 Main Street
East Hartford, CT 06180
Phone: (860) 565-4682
Fax: (860) 755-1976

7.2.12 XTE67/2

FY 06 (1st Qtr)

Objectives: Demonstrate the temperature, speed, and structural capability of the engine to run Integrated High Performance Turbine Engine Technology Program (IHPTET) Phase III conditions. Incorporate new HCF tools and component technologies into the IHPTET Phase III demonstrator.

HCF Technologies to be Demonstrated: A candidate list of technologies for the XTE67/2 engine has been identified.

Progress to Date: The proposal for this activity is scheduled for delivery March 2002.

Participating Organizations: Air Force Research Laboratory (AFRL), Pratt & Whitney

Points of Contact:

Government
Mr. David Jay
U.S. Air Force, AFRL/PRTP
1950 Fifth St., Bldg. 18D
Wright-Patterson AFB, OH 45433-7251
Phone: (937) 255-2767
Fax: (937) 255-2278

Contractor
Mr. Willard Pospisil
Pratt & Whitney M/S 161-22
400 Main Street
East Hartford, CT 06180
Phone: (860) 565-0028
Fax: (860) 755-4293

7.3 Allison Advanced Development Company

The main focus of the AADC demonstrator programs is to provide the test beds for the evaluation of Integrated High Performance Turbine Engine Technology (IHPTET) Program technologies and new HCF technologies. These critical core and engine demonstrations assess the performance and mechanical characteristics of HCF technologies in a realistic engine environment and provide the data necessary to validate and update advanced HCF prediction tools.

7.3.1 XTL17/SE1

FY 03 (2nd Qtr)

Objectives: Conduct a baseline AE3007 engine test to calibrate a strain-gauged fan with NSMS and Tip Timing probes.

HCF Technologies Demonstrated: NSMS (line probe) and Tip Timing (spot probe) data correlated with strain gage data.

Final Results: The test results will be used to evaluate the data obtained from a strain-gauged fan and compared to NSMS and Tip Timing Light probes.

Participating Organizations: Air Force Research Laboratory (AFRL), Allison Advanced Development Company (AADC)

Points of Contact:

Government
Mr. Mark Dale
U.S. Air Force, AFRL/PRTP
1950 Fifth St., Bldg. 18D
Wright-Patterson AFB, OH 45433-7251
Phone: (937) 255-2767
Fax: (937) 656-4179

Contractor
Mr. Bernie Rezy
Allison Advanced Development Co.
2056 South Tibbs Ave.
Indianapolis, IN 46207
Phone: (317) 230-6543
Fax: (317) 230-3009

7.3.2 XTL17

FY 03 (4th Qtr)

Objectives: Demonstrate the core technologies required to meet the IHPTET Phase III specific thrust goal.

HCF Technologies Demonstrated: Design of engine components predates advent of modern HCF computer codes.

Details/Progress: Design of an advanced, high performance combustor is underway. Repair and refurbishment of XTL16 hardware is underway and will be completed in 2002.

Participating Organizations: Air Force Research Laboratory (AFRL), Naval Air Warfare Center-Aircraft Division (NAWC-AD), Allison Advanced Development Company (AADC)

Points of Contact:

Government
Mr. Mark Dale
U.S. Air Force, AFRL/PRTP
1950 Fifth St., Bldg. 18D
Wright-Patterson AFB, OH 45433-7251
Phone: (937) 255-2278
Fax: (937) 656-4179

Contractor
Mr. Bernie Rezy
Allison Advanced Development Co.
2056 South Tibbs Ave.
Indianapolis, IN 46207
Phone: (317) 230-6543
Fax: (317) 230-3009

7.3.3 XTL17/SE2

FY 05 (3rd Qtr)

Objectives: Demonstrate the durability characteristics of HCF technologies in a 200-hour AE3007 engine test sponsored by DoD and MOD.

HCF Technologies Demonstrated: Damping technologies including hard coatings, air film damping, NSMS, and Tip Timing. Mistuning and probabilistic analysis will be conducted for the baseline and damped fans.

Details/Progress: Notification of intent to award program has been received. Contract negotiations should commence in second quarter of FY2002.

Participating Organizations: Air Force Research Laboratory (AFRL), Allison Advanced Development Company (AADC), Rolls-Royce plc., UK Ministry of Defense

Points of Contact:

Government
Mr. Mark Dale
U.S. Air Force, AFRL/PRTP
1950 Fifth St., Bldg. 18D
Wright-Patterson AFB, OH 45433-7251
Phone: (937) 255-2278
Fax: (937) 656-4179

Contractor
Mr. Bernie Rezy
Allison Advanced Development Co.
2056 South Tibbs Ave.
Indianapolis, IN 46207
Phone: (317) 230-6543
Fax: (317) 230-3009

7.4 Conclusion

The HCF program has taken advantage and will continue to take advantage of IHPTET core and engine demonstrators to validate HCF-related technologies by piggy-backing the HCF technologies onto those demonstration tests. The "relevant environment" provided by each of these tests is the key that enables the technology to transition ultimately into use in operational systems. The HCF technologies, be they analytical methodologies capable of predicting outcomes (of the tests or of actual operational usage) or be they actual concepts implemented in hardware (like dampers or surface treatments), get a major portion of their validation from successful completion of their engine demonstrations. Challenges remain in how to adequately demonstrate durability under vibratory conditions and how to provide statistical significance for the test data from the necessarily limited test assets and test times that are available in these demonstrators. These challenges may ultimately have to be met by the synergistic combinations of engine demonstration with other validation methodologies.

8.0 TEST AND EVALUATION

PROGRAM CHAIR

DR. ROBERT W. MC AMIS
U.S. Air Force
AEDC/SVT
1099 AVE C
Arnold AFB, TN 37389-9013
Phone: (931) 454-4951
Fax: (931) 454-3644

BACKGROUND

High cycle fatigue (HCF) issues have resulted in distress to engines impacting the operation and maintenance of fielded USAF systems. The Test Protocol section describes the methods and practices used to ensure that engines have been adequately designed and developed to minimize the occurrence of high cycle fatigue failures during operational use.

Operational aircraft engines must not experience high cycle fatigue problems which result in failures, operational restrictions, undue maintenance, and inspections that hamper or hinder field availability for warfighters. The intent of the Test Protocol section is to provide information relative to the design, testing, and integration of components into full scale engines to minimize the occurrence of high cycle fatigue failures throughout the flight envelope of the engine.

Gas Turbine Engine failure mechanisms include:

- High cycle fatigue
- Low cycle fatigue
- Thermo-mechanical fatigue
- Creep
- Overstress
- Corrosion
- Erosion
- Fretting and wear

The ability of a component to avoid these failure mechanisms depends on the component design, material properties, and the operating environment. The component design and the material used are fixed. The operating environment may change and have a detrimental effect on the life of the component. The interrelation of all these factors impacts the rate of component life consumption. Other factors affecting life consumption include:

- Manufacturing and material defects
- Build and maintenance errors
- Foreign object damage (FOD)

- Limit exceedances (i.e. overspeeds, overtemperatures . . .)

Controlling these factors is the responsibility of the engine manufactures, operators, and maintainers. Avoiding them is possible but difficult. One factor is the engine internal flow path configuration (number of blades, vanes, and struts) which can excite the blade natural frequencies with engine integral-order drivers. Flow distortion can also create engine integral-order drivers. Another factor is nonintegral order excitations which are caused by flow separation, rotating stall, buffeting and flutter.

In particular, High Cycle Fatigue (HCF) is primarily a function of engine design. A component that fails in HCF does so because it has been subjected to a large number ($>10^7$) of elastic stress cycles. A number of factors may cause high-frequency loading of components. These are generally known as drivers and include the engine internal flow path configuration (flow perturbations), self-excited vibration (flutter, buffeting flow separation), flow distortion (pressure or temperature), and rotor balance.

HCF has become more of a concern recently because advanced rotor blade designs have undergone a fundamental change to achieve higher thrust to weight ratios and increased performance. New blade designs tend to be low-aspect-ratio, unshrouded, and an integral part of the disk. Low-aspect-ratio blades inherently have more natural modes in the engine operating range because frequencies are closely spaced. Mode shapes and corresponding vibratory stress fields tend to be highly variable among a population of blades because of small manufacturing variations. These variations create increased opportunity for mistuning. The integrally bladed-disk design and the elimination of inter-blade shrouds can reduce damping and contribute to higher dynamic stresses caused by integral and nonintegral order vibration. Another impact on HCF avoidance is simply that reduced part counts and stage counts translate into smaller design margins and increase reliance on the design system.

Structural failures attributable to HCF impact development (including test), production, and field operation and can cause attendant cost and schedule impacts. To minimize the potential for HCF, an HCF Test Protocol has been developed that permeates the design, development, test, and operation of the part. The approach is often referred to as “holistic” in that it is concerned with wholes rather than with the individual parts. Focus has been placed on improving the generation of key information at each stage of development and operation and the application of this information to other parts of the process. An integrated development process to include analytical-model-based aspects and experimental results has replaced the paradigm of design-then-test. The protocol includes a characterization phase and a demonstration phase. The overall intent of the protocol is to acquire information about the system in order to decrease probability of failure as the concept matures through design to production and maintenance. The probability of failure can be shown schematically, decreasing as development time increases (Figure 8.0.1). Additionally, the confidence bands narrow as system knowledge is gained. The dashed line is the mean probability of failure and is shown to decrease as the system proceeds through the design cycle. The characterization test protocol is in the concept, design, and prototype (EMD) phase, and is intended to reduce the uncertainty. The demonstration test protocol phase continues to reduce the probability of failure and occurs prior to production. The demonstration test then demonstrates an acceptable probability.

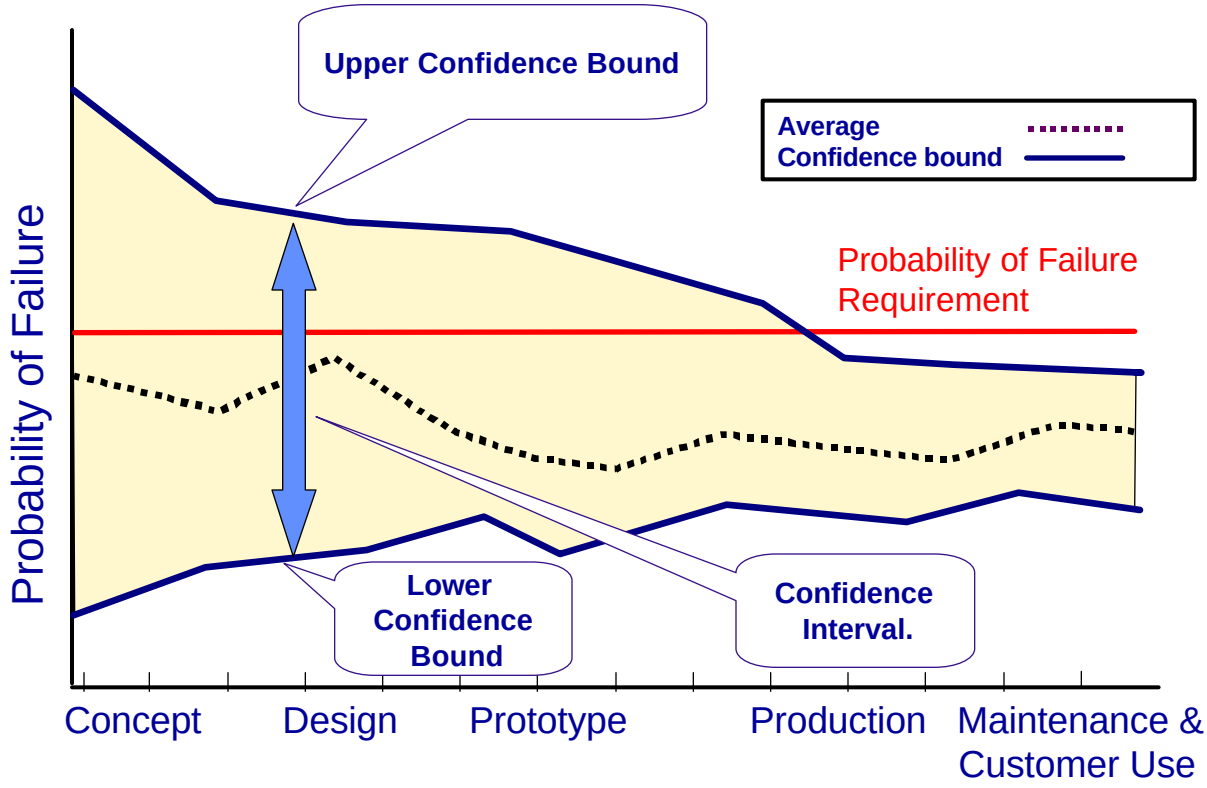

FIGURE 8.0.1 Decrease in Uncertainty and Risk over a System's Life Cycle

FIGURE 8.0.2 Test and Evaluation Development

Product	FY01	FY02	FY03	FY04	FY05	FY06
8.1 Characterization Test Protocol Development						
8.2 Demonstration Test Protocol Development						
8.3 Development of Multi-Axial Fatigue Testing Capability						

8.1 Characterization Test Protocol

FY 00-05

Background

The enhanced HCF Test Protocol has been developed as the understanding of failure mechanisms, drivers, and test planning criteria have evolved. New instrumentation and sensors, recording devices, analysis tools, and information management tools have provided better insights to the failure

mechanisms and means to counter HCF. Fig 8.1.1 provides a high level overview of some of the individual processes. The test protocol must ensure the following are accomplished:

- Identification of mode shapes and their variation
- Identification of critical locations with minimum HCF margins
- Exposure to relevant drivers and sufficient range of influence parameters
- Amplitude response ranges (including maximum) are known
- Fatigue mechanisms are known

Recent progress

A methodical systems engineering approach was defined and documented to fully understand the design and test parameters needed to identify and resolve high cycle fatigue issues within gas turbine engines. Figure 8.1.1 provides the key stages of conducting a high cycle fatigue program.

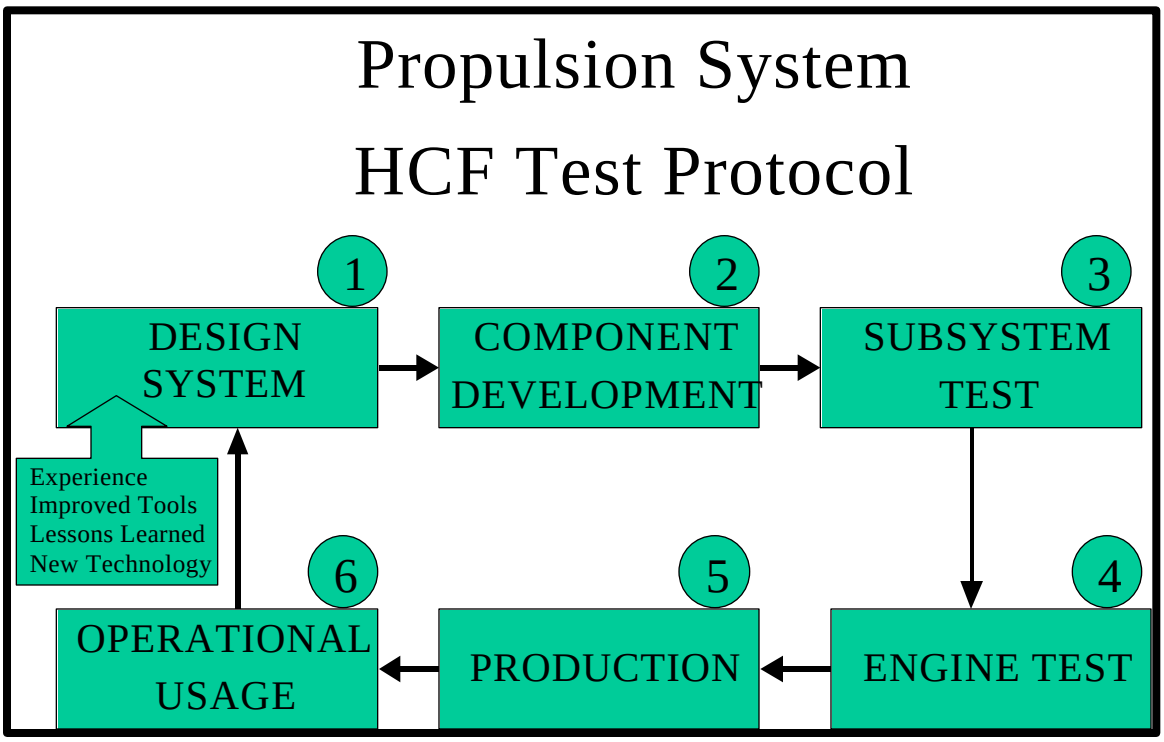

Figure 8.1.1 Approach for Addressing Turbine Engine HCF

(a) Design system: The holistic test and evaluation approach recommended herein begins with the contractor's design system. The manufacturer's design system defines the tools, margins, criteria, and material data that are used for the design of a gas turbine engine. Considering that a definition of robustness is insensitivity to variation, the test protocol first recommends that numerical assessments, including probabilistic predictions, be made to bound the range of variation that will potentially be present in a component. This requires the understanding of the relevant influence parameters. Some influence parameters may be geometric variations, variations in boundary conditions, local environment and body forces (e.g., RPM), etc. Assessments such as these can be performed by "brute-force" or using techniques like eigensensitivity analysis. The latter has the advantage of being useful for identifying model regions where modal frequencies may be especially sensitive to geometric variations. These results can be used to create specific models for parts that are off-nominal if

geometric differences are known (by coordinate measuring machine measurements, for example) or to correct/understand discrepancies between experimental results and nominal model results.

The manufacturer should insure that structural models used for these studies be sufficiently representative of the actual structure. One way to address this is to perform a mesh density investigation to ensure that computed frequencies for normal modes don't change as a function of model discretization. Use of solid elements (isoparametric) with parabolic shape functions is recommended.

The result of a sensitivity conscience design or probabilistic approach is a basic understanding of potential design variations that may exist once the structure is manufactured. Also, this process generates the structural models used to assess uninstrumented locations and perform detailed analysis of experimental results under operational conditions in subsequent phases of the recommended protocol.

(b) Component testing: The key focus of component tests, which are generally performed on shaker tables or using stingers, is to validate the analytical models generated above. The objective is to insure that the finite element model can accurately capture the stress field for steady loads and modal responses. Component tests should be performed to experimentally determine modal frequencies and mode shapes for comparison to analytical results. Impedance tests can be conducted inexpensively to define experimental frequencies. Care should be taken to insure that boundary conditions and physical characteristics (e.g., crystal orientation of anisotropic materials) of the part being tested are consistent with the model. Experimental and analytical frequencies should match mode-for-mode within five percent through the frequency range of interest. If they don't, the designer can utilize sensitivity data generated earlier to understand where problems may exist in the model.

Assuming sufficient agreement exists between experimental and analytical frequencies, attention should next be given to rigorous comparison of mode shapes. Utilization of a criterion such as the modal assurance criterion (MAC) is recommended for this purpose. Accuracy of the MAC is increased as the number of measurements used approaches the number of degrees of freedom in the analytical model. For this reason, utilization of scanning laser vibrometry or other field measurement techniques are recommended. These methods are also non-intrusive. Again, care should be taken to ensure that boundary conditions are sufficiently comparable between the model and the test.

Once it is verified that the analytical and experimental frequencies and modes are in sufficient agreement, the model can be trusted to describe the stress field at all locations on the component for any linear loading situation (steady or vibratory). Variations in stress resulting from changes in boundary conditions can be assessed and operational effects can be addressed.

If the experimental and analytical results do not agree, every effort should be made to reconcile differences, since failure to do so indicates that the analytically predicted design intent will not be achieved.

Specifically in the case of mistuning assessments, bench top experimental analysis of bladed disks can be subdivided into two types of testing: forced response and modal analysis.

Forced response analysis is excitation of the disk assembly in a spatial pattern comparable to that expected in operation. This means application of a traveling wave excitation of m cycles per revolution, m being the number of upstream excitations in operation per revolution (downstream if back propagation of excitations is being studied). Excitation of this form has been generated in the

past using screens, piezo-electric actuators, speakers, air jets, magnets, and fans. Careful control of the timing (for electronically controlled actuators) or spacing (for spinning excitations) should be maintained to ensure true on-resonant excitation. Slight variations can cause significant degradation of the desired results by impacting combined system modal responses. In general, multiple system modes are combined in the system forced response. (Mode localization could not occur without this happening.) These modes are often highly sensitive to mistuning, and as a result, forced response analysis is useful for evaluating specific stress distributions determined analytically, but cannot be used as a means of model correction when that model will be used for mistuned analysis, statistically or otherwise.

The term modal analysis is used to represent the traditional systematic identification of a set of system modal frequencies and mode shapes. Modes in bladed disk assemblies are often paired with an orthogonal mode with the same natural frequency. Consequently, traditional Single Input, Multiple Output (SIMO) or Multiple Input, Single Output (MISO) modal testing techniques are not applicable in the ideal tuned case (they cannot pick up the repeated frequency and associated mode shape). As a result, Multiple Input, Multiple Output (MIMO) techniques such as Polyreference Time Domain (PTD), Polyreference Frequency Domain (PFD), or the Eigenvalue Realization Algorithm (ERA) are necessary, the latter being freely available from NASA Langley for US citizens to use in government, industry, or academia. In the mistuned case, SIMO or MISO techniques work in theory, but in practice, modes are so closely spaced within a group that they tend to be very difficult, if not impossible, to identify.

Results from the use of "rainbow wheels" to validate damping can be misleading with the existence of modal interaction. Damping itself can be a source of mistuning, and results obtained can be measures of energy transfer to the rest of the system rather than the desired energy dissipation. Ideally, rainbow wheels should be avoided. When used, great care must be taken to assure that the measured results are interpreted correctly. Damping that is applied to a single blade (i.e., not dependent on adjacent blade motion) can be accurately tested by detuning the blade sufficiently such that the test frequency for the blade is far enough from the system frequencies to avoid modal interaction. For a rainbow wheel with a large number of different dampers, this could necessitate a system finite element model (FEM) to determine whether system modes interact with any of the damped blade's modes. When blade interactive dampers are tested, the band of blades must be mistuned from the rest of the disk and experimental data must validate that 1) no modal interaction occurs between the group of damped blades, and 2) the number of blades used is sufficient that extrapolation to a complete disk is valid. For such extrapolation to the entire disk to be valid, the group must demonstrate at least two special cycles of the same behavior in the middle of the group. This corroborates that forward and backward blade interaction is fully developed for the center groups.

(c) Subsystem testing: Once a physically representative analytical model of the structure is available, it can be utilized to define instrumentation locations for use in tests where nonintrusive field measurements are not practical. Definition of these locations can be performed using "brute-force" or by utilizing optimization schemes. Locations selected for instrumentation should provide sufficient detection of responses and should also permit mode delineation by using MAC-like approaches. In order for the latter to be accomplished, more than one sensor should be applied to the component. Locations selected for instrumentation should also be insensitive to sensor application tolerances.

Once sensor locations have been defined, it is necessary to establish experimental limits. These limits serve two functions: to insure test article safety and to establish experimental success criteria. Again, since a physically representative analytical model is now available, it can be used to assess the various combinations of steady and vibratory stresses at each location represented in the model and to compare

each of these to a fatigue criterion. Modal responses can be analytically scaled until the fatigue criterion is met at the minimum margin location. The minimum margin location is easily identified since all locations are monitored. Predicted sensor output can then be "read-off" to define the limit.

Once instrumentation locations, test limits, and success criteria have been established, instrumentation can be applied and tests can be performed in rigs or engines. Test conditions should be selected so that ranges of local influence parameters are sufficiently tested. For example, a turbine rig test should seek to test a sufficient combination of pressure and temperature as defined by the local P-T map. Additional influence parameters that should be considered include RPM, distortion, inlet profile, or perhaps others.

HCF responses should be compared to previously defined limit and success criteria. Data generated to assess component variabilities can now be used to prescribe corrections to the design, should limits be exceeded.

(d) Engine test: Engine testing should proceed with the intent of expanding the exposure of each component to its range of influence parameters. The same instrumentation locations used during subsystem testing, or a subset of it, should be used during engine test. To expand visibility despite the need to cover a large number of components during engine test, other tools, like the Non-interference Stress Measurement System, or NSMS, are being developed. Also, because multiple components are usually tested concurrently during engine test, optimization techniques may be needed to define a minimum number of test conditions that expose each component to its maximum range of local influence parameters.

The volume of data recorded during engine tests, particularly during simulated altitude ground tests, can be quite extensive. HCF failures have occurred that would have been avoidable had all the data that were acquired been processed and analyzed. Because of this, new technologies and systems that can process, analyze and store all acquired data in a database should be employed.

New tools developed for analysis of large volumes of engine test data make it possible to statistically assess the range of responses encountered as the local operational range of influence parameters is expanded. These assessments are naturally extendable to operational scenarios and form the foundation of enhancements to the design system, such as development of probabilistic methods. For example, these new statistical tools should be combined with probabilistic models for the system or component to validate structural modeling.

(e) Production/Operational Usage: Databases established during development or component improvement programs, when used in concert with production and operational use experience, can potentially be used for health monitoring and/or prognostic approach development. All information resulting from "real" use should be used to enrich design and development tools by expanding understanding of response variabilities.

To implement the Characterization Test Protocol, a simple checklist was created (Figure 8.1.2). The checklist denotes the Test Protocol items defined in serial order, which, when executed, populates the information system required for proper T&E assessment.

	Test Protocol Item	Yes ✓ / No ×	
I.	Design per Standard Work		
II.	Construct FEM		
	Solid Elements		
	Parabolic Displacements Functions		
III.	Perform Normal Modes Analysis		
	Mesh Density Assessment		
IV.	Sensitivity Assessment		
	Geometry/Eigensensitivity		
	Boundary Conditions		
V.	Define Optimum Sensor Locations		
	Mode Measurement Capability		
	Modeshape Identification		
	Sensitivity to Sensor Misplacement		
VI.	Validate FEM		
	Frequency Comparison		
	Strain Ratio Comparison		
	MAC or Similar		
VII.	Compute Normal Modes at Speed		
VIII.	Define Limits for All Component Locations		
IX.	Design Experiment to Maximize Exposure to Influence Parameters		
X.	Test Rig and/or Engine		
	Process All Dynamic Data		
	Transform to Frequency Domain		
	Identify Modes Using Frequency and MAC		
	Apply Limits/Use FEM or FEM Derived Look-up Table		
	Database Results		
	Establish Statistical Variations from Database		
XI.	Assess Robustness		
XII.	Fix as-needed using Eigensensitivity to Move Problem Modes		

Partial ~
Yes ✓
No ×

Figure 8.1.2 HCF Characterization Test Protocol Checklist

8.2 Demonstration Test Protocol
FY 00-05

Background

In addition to developmental engine tests aimed at characterizing component HCF margins, demonstration tests should be run. These tests are particularly useful for uncovering HCF problems on engine external components. The value, as it relates to internal components, is less clear since there are so many discrete frequencies for each of the parts that ensuring sufficient exposure to relevant modes is nearly impossible. Nonetheless, current practice is to perform an up and down HCF stairstep test prior to the beginning of an accelerated mission test (AMT), and at the end of the AMT. These stairsteps are typically run at 50 RPM increments with, $5x10^5$ cycles (assuming a 3E driver) at each increment which equates to 10^6 cycles in each 100-RPM band. In addition, the engine tests should

include dwell time (10^7 cycles) at each of the critical speeds above idle where the response in the rotor system dynamic verification testing shows peak values above the Goodman allowable. The procedures should be repeated for the other critical speeds below maximum speed if these critical speeds lead to maximum response at any point in the engine. Modes above and close to the maximum speed should be checked with the unbalance distribution required to excite these modes. If required, the phase of unbalance distributions should be changed to help determine residual unbalance.

Recent Progress

The emphasis for the demonstration test is driven by the probability of failure requirement defined in the Engine Structural Integrity Program (ENSIP) Guide, section A.4.13.3 High Cycle Fatigue: the probability of failure due to HCF for any component within or mounted to the engine should be below $1x10^{-7}$ per engine flying hour (EFH) provided the system level safety requirements are met.

The demonstration test protocol was identified as occurring during the latter portions of the design cycle and aimed primarily at improving confidence in the probabilistic performance metric. Because of this, it is likely that so-called demonstration tests will be engine specific depending on the type of confidence increase required.

Coordination with the Components Action Team (through the probabilistics element) was initiated. Guidance from the Components Action Team was received: (1) tests alone are impractical (a holistic approach needed); (2) define tests to validate probabilistics model inputs (e.g., means and variances); (3) define tests to validate physics based models (e.g., FEM validation); (4) define the uncertainties (e.g., eigensensitivity, sensor misplacement).

At this time, it is envisioned that the demonstration test will not be a single engine test or single component test. Rather, it will be composed of laboratory, component, rig, and engine tests. To enhance implementation of such a demonstration test protocol, communication was established among the Compressor Research Laboratory at AFRL, the Navy Spin Pit facility and Turbine Engine Test Facilities at AEDC. It is anticipated that data will be collected at all facilities and analyzed as a single set for adequate probabilistic assessment.

8.3 Development of Multi-Axial Fatigue Testing Capability
FY 00-01

Background

The objective of this task was to develop the capability to test turbine engine components in a bench-test environment that simulates vibrational loading effects experienced during engine operation. Research goals were to develop a test system that simulates operational blade loading, including simulated rotational effects, and to develop a data acquisition system that accurately monitors critical test parameters. This test capability was to provide a low-cost method to evaluate turbine engine blades for HCF. A test frame was designed and constructed to test gas turbine blades under multi-axial loading conditions. A load cell on the primary axis was employed to simulate the centrifugal loading experienced by the blade. Two rams were positioned on the second axis; and, depending on their relative position, either bending or torsion could be induced in the airfoil. Combined, the loading allows for fatigue testing under simulated operational environments.

Final Results

The multi-axial fatigue frame (Figure 8.3.1) was procured and built under an SBIR effort which was completed in 2000. Upon completion of the frame, a parametric study was initiated to determine the full range of capabilities of the system. Through this effort, numerous tests have been performed including cruciform specimens made from composite material and the torsion fatigue testing of simulated airfoils under both vibrational and simulated rotational loading. The fixture is now fully operational.

Currently, a joint effort with the Air Force Institute of Technology to investigate fretting fatigue is being performed utilizing the frame.

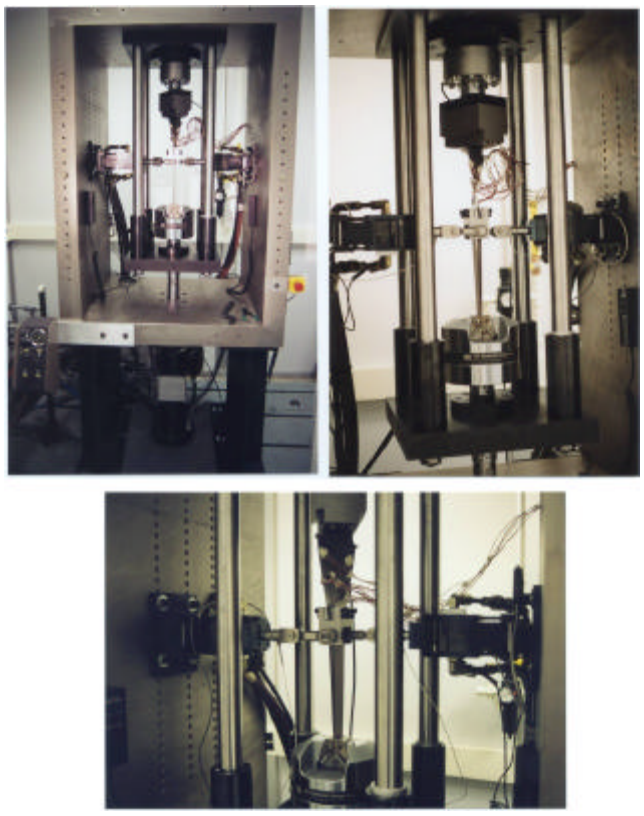

FIGURE 8.3.1 Multi-axial Fatigue Frame

Participating Organizations: Air Force Research Laboratory (AFRL)

Points of Contact:

Government
Mr. Gary Terborg
U.S. Air Force, AFRL/PRTC
1950 Fifth St., Bldg. 18D
Wright-Patterson AFB, OH 45433-7251
Phone: (937) 255-2611
Fax: (937) 255-2660

THIS PAGE INTENTIONALLY LEFT BLANK

9.0 TRANSITION

BACKGROUND

The Transition Action Team is responsible for identifying those technologies, methodologies, and criteria developed through the HCF Science and Technology Program which have reached sufficient maturity for incorporation into the Engine Structural Integrity Program Handbook and the Joint Service Specification Guide for Turbine Engines. The goal of this task is to insure that the knowledge gained from the Action Team efforts is successfully transitioned into design practice and actively applied in future military engine design efforts. Three groups (Analysis, Testing, and Materials) actively communicate and coordinate with other Action Teams, industry, and academia to identify opportunities and recommend proposed changes.

ACTION TEAM CHAIRS

Chair
Mr. Vincent S. Spanel
ASC/ENFP
2530 Loop Road West
Bldg. 560
WPAFB OH 45433-7101
Phone: (937) 255-8604
Fax: (937) 656-4546

Figure 9.0 HCF Technology Transition

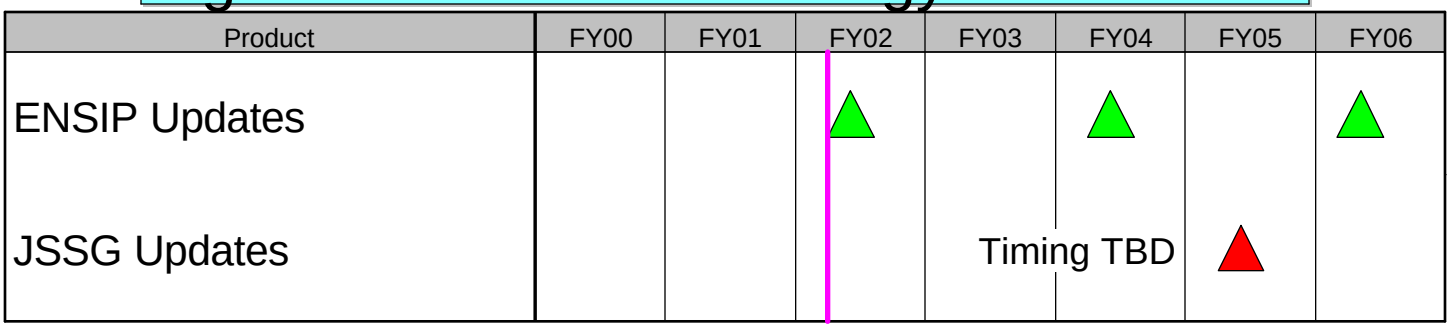

9.1 Engine Structural Integrity Program (ENSIP) / Joint Service Specification Guide (JSSG):

Background

The initial effort was started in 1998 based on a recommendation of the Executive Independent Reviews Team (EIRT). The groups worked throughout 1998 and 1999 and made initial recommendations for changes to the ENSIP Handbook at the end of the year. In 2000, the recommendations were incorporated into a draft update of the ENSIP Handbook and underwent a detailed and lengthy review cycle with government and industry experts. Some of the updates include new analyses for mistuning and damping, changes in test procedures and updated requirements for material characterization. After several iterations, the revised document was finished in December of 2000.

Recent Progress

The status of the effort and content of the revised handbook was presented at the EIRT review in February of 2001. Several follow-up meetings were held to address some remaining issues through early 2001. In mid-2001, the release of the document was delayed for incorporation of recent lessons learned relating to hold-time effects on crack growth behavior. The Team reviewed the task status at the HCF Mid-Term Steering Committee Meeting in August 2001 and the final draft was provided to the Engineering Standards Office (ASC/ENOI) at Wright-Patterson AFB immediately afterwards. The formal approval cycle was initiated in September 2001, when it was released for government and industry review and concurrence with a target complete date of November 2001. The Standards Office received several comments from industry and those were reviewed for possible incorporation into the final official release which is now expected in early 2002.

All of the recommended changes to the ENSIP handbook are also being provided to the JSSG team for incorporation into the next release of JSSG-2007. However, current funding is being targeted to develop system level JSSG documents, and a scheduled date for the next release of the Turbine Engine JSSG document has not been established. All recommendations are being gathered and held until funding is available to begin the update cycle.

10.0 AEROMECHANICAL CHARACTERIZATION

The Aeromechanical Characterization Action Team was disbanded in CY 2001. The responsibilities for its remaining projects were transferred to the Forced Response Action Team and to the HCF Test and Evaluation Program. The former Aeromechanical Characterization activities listed below are addressed in this report in the sections indicated:

Development of Multi-Axial Fatigue Testing Capability – 8.3
Spin-Pit Excitation Methods – 5.2.7
Inlet Distortion Characterization – 5.2.8
Engine Structural Integrity Program (ENSIP) / Joint Service Specification Guide (JSSG) – 9.0

Definition of Acronyms

Acronym	Definition
3D	Three-Dimensional
AADC	Allison Advanced Development Company
ACIS	Advanced Compact Inlet System
AEDC	Arnold Engineering Development Center
AFD	Air Film Damping
AFDS	Air Film Damping System
AFIT	Air Force Institute of Technology
AFOSR	Air Force Office of Scientific Research
AFRL	Air Force Research Laboratory
AMT	Accelerated Mission Test
AT	Action Team
ATEGG	Advanced Turbine Engine Gas Generator
BAA	Broad Agency Announcement
BDSP	Blade Deflection Signal Processor
BTG	Blade Timing Generator
CAD	Computer Aided Design
CARL	Compressor Aero Research Laboratory
CCB	Chu Conle Bonnen (model)
CDA	Controlled Diffusion Airfoil
CECM	Comprehensive Engine Condition Management
CEP	Common Engine Program (Army)
CFD	Computational Fluid Dynamics
CLDEF	Centrifugally Loaded Dynamic Excitation Facility
CLDS	Constrained Layer Damping System
CLDT	Constrained Layer Damping Treatment
CM	Chem Milled
CMU	Carnegie Mellon University
CPU	Central Processing Unit
CRF	Compressor Research Facility
CY	Calendar Year
DCT	Diamond Cross-section Tension
DEN	Double Edge Notch
DSP	Digital Signal Processor
DUST	Dual Use Science and Technology
ECS	Eddy Current Sensor
EDAS	Engineering Design & Analysis Solutions (company)
EDM+CM	Electrodischarge Machining plus Chem Milling
EIRT	Executive Independent Review Team
ENSIP	Engine Structural Integrity Program
E-O	Electro-Optics
ERA	Eigenvalue Realization Algorithm

Acronym	Definition
FEA	Finite Element Analyses
FEM	Finite Element Model
FFT	Fast Fourier Transform
FIFO	First-In-First-Out
FOD	Foreign Object Damage
FRAT	Forced Response Action Team
FY	Fiscal Year
G4F	Generation-4 Front End (NSMS)
G4P	Generation-4 Processor (NSMS)
GDATS	General Dynamics Advanced Technology Systems
GE	General Electric
GEAE	General Electric Aircraft Engines
GRC	Glenn Research Center (NASA)
GUI	Graphical User Interface
GUIde	Government, University, Industry (consortium)
HCF	High Cycle Fatigue
HPC	High Pressure Compressor
HPT	High Pressure Turbine
HTC	Hood Technology Corporation
I/O	Input/Output
IAP	Industry Advisory Panel
IBR	Integrally Bladed Rotor
IDDS	Infrared Damage Detection System
IGV	Inlet Guide Vane
IHPTET	Integrated High Performance Turbine Engine Technology
IR&D	Independent Research and Development
ISSI	Innovative Scientific Solutions, Inc.
JSF	Joint Strike Fighter
JSSG	Joint Service Specification Guide
JTDE	Joint Technology Demonstrator Engine
ksi	kilo-pounds per square inch
LANL	Los Alamos National Laboratory
LCF	Low Cycle Fatigue
LE	Leading Edge
LED	Light Emitting Diode
LPC	Low-Pressure Compressor
LPT	Low-Pressure Turbine
LSG+CM	Low Stress Grinding plus Chem Milling
LSP	Laser Shock Peening
MAC	Modal Assurance Criteria
ManTech	Manufacturing Technology
MEMS	Micro-Electromechanical System
MIMO	Multiple Input, Multiple Output
MIP	Multiple Individual Particles

Acronym	Definition
MISO	Multiple Input, Single Output
msi	Mega-pounds per square inch
MURI	Multi-University Research Initiative
NASA	National Aeronautics and Space Administration
NAVAIR	Naval Air Systems Command
NAWC	Naval Air Warfare Center
NPS	Naval Postgraduate School
NSMS	Non-Contact Stress Measurement System
NSMS	Non-Intrusive Stress Measurement System
O&S	Operations and Support
OSU	Ohio State University
P&W	Pratt & Whitney
PC	Personal Computer
PDAS	Probabilistic Design Analysis System
PFD	Polyreference Frequency Domain
PIV	Particle Image Velocimetry
PIWG	Propulsion Instrumentation Working Group
plc	Public Limited Company (UK)
POD	Proper Orthogonal Decomposition
PPGM	Propulsion Product Group Manager
PR	AFRL Propulsion Directorate
PRDA	Program Research and Development Announcement
PRDS	Probabilistic Rotor Design System
PSP	Pressure Sensitive Paint
PTD	Polyreference Time Domain
PWA	Pratt & Whitney Aircraft
Q	Vibratory Amplification Factor
QA	Quality Assurance
QC	Quality Control
RFL	Random Fatigue Limit
ROM	Reduced Order Model(ling)
RPM	Revolutions Per Minute
RR	Rolls-Royce
SBIR	Small Business Innovative Research
SDD	System Design & Development
SEM	Scanning Electron Microscope
SIMO	Single Input, Multiple Output
SLS	Selective Laser Sintering
SMI	Stage Matching Investigation
SN	Stess versus Cycles
SNM	Subset of Nominal Modes
SRA	Stress Relieve Anneal
SSR	Shear Stress Range
STOA	Solution Treated Over-Aged

Acronym	Definition
T/PSP	Temperature/Pressure Sensitive Paint
TACs	Total Accumulated Cycles
TBC	Thermal Barrier Coating
TEFF	Turbine Engine Fatigue Facility
TF	Transfer Function
TM	Trademark
TP	Thermographic Phosphor
TPT	Technical Plan Team
TSP	Temperature Sensitive Paint
UAV	Uninhabited Air Vehicle
UCAV	Uninhabited Combat Aerial Vehicle
UDRI	University of Dayton Research Institute
UK	United Kingdom
USAF	United States Air Force
UTC	Universal Technology Corporation
UTRC	United Technologies Research Center
VDC	Vacuum Die Casting
VE	Viscoelastic
WI	Williams International
YAG	Yttrium Aluminum Garnet

Alternate Description of Figures

Figure Number	***Title*, Description**
FIGURE 0.1	*HCF Team Organizational Structure* The organization chart shows a Steering Committee, Chaired by Mr. May, supported by an Executive Independent Review Team, Chaired by Dr. Heiser and an Industry Advisory Panel, with a currently vacant chair, overseeing the efforts of a Technical Planning Team, chaired by Mr. Fecke supported by the activities of the Science and Technology Action Teams managed by Mr. Thomson, the Test and Evaluation effort led by Dr. McAmis, and the MIL-HDBK-1783B effort led by Mr. Spanel. A separate US-UK Project Arrangement Steering Committee and Management Group coordinates their effort with the HCF Steering Committee and transitions the results of the effort to applicable systems.
FIGURE 1.0	*Component Surface Treatment Research Schedule* 1.1 LSP vs. Shot Peening Competition – All FY95 1.2 Laser Optimization Development – All FY95 1.3 Production LSP Facility Development – FY96 through FY98 1.4 LSP Process Modeling – FY96 through FY99 1.5 RapidCoater (TM) for LSP – FY97 through 2QFY02 1.6 Manufacturing Technology for Affordable LSP – FY98 through 2QFY03 1.7 Laser Peening of F119 Fourth-Stage Integrally Bladed Rotors – FY00 and 2QFY03 1.8 Processing and Manufacturing Demonstration for High Strength Affordable Castings – FY00 – FY02
FIGURE 1.5.2.1	*A Single RapidCoater™ Head (a) for Single-Sided Processing and a Dual RapidCoater™ Head, and (b) for Processing a Thin Section, Such as Compressor Blades* This two-photograph figure shows the following: a) A single head with mounted paint spray nozzle, water curtain nozzle, and paint wash-off nozzle b) A head mounting two fixtures like that shown in a) aimed at what would be opposite sides of the part to be processed
FIGURE 1.5.2.2	*Spatial Profiles of the Laser Beam Showing the Transformation from a Round Spot (a) to a Square Spot (c) with the Use of Optics (b)* This illustration shows two color-coded brightness images (a and c), one round and one square, and a line drawing showing the laser light rays being bent by using a specially-shaped prism between the laser and the target (c).
FIGURE 1.6	*(a) The Small Parts Laser Peening Cell for Processing Parts such as*

Turbine Engine Airfoils, (b) The Large Parts Cell for Laser Peening Parts such as F119 IBRs.
This two-photograph figure shows the following:
(a) A multi-axis robot arm, about four feet tall, and the cabinets and support structure that house the laser peening and control equipment.
(b) Two multi-axis robot arms, the smaller of which (about 4 feet tall) holding the coating system and the larger of which (about 6 feet tall) with a fixture for mounting parts.

FIGURE 1.7 *(a) A 4th Stage IBR Positioned for Processing in the Large Parts Peening Cell, (b) A Close-up Schematic of Laser Peening of a 4th Stage IBR (Laser Beams Added for Visualization).*
This two-photograph figure shows an IBR mounted to the large multi-axis robot arm and a detail view of the water curtain nozzles spraying water on one of the rotor blades with a red line indicating a path for the laser peening beam through the water curtain onto the blade.

FIGURE 1.8 *(a) Vacuum Die Cast Titanium Alloy Blades Prepared for Laser Peening, (b) Fatigue Testing of a Laser Peened Blade on an Electro-Dynamic Shaker Table.*
This two-photograph figure shows (a) twelve compressor blades laid out on a table and (b) a blade mounted on a shaker with instrumentation for measuring strain and vibratory amplitude.

FIGURE 1.9 *Interrelationship among LSP Programs*
This development process schematic shows that the completed Laser Optimization Development supported the Production LSP Facility Development, which with the completed Process Modeling of LSP, supports the yet-to-be-completed Manufacturing Technology for Affordable LSP. The completed Overlay Concept Development supports the yet-to-be-completed RapidCoater program which then supports both the yet-to-be-completed Manufacturing Technology for Affordable LSP and the yet-to-be-completed Laser Peening of F119 4th Stage IBRs. The Manufacturing Technology for Affordable LSP supports both the Laser Peening of F119 4th Stage IBRs and the Processing and Manufacturing Demonstration for High Strength Affordable Castings.

FIGURE 2.0 *Materials Damage Tolerance Research Schedule*
2.1 Microstructure Effects of Titanium HCF (Fan) – FY96 through FY98
2.2 Air Force In-House Research (Fan and Turbine) – FY96 through FY03
2.3 HCF and Time-Dependent Failure in Metallic Alloys for Propulsion Systems (Fan and Turbine) -- FY96 through FY01
2.4 Improved HCF Life Prediction (Fan) – FY96 through FY00
2.5 Advanced HCF Life Assurance Methodologies – FY99 through FY02
2.6 Probabilistic HCF Life Prediction – 2nd half FY01 through FY06
2.7 Future Efforts

2.7.1 Advanced High Cycle Fatigue Mechanics – FY02 through FY04
2.7.2 HCF Properties of Welds on Nickel-Based Alloys – FY02 through FY06

FIGURE 2.2.1 *Pre-Crack and Step-Test Loading Technique Used to Determine LCF/HCF Thresholds*
This plot of stress versus time shows a series of LCF precrack cycles followed by blocks of 10^6 HCF cycles, each block with increasing amplitude, all at a constant frequency of 600 Hz building up to the last block in which the peak stresses in the cycle exceed sigma-max-threshold.

FIGURE 2.2.2 *Schematic of Double Edge Notch (DEN) Specimens Used for HCF/LCF Interaction Study*
This multi-view line drawing shows cylindrical notches perpendicular to the pull direction opposite each other on the two narrow sides of a rectangular cross-section pull-test specimen. This creates a high-stress plane perpendicular to the pull direction. The notches are the same depth but with a different radius, forcing the higher stress, at a K_t of 2.25, at the smaller-radius notch versus the lower stress at the larger-radius notch, at a K_t of 1.94. A crack grows out of the smaller notch at a depth = c and a half-length = a.

FIGURE 2.2.3 *Micrograph of Typical Damage Identified by the Infrared Damage Detection System (IDDS)*
The micrograph shows the material's grains with a crack in the center of the image growing through two grains and along the grain boundary of a third.

FIGURE 2.2.4 *Comparison of Cycles to Failure in Last HCF Loading Block for Specimens with and Without Damage.*
This plot of Percentage of Last Loading Block Complete shows about two dozen data points in a range of percentages from 0 to 100 for Pure HCF, while a similar number of data points from testing with LCF cracks only range between 0 and 15.

FIGURE 2.2.5 *Kitagawa Diagram Showing the Relationship between Crack Depth and Failure Stress at 10^7 Cycles.*
In this log-log plot of maximum stress (MPa) versus crack depth c in micro-meters, the long crack delta-K_{th} with short crack correction curve is close to but always below the test data points for Rs at 0.1 and -10 both with and without stress-relieve anneal. The curve declines from almost tangent to the 330 MPa constant fatigue limit through a point at 180 MPa and 100 micro-meters down to 100 MPa at 340 micro-meters.

FIGURE 2.2.6. *Notional Goodman Diagram*
This plot shows the declining straight line allowable alternating stress with

increasing mean tensile stress at 10^7 cycles. It illustrates the unknown allowable alternating stress as mean stress transitions from tensile to increasing compressive stress.

FIGURE 2.2.7 *Goodman Diagram with Jasper Equation and Compressive Mean Stress Data*

This plot of alternating stress (MPa) versus mean stress (MPa), for Ti-6Al-4V for 10^7 cycles at 50-70 Hz, shows the Jasper curve agreeing well with test data. This smooth curve starts at +600 alternating stress at -400 mean stress rising slightly to 610 at -300 and then curving downward to 500 at 0 mean stress to 220 at 350 and then flattening through 140 at 600 to 90 at 1000 mean stress.

FIGURE 2.2.8 *Fretting Fatigue SN Data Compared to Plain Fatigue Curve*

This plot of effective stress (MPa) in a linear scale versus cycles (N) in a logarithmic scale shows a curve for plain fatigue running from 1000 MPa stress at $1.7x10^4$ cycles through 700 at $1.0x10^{5,}$ flattening to 475 at $1.0x10^8$. The data points for fretted surfaces from fretting pads with radii of 2, 4, and infinity (flat) follow a trend that is well below the plain fatigue curve at plus or minus 70 MPa to a curve that runs from 700 MPa at $2x10^4$ cycles through 250 at $3x10^5$, flattening at 200 from $1x10^6$ through $5x10^7$.

FIGURE 2.2.9 *Insensitivity of Fretting Fatigue Debit to Normal and Shear Stress*

This figure shows two plots:

1) Fretted stress divided by baseline stress versus normal stress (MPa) which shows data points (at R=0.5 for 1 mm [2 points], 2 mm [15 points], and 4 mm [7 points] samples) scattered around a level line at 0.35 plus or minus 0.15 for normal stresses between -560 and -50 MPa.

2) Fretted stress divided by baseline stress versus shear stress (MPa) which shows data points (at R=.5 for 1 mm [2 points], 2 mm [15 points], and 4 mm [7 points] samples) scattered around a level line at 0.35 plus or minus 0.15 for normal stresses between 10 and 70 MPa.

FIGURE 2.2.10 *Fretting Pad (Top) and Non-Traditional "Golden Arch" Specimens (Bottom)*

This photograph shows the following: the Fretting Pad, which is a 3" by 0.75" by 0.5" bar with slightly cylindrically rounded ends on which the fretting occurs; two views of the "Golden Arch" specimens, which are machined from the ends of the bar in a 1" by .075" by .05" "U" shape with the bottom of the U being the fretting surface.

FIGURE 2.2.11 *Micrograph of Arch Specimen Fretting Surface.*

The photograph shows an irregular area of fretting damage about 0.002 inches wide and 0.05 inches long with three identified cracks along the length of the damaged area (i.e., perpendicular to the rub direction) in this damaged area. The cracks are about 0.0015 inches, 0.005 inches, and

0.004 inches long.

FIGURE 2.2.12 *Kitagawa Diagram with Data from Fretted Arch Specimens*
This is a log-log plot of Maximum stress (MPa) versus crack depth (micro-meters) for fretting cracks in Ti-6Al-4V at R=0.1 showing the constant fatigue limit at 550 MPa, a "straight line" for the prediction without small crack correction from 800 MPa at 11 micro-meters to 160 MPa at 250 micro-meters, and a curve of the prediction WITH small crack correction that approaches tangency to the fatigue limit at 1 micro-meter and tangency with the uncorrected prediction at 250 micro-meters and running through a point at 400 MPa at 20 micro-meters. Eleven experimental data points from 20 to 160 micro-inches scatter plus or minus 50 MPa around the corrected curve, which fits the data better than the uncorrected line (which is at or above all of the data points).

FIGURE 2.2.13 *Overview of the Dovetail Fretting Fatigue Fixture*
This photograph shows a specimen metal rod with a flat "Y-shaped" end about the thickness of the rod, with the arms of the "Y' filled in. The mating fixture is the same thickness as the flat part of the specimen and has a cutout the same shape as the mating "Y" about 20% larger. Two rectangular fretting pads about 1/3 the length of the arms of the "Y" are mounted in cutouts in the fixture and contact the middle of the outside of the arms of the specimen's "Y."

FIGURE 2.2.14 *Variation of Fatigue Failure Loads for Three Different Fretting Pad Geometries*
This bar graph shows the maximum load (kN) for 10^6 cycles to failure (at a 45 shoulder angle, R=0.1): 20 kN for the 0.25 inch "long" flat fretting pad; 19 kN for the 2-inch radius cylindrical fretting pad and 18 kN for the 0.04 inch "short" fretting pad with 11-degree sloped taper on either side of the flat.

FIGURE 2.2.15 *Section View of Ultrasonic Fatigue System*
This line drawing shows the support fixture bottom platen with an ultrasonic exciter at the bottom, two resonant boosters above it attached to the specimen above them, attached to another resonant booster above that, attached to the spring-mounted upper holding fixture which has an eddy current gauge to measure motion. The upper holding fixture is loaded against the crosshead (attached via columns to the platen base) by an air cylinder, with the load measured by a load cell.

FIGURE 2.5.1 *Room Temperature Crack Growth Rates for Ti-17b*
This log-log plot of da/dN (in/cycle) versus delta K, a position (ksi-in^0.5) for Ti-17Beta, at 75 degrees F, shows data points that follow three basic curves:
1) For R=0.1 and 0.5 the data points go vertically at delta K of 2.5 from

da/dN of 2E-10 to 8E-9 then curve to the right becoming linear from da/dN of 1E-7 at 4.5 to 4E-6 at 15
2) For R=0, the data points go vertically at delta K of 3.2 from da/dN of 9E-10 to 5E-9 then curve to the right becoming linear form 3E-7 at 7 to 4E-5 at 35
3) For R=1.0, 1.1, and 1.2, the data points start at da/dN of 5E-9 at 6.1 curving slightly to the right through 4E-7 at 14 and becoming linear from 1E-6 at 21 to 5E-5 at 90

FIGURE 2.5.2 *Fatigue Data at 10^7 Cycles for Axial FOD Specimens*
The plot of Smax (ksi) versus FOD depth in inches shows data points for Ti-17 at room temperature with R= -1:
For 20-degree notches: 26 ksi at 0.013, 21 at 0.015, 13 at 0.016
For 20-degree notches stress relieved: 31 at 0.012, 26 at 0.0155, 25 at 0.016
For 40-degree notches: 27 at 0.008, 20 at 0.01
For a 40-degree notch stress relieved: 28 at 0.01

FIGURE 2.5.3 *Fatigue Data at 10^7 Cycles for Leading Edge FOD Specimens*
This is a plot of Smax (ksi) versus FOD depth in inches for blunt and sharp tip radius Ti-17 Pizza Hut FOD for 10^6 step tests at 75 degrees F, R= -1 with data points at the following:
FOD with step >0: 31 ksi at 0.0075 in
FOD with 0 steps, stress relieved: 24 at 0.017, 25 at 0.025
FOD with stress relief and >0 steps: 57 at 0.007, 38 at 0.009, 28 at 0.015, 28 at 0.023

FIGURE 2.5.4 *S-N Diagram for PWA 1484 at 1100^oF*
This is a plot of linear-scaled max cyclic stress (ksi) versus logarithmic-scaled life (cycles) for R= 0.1 for three crystal orientations:
<001+15> : 135 ksi at 1.3E4 (=$1.3x10^4$) cycles, 125 at 2.4E4, 125 at 4.0E4, 115 at 1.6E5
<010> : 140 at 4E4, 125 at 6.5E4, 130 at 7E4, 130 at 1.8E5, 120 at 4.2E5, 120 at 6E6, 118 at 7.5E6
<001> : 140 at 4E4, 130 at 1E5, 120 at 2.4E5, 120 at 1.8E6, 110 at 8E6

FIGURE 2.5.5 *Application of Walls Parameter to S-N Data for PWA 1484 at 1100^oF*
This is a plot of linear-scaled Walls Damage Parameter versus logarithmic-scaled life (cycles) for R= 0.1 for three crystal orientations:
<001+15> : 0.525 at 1.3E4 (=$1.3x10^4$) cycles, 0.522 at 2.4E4, 0.535 at 4.0E4, 0.495 at 5E4, 0.550 at 7E4, 0.475 at 7.5E4, .0480 at 8E4, 0.495 at 1.7E5
<010> : 0.540 at 4E4, 0.555 at 4.2E4, 0.500 at 7E4, 0.515 at 1.7E5, 0.475 at 4.2E5, 0.475 at 6E6, 0.465 at 7.5E6
<001> : 140 at 4E4, 130 at 1E5, 120 at 2.4E5, 120 at 1.8E6, 110 at 8E6
A curve fit of the data points is approximately a line that runs from 0.540 at

1.0E4 to 0.455 at 1.0E7

FIGURE 2.5.6 *Crack Growth Rates for PWA 1484 at 1900^{o}F*

This log-log plot of da/dn (in/cycle) versus delta K (ksi-in$^{1/2}$) run at 10 Hz shows data series of multiple points spaced closely enough together to produce what appear to be smooth curves as look as follows:

- Run A2LRX-2 for R=0.8 begins at 1.6E-8 at 2.6 and rises linearly to the right to 1.5E-7 at 3.2 then changes direction rising linearly to the left to 3E-7 at 3.0
- Run T20VW-2 for R=0.7 begins at 1.5E-8 at 4.3 and rises vertically to 2.4E-8 then rises linearly to 6.4E-8 at 5.1 then rises linearly to 3.2E-7 at 5.2
- Run A2LRX-4 for R=0.5 begins at 5.3E-9 at 4.2 rising linearly to 1.9E-7 at 4.7 then jogs linearly upward to the right to 2.2E-8 at 5.3 then rises approximately linearly to 1E-06 at 8.5
- Runs A2LPF-1 and A2LPE-1 for R=0.05 begin at da/dn of 2E-9 at delta K of 6.0 rising almost linearly to 1E-8 at 6.2 then curve to the right to 2E-8 at 7.2. From there the curvature reverses upward through 5E-8 at 9.0 to 2E-7 at 10.5 then becomes almost linear to 1.4E-6 at 15.0
- Run A2LPX-1 for R= -1 begins at 1.1E-9 at 12.0 rising linearly to 1E-8 at 13.0 then curving sharply to the right and back down through 1.8E-8 at 16.0 to 1.7E-8 at 17.0. At that point it abruptly changes direction, rising linearly to 4.5E-8 at 20. It jogs to the right to 5E-8 at 23 and then rises again almost linearly to 1.6E-6 at 29.
- Run A2LRX-3 for R= -1 begins at 9E-8 at 20.5 and rises linearly to 7E-7 at 34. Between 7E-7 and 1.7E-6, the data shows two linear trends one from 26 to 33 the other from 34 to 36. The two lines are joined by a smooth curve above 1.7E-6 peaking at 1.9E-6 at 34.
- Run T20VW-1 for R= -1 begins at 9.5E-9 at 16 and rises approximately linearly to 9.5E-7 at 29

FIGURE 2.5.7 *Crack Growth Rates for PWA 1484 at 1100^{o}F*

This log-log plot of da/dn (in/cycle) versus delta K (ksi x SQRT in) for R= 0.1 at 10 Hz shows two runs with series of data points and their curve fits that look as follows:

- Run T20WF-1 begins at 1E-9 at 4.9 and rises linearly to 6E-8 at 5.0 then curves to the right to 2.6E-7 at 5.5 then curves more sharply to the right to 3E-7 at 6.0. It then curves upward through 4.8E-7 at 9 to 8.5E-7 at 12. It breaks to the right and then curves more tightly upward through 1E-6 at 13 to 2E-6 at 14.
- Run T20Wf-2 begins at 1E-9 at 5.5 rising vertically to 6.5E-8. It then curves smoothly to the right through 3E-7 at 6.1 to 4E-7 at 7. It then curves upward through 7.2E-7 at 10 to 3E-6 at 14.

FIGURE 2.5.8 *Walker Effective K Model for Fatigue Crack Growth of PWA 1484 at 1900^{o}F, 10 hz.*

This log-log plot of da/dN (in/cycle) versus K(effective) (ksi x sqrt in)

shows a predicted crack growth line from da/dN of 7E-9 at a K(effective) of 6.2 to 1.4E-6 at 18 (based on the equation da/dN=7.899E-13x[K(effective)raised to the power 4.941].
K(effective) threshold is ~6.5 ksi sqrt in.
The data points for R ranging from 0.8 to -1 follow a linear trend on the plot that rises more steeply than the model in lines parallel to and approximately centered on a line from 1E-8 at 8.3 to 2E-6 at 16.
The data scatter in K(effective) is about 4 ksi sqrt in.

FIGURE 2.5.9 *Ti-6Al-4V Single Load Plus Interpolated Step Test Failure Random Fatigue Limit Model Fit.*

This plot of linear Walker stress versus logarithmic cycles at failure for Ti6-4 with the Walker exponent, w, = 0.362. The B50 life of the Random Fatigue Limit model is shown by a curve starting at 77 ksi at 5E+3 cycles running through 50 ksi at 1E+5 cycles to 35 ksi at 1E+9 cycles. The plot also has model curves for various lives up to B99 at 6.5 ksi higher than the B50 and down to B.135 at 14 ksi lower. Numerous data points for failures and some runouts are plotted within these bounds.

FIGURE 2.5.10 *Ti-17 Step Test with Last Surviving Stress Level as Runout Random Fatigue Limit Model Fit.*

This plot of linear Walker stress versus logarithmic cycles at failure for Ti17 with the Walker exponent, w, = 0.328. The B50 life of the Random Fatigue Limit model is shown by a curve starting at 89 ksi at 5E+3 cycles running through 63 ksi at 1E+5 cycles to 59 ksi at 1E+9 cycles. The plot also has model curves for various lives up to B99 at 4 ksi higher than the B50 and down to B.135 at 12 ksi lower. Several data points for failures and runouts are plotted within these bounds.

FIGURE 3.0.1 *Instrumentation Research Schedule*

3.1 Improved Non-Contacting Stress Measurement System (NSMS)
- 3.1.1 Improved NSMS Hardware – FY96 through FY02
- 3.1.2 Alternate Tip Sensors – FY97 through FY01
- 3.1.3 Enhanced NSMS Data Processing Capability – FY99 through FY02
- 3.1.4 Spin-pit Validation of NSMS – FY99 through FY01
- 3.1.5 High-Temperature NSMS Sensor Development – 2nd half FY01 through FY04
- 3.1.6 Dual Use Science and Technology (DUST) Program – 2nd half FY01 through FY04
  - 3.1.6.2 Durable Small Engine NSMS – FY01 through FY02

3.2 Environmental Mapping System
- 3.2.1 Pressure/Temperature Sensitive Paint (PSP/TSP) – FY95 through FY02
  - 3.2.1.1 PSP: Improved Dynamic Response – FY97 through FY01
  - 3.2.1.2 PSP: Light Emitting Diodes – FY99 through FY01

FIGURE 3.1.1 *Next-Generation NSMS Overview*

The schematic shows a bladed rotor with 8 optical sensors pointed at the blade tips and one 1/rev trigger sensor. The blade tip sensors are fed from the Generation 4 NSMS hardware system by a laser illuminator and return a signal to a detector module which feeds both the Signal Monitor and Control module and the Timing Generator and the Blade Deflection Signal Processor. The latter feeds a PC Display and Digital Recorder which handles the Raw Mils (displacement), rpm, and time-code data which represent the Raw Time of Arrival. This system feeds the NSMS Computer System with its Generation 4 Analysis Software, which uses the Raw Time of Arrival Data in conjunction with a Deflection to Stress Calibration Table to produce the final output: multiple mode integral and non-integral vibratory response (frequency, stress in ksi, and phase).

FIGURE 3.1.4.1 *Turbine Rotor Spin Test with Magnet Excitation and 2-Light Probe NSMS System.*

The photograph shows a section of an instrumented turbine rotor in a spin pit fixture viewed in the plane of the rotor with two magnets held by fixed brackets near the leading edge of the blades about 10% blade span from the tips of two blades and spaced 6 blades apart. It also shows the supporting structure for the NSMS light probes.

FIGURE 3.1.4.2 *Example of Resonant Response of One Blade from One Light Probe Signal*

This is a computer screen shot with multiple graphic windows, the primary one being Magnitude versus Rotor Speed showing a trace of vibratory response of blade #3 from 4050 to 6270 with a resonant peak at about 5660 rpm.

FIGURE 3.1.4.3 *Micro-Strain in Each Blade Deduced from (Calibrated) Light Probe Measurements.*

This figure shows two plots of zero-to-peak strain versus blade number for probe # 1 with plastic inserts. The top figure shows runs 1 through 5; the

bottom plot shows only runs 3 through 5. For all of the runs plotted, the inferred strain is very repeatable, with high responding blades consistently having high response and low responding blades consistently having low response.

FIGURE 3.1.6.2.1 *Installation of the Fiber Optic Sensors in the Compressor Case*
This computer-generated drawing shows two views of a ring-shaped compressor case with the routing shown of the optical fibers on the outside of the case from the sensors then gathered into a bundle, held onto the case with three brackets, then leading away from the case.

FIGURE 3.1.6.2.2 *Fiber Optic Sensor Installation Array Pattern*
This computer-generated drawing shows the fiber-optic sensors that "look" through the compressor case in the area where the blade tips pass. The pattern of sensors is an equilateral parallelogram with five axial rows of seven sensors circumferentially. The axial rows would be spaced evenly if there were seven rows, but in this spacing there are no sensors where rows 3 and 5 would be in an even spacing.

FIGURE 3.2.1.1 *Spanwise Temperature Distribution at 10% Blade Chord. Blue – Using Scaled Temperature Data. Red – Using CFD Temperature Distribution and Experimental Pressure Data*
This is a plot of Temperature (deg. C) versus spanwise distance S (arbitrary units) with two curves. The blue curve, described in the text, starts at 50 deg. C and 12 units, jumps up to 58 deg. at 12, then goes down to the right but curving upward through a minimum of 56 deg. C at 24 to 58 deg. C at 60, then rises almost linearly to 86 deg. C at 160, then drops almost linearly to 75 at 170, and then drops vertically to the horizontal axis at 50 deg. C. The red curve, described in the text, begins at 57 deg. C. and 31, following the red curve up and to the right within 3 C degrees but peaking at 87 deg. C at 165 and then curving downward to the right to 84 at 170.

FIGURE 3.2.1.2 *Temperature Fields Obtained From Scaled TSP Data and Temperature Fitting of the CFD Pressure and PSP Relative Intensity Distributions*
This computer-generated image shows color-coded temperature fields, for the two methods described in the text, on the spanwise outer 2/3rd and chordwise forward 4/5ths of a compressor blade ranging from 56 deg. C spanwise inboard to 88 deg. C outboard. It also graphically compares the TSP temperature results with CFD results for a chordwise section at about half span for the scaled TSP method, which shows poor agreement; and it graphically compares the TSP temperature results with CFD for a spanwise section at about 10% chord aft of the leading edge for the Temperature Fitting of the CFD Pressure method, which shows good agreement.

FIGURE 3.2.1.3 *Pressure Fields Obtained from PSP (Left) and CFD (Right)*
This computer-generated image shows a color-coded pressure field, derived

from the PSP using the scaled temperature method, on the spanwise outer 2/3rd and chordwise forward 4/5ths of the suction side of compressor blade ranging from a pressure ratio 0.1 at the leading edge to 0.6 at 40% chord. It also shows a color-coded pressure field derived from CFD which shows similar regions of low pressure ratio, but at a lower intensity than the TSP-derived field. The figure also graphically compares the TSP pressure results with CFD results for a chordwise section at about half span for the scaled TSP method, which shows limited agreement (plus or minus 0.1 pressure ratio) in the forward 10% of the chord slightly aft of the leading edge; and it graphically compares the TSP pressure results with CFD for a spanwise section at about 10% chord aft of the leading edge, which shows similar trends of pressure increase and decrease but shows poor agreement in pressure magnitudes.

FIGURE 3.2.1.4 *Decay Time Verses Temperature for Cerium-Doped Yttrium Garnets*

This is a plot of decay time (ns) versus temperature (deg. C) for various ratios "x" of Gallium to the Gallium-Aluminum total in the garnets:

x=0, sample 1 – the data points run from 58 ns at 180 deg. C almost linearly to 24 ns at 290 deg. C

x=0, sample 2 – the data points run from 45 at 20 linearly to 41 at 210 then curve downward to 30 at 300

x=0.25 – the data points run from 50 at 0 linearly to 45 at 210 then curve downward to 31 at 300

x=0.5 – the data points run from 43 at 0 linearly to 9 at 160 then flatten to 4 at 250

x=0.625 – the data points run from 40 at 0 almost linearly to 22 at 90

x=0.69 – the data points run from 32 at 0 linearly to 20 at 40 then flatten to 17 at 90

x=0.75 – the data points run from 16 at 0 linearly to 10 at 40 then flatten slightly to 8 at 90

FIGURE 3.2.1.5 *Decay Time Verses Temperature for Cerium-Doped Silicates*

This is a plot of decay time (ns) versus temperature (deg. C) for three silicates:

Y_2SiO_5:Ce – the data points run from 64 ns at 20 deg. C curving smoothly downward through 61 at 50 to 32 at 120 then reversing curvature and running through 11 at 170 to 6 at 220

La_2SiO_5:Ce – the data points run from 20 at 0 linearly to 7 at 270

Gd_2SiO_5:Ce – the data points run from 18 at 20 curving downward through 17 at 90 then linearly to 6 at 220 then linearly to 2 at 290

FIGURE 3.2.1.6 *Response Time of the PSP to a Pressure Step Versus Weight Percent of Polymer (Scroggin)*

This plot of logarithmic response time versus linear weight % of polymer shows a smooth curve through data points at the following:

$6x10^{-5}$ ns at 2.5 %

0.00011 at 3.5
0.0003 at 6.5
0.0008 at 10
0.011 at 15
0.09 at 19
0.1 at 24

FIGURE 3.2.1.7 *Experimental Setup for Response of PSP to Pressure Step*
This line-drawing schematic shows the test specimen inside an evacuated chamber with a burst cover at one end and a window at the other end. A 460 nm wavelength LED array illuminates the specimen through the window and the reflected light exits from the specimen through the window and passes through a 610 LP filter to a photo-multiplier tube, which sends its signal to a digital oscilloscope.

FIGURE 3.2.1.8 *Temporal Response of Several PSPs to a Pressure Step*
This is a plot of linear I/Io versus logarithmic time (sec.) for various PSPs:
FIB+TiO2 – the data is a smooth curve upward from 0.03 at .0001 sec through 0.04 at 0.00011 sec. to 0.1 at 0.0002 then linear to 0.8 at 0.0008 sec. then curves to the right through 0.9 at .001 to 0.97 at 0.002 then linear to 0.975 at 0.006
FIB – the data starts at 0.07 at .0002, curving slowly upward through 0.25 at .001 to 0.7 at .01, then curving to the right through 0.85 at 0.03 to 0.97 at 0.1
SolGel – the data starts at 0.07 at .0002, curving slowly upward through 0.16 at .0008 through 0.51 at 0.01, then curving to the right through 0.87 at 0.1 to 0.97 at 0.3
HiT – the data starts at 0.03 at .0001, curving slowly upward through 0.09 at 0.001, through 0.025 at 0.01, through 0.55 at 0.1 to 0.97 at 1.0

FIGURE 3.2.1.9 *Driver Pulse and Corresponding LED Light Output for ISSI's 4" LED Array*
This plot of amplitude versus time (sec) shows the driving pulse on at time=zero and off at time $=3.5 \times 10^{-6}$ sec. The LED response starts increasing amplitude at time$=0.1 \times 10^{-6}$ sec., rising rapidly then curving to the right, becoming almost level by the time it reaches the same amplitude as the driver at 2.4×10^{-6} sec., rising slowly to 2% above the driving amplitude. The decay is almost linear from time$= 3.65 \times 10^{-6}$ to 3.85×10^{-6} sec.

FIGURE 3.3.1.1 *a) Sensor and Cabling b) Signal Processor*
This two-part figure shows the following:
a) a photo of the flanged sensor and the connected cabling which ends in a two-connector pigtail,
b) a photo of the rectangular signal processor box with eight connector ports.

FIGURE 3.3.1.2 *Eddy Current Sensor Signal Processing System*

This line drawing schematic shows the input coming from 1 to 4 eddy current sensors through a power/sense module which processes the signal with modulation, demodulation and amplification. The signal then passes through Low Noise Amplifiers into an HEDG 11 1MHz Analog Input/Output unit through a first-in-first-out (FIFO) transfer into a HERON 4 6701 Digital Signal Processor (DSP) which does key parameter extraction. The signal then passes via FIFO transfer to a second HERON 4 DSP which does data management. The signal is then passed again via FIFO transfer through a PCI interface and PCI bus to a computer with a Pentium III CPU and data storage and is presented to an operator via a graphical user interface and input/output controls (e.g., monitor, keyboard, mouse, etc.). The Analog I/O, the two 6701 DSPs and the PCI interface are all housed in a HERON Carrier (HEPC8)

FIGURE 4.0 *Component Analysis Research Schedule*

4.1 Assessment of Turbine Engine Components – FY98-01
4.2 Probabilistic Design of Turbine Engine Airfoils, Phase I – FY99-03
4.3 Probabilistic Design of Turbine Engine Airfoils, Phase II – FY01-05
4.4 Probabilistic Blade Design System – FY98-01
4.5 Efficient Probabilistic Analysis Methods for Turbine Engine Components – FY99-01
4.6 PREDICT – FY01-03

FIGURE 4.5 *Airfoil Stochastic Analysis*

This illustration shows a notional compressor blade and a potential variation in displacement (in response to load) that is due to statistical influences (like an uncertain thickness). The illustration highlights the concept that uncertainty analysis will produce descriptions of the distributions of the variation that result from the uncertainties in the form of probability density functions and cumulative density functions.

FIGURE 5.0.1 *Forced Response Research Schedule (1)*

5.1 Development of Physical Understanding and Models
- 5.1.1 Development of TURBO-AE – FY96 through FY99
- 5.1.2 Nonlinear Modeling of Stall/Flutter – FY97 through FY01
- 5.1.3 Force Response: Mistuned Bladed Disk (REDUCE Code) – FY95 through FY96
- 5.1.4 Design Guidelines for Mistuned Bladed Disk (REDUCE Code) – FY96 through FY01
- 5.1.5 Tip Modes in Low-Aspect-Ratio Blading – FY95 through FY96
- 5.1.6 Sensitivity Analysis of Coupled Aerodynamic/Structural Behavior of Blade Rows – FY96 through FY02
- 5.1.7 Dynamic Analysis and Design of Shroud Contact (BDAMPER

Code) – FY95 through FY01

5.1.8 Friction Damping in Bladed Disks – FY97 through FY01

5.1.9 Compressor Mistuning Characterization – FY97-99

5.1.10 Fretting Characterization – FY98-02

FIGURE 5.0.2 *Forced Response Research Schedule (2)*

5.2 Acquisition of Experimental Data

5.2.1 High Mach Forcing Functions – FY95 through RY96

5.2.2 Forward Swept Blade Aerodynamics – FY95 through FY96

5.2.3 Oscillating Cascade Rig – FY95 through FY02

5.2.4 F109 Unsteady Stator Loading – FY95 through FY02

5.2.5 Fluid-Structure Interaction – FY96 through FY01

5.2.6 Experimental Study of Forced Response in Turbine – FY96 through FY01

5.2.7 Spin Pit Excitation Methods – FY98 through FY01

5.2.8 Inlet Distortion Characterization – FY98 through FY01

FIGURE 5.0.3 *Forced Response Research Schedule (3)*

5.3 Validation of Analytical Models

5.3.1 Evaluation of Current State-of-the-Art Unsteady Aerodynamic Models for the Prediction of Flutter and Forced Vibration Response – All FY97

5.3.2 Evaluation of State-of-the-Art Aerodynamic Models – FY99 through FY05

5.3.3 Forced Response Prediction Systems (Fans) – FY95 through FY03

5.3.4 Aeromechanical Design System Validation – FY96 through FY01

5.4 New Efforts – FY01 through FY06

FIGURE 5.2.3 *Oscillating Cascade Rig Test Results*

This eight part figure shows four shadow graphs on the left and the matching graphs of unsteady pressure p (kPa) (on the suction side of the vane past the leading edge) versus time (ms) for four conditions:

1. Subsonic inlet flow -- showing portions of four vanes and the high pressure stagnation point at the vane leading edges and the adjacent low pressure regions. The graph shows a constant mean unsteady pressure of about 32 kPa with high frequency hash plus or minus 10 kPa about this mean.

2. Low transonic inlet flow – showing weak oblique shocks from the vane leading edges intersecting a normal shock emanating from the vane at about 1/3 chord. The graph shows a constant mean unsteady pressure of about 28 kPa with high frequency hash plus or minus 20 kPa about that mean.

3. High transonic inlet flow – showing a stronger oblique shock from the leading edge on alternate vanes intersecting a slightly oblique shock emanating from the vane at about ¼ chord. The intervening vanes show no

oblique shock, only a normal shock emanating from the vane at about 40% chord. The graph shows a constant minimum unsteady pressure at 21 kPa with higher frequency hash going upward only to peaks as high as 32 kPa.
4. Supersoninc inlet flow – showing a strong oblique shock from the leading edge intersecting another strong oblique shock emanating from the vane at about the 1/3 chord point. The graph shows a constant unsteady pressure of 21 kPa with less than 1 kPa of high frequency hash.

FIGURE 5.2.4.1 *F109 Fan and Vane Configuration*
This line drawing cross section of the F109 fan shows a two-inch span vane with an end plate at the outer diameter of the fan case with four pressure taps in a line from 2/3 span and 2/3 chord to almost the trailing edge at mid span of the vane. The aft-most pressure tap is 0.6 fan chord lengths from the leading edge of the fan rotor. A piece of reflective tape is located on the engine spinner, just ahead of the fan as an indicator for an optical trigger for fan rotational position (fan speed detection).

FIGURE 5.2.4.2 *Normalized, RMS Unsteady Pressure vs. Fan RPM*
This is a plot of the data points of RMS delta P/q versus Fan RPM for the following vane configurations:
1. Sharp Trailing Edge: 0.1 at 11000 RPM , 0.25 at 12100, 0.37 at 12300, 0.9 at 12800, 0.95 at 13300, 0.7 at 13800, 2.20 at 14400.
2. Bluff Trailing Edge: 0.3 at 11000, 0.4 at 12100, 0.45 at 12300, 1.1 at 13300, 1.2 at 13800, 1.3 at 14400.
Semi-Bluff Trailing Edge: 0.1 at 11000 RPM , 0.3 at 12100, 0.45 at 12300, 0.85 at 12800, 1.15 at 13300, 0.95 at 13800, 1.35 at 14400.

FIGURE 5.2.8.1 *CFD Solutions at an Axial Plane in the Inlet Section of the F-16*
This computer-generated image shows a circular map of the total pressure differential and a circular map of the static pressure differential, with color gradations to indicate the degree of pressure differential. The total pressure map shows a small region with no pressure differential at the inlet wall at the 4 o'clock position and a gradient of increasing total pressure differential, represented by 20 gradations in color, radiating outward from that position across the inlet to an almost constant, and maximum, total pressure differential covering almost all of the right half of the map. The static pressure map, on the other hand, shows only one gradation in color covering approximately the upper right quadrant of the map.

FIGURE 5.2.8.2 *CFD Solutions at an Axial Plane in the Inlet Section of the ACIS*
This computer-generated image shows a half-circle map of the total pressure differential and a half-circle map of the static pressure differential, with color gradations to indicate the degree of pressure differential, with the centerline of the circle at the right side of the maps. The total pressure map shows a small island with the lowest pressure differential, three gradations, at about one third of the inlet radius from the inlet wall, 20% of

the radius in width, running from about 8 o'clock to 10 o'clock position. A gradient of increasing total pressure differential, represented by 13-15 gradations in color, radiates outward from that position across the inlet half with the maximum total pressure differential at the upper half of the inlet centerline and in a small region from 7 to 8 o'clock near the inlet wall. The static pressure map shows a small round island of no static pressure differential, with a diameter of about 20% of the inlet radius, centered in the upper third of the map. Gradations in color radiate outward from that island, 3 gradations both clockwise and counterclockwise in the circumferential direction, 4 gradations in the radial direction toward the inlet's center, and 2 gradations toward the inlet wall. The maximum differential, 4 gradations, is at the inlet center in an island about 20% of the inlet diameter high and 10% wide.

FIGURE 5.2.8.3 *Total Versus Static Pressure Excitations across Spectrum of Conditions*
This is a plot of the ratio of MEI total pressure to MEI static pressure versus test condition for the F-16 and the ACIS inlets:
Test condition 58: 5.5 for F-16, no ACIS data
Test condition 54: 20 for F-16, 10 for ACIS
Test condition 38: 5 for F-16, no ACIS data
Test condition 59: 12 for F-16, no ACIS data
Test condition 47: 3.5 for F-16, no ACIS data
Test condition 36: 3.5 for F-16, 8.5 for ACIS
Test condition 29: 4.5 for F-16, no ACIS data
Test condition 49: 7.5 for F-16, no ACIS data
Test condition 33: 7.5 for F-16, no ACIS data
Test condition 24: 19 for F-16, 6 for ACIS

FIGURE 5.3.4.1 *Forced Response Prediction Process*
This schematic diagram shows the analytical models and their interrelationships needed to model resonance stress: modal analysis supports structural damping analysis, aerodynamic damping analysis, and forced response. Steady flow supports aerodynamic damping analysis and unsteady flow analysis. Forced response needs the inputs form modal analysis, aerodynamic damping analysis, structural damping analysis and unsteady flow analysis to generate the final resonance stress output.

FIGURE 5.3.4.2 *CFD Model of Inlet Guide Vane and Rotor*
This computer model drawing shows a six-inlet-guide-vane-with-flap stator segment and a six-blade rotor segment . Each blade and vane has about 20 spanwise by 20 chordwise four-sided surface elements.

FIGURE 5.3.4.3 *Rotor Blade Sector Finite Element Model Used in Tuned Analysis*
This computer model drawing shows a single fan blade and its sector of attached rotor, with a very high mesh density.

FIGURE 5.3.4.4 *Comparison of Predicted and Measured Vibratory Stresses*

This plot of vibratory stress versus RPM has no numerical scales. The following description is for five RPMs (low , low- medium, medium, high-medium, high) with the numbers being percent of the vertical scale height.

- Low RPM:
  Engine Test Data: 21
  Predicted Stress, Design Intent: 14
  Predicted Stress, Ave. Measured Blade: 20
  Predicted Stress, Max. Measured Blade: 26
  Predicted Stress, Min. Measured Blade: 16
- Low-Medium RPM:
  Engine Test Data: 18
  Predicted Stress, Design Intent: 42
  Predicted Stress, Ave. Measured Blade: 28
  Predicted Stress, Max. Measured Blade: 38
  Predicted Stress, Min. Measured Blade: 20
- Medium RPM:
  Engine Test Data: 69
  Predicted Stress, Design Intent: 78
  Predicted Stress, Ave. Measured Blade: 76
  Predicted Stress, Max. Measured Blade: 82
  Predicted Stress, Min. Measured Blade: 67
- High-Medium RPM:
  Engine Test Data: 64
  Predicted Stress, Design Intent: 35
  Predicted Stress, Ave. Measured Blade: 49
  Predicted Stress, Max. Measured Blade: 53
  Predicted Stress, Min. Measured Blade: 46
- High RPM:
  Engine Test Data: 36
  Predicted Stress, Design Intent: 75
  Predicted Stress, Ave. Measured Blade: 69
  Predicted Stress, Max. Measured Blade: 75
  Predicted Stress, Min. Measured Blade: 63

FIGURE 6.0.1 *Passive Damping Research Schedule*

6.1 Identification and Characterization of Damping Techniques
- 6.1.1 Mechanical Damping Concepts – FY 95-01
- 6.1.2 Air Force In-House Damping Investigations – FY 01-06
- 6.1.3 Centrifugally Loaded Viscoelastic Material Characterization Testing – FY 96-98
- 6.1.4 Damping for Extreme Environments – FY 97-01
- 6.1.5 Centrifugally Loaded Particle Damping – FY 96-01
- 6.1.6 Evaluation of Damping Properties of Coatings – FY 00-02
- 6.1.7 Development of Air Film Damping for Turbine Engine

FIGURE 6.1.2.1 *Turbine Engine Fatigue Facility*
This schematic overview shows the facility rooms and the locations of the shakers, the single and multi-axial fatigue frames, and the digital holography area.

FIGURE 6.1.2.2 *(a) 700 lb, (b) 6,000 lb and (c) 18,000 lb Shakers*
This figure has three photographs of the three shakers.

FIGURE 6.1.2.3 *Single Point Laser Vibrometer*
This is a photograph of the laser (about the size of a quart carton of milk) and the cable connecting it to the electronics box, about the size of an briefcase that houses the controller-analyzer.

FIGURE 6.1.2.4 *AE3007 Blade Bench Test Results*
This plot of Q versus temperature for various blades shows the undamped blade with Qs around 300, plus or minus 30 between 75 and 325 degrees F. Most of the other blades have Qs around 150 in that same temperature range varying by plus or minus 100. The one exception is blade number 809 which shows a steadily rising Q from 100 at 110 deg. F peaking at 450 at 250 deg. F then declining to 360 at 325 deg. F. The line for the predicted damping has the following points: 170 at 50 deg. F, 210 at 70, 165 at 80, 30 at 90, 30 at 125, 100 at 150, 175 at 175.

FIGURE 6.1.2.5 *AE3007 Blade and Test Fixture*
This photograph shows an L-shaped fixture with gussets on the two sides supporting the vertical leg of the L. The blade is mounted in a circular fixture between the gussets on the base of the L.

FIGURE 6.1.2.6 *Undamped AE3007 Blade Bench Test*
This plot of Q versus temperature in degrees F is a smooth curve that begins at 830 at 70 deg. F and runs through 1240 at 170 deg., peaking at 1340 at 250 deg. F, and ends at 1330 at 270 deg. F.

FIGURE 6.1.2.7 *AE3007 Damped Blade #809 Test Results*
This is a smooth curve that begins at 160 at 70 deg. F, declines to 130 at 96, then curves upward to 340 at 160, then changes curvature downward, peaking at 535 at 192 to 420 at 240. There it changes curvature again (upward) through a local minimum at 360 at 233 deg. F to 420 at 245. It changes curvature one last time, peaking at 530 at 260 deg. F declining to 320 at 310 deg. F.

FIGURE 6.1.2.8 *Simulated Blade Specimen*
This is a photograph of a metal plate about twice as long as it is wide, with a thickened area at one end going the full width and about ¼ of the length.

FIGURE 6.1.2.9 *Typical Broad Band Sweep*
This graph vibration amplitude versus frequency showing five peaks, each at the resonance for one of the vibratory modes within the tested frequency range. The scales and details of the test are not legible in this sample plot.

FIGURE 6.1.2.10 *Specimen Baseline Test Setup in the Intermediate Temperature Furnace*
The blade-like specimen is shown clamped in a support fixture inside the furnace with a magnetic exciter held by a support fixture near the “blade” tip.

FIGURE 6.1.2.11 *Baseline Test Results*
This is a plot of frequency versus temperature (deg. F) for the various specimens (test series):
Series 1: 1920 at 75 deg. F, 1900 at 100, 1890 at 125, 1882 at 150, 1874 at 175, 1868 at 200, 1871 at 225, 1854 at 250, 1844 at 275, 1837 at 300, 1828 at 325, 1818 at 350, 1812 at 375, 1802 at 400
Series 2: 1920 at 75 deg. F, 1905 at 100, 1897 at 125, 1889 at 150, 1878 at 175, 1866 at 200, 1860 at 225, 1854 at 250, 1844 at 275, 1834 at 300, 1824 at 325, 1812 at 350
Series 3: 1952 at 75 deg. F, 1944 at 100, 1936 at 125, 1928 at 150, 1920 at 175, 1912 at 200, 1905 at 225, 1898 at 250, 1890 at 275, 1880 at 300, 1873 at 325, 1865 at 350
Series 4: 1952 at 75 deg. F, 1944 at 100, 1936 at 125, 1928 at 150, 1920 at 175, 1915 at 200, 1912 at 225, 1907 at 250, 1902 at 275, 1895 at 300, 1890 at 325, 1883 at 350, 1879 at 375
Series 5: 1952 at 75 deg. F, 1940 at 100, 1936 at 125, 1928 at 150, 1920 at 175, 1912 at 200, 1909 at 225, 1894 at 250, 1900 at 275, 1895 at 300, 1891 at 325, 1887 at 350, 1882 at 375, 1878 at 400

FIGURE 6.1.2.12 *Low Temperature Coating Test Specimen*
This photograph shows a long narrow metal beam about 13 times as long as it is wide, with a thickened section at its left end, 20% of its length, with a hole in the center of the thickened section.

FIGURE 6.1.2.13 *Low Temperature Coating Test Specimen in the Test Setup*
This photograph shows the beam specimen securely clamped in a fixture, with four bolts providing the clamping, mounted on top of a shaker. There is also an accelerometer mounted to the top of the shaker.

FIGURE 6.1.2.14 *High Temperature Damping Coating Specimens*
This photograph shows two flat metal specimens about 2½ times as long as they are wide, with a thickened section at the lower third. One of the two specimens is coated on all but the thickened section.

FIGURE 6.1.5.1 *Examples of Damper Trial Inserts*
This photograph shows five cylindrical metal inserts about the same diameter as a dime (shown for comparison) about half their diameter in length, open at one end, each with a different shaped cavity. Two have circular cavities; three have slotted cavities.

FIGURE 6.1.5.2 *Examples of Results of Particle Damping Behavior at 4500 G's Centrifugal Load at Increasing Out-of-Plane Dynamic Excitation Levels*
This is a plot of the Response Transfer Function (G/V) versus Frequency (Hz) at 5000 RPM. The peak response at the 5% (plus or minus 5 V excitation) is 2.65 G/V at 309.5 Hz. As excitation increases, the peak gets lower as does the frequency. At the maximum excitation (100% = plus or minus 200 V) the peak has flattened to a maximum of 0.55 G/V centered at about 306 Hz, with the flat peak extending from 301 Hz to 311.

FIGURE 6.1.5.3 *Representative Results Comparing First Mode Results for the Baseline (Undamped) Versus a Particle Damped Configuration at a Variety of RPMs Corresponding to 180 to 4500 Gs Centrifugal Load. Full Scale Excitation Was 200V*
This is a plot of Response Transfer Function (G/V) versus Frequency (Hz) for five RPMs with and without damping treatment #2 at 100% excitation.
- At 1010 RPM the peak Response Transfer Function is reduced by the added damping from 1.2 to a 0.40
- At 2000 RPM it is reduced from 1.33 to 0.40
- At 3000 RPM it is reduced from 1.36 to 0.43
- At 4000 RPM it is reduced from 1.36 to 0.47
- At 5000 RPM it is reduced from 1.35 to 0.57

FIGURE 6.1.5.4 *Comparison of Peak Reduction Versus Centrifugal Load and Dynamic Excitation Amplitude for Two Different Damping Configurations*
This figure shows two three-dimensional surface plots of Response

Amplitude Ratio (Baseline Case BL07/Damped Case D025 and Baseline Case BL07/Damped Case D15T) versus RPMs versus Drive Amplitude (% full scale value). Case D025 peaks at a response amplitude ratio of 3.2 at 2000 RPM at 100% drive amplitude. Case D15T peaks at a response amplitude ratio of 2.4 at 1000-2000 RPM at 90-100% drive amplitude.

FIGURE 6.1.6.1.1 *Frequency Response Function for Sweep-Up and Down Excitation of the Coated Beam.*
This plot of Frequency Response Function (M/s/N) versus Frequency shows the sweep up and sweep down curves.
The sweep up rises sharply from 0.012 at 308.2 Hz to a peak at 0.0285 at 308.4 Hz then declines again to 0.011 at 311 Hz.
The sweep down rises from 0.012 at 311 Hz to a peak at 0.029 at 308.2 and then declines to 0.010 at 307.6 Hz.

FIGURE 6.1.6.1.2 *Time History of Beam Tip Velocity in a Ring-Down Approach for a Coated Beam*
This plot of velocity (m/sec) versus time (sec) shows an oscillation with a period of just over 0.02 sec whose peaks decline from 1250 m/sec at time 0.02 to 495 m/sec at 0.24 sec.

FIGURE 6.1.6.1.3 *Strain and Q vs. Forces for the Coated Beam*
This is a dual plot of Maximum strain (micro-strain units) versus Force (N) and Q versus Force. The data points are as follows:
-- 0 strain at 0 force, 90 micro-strain units at 8 N, 110 at 12, 180 at 25, and 260 at 42
-- Q = 305 at 0 N, 245 at 8, 230 at 12, 190 at 25 and 155 at 42

FIGURE 6.1.6.1.4 *Strain and Maximum Tip Velocity vs. Force for the Coated Beam*
This is a dual plot of Maximum strain (micro-strain units) versus Force (N) and Maximum Tip Velocity (m/sec) versus Force. The data points are as follows:
-- 0 strain at 0 force, 90 micro-strain units at 8 N, 110 at 12, 180 at 25, and 260 at 42
-- 0 m/sec at 0 N, 245 at 8, 300 at 12, 600 at 25 and 750 at 42

FIGURE 6.1.7.1 *AFDS Integrated into a Fan Blade*
This is a photograph of the suction side of a fan blade with the air film damper cover sheet installed, running from 5% chord to 95% chord and from 40% span to 95% span. It also shows a separate contoured cover sheet.

FIGURE 6.1.7.2 *FEA Prediction of AFDS Performance*
This is a plot of logarithmically-scaled predicted compliance (in/lb) from 1E-6 to 1.0 versus linear-scaled frequency (Hz) from 0 to 3500 Hz. The compliance for the baseline AE3007 fan blade shows resonant spikes as

high as 0.03 with minimums as low as 3E-6. The air film damped blade's compliance matches the baseline's from 0 to 250 Hz after which its peaks get continuously lower and minimums continuously higher as frequency increases. The Two-Stripe Mode is singled out, showing a baseline peak at 6E-3 at 1750 Hz while the damped peak is at 4E-4 at 1720 Hz.

FIGURE 6.1.7.3 *Measured AFDS Performance*
This is a plot of logarithmically-scaled measured compliance (in/lb) from 1E-6 to 1.0 versus linear-scaled frequency (Hz) from 0 to 3500 Hz. The compliance for the baseline AE3007 fan blade shows resonant spikes as high as 0.025 with minimums as low as 6E-6. The air film damped blade's compliance peaks begin slightly less than the baseline's from 0 to 250 Hz after which its peaks get continuously lower and minimums continuously higher as frequency increases. The Two-Stripe Mode is singled out, showing a baseline peak at 1.2E-2 at 1750 Hz while the damped peak is at 8E-4 at 1740 Hz.

FIGURE 6.1.7.4 *AFDS Optimization via FEA*
This computer image showing a view of the suction side of the Finite Element Model of the AE3007 fan blade, with the air film cover sheet 6.3 spanwise inches long at the front, one inch from the blade's leading edge, to within ½ inch of the blade tip and 5.6 spanwise inches at the back, ½ from the blade's trailing edge. The sheet is 4.0 inches long chordwise at its outboard end, ½ inch from the blade tip, and 3.75 inches long chordwise at its spanwise inboard end. The FEM uses 20 x 20 quadrilateral elements for the cover sheet.

FIGURE 6.1.7.5 *FEA Prediction of C-1 AFDS Performance*
This is a plot of logarithmically-scaled predicted compliance (in/lb) from 1E-6 to 1.0 versus linear-scaled frequency (Hz) from 0 to 3500 Hz. The compliance for baseline AE3007 fan blades, with Qs equal to 500, 200, and 70, shows resonant spikes as high as 0.012 with minimums below as 1E-6. The air film damped blade's compliance peaks begin almost equal to those of the baseline blades from 250-350 Hz after which its peaks get continuously lower and minimums continuously higher as frequency increases. The Two-Stripe Mode is singled out, showing a baseline peak at 2.3E-3 at 1750 Hz for Q=500, 1E-3 for Q=200, 3.5E-4 for Q=70 all at 1760 Hz, while the damped peak is at 5E-5 at 1740 Hz.

FIGURE 6.1.8.1 *Typical Solid Blisk Design*
This is a photograph of a three-stage blisk

FIGURE 6.1.8.2 *PRDA V Constrained Layer Damping System Viscoelastic Damper Successfully Tested on an AE3007 Fan Blade (1999)*
This photograph of the blade perpendicular to the suction side at mid chord at about 60% span shows the constraining layer cover sheet on the outer

third of the blade span from 35% aft of the leading edge to 5% forward of the trailing edge.

FIGURE 6.2.7.1 *Planned AE3007 Engine Testing*

This diagram shows a cutaway schematic of the AE3007 engine with bubbles surrounding it indicating the technologies that will be included in the planned test program:

- Non Contacting Stress Measurement (PRDA VII)
- Blade Tip Timing (UK)
- Air Film Damping (PRDA VII)
- Aeromechanical and Probabilistic Analysis (AADC IRAD)
- Damping Hard Coatings (UK)

FIGURE 6.2.7.2 *SBIR Phase 1 Damping installed on an AE3007 Fan Blade*

This is a photograph of the suction side of an AE3007 fan blade with the air film damper cover sheet installed, running from 5% chord to 95% chord and from 40% span to 95% span. It also shows a separate contoured cover sheet.

FIGURE 6.2.7.3 *Gen IV NSMS System*

This line drawing schematic shows the test stand side of the system with an engine with a 1/rev sensor mounted on it and the fiber optic transmit and receive cables going to and from the optical sensors also mounted on the engine. The Control room houses the following parts of the system. The Laser illuminator feeds the fiber optic transmit cable. It is controlled by the Laser Illuminator Control and Signal Monitor. An Analog Detector/Trigger Module gets the signals from the 1/rev sensor and from the optical sensors on the engine and feeds both the Laser Illuminator and Signal Monitor and a processing unit that contains the Blade Timing Generator and the Data Display and Control Interface Module and feeds a Data Display, a Hard Disk, a Removable Storage Medium unit and a User's Computer. The processing unit also get an IRIG Time Code input from the test cell facility. The processing unit also can receive inputs from the Hard Disk and from the User's Computer.

FIGURE 7.0 *HCF Demonstrator Engine Plan*

This schedule chart shows the expected run and data analysis schedule times for each of the upcoming HCF-relevant engine demonstrators:

General Electric / Allison Advanced Development Company
XTC76/2 – 4th Qtr. CY98
XTC76/3 – 4th Qtr. CY01
F110 – 3rd Qtr. CY03-1st Qtr. CY04
XTC77/1 – 3rd -4th Qtr. CY05
XTE76/1 – 4th Qtr. CY03-1st Qtr. CY04
XTE77/1 – 4th Qtr. CY05-2nd Qtr. CY06

XTE77/SE1 – 3rd -4th Qtr. CY03
XTE77/SE2 – 4th Qtr. CY04-1st Qtr. CY05

Pratt & Whitney
XTC66/SC – 2nd Qtr. CY 97
XTC66/1B – 4th Qtr. CY 97
XTC67/1 – 1st Qtr. CY 02
XTC67/2 – 3rd-4th Qtr. CY05
XTE66/1 – 1st Qtr. CY99
XTE65/3 – 3rd Qtr. CY00
XTE67/1 – 4th Qtr. CY02-2nd Qtr. CY03
XTE67/2 – 4th Qtr. CY05-2nd Qtr. CY06
XTE66/SE – 1st Qtr. 98
XTE67/SE1 – 1st – 2nd Qtr. CY03
XTE67/SE2 – 4th Qtr. CY04-2nd Qtr. CY05

Allison Advanced Development Company
XTL17 – 3rd Qtr. CY03
XTL17/SE1 – 1st - 3rd Qtr. CY03
XTL17/SE2 – 2nd – 4th Qtr. CY05

Honeywell
XTL57/1 – 4th Qtr. CY02-2nd Qtr. CY03

Williams International
FJ22 – 1st-3rd Qtr. CY 02
EJ22 – 2nd -3rd Qtr. CY03

CEP (Army): 3rd Qtr. CY03-1st Qtr. 03 and 1st – 3rd Qtr. 05

FIGURE 8.0.1 *Decrease in Uncertainty and Risk over a System's Life Cycle*

This is a notional plot of Probability of Failure versus Time (engine life cycle phases: from Concept through Design through Prototype through Production through Maintenance and Customer Use). It shows a constant probability of failure requirement and an average probability of failure varying up and down, but always below (better than) the requirement. The figure also shows an upper and a lower confidence bound above and below this average (the confidence interval is the distance between the upper and lower bounds). Early in the system life cycle, the upper confidence bound can be well above the probability of failure requirement, but as time (and system development and knowledge of the system) progresses, the upper bound decreases toward the average until, during the production phase, it too (and therefore the entire confidence interval) is below the requirement line, indicating that, even with the remaining uncertainty, the probability of failure is acceptable relative to the requirement.

FIGURE 8.0.2 *Test and Evaluation Development*

This is a schedule chart for the following tasks:
8.1 Characterization Test Protocol Development – FY01-05
8.2 Demonstration Test Protocol Development – FY01-05
8.3 Development of Multi-Axial Fatigue Testing Capability –

FIGURE 8.1.1 *Approach for Addressing Turbine Engine HCF*

This is a schematic of the steps in the HCF Test Protocol:

1. Design System establishment or modification, leads to
2. Component Development, leads to
3. Subsystem Test, leads to
4. Engine Test, leads to
5. Production, leads to
6. Operational Usage, which when added to Experience, Improved Tools, Lessons Learned, and New Technology leads back to modifications to the Design System

FIGURE 8.1.2 *HCF Characterization Test Protocol Checklist*

Test Protocol Item

I. Design per Standard Work
II. Construct FEM
    - Solid Elements
    - Parabolic Displacements Functions
III. Perform Normal Modes Analysis
    - Mesh Density Assessment
IV. Sensitivity Assessment
    - Geometry/Eigensensitivity
    - Boundary Conditions
V. Define Optimum Sensor Locations
    - Mode Measurement Capability
    - Modeshape Identification
    - Sensitivity to Sensor Misplacement
VI. Validate FEM
    - Frequency Comparison
    - Strain Ratio Comparison
    - MAC or Similar
VII. Compute Normal Modes at Speed
VIII. Define Limits for All Component Locations
IX. Design Experiment to Maximize Exposure to Influence Parameters
X. Test Rig and/or Engine
    - Process All Dynamic Data
    - Transform to Frequency Domain
    - Identify Modes Using Frequency and MAC
    - Apply Limits/Use FEM or FEM Derived Look-up Table
    - Database Results
    - Establish Statistical Variations from Database
XI. Assess Robustness
XII. Fix as-needed using Eigensensitivity to Move Problem Modes

FIGURE 8.3.1 *Multi-axial Fatigue Frame*

This is a three-photograph figure showing three views of the multi-axial fatigue frame. It shows four columns supporting the top and bottom holding fixtures for the specimen. The bottom holding fixture is attached to the radial load actuator. The four-column support is surrounded by a rectangular structure, open on two sides, that holds the actuators that impart the side loads to the specimen through the spaces between the four columns. The entire assembly is solidly mounted to a solid structural base.

FIGURE 9.0 *HCF Technology Transition*

This schedule charts show ENSIP updates in mid FY2002, mid FY2004 and mid FY2006. A JSSG update is planned for some time in FY005.